Modelling the Distribution of Mercury in Oil and Gas Processing Facilities

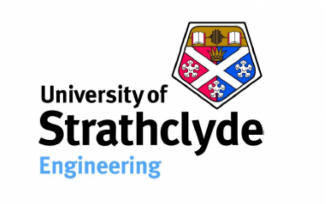

Manssor Khalifa

Department of Chemical and Process Engineering

University of Strathclyde

A thesis submitted for the degree of

Doctor of Philosophy

2018

Dedication

This thesis is the result of the authors original research. It has been composed by the author and has not been previously submitted for examination which has led to the award of a degree. The copyright of this thesis belongs to the a uthor under the terms of the United Kingdom Copyright Acts as qualified by University of Strathclyde Regulation 3.50. Due acknowledgement must always be made of the use of any material contained in, or derived from, this thesis.

Acknowledgement

This PhD would never have been possible without the support and guidance of various people at the Chemical and Process Engineering Department, University of Strathclyde.

Firstly, I would like to extend my sincere gratitude to my supervisor, Dr. Leo Lue for giving me the wonderful opportunity to complete my PhD under his supervision and support. Thank you for giving me the opportunity to grow in this field of research.
Special thanks should also be given to Dr. Karen Johnston for useful discussions and guidance throughout the writing and editing of our journal paper.
I would also like to acknowledge Mr. Brian Dickson for his guidance and support to improve my teaching skills.
Special thanks should be given to Dr. Moinul Hossain for his help and support.
I would like to thank, all members of my family and friends for their encouragement. I would specially like to thank my supportive wife, Heba, and my lovely son Sanad for their patience.

I would also like to extend appreciation to my colleagues and friends, within the Chemical Engineering Department.

Grateful to the Department of Chemical and Process Engineering at the University of Strathclyde and to the Libyan Ministry of Higher Education and Scientific Research for their financial support.

Abstract

Mercury is not only considered a toxic pollutant in the environment but also a corrosive element in processing equipment. The presence of mercury in oil and gas can increase the exposure risk to field operators and can cause serious corrosion problems. Furthermore, it may cause catalyst poisoning and deactivation; these could lead to long, unplanned shutdowns which are neither operationally nor financially desirable as they negatively impacts the equipment life and profit. Therefore, producing oil and gas from reservoirs that contain mercury is a challenging task. This work is concerned with the thermodynamic modelling of mercury distribution in oil and gas process facilities. The main objectives of this research are to investigate the distribution of mercury in oil and gas process facilities in order to eliminate mercury impact and unplanned shutdowns. In addition it aims to identify the best location of mercury removal units in an effort to alleviate mercury exposure risks and damage. This work allows the prediction of the thermodynamic behavior of elemental mercury in a wide variety of solvents, hydrocarbon mixtures, and operating conditions where experimental data are unavailable. This was successfully achieved by using two approaches; introducing binary interaction parameters between mercury and other molecules, and modelling mercury atoms as an associating atoms. The effectiveness of the developed models is validated against experimental data.

It has been observed that the process operating conditions play an important role in mercury distribution in various phases. Reducing the operating pressure and increasing operating temperature allows more heavy hydrocarbons to flash out carrying over more mercury to the gas stream. This increases the possibility of mercury accumulation in the gas processing units. The presence of heavy hydrocarbons in the produced water streams increases the solubility of elemental mercury in these streams. This negatively impacts the biosphere due to mercury pollution.

Contents

Dedication 1

Acknowledgement 2

Abstract 3

Contents 4

List of Figures 8

List of Tables 13

1 Introduction 19

2 Mercury in the environment and hydrocarbon processing 23

2.1 Introduction . . . 23

2.2 Sources of mercury . . . 25

2.2.1 Mercury species in the environment . . . 28

2.3 Mercury in oil and gas . . . 30

2.3.1 Mercury concentration in crude oil and refinery products . . . 32

2.3.2 Mercury concentration in natural gas and condensate . . . 36

2.3.3 Mercury in produced water . . . 37

2.3.4 Mercury impact in oil and gas processing facilities . . . 38

2.3.5 Corrosion mechanisms of mercury in oil and gas facilities . . . 39

2.4 Mercury removal technologies . . . 42

2.4.1 Mercury removal from the condensate . . . 43

2.4.2 Mercury removal from natural gas . . . 43
2.5 Remediation cost of mercury pollution . . . 44
2.6 Thermophysical properties of mercury . . . 45
2.6.1 Elemental mercury vapor pressure . . . 46
2.6.2 Density of mercury . . . 47
2.6.3 Solubility of mercury . . . 47
2.7 Modeling approaches . . . 50
2.8 Conclusion . . . 52

3 Thermodynamic modelling **53**
3.1 Introduction . . . 53
3.2 Thermodynamic Potentials . . . 54
3.3 Ideal gas system . . . 58
3.4 Non ideal system . . . 60
3.5 Phase equilibrium . . . 63
3.6 Equations of State . . . 65
3.6.1 Soave-Redlich-Kwong equation of state . . . 66
3.6.2 Group contribution method . . . 69
3.7 Perturbed-chain statistical associating fluid theory . . . 73
3.8 Conclusion . . . 79

4 Prediction of the thermophysical properties **80**
4.1 Introduction . . . 80
4.2 Thermophysical properties prediction using SRK EoS . . . 81
4.2.1 Modelling vapor pressure of pure components using SRK EoS . 83
4.2.2 Modelling the solubility of elemental mercury in water using SRK EoS . . . 85
4.2.3 Modelling the solubility of elemental mercury in normal alkanes using SRK EoS . . . 86
4.2.4 Modelling the solubility of elemental mercury in aromatics using SRK EoS . . . 90
4.2.5 Modelling the solubility of elemental mercury in alcohols using SRK EoS . . . 91

4.2.6 SRK EoS model validation for predicting the soubility of elemental mercury in multi component systems 93
4.3 Thermophysical properties prediction using PC-SAFT EoS 96
4.3.1 PC-SAFT prediction with non associating scenario 97
4.3.1.1 Modelling vapor pressure of pure components using PC-SAFT EoS 98
4.3.1.2 Modelling the solubility of elemental mercury in water using PC-SAFT EoS 101
4.3.1.3 Modelling the solubility of elemental mercury in normal alkanes using PC-SAFT EoS 102
4.3.1.4 Modelling the solubility of elemetnal mercury in aromatics using PC-SAFT EoS 104
4.3.1.5 Modelling the solubility of elemental mercury in alcohols using PC-SAFT EoS 105
4.3.2 PC-SAFT EoS prediction with the associating scenario 106
4.3.2.1 Modelling vapor pressure of pure components 106
4.3.2.2 Modelling the Solubility of elemental mercury in water using PC-SAFT EoS 107
4.3.2.3 Modelling the solubility of elemental mercury in normal alkanes using PC-SAFT EoS 108
4.3.2.4 Modelling the Solubility of elemental mercury in aromatics using PC-SAFT EoS 110
4.3.2.5 Modelling the Solubility of elemental mercury in alcohols using PC-SAFT EoS 111
4.3.3 PC-SAFT model validation for predicting the solubility of elemntal mercury in multicomponent system 113
4.4 Conclusion 114

5 Mercury distribution in an oil and gas processing plant 116
5.1 Introduction 116
5.2 Obaiyed gas processing plant 117
5.3 Process simulation model and validation 121
5.4 Results and discussion 125

5.5 Location of mercury removal unit 128
5.6 Conclusion 130

6 Speciation of mercury **132**
6.1 Introduction 132
6.2 Mercury species in the oil and gas process streams 133
6.3 Stability of mercury species in hydrocarbons 135
6.4 Mercury species transformation in the flue gases 138
6.5 Mercury chloride property prediction 139
6.5.1 Mercury chloride vapor pressure prediction 141
6.5.2 Mercury chloride solubility prediction 142
6.6 Species transformation 145
6.6.1 Ideal gas equilibrium reaction 148
6.6.2 Non ideal system equilibrium reaction 148
6.7 Conclusion 150

7 Conclusions and recommendations **152**
7.1 Conclusions 152
7.2 Recommendations and future work 154
.1 Appendix A 156
.2 Appendix B 158
.3 Appendix C 165

Bibliography **175**

List of Figures

2.1 Location of Chisso company in Japan 24
2.2 Mercury emissions from natural sources 26
2.3 Mercury emissions from anthropogenic sources 27
2.4 Transformation of mercury species 29
2.5 Total world energy consumption in $\times 10^{15}$ Btu 31
2.6 World oil production and consumption in million barrels per day 33
2.7 Inlet nozzle fatigue due to mercury 38
2.8 Mercury pitting corrosion 40
2.9 Mercury removal unit (MRU) installed upstream and downstream of CO_2 removal unit 42

3.1 The green symbols represent the accepter sites of a molecule and the red symbols represent the donor sites of a molecule 74

4.1 Relative deviation error between experimental and calculated values using SRK EoS in the vapor pressure of elemental mercury (black), water (red), methanol, (yellow), and isopropanol (blue) 84
4.2 Relative deviation error between experimental and calculated values using SRK EoS in the vapor pressure of (a) n-alkanes and (b) aromatic compounds 85
4.3 Solubility of mercury in water. The symbols represent the experimental data. The dashed line is the correlation of the SRK EoS with $k_{ij} = 0$, and the solid line is the correlation with k_{ij} estimated using the group contribution method. (b) The variation with temperature of the binary interaction parameter between mercury and water for SRK EoS 86

4.4 Solubility of mercury in normal alkanes: C_5 (black), C_6 (red), C_7 (green), C_8 (blue), C_9 (orange), and C_{10} (indigo). The symbols represent experimental data, the solid lines represent predicted solubility with the binary interaction parameters estimated using the GCM, and the dashed lines represent the solubility without introducing the binary interaction parameter. 87
4.5 Solubility of mercury in (a) propane and (b) butane. The symbols represent experimental data, the solid lines represent SRK EoS predicted solubility by introducing k_{ij} estimated using the GCM, and the dashed lines represent the solubility with $k_{ij} = 0$ 88
4.6 SRK EoS binary interaction parameter for mercury-alkane mixtures. . . 89
4.7 (a) Solubility and (b) binary interaction parameter of mercury with in benzene (black), toluene (red), and o-xylene (green)for SRK EoS. The symbols represent experimental data 90
4.8 Solubility of mercury in methanol (black) and isopropanol (red). The symbols represent experimental data, the solid lines are predicted solubilities using SRK EoS with the binary interaction parameter estimated using the GCM, and the dashed lines are correlations with the binary interaction parameter set to zero 93
4.9 (a) Solubility of mercury in LHC mixture. The black symbols represent experimental data at different pressures, and the red is the SRK EoS correlation without k_{ij}, and the green symbols represent SRK EoS correlation with k_{ij} estimated using the group contribution method. (b) Solubility of mercury in HHC mixture 97
4.10 Relative deviation error between experimental and calculated values in vapor pressure using PC-SAFT for elemental mercury (black), water (red), methanol, (yellow), and isopropanol (blue). 98
4.11 Relative deviation error between experimental and calculated values using PC-SAFT in the vapor pressure of (a) n-alkanes and (b) aromatic compounds. 100
4.12 (a) Solubility of mercury in water. The solid line is the correlation of the PC-SAFT EOS with k_{ij}. (b) The variation with temperature of the binary interaction parameter between mercury and water. 101

4.13 Solubility of mercury in normal alkanes: C_5 (black), C_6 (red), C_7 (green), C_8 (blue), C_9 (orange), and C_{10} (indigo). The symbols represent experimental data, the solid lines represent predicted solubility using PC-SAFT EoS without association term. 102
4.14 Solubility of mercury in (a) propane and (b) butane using PC-SAFT EoS. The symbols represent experimental data, the solid lines represent predicted solubility with the binary interaction parameters, and the dashed lines represent the solubility without introducing the binary interaction parameter. 103
4.15 Solubility of mercury in benzene (black), toluene (red), and *o*-xylene (green), The symbols represent experimental data, the solid lines represent predicted solubility with the binary interaction parameters, and the dashed lines represent the solubility without introducing the binary interaction 104
4.16 Solubility of mercury in methanol (black) and isopropanol (red). The symbols represent experimental data, the solid lines are predicted solubilities with the binary interaction parameter estimated using PC-SAFT. 105
4.17 Relative deviation error between experimental and calculated vapor pressure using PC-SAFT and SRK for elemental mercury: SRK EoS (red), PC-SAFT without association (black), PC-SAFT with 2 associating site (blue), PC-SAFT with 4 associating site (green). 106
4.18 (a) Solubility of mercury in water using PC-SAFT EoS. The symbols represent the experimental data, the black dashed line is the correlation with 2(1:1) without k_{ij}, the red dashed line is the correlation with 4(2:2) without k_{ij}, and the solid line is the correlation with 2(1:1) with k_{ij}. (b) The variation with temperature of the binary interaction parameter between mercury and water. 107
4.19 Solubility of mercury in normal alkanes: C_5 (black), C_6 (red), C_7 (green), C_8 (blue), C_9 (orange), and C_{10} (indigo). The symbols are experimental data, the dashed lines are predicted without association and k_{ij}, the solid lines are predicted using 2(1:1), and the used dotted-dashed lines are predicted using 4(2:2). 109

4.20 Solubility of mercury in (a) propane and (b) butane. The symbols are experimental data, the dashed lines are predicted without association and k_{ij}, the solid lines are predicted using 2(1:1), and the dotted-dashed lines are predicted using 4(2:2). 109
4.21 Solubility of mercury in benzene (black), toluene (red), and o-xylene (green). The symbols represent experimental data, the dashed lines are predicted solubilities using PC-SAFT EoS without association and introducing k_{ij}, the solid lines are predicted solubilities using PC-SAFT EoS with 2(1:1) association site, the dotted−dashed lines are predicted with 4(2:2) mercury association site 110
4.22 Solubility of mercury in methanol (black) and isopropanol (red). The symbols represent experimental data, the solid lines are calculated solubility with k_{ij} and the dashed lines are correlated results without k_{ij} for 2(1:1) associating sites, and the dotted dashed lines are predicted solubilities with k_{ij} for 4(2:2) associating sites 111
4.23 (a) Solubility of mercury in LHC mixture. The (black) symbols represent experimental data, (red) symbols are the PC-SAFT correlation without association, the (blue) symbols are PC-SAFT correlation with 2(1:1), the (brown) symbols are PC-SAFT correlation with 4(2:2), and the (green) symbols are the SRK with GCM. (b) Solubility of mercury in HHC mixture. 113

5.1 Obaiyed natural gas process flow diagram 118
5.2 (a) Gas composition from the gas outlet stream. The (gray) bars represent experimental measurement, and the (green) is the estimated values (b) condensate composition from the condensate outlet stream. The (gray) bars represent experimental measurement, and the (green) is the estimated compositions 123
5.3 Obaiyed natural gas process flow diagram with MRU 130

6.1 Stability of mercury species 135

6.2 Vapor pressure of $HgCl_2$, the (blue) symbols represent experimental data, the red solid line represents the vaporization from liquid state to vapor, the black solid line represents the sublimation from solid to vapor. 141
6.3 Solubility of $HgCl_2$, the symbols represent experimental data. The green dashed line represents the predicted solubility using PC-SAFT EoS. . . 145

List of Tables

2.1 Mercury content in crude oils imported to the USA and the UK by country and region . . . 34
2.2 Range of mercury levels in refinery products . . . 35
2.3 Mercury levels in natural gas and condensate in different regions . . . 36
2.4 Stainless steel SS316L composition in weight present . . . 39
2.5 Mercury removal adsorbent scrubbers . . . 44

3.1 Thermodynamic model selection based on system application . . . 66

4.1 Group interaction parameters A^0 and B^0 for mercury with other groups. 82
4.2 Pure component critical properties and acentric factor. . . . 83
4.3 Mole fraction of hydrocarbon mixtures . . . 95
4.4 Coefficients for the temperature dependence . . . 96
4.5 PC-SAFT Pure component parameters . . . 99
4.6 PC-SAFT elemental mercury−alkanes k_{ij} . . . 103
4.7 PC-SAFT elemental mercury and other solvents k_{ij} . . . 104

5.1 Obaiyed plant feed characterized groups . . . 119
5.2 Concentration of mercury species in the process streams . . . 120
5.3 Estimated hydrocarbon feed composition to Obaiyed plant. . . . 123
5.4 Estimated feed composition to Obaiyed plant. . . . 124
5.5 Elemental mercury distribution through the plant using SRK EoS . . . 126
5.6 Elemental mercury distribution through the plant using PC−SAFT EoS 127
5.7 Mercury risk levels in crude oil and natural gas . . . 128

6.1 Speciation processes of mercury specie in the flue gas . . . 140

6.2 PC-SAFT parameters for mercury species 142

B-1 Universal PC-SAFT model constants 159

Nomenclature

Greek Symbols

ϵ	Depth of pair potential, J
η	packing fraction
μ_i^{ig}	Ideal gas chemical potential
μ_i^o	the chemical potential of species i at reference state
ϕ_i	The fugacity coefficient of species i
σ	Segment diameter in Å
ϵ_{ij}	Average dispersion energy
σ_{ij}	Average segment diameter Å
ζ_n	abbreviation defined by Eq. (3.77)

Superscripts

AA_i	Compressibility factor parameter for SRK EoS
BB_i	Compressibility factor parameter for SRK EoS
f_i	the fugacity of species i in the solution
f_i^o	the fugacity of species i at reference state
n_i	Number of moles of component i

x_i Mole fraction of component i

Other Symbols

A The Helmholtz free energy

a SRK EoS parameter

a_i universal PC-SAFT constants

A^{disp} the dispersion contribution to Helmholtz free energy

A^{elec} Electrolyte contribution to Helmholtz free energy

A^{hc} the hard chain contribution to Helmholtz free energy

A^{hs} the residual contribution of hard-sphere system to Helmholtz free energy

A^{ig} Ideal gas Helmholtz energy

$A_{kl}(T)$ The temperature dependence of the interaction parameter

A^0_{kl} Group contribution method interaction parameter

A^{polar} the polar contribution to Helmholtz free energy

A^{res} Residual Helmholtz free energy

A^{assco} the association contribution to Helmholtz free energy

b SRK EoS parameter

b_i universal PC-SAFT constants

B^0_{kl} Group contribution method interaction parameter

C_p Heat capacity at constant pressure

C_p The heat capacity at constant pressure

C_v Heat capacity at constant volume

C_v The heat capacity at constant volume

d_i temperature-dependent segment diameter in Å

$E(T, x)$ the dependence of the attractive interactions

E_{ij} The free energy of interaction

G The Gibbs free energy

g^{hs} Radial distribution function of hard-sphere fluid

G^{ig} Ideal gas Gibbs free energy

$G_k^{o,ig}$ Pure ideal gas Gibbs free energy

I_1 abbreviation defined by Eq. (3.83)

I_2 abbreviation defined by Eq. (3.83)

I_{exc} The contribution from excluded volume interactions

m Mean segment number in the mixture

M^{res} Residual property

P^{res} Residual pressure

V^{res} Residual volume

m_i Number of segments per chain

V the pressure of the system

S Entropy of the system

V the temperature of the system

U Internal energy of the system

V the volume of the system

V^{ig} Ideal gas volume

X^{A_i} Mole fraction of molecule i not bonded at site A

Z Compressibility factor

Z_{att} Attractive interactions

Z_{exc} Excluded volume interactions

Chapter 1

Introduction

Mercury occurs naturally in the environment and can be found in soil, air and water. It has two forms: elemental and compound. The elemental form of mercury is denoted by Hg and has several common names such as metallic mercury, liquid mercury, liquid silver and quicksilver [1, 2]. The compound forms are classified as inorganic (e.g. mercuric oxide, mercuric chloride, mercuric sulfide, mercuric hydroxide) and organic (e.g. methylmercury and dimethylmercury) [3]. Elemental mercury accounts for 80% of the mercury in the atmosphere, and it can circulate in the atmosphere for more than a year to reach a place far from its original source [1].

There are two sources of mercury in the biosphere: natural sources and anthropogenic (e.g. industrial). Both are considered to be equally significant causes of mercury accumulation in the environment. The natural sources include volcanic activity, erosion of terrain and dissolution of mercury minerals in oceans, lakes and rivers [3, 4]. The anthropogenic sources include the combustion of coal, oil, and gas as fuel to generate electricity or energy, manufacturing of cement, paper milling, flared gas from inshore and offshore oil and gas platforms and discharge of produced water from oil and gas processing, such as in chemical plants and refineries [5, 6, 7].

Although mercury occurs only in trace amounts in crude oil, natural gas and bitumen, they are considered a major source of mercury emissions in the environment [3, 6, 8, 9]. The release of mercury to the environment from burning oil and gas, waste from petrochemical plants, process treatment facilities and refineries are considered the main sources of mercury emissions in the US [5].

It has been reported that one-third of the global mercury emissions in the environment is from China, as it is the largest energy consumer in the world and the largest developing country [10]. As oil and natural gas are still the main source of energy in the world, this encourages producers to produce more in order to increase their profit, no matter if the reservoir is of low quality due to some undesirable, such as mercury or sour gases.

In addition to the contribution of mercury to environmental pollution, the presence of mercury in oil and gas processing plants has a negative impact on production and processing facilities. Mercury can cause equipment degradation, catalyst poisoning, generation of toxic waste streams and increase the risk of exposure of workers [5]. Mercury has an ability to accumulate in primary and secondary process treatment units, such as amine units, glycol units, cryogenic units and heat exchangers, eventually causing process failure [11].

As mercury is present in some major oil fields, maintenance and operation teams in those locations are exposed to the highly dangerous element on a daily basis. Examples of activities that expose workers to mercury are equipment cleaning, oil sampling, vessel and tank inspections and hot work activities on restricted areas. The exposure risks are proportional to the concentration of mercury in the process facilities [11]. Mercury exposure risks can be eliminated by determining its concentration and understanding the exposure pathways in the work locations and adopting effective health and safety policies and procedures accordingly. Consequently, understanding the distribution of mercury in process facilities is crucial not only for the proper design of mercury removal units (MRU) but also to eliminate the exposure risks. It can also prevent mercury from accumulating which can lead to equipment failure and eventually process shutdown. Avoiding mercury pollution and damage is far more cost effective than remediation of polluted areas.

Therefore, the main objective of this study is to accurately predict the distribution of mercury in oil and gas processing facilities by developing the thermodynamic models that were widely used in the industry. In order to meet the above objective, thermodynamic models have been developed in this study which have the ability to predict the thermodynamic behavior of mercury by taking vapor−liquid equilibrium and liquid−liquid equilibrium calculations into account more precisely. This has been achieved by two ways; introducing binary interaction parameters between mercury and

other molecules, and modeling mercury atoms as a bonded atoms. Also, the models are able to calculate thermodynamic properties, such as chemical potential, vapor pressure, solubility and phase change of the system. The models were validated with the binary system and multi-components solubility data. Finally, the stability and transformation of the presence of mercury compounds in oil and gas process streams are investigated from the thermodynamic and kinetic concepts.

The thesis is structured as follows; firstly consideration is given to the environment where an overview of mercury sources in the ecosystem and its health effects are presented. These are discussed in **Chapter 2** with an emphasis on the presence of mercury in oil and gas processing facilities, its consequence and negative impact on the production from an operational, safety and financial point of view. Then mercury removal technologies used in oil and gas industry are reviewed. Afterwords, in the same chapter, the importance of measuring or predicting the thermophysical properties of mercury is highlighted.

In **Chapter 3**, a review of the thermodynamic models in literature for predicting the solubility behavior of mercury in several solvents is presented. Review of the literature revealed that equations of state (EoS), such as Soave Redlich-Kwong (SRK), Peng Robinson (PR), perturbed-chain statistical associating fluid theory (PC-SAFT) are the primary choice for this purpose. Therefore, both SRK and PC-SAFT EoS's are presented in detail. The use of group contribution method as an approach to provide a good estimate for SRK EoS binary interaction parameters is discussed. The importance of the thermodynamic potential state functions for predicting the equilibrium behavior and the thermodynamic properties of any given system is discussed in detail. The use of $\phi - \phi$ approach technique for solving fluid-fluid phase equilibria and solubility calculations is introduced. Solubility provides better description of the concentration of a solute in a solvent than the phase diagram specially for dilute solutions such as mercury in water.

The main results of the thesis are described into two chapters. In **Chapter 4**, the vapor pressure of pure elemental mercury and several solvents, and the solubility of elemental mercury in these solvents were predicted using both the SRK and PC-SAFT EoS's, described in Chapter 3. Afterwords, both models were validated for predicting the solubility of mercury in light and heavy hydrocarbons mixtures. In **Chapter 5**, both

models are used to predict the distribution of mercury in oil and gas processing facilities. The results of the models were compared to real field experimental measurements. The proper location of mercury removal unit is selected accordingly.

As the elemental mercury chemically transforms or changes phase in the process facilities, based on Chapter 5 obtained results, speciation of mercury compounds in oil and gas streams is reviewed in **Chapter 6**. The stability of mercury compounds and their transformation are investigated from both thermodynamic and kinetic point of views. The required parameters for modeling the transformation of any component from one form to another are discussed.

As is the case with all work, there are many conclusions, recommendations and questions which remain upon the completion of the work. **Chapter 7** highlights the main conclusions and further work that could be undertaken in future.

Chapter 2

Mercury in the environment and hydrocarbon processing

2.1 Introduction

Due to its toxicity and accumulative nature, mercury is classified as a highly dangerous element by the US Environmental Protection Agency (EPA) [6]. Human health and the ecosystem are highly affected by mercury pollution. Since 1950, when the waste of a chemical plant was dumped into the Minamata Bay in Japan by the Chisso Corporation, mercury pollution has become a world-wide concern [12]. The Chisso corporation built a chemical plant to produce acetaldehyde in 1932 (see Figure 2.1), and the production process required inorganic mercury ($HgSO_4$) as a catalyst. The byproduct stream from the plant contained the toxic mercury species methylmercury (MeHg). It accumulated in the aquatic food chain, which was the main source of food of that area [13]. Its symptoms were recognized in 1956 and called Minamata disease [14]. This toxic species poisoned around 2264 people by the end of 2000. The MeHg from the chemical plant spread and distributed into nearby areas, such as the Shiranui Sea (shown in Figure 2.1). Minamata in Japan is not the only mercury contaminated area in the world. There are several mercury polluted sites in other countries, such as Sweden, Russia, Indonesia, China, Brazil, Tanzania, USA, South Africa, and the Philippines [6, 15, 16, 17]. The Arctic region is one of the most affected areas by mercury pollution. Greenland is the one of the 20 countries located in the Arctic, and the food sources for its traditional diet

include fish, seabirds, seals and whales, which all have high mercury levels [18].

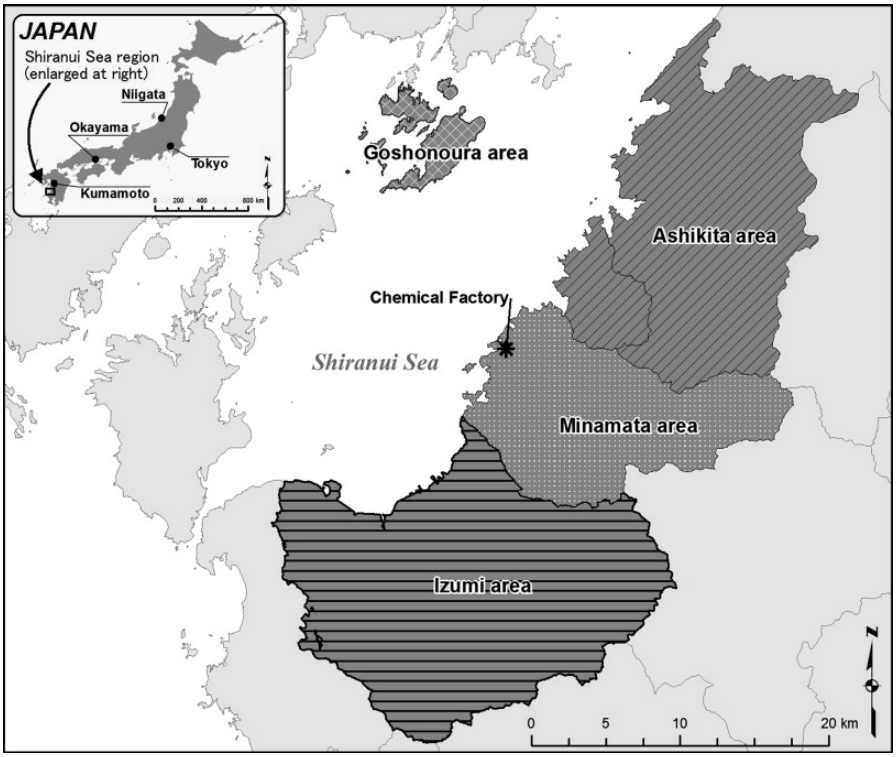

Figure 2.1: Location of Chisso company in Japan. Taken from Ref. [19].

Mercury accumulates in the human body either by inhalation or from the food chain. The human body can detoxify the entire accumulated mercury but this depends on several parameters, such as exposure level and species, genetics and human body health [20]. Inhalation of mercury generally happens either when vapor mercury is breathed in from dental fillings or breathing polluted air. Fish and other seafoods are the major source of human exposure to methylmercury. However, they are a beneficial food and should not be withdrawn from human consumption [6]. Fish tissue can hold up to 106 times higher mercury concentrations than sea water. In Greenland, the daily mercury intake ranges from $48\,\mu g\,d^{-1}$ per person in autumn to $66\,\mu g\,d^{-1}$ in spring [21]. This is about 10 times higher than in Denmark [18].

Mercury exposure causes several neurological disorders, because it impairs brain development, the nervous system, heart, lungs, cardiovascular system as well as the immune system [6, 22]. It also has a negative impact on unborn babies and reduces

the fetus ability to learn prior to birth. If the level of methylmercury reaches $5.8\,\mu g\,L^{-1}$ in the placental blood, the risk of loss of intelligence quantified by the intelligence quotient (IQ) becomes higher, as reported by National Research Council [23]. Around 74% of newborn children in Greenland recorded mercury level in the placental blood higher than $5.8\,\mu g\,L^{-1}$ [6], and more than 80% of the population in North Greenland has exceeded the acceptable mercury level $58.0\,\mu g\,L^{-1}$ in their blood [24].

Mercury not only affects human health and the environment, but the presence of mercury in oil and gas reservoirs also negatively impacts oil and gas processing, transport and storage facilities. Workers can be exposed to the toxic species on a daily basis. It may also cause unplanned shutdowns due to mercury corrosion. These unplanned shutdowns and remediation of polluted areas are very expensive. Therefore, understanding the distribution of mercury and its pathways in the ecosystem and oil and gas processing facilities is of vital importance. It allows the evaluation of strategies to reduce its environmental and financial risks.

This chapter aims to discuss the contribution of natural and anthropogenic sources of mercury to environment in detail. In addition to that, the most dominant mercury species and their pathways in the environment are highlighted. Afterwords, it is worth to take into consideration the presence of mercury compounds in oil and gas the largest nonrenewable energy sources in the world and their concentration levels. Then the negative impact of the presence of mercury species to the oil and gas processing facilities is discussed in detail. The conventional removal technologies used in the oil and gas industry to capture mercury compounds from process streams are reported. Finally, a review of the importance of measuring, estimating or predicting the thermophysical properties of mercury is given.

2.2 Sources of mercury

The presence of mercury in the biosphere is due to natural and anthropogenic sources. The release of mercury in the atmosphere is considered as the route for mercury spreading through the environment [15, 25].

There are several natural sources responsible for mercury emissions to the ecosystem, which include volcanic activity, erosion of terrain and dissolution of mercury minerals in the oceans, lakes, rivers and others [3]. Due to the geological complexity of

those natural phenomena, the estimates of the emitted mercury to the biosphere from these sources are inaccurate [26]. It is reported that the amount of mercury released to the atmosphere from natural sources is around 5207 tons per year, where oceans contribute around 52% of the emitted mercury from natural sources [25], as shown in Figure 2.2. Biomass burning, which includes wood burning and biofuel combustion, is considered the second major natural mercury emission source, and it accounts for 13% of the natural sources. Deserts and non−vegetated areas account for around 10% followed by volcanoes and geothermal activities which contribute around 9%. Forest fires release around 7% of the total nature mercury. Therefore, countries that have large areas of forest, such as United States, China, South Australia and others might emit more mercury to the ecosystem. Agricultural areas contribute around 2%, where countries such as China and United States might increase the emitted mercury due to their agriculture products.

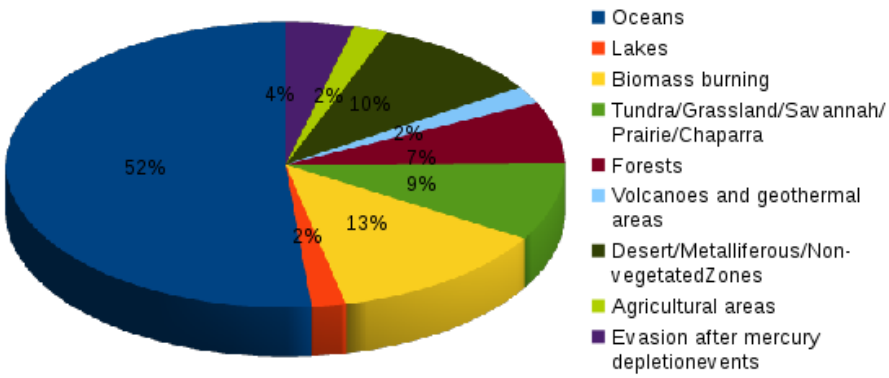

Figure 2.2: Mercury emissions from natural sources. Data taken from Ref. [25].

The amount of mercury released due to anthropogenic sources accounts for about 50% of the global mercury emissions in the ecosystem [27]. Moreover, several studies reported that the anthropogenic sources of mercury are responsible for the increase of mercury concentration in the ocean by a factor of 3 of its original concentration since the lowest mercury concentration of 0.8 picomoles in the Antarctic Ocean [28, 29, 30].

The combustion of fossil fuels accounts for most of the emitted mercury from anthropogenic sources. It accounts for around 41.9% of the total global anthropogenic emissions to the atmosphere, as shown in Figure 2.3 [31]. The use of coal to generate

power and heat contributes around 26% of the global anthropogenic mercury emissions. As a result, several attempts have been made in order to reduce mercury emitted from some coal-fired heaters in the USA and China, such as installing an air pollution control devices or installing mercury capture units in order to capture mercury from fired heaters flue gases [32]. Due to the lack of data for the concentration of mercury compounds in the world crude oil, natural gas and petroleum products, the emitted mercury from burning crude oil and natural gas can not be confidently reported [3, 5]. The total mercury concentration was measured in some exported crude oils and natural gases to the USA and UK. This will be discussed in Sec. 2.3 in detail. The second major industrial mercury emission source is gold production, which contributes to around 23.81% [31], as shown in Figure 2.3. Even though there are several new technologies that can be used for gold extraction that do not involve Hg, the use of the gold amalgamation process is still the most widely used extraction process because of its high efficiency [33]; however, its main drawback is the high release of mercury to the environment. Both cement and metal productions, as shown in Figure 2.3, provide an almost equal percentage of 9.5% of anthropogenic mercury emissions to the ecosystem. This might be due to the fact that both require raw materials that contain the same concentration of mercury.

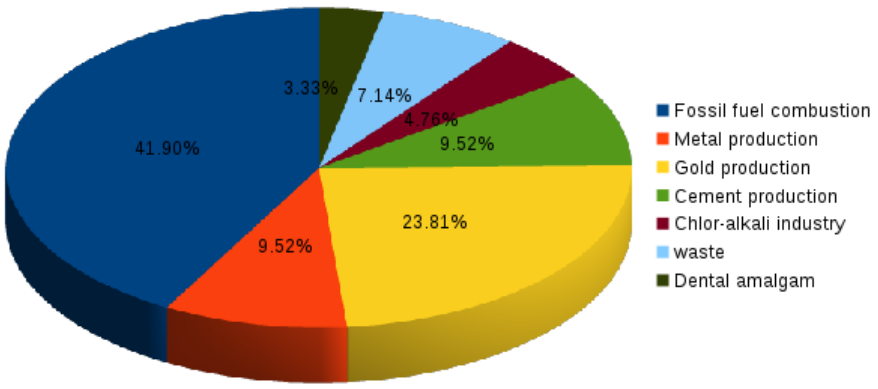

Figure 2.3: Mercury emissions from anthropogenic sources. Data taken from Ref. [31].

Mercury has several forms as described in Chapter 1, and each form has its own

physical properties, toxicity and behavior. Knowing the most dominant mercury specie in the environment is of vital importance, as it helps to understand their risk. The next section covers mercury species, concentration and their pathways in the environment.

2.2.1 Mercury species in the environment

Mercury compounds can be found in the ecosystem in the form of inorganic or organic mercury. The inorganic form can either be found in an unoxidized state, such as elemental mercury (Hg), mercury sulfide (HgS) and mercury chloride ($HgCl_2$) or an oxidized form like Hg^{+2}. Organic mercury exists in the environment in the form of methylmercury (MeHg) or dimethylmercury (DMHg) [31, 34]. Figure 2.4 shows mercury species transformation, from a toxic specie like elemental mercury to a much more toxic species, like methylmercury in the ecosystem in the presence of methylation bacteria. Organic forms have higher lipid solubility which can be absorbed completely by the gastrointestinal tract [35]. Therefore, they are considered as more toxic than other mercury forms. Each specie has its own chemical and physical properties and residence time in the atmosphere, soil and water. Some mercury compounds have the ability to travel over long distances. The instability and movement of mercury compounds in the ecosystem are challenging problems for researchers. Natural phenomena, industrial waste, as well as global warming are all responsible for mercury transport in the biosphere, from the atmosphere to the earth and water during rainfall and snow as shown in Figure 2.4. Afterwards, it can be evaporated from oceans, the leaves of plants and other ecosystem surfaces to the air [36].

Elemental mercury is considered the predominant mercury species in the air, due to its low water solubility and high vapor pressure compared to other mercuric compounds [34]. It is in a liquid state at ambient conditions due to the valence electron in the outer shell unlike other metals [37]. It has the longest lifetime in the aerosphere, and it is considered as the most predominant mercury pollutant and ruling specie in the air where it contributes to around 95% of the total mercury species in the air [38, 39]. The Hg^{2+} species can be found in the air and accounts for less than 5% of the total mercury concentration [40]. In water and soil, both Hg and Hg^{2+} are present, and the dissolved elemental mercury can be transformed to methylmercury by bacteria as shown in Figure 2.4 [41]. The Hg^{2+} specie can be transformed into organic or inorganic species

in the presence of reducing agent.

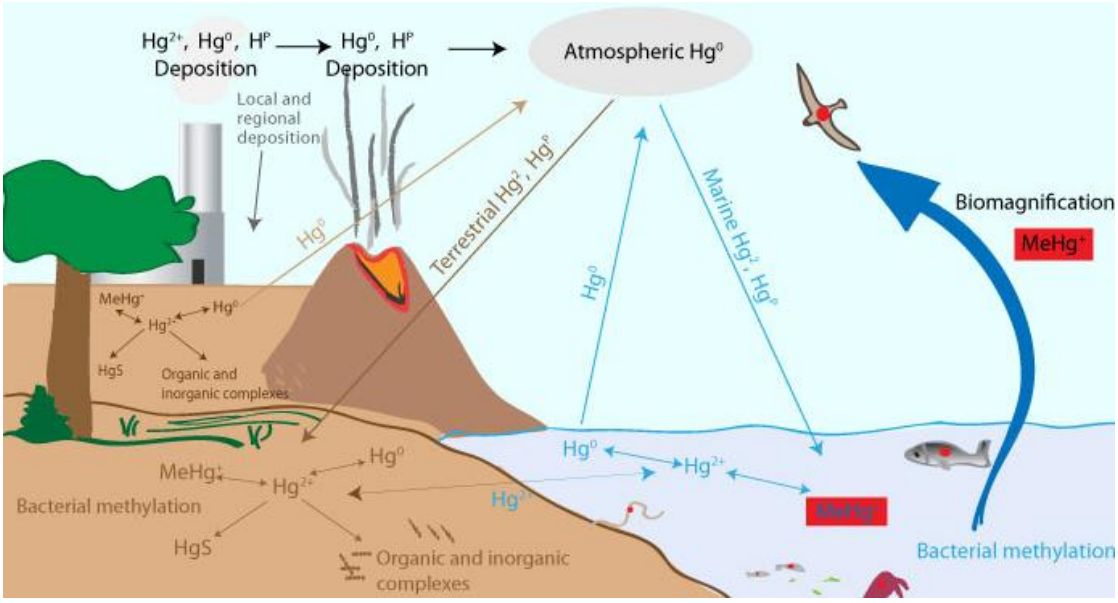

Figure 2.4: Transformation of mercury species. Taken from Ref.[27].

Measuring the concentration of these species in air, water and soil is a challenging task. Many techniques have been used to measure the concentration of these species in the environment. For instance, mercury species in soil can be measured by chemical extraction, X-ray absorption spectroscopy or thermo-desorption methods [42]. The first measurement of mercury in soil was conducted by Giulio and Ryan using chemical extraction [43], but nowadays, thermo-desorption is the most widely used technique. For measuring mercury species in water, cold vapor atomic absorption or cold vapor atomic fluorescence spectrometry is used; organic mercury species in water can be measured also using gas chromatography [42]. The first measurement of mercury solubility in water was in 1929 by Bonhoeffer and Reichardt [44]. Mercury ions, such as mercuric specie Hg^{2+}, can be measured in solution using ion selective electrodes [45]. For mercury measurements in the gas phase, several techniques such as uorescence, gas chromatography and mass spectrometry methods were used to detect its species [46]. This means that each mercury specie requires proper technique to measure depends on its environment.

As shown in Figure 2.4 and discussed in Sec. 2.2, generating energy from non−renewable

energy sources, such as oil, natural gas and coal, is one of the main sources of mercury in the ecosystem. Thus, understanding the origin of mercury species and concentration levels in the consumable energy sources is essential. This will be discussed in detail in the next section. In addition to that, distinguishing the negative impact of the presence of mercury compounds in these resources is explored.

2.3 Mercury in oil and gas

Fossil fuels, coal, oil and natural gas are still the main sources of energy in the world. Among these, oil and gas will continue to be the most consumed fuels over the next years, as reported by the International Energy Outlook 2016 and shown in Figure 2.5 [47, 48]. It is estimated that by 2020, the total world energy consumption will reach around 350×10^{15} Btu by burning oil and gas and 170×10^{15}Btu by burning coal. This means that the required burning quantity from oil and gas is almost double the coal quantity. Consequently, oil and gas are considered a major mercury emission source to the environment, even though they only contain trace amounts of mercury.

The blue and orange solid lines in Figure 2.5 represent, the crude oil and natural gas consumption while the black line represents the coal consumption. The green solid line is the energy generated from renewable sources, such as wind, solar, oceans and others. It is clear that the natural gas demand is increasing rapidly compared to coal and crude oil where will exceed the coal consumption by the end of 2030. This is due to the fact that natural gas is cheaper and more environmentally friendly than oil and coal. Moreover, Figure 2.5 indicates that coal consumption has been almost constant since 2012. The dotted lines (black and green) represent the expected increase in renewable energy production and decrease in coal consumption, in case of further improvements applied to their generation systems, such as installing proper air quality control devices in the coal fired heaters. The presence of mercury might negatively impact their operating performance. Preventing this to occur, requires a comprehension of mercury species and distribution via process facilities and production streams. Understanding the origin of mercury species, their concentration in oil and gas helps to estimate and reduce its emissions. This section covers an overview of the concentration level of mercury in some crude oil, refined products and natural gas that exported to the USA and the UK. The negative impact of its presence to oil and processing facilities is also highlighted.

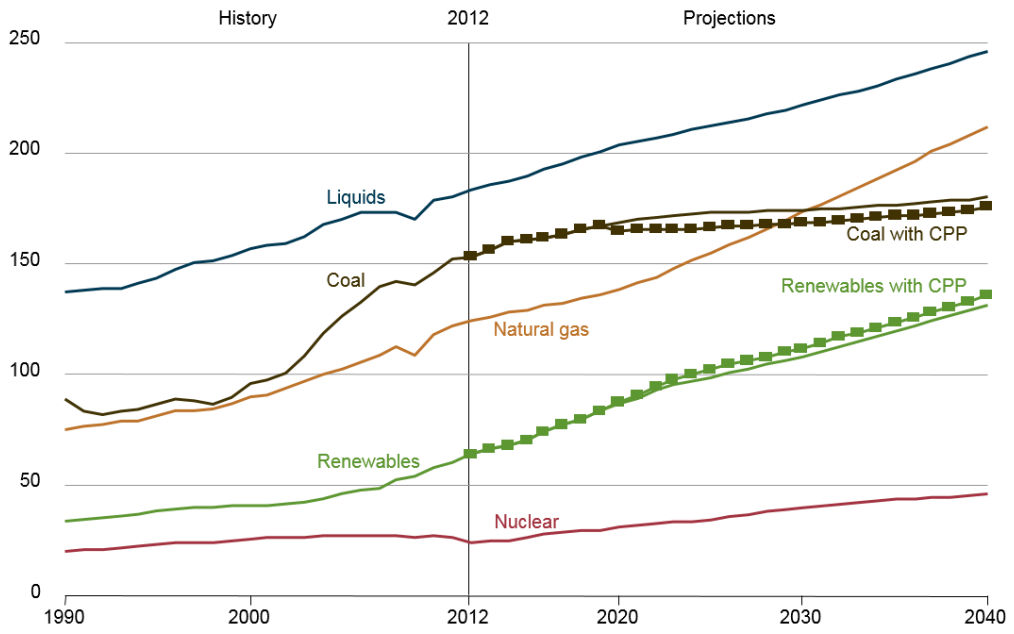

Figure 2.5: Total world energy consumption in $\times\ 10^{15}$ Btu. Taken from Ref. [47].

Most crude oil and natural gas reservoirs are sour and contain undesirable elements such as hydrogen sulfide, carbon dioxide and mercury [49]. Oil and gas producers even produce and process lower quality crude oil and natural gas in order to satisfy and provide the required energy demand. The undesirable elements must be removed prior to oil and gas processing and export for safety, environmental and operational issues.

Very little information and research are available in the literature on the origin of mercury in oil and gas. One source of mercury is the organic form of mercury deposited prior to burial and hydrocarbon formation [50]. Another source is secondary processes like the interaction of oil with metal rich fluids and the formation of water during migration, maturation or biodegradation. Evidence of this process has been demonstrated in the Cymric field in California, where high mercury levels in crude oil have been reported [51]. The deposition of atmospheric mercury in the soil, which reached the hydrocarbon formation layer, accounts for the presence of mercury in crude oil and natural gas [3].

The concentration of mercury in oil and gas reservoirs might decrease or increase with time. A study conducted by Ryzhov et al. [8] concluded that mercury concentration in an oil well varies from one year to another in the range from 10% to 80% of

the average mercury content of the gas in the reservoir. This huge change in mercury concentration is a challenging task for oil and gas producers, as monitoring the concentration of mercury is required over the field production lifetime. This impacts the design capacity of processing facilities as well as mercury removal units.

Mercury compounds in crude oil and natural gas are classified based on their solubility and ability to move from one phase to another into three categories, dissolved mercury compounds, inorganic mercury compounds and suspended mercury compounds [9]. Dissolved mercury compounds, such as elemental mercury and organic mercury are soluble in liquids and have the ability to move from the liquid phase to the gas phase. They distribute among the liquefied petroleum gas (LPG) and naphtha product streams during the refining process. Inorganic mercury compounds, such as mercury chloride, mercury bromide and mercury iodide are also soluble in water and solvents. The last category is the suspended mercury compounds which is mercury atom associated with another element to form solid particles, such as mercury sulfide HgS, and are insoluble in water and solvents.

The composition and heating value of the most consumable energy source (crude oil and natural gas) plays an important role in the oil and gas market. Crude oil and natural gas are a mixture of light and heavy hydrocarbons. This mixture must be separated, purified from its undesirable elements and stabilized prior to export and storage. This requires several processing steps, such as separation processes in which gas, condensate, oil and water are separated, gas sweetening process in which separated gas treated from carbon dioxide and hydrogen sulfide, dehydration processes in which water is removed, and stabilization processes in which the condensate and heavy crude oil where stabilized. These processes contain various units, such as separators, stabilization columns, heat exchangers, pumps and compressors. Each of these units is operated at different pressure and temperature in order to achieve required gas, condensate, and oil specifications. In the next subsections, an overview of mercury levels in crude oil and its refined products will be presented.

2.3.1 Mercury concentration in crude oil and refinery products

There are two reasons to produce and buy oil that contains mercury; the first reason is to cover the world energy demand, and the second is the cheaper price of crude oil

containing mercury. Due to the huge energy demand, world oil production is almost equal to its consumption, as shown in Figure 2.6. The world oil production hit 98.41 million barrels per day in 2017 as reported by U.S. Energy Information Administration (EIA) [52]. In addition, in the first quarter of 2018 as shown in Figure 2.6, that a drew nearly 0.2 million barrels per day of the implied stock change. This means that, there is a growing demand in refining products, which requires an increase oil exploration and production activities.

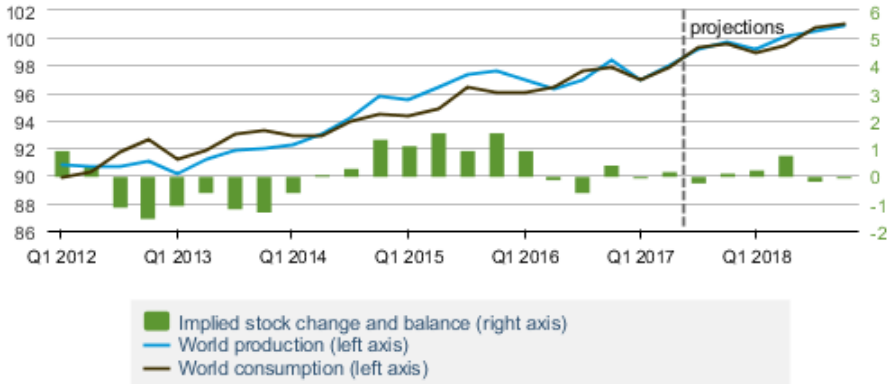

Figure 2.6: World oil production and consumption in million barrels of oil per day. Taken from Ref. [52].

Crude oil containing mercury is cheaper than mercury free crude oil by 20 US $/bbl [53]. Therefore, refineries aim at increasing their profit by choosing a feedstock with lower quality, however, the impact of mercury on refinery process facilities should be considered in order to protect the them from damage. Mercury concentration varies from one oil reservoir to another. A study carried out by the United States Environmental Protection Agency (EPA) on 170 crude oil streams produced and imported to the USA reveals useful information on worldwide mercury concentrations in crude oil [54]. The study indicated that the average total mercury concentration of the processed crude in the USA is around $3.5\,\mu g\,kg^{-1}$. The samples were taken upstream of refinery tank farms. In other words, losses of mercury during production, separation, and transportation were not taken into account. As a result, the mercury concentration in crude oil is expected far beyond $3.5\,\mu g\,kg^{-1}$. Moreover, the Integrating Knowledge to Inform Mercury Policy (IKIMP) in the UK has reported that the emitted mercury from imported and processed oil in the UK was around 270 kg to 850 kg per annum, which is

expected to be present in the feedstock of the UK refineries [50].

Table 2.1 shows the concentration of mercury in some crude oil imported to the USA and the UK. It is clear that, the concentration of mercury changes with the reservoir and region.

Table 2.1: Mercury content in crude oils imported to the USA and the UK by country and region [50, 54].

Country	Imports to the USA	Imports to the UK
	Mercury $\mu g\,kg^{-1}$	
Algeria	13.3	
Angola	1.6	
Nigeria	1.8	
Africa	2.7	—-
Venezuela	4.2	
Mexico	1.3	—-
Kuwait	0.8	—-
Norway	19.5	3.6-19.5
UK	3.6	—-
Thailand	593.1	——
Canada	2.1	——
Iraq	0.7	——
Viet Nam	66.5	—-
US	4.3	—-
S. America	5.3	—-
Middle East	0.8	—-
Russia	3.1	

These data in Table 2.1 are useful as they supply information about the concentration level of total mercury in the feedstock, but they do not provide important insights into the distribution of mercury in the refinery products, as well as the impact of mercury in the refinery processing facilities. Moreover, these data are not useful for modeling mercury pathways in the refinery processing equipment, as it is only for the feedstock rather than the entire product stream.

Most refinery products, such as gasoline, diesel, heavy oil and liquefied natural gas (LNG) are used as fuels or lubricants for automobiles. If mercury compounds are not captured prior to refining the crude oil, they will distribute through the refinery prod-

ucts. Table 2.2 shows mercury levels in refinery products. The presence of mercury compounds in those products increases the amount of released mercury to the environment. Various studies report that the use of refined products in automobiles are considered a significant mercury source in the atmosphere [55, 56]. This might due to the high increase in car production and use in the world. Several water samples were collected in different places in the USA, and the analysis indicated that there is a relation between vehicular traffic sources and Hg levels in water [57].

Table 2.2: Range of mercury levels in refinery products.

Product Type	Hg conc. ng g^{-1}	Ref.
Gasoline, USA	0.2-1.4	[58]
Gasoline, Algeria	3.2	[58]
Gasoline, Slovenia	1.2	[58]
Diesel, USA	0.4	[58]
Diesel, Slovenia	2.97	[58]
Kerosene, USA	0.04	[58]
Heating Oil, USA	0.59	[58]
Light distillates, USA	1.32	[59]
Utility fuel oil, USA	0.67	[59]
Asphalt, USA	0.27	[59]

Having a clear knowledge of mercury distribution in crude oil and refinery products is very important, as it can eliminate unplanned shutdowns and reduce the mercury emission rate to the environment. In addition to that, buying cheap feedstock can increase the refinery profit, if the knowledge and insight of mercury distribution are clearly identified. Natural gas is considered as of the cleanest fossil fuels; knowing its mercury level is of vital importance. Therefore, next section covers the presence of mercury in the natural gas and associated water obtained when oil and gas are separated in the processing facilities.

2.3.2 Mercury concentration in natural gas and condensate

Natural gas and condensate contain light hydrocarbons that have a low boiling range. In order to avoid corrosion, damage, and pipelines blockage problems, natural gas and condensate streams have to be treated prior to export [60]. Treating natural gas requires

several steps, including primary and secondary separation, sweetening, dehydration and mercury removal. In the primary separation, three phase separator is usually used to separate crude oil, natural gas and water. The gas stream is sent to further gas treatment units, such as gas sweetening process in order to remove sour gases and dehydration unit to the remaining water. The liquid hydrocarbon is then routed to the secondary separation units which contain several separation processes. These steps may differ from one plant to another depending on the nature of impurities in the produced gas [60].

The concentration of mercury in natural gas fields varies from one reservoir to another. Mercury has been detected in several gas fields in the world, such as South-East Asia, North Africa and Eastern Europe. Table 2.3 summarizes range of mercury levels in natural gas and gas condensate in different regions [61].

Table 2.3: Mercury levels in natural gas and condensate in different regions [51, 61]

Location	Hg conc.	
	Gas µg/m^3	Condensate (ng/g)
Europe	100–150	—
South America	50–120	50–100
Gulf of Thailand	100–400	400–1200
Africa	80–100	500–1000
Gulf of Mexico (USA)	0.02–0.4	—
Overthrust Belt (USA)	5–15	1–5
North Africa	50–80	20–50
Malaysia	1–200	10–100
Indonesia	200–300	10–500
Netherlands(Natural Gas Exported to the UK by pipeline)	180–200	—
Algeria Exported to the UK	50–80	—

Despite the fact that it has been reported that there is no mercury in UK gas fields [51], there is evidence of the presence of mercury in natural gas and LNG imported to the UK, as indicated in Table 2.3, where the level in Netherlands exported gas reaches 200 µg/m^3[51]. This exceeds mercury allowed levels in the natural gas streams which should be limited to less than 0.01 µg/Nm^3 prior to gas liquefaction [62]The presence of mercury in high levels impacts natural gas process treatments, such as liquefaction and separation after and prior its use as domestic gas, production of chemicals, and hydrogen production. Mercury compounds might precipitate in these processes or eventually

release to the environment. Purifying natural gas and crude oil leads to some waste streams, such as produced water. Taking into consideration mercury in the produced water is of vital importance. Therefore, mercury in the produced water is discussed in detail in the next section.

2.3.3 Mercury in produced water

Produced water is water associated and removed in the production of oil and gas during the primary and secondary separation processes. It is naturally present with crude oil and natural gas in the reservoir [63]. It is water contaminated with hydrocarbons and other undesirable elements, such as mercury. Produced water increases over field life as the reservoir becomes more depleted. Therefore, produced water streams are the largest oil and gas waste streams. Although oil and gas companies have an obligation to remove hydrocarbons from produced water prior to re-injection or disposal [64], there is no obligation to remove mercury compounds. However, there is an obligation for producers to analyse its concentration and report its level to the Department for Energy and Climate Change (DECC), in accordance with the Oil Pollution Prevention and Control Regulations [65]. DECC in the UK reported that $91\,\mathrm{kg}$ of mercury was discharged with $198\,\mathrm{million\ m^3}$ of produced water in 2008, while it increased to $186\,\mathrm{kg}$ of Hg in 2009 with produced water capacity of $197\,\mathrm{million\ m^3}$ [50]. Moreover, high concentrations of mercury around natural gas processing facilities were reported by Wilhelm and Bloom [3] in the range of $0.32\,\mathrm{mg\,kg^{-1}}$ to $40\,\mathrm{mg\,kg^{-1}}$ in the atmosphere and $3000\,\mathrm{mg\,l^{-1}}$ in the waste water. It is clear from this section and previous sections that mercury has the ability to distribute via oil and gas processing streams (condensate, gas, and water) and eventually reach the environment via different pathways, as described. The presence of mercury has a footprint in oil and gas processing facilities prior to polluting the ecosystems. This will be discussed in the next section in detail.

2.3.4 Mercury impact in oil and gas processing facilities

Damage has been widely reported due to the presence of mercury in gas processing facilities. The first fatal damage attributed to mercury was reported in 1973 in Algeria, where it was discovered that mercury is the main cause of corrosion in the aluminum

heat exchangers [7]. The same failure was discovered in the Groningen field in Holland and the Moomba field in Australia. In the Groningen field, it was initially believed that CO_2 was the source of corrosion in the gas-gathering system, but more investigations revealed that corrosion was due to the high mercury concentration in the system (ranging from 0.001 to $180\,\mu g/m^3$) [61, 66]. In the Moomba gas processing plant in Australia in 2004, a gas leak led to an explosion due to a failure in the inlet nozzle of an aluminium heat exchanger, as shown Figure 2.7. The main cause of this nozzle fatigue was revealed to be liquid metal embrittlement as a result of the direct contact of some molten metals as mercury with several material, such as alloys [67].

Figure 2.7: Inlet nozzle fatigue due to mercury. Taken from Ref.[67].

Furthermore, in 1981 mercury corrosion problems were reported in Indonesia and Thailand. In the Arun gas plant in Indonesia, mercury spread across the entire plant, due to a malfunction of the mercury removal beds, and led eventually to a failure in an aluminum heat exchanger box [61].

Mercury has a negative impact on the gas pipelines, as well. An $18\,km$ gas pipeline in Egypt was repaired due to mercury corrosion, and the owner lost millions of dollars due to the unplanned shutdown lasting two months [61]. Thus, taking into consideration mercury corrosion mechanism into account is of vital importance. Next section covers, the types of mercury corrosion in oil and gas and their mechanisms, with an emphasis on the loss of money due to corrosion problem in oil and gas processing facilities.

2.3.5 Corrosion mechanisms of mercury in oil and gas facilities

Selecting the proper material of construction for processing equipment depends on several factors, such as operating conditions and fluid corrosivity. If the fluid contains acid gases, such as hydrogen sulfide H_2S or carbon dioxide CO_2, corrosion allowance has to be take into account in order to avoid equipment failure. Equipment failure might lead to a decrease in production capacity or total shutdown. It costs the oil industry in the USA around US$ 1.4 billion in 2002 [68].

As mercury is a corrosive element, like H_2S and CO_2, it must be removed prior to oil and gas processing in order to protect the downstream processing facilities. It might deposit or spread from one place to another in the pipelines and processing equipment and cause equipment failure. This is a challenge for oil and gas companies as it is difficult to decide where mercury removal units should be installed. Mercury has the ability to react with copper, copper-containing alloys, iron, chromium or nickel, causing cracking of distillation trays, heat exchanger tubes and process valves [69]. This is costly in terms of capital cost and operation shutdown period. The reaction of mercury with iron, nickel and chromium requires water or acidic phases prior to occur [70]. Elemental mercury can cause several types of corrosion, such as amalgam corrosion, galvanic corrosion and degrade materials by liquid metal embrittlement, as shown in Figure 2.7.

Amalgam corrosion occurs when elemental mercury forms an alloy with various metals such as aluminum, tin, silver, iron, and zinc [71]. SS316L stainless steel material which is widely used as material of construction of oil and gas processing facilities, was tested for mercury corrosion by AL-Hinai and Nengkoda [70]. The SS316L contains several elements,such as nickel, chromium and others, as shown in Table 2.4.

Table 2.4: Stainless steel SS316L composition in weight present. Taken from Ref. [70]

Grade	C	Mn	Si	P	S	Cr	Mo	Ni	N
316L	0.03	2	0.75	0.045	0.03	18.0	3.0	14.0	0.1

A solution of elemental mercury in cyclohexane was prepared by Nengkoda and Al-Hinai [70]. Then an acid gas contains H_2S was passed through the solution for around an hour. Afterward, the SS316L was exposed to the prepared solvent at different temperatures ranging from 100 to 200°C. The results of their study concluded that the

stainless steel was corroded by mercury, as shown in Figure 2.8, where mercury can cause pitting corrosion.

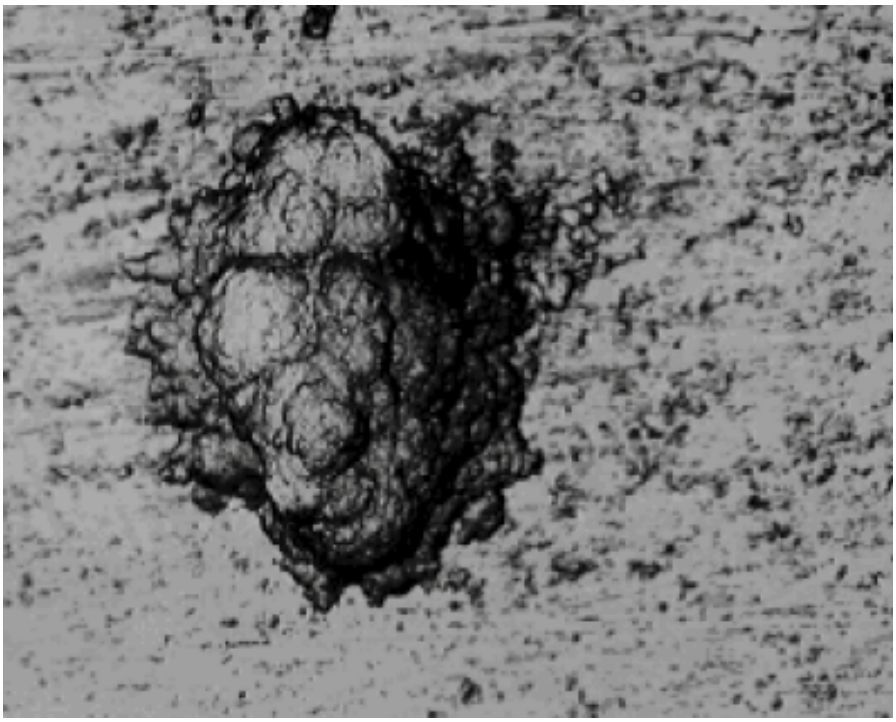

Figure 2.8: Mercury pitting corrosion. Taken from Ref. [70].

The corrosion mechanism of SS316L was expressed into two steps. First, both nickel and chromium in the SS316L reacts with water according to the following reaction;

$$\text{Metal} + \text{Water} \longrightarrow \text{Metalhydroxide} + \text{Hydrogen} \tag{2.1}$$

Afterwards, an alloy of mercury with corroded metal will be generated due to the presence of mercury. The alloy "amalgam" of mercury with aluminum or any other metal is weaker than pure aluminum and by exposing this layer to an aqueous electrolyte, aluminum corrosion occurs according to the following chemical reactions [66].

$$\text{Al(s)} + \text{Hg(aq)} \longrightarrow \text{AlHg(s)} \tag{2.2}$$

$$2\mathrm{AlHg(s)} + 6\mathrm{H_2O(l)} \longrightarrow 2\mathrm{Al(OH)_3(aq)} + 3\mathrm{H_2(q)} + 2\mathrm{Hg(aq)} \tag{2.3}$$

It is clear that the reaction in Eq. (2.3) leaves free mercury to continue the corrosion process and speed up the failure rate of the equipment. This means that even with a small amount of elemental mercury, the reaction will continue.

Galvanic corrosion is one of most known corrosion types which occurs when a corrosive environment is exist in the process. It is one of the corrosion types occurs when two different materials are coupled or uncoupled in a corrosive solvent [72]. The presence of acid gases and elemental mercury in the fluid streams lead to speed up galvanic corrosion. As mercury gets in flowlines and process facilities, its concentration can be reduced from 50 to $20\,\mu g/m^3$ due to its deposition as indicated in the Eq. (2.4) and Eq. (2.5) below [66, 73].

$$3\,\mathrm{H_2S} + \mathrm{Fe_2O_3} + \mathrm{H_2O} \longrightarrow 2\,\mathrm{FeS_3} + \mathrm{H_2O} \tag{2.4}$$

$$\mathrm{Hg} + \mathrm{Fe_2S_3} \longrightarrow \mathrm{HgS} + 2\,\mathrm{FeS} \tag{2.5}$$

The presence of H_2S and CO_2 compounds in the previous reaction mechanism enhances the corrosion rate, where H_2S act as a catalyst and CO_2 increases the acidity of the fluid. Even very small quantities of H_2S are adequate to generate reaction [68, 73].

Liquid metal embrittlement (LME) is a phenomenon in which some materials, such as aluminum, nickel, copper alloys, and others became like a fragile metal [71]. It occurs in the presence of mercury where mercury diffuses in the grain boundary of the metal and eventually causes crack or fatigue as shown in Figure 2.7.

The pigging operations or solvents used in chemical treatments, such as corrosion, wax, and hydrate inhibitors can cause a transitory increase of mercury concentration in downstream process facilities and moves mercury to another unit passing through contaminated pipelines and accumulates in another unit [74]. Consequently, this can speed the corrosion process through the entire processing facilities. In order to avoid mercury corrosion, industrial experts prefer to install mercury removal units. Thus next section will discuss, mercury removal technologies that used in oil and gas industry in detail.

2.4 Mercury removal technologies

Oil and gas fields contain several light and heavy hydrocarbon components. The light hydrocarbons account for more than 70% of the natural gas composition. The heavy hydrocarbons are the dominant components of crude oil composition. The gas stream is rich in light hydrocarbon while the condensate stream is rich in heavy hydrocarbon. Therefore, each stream has its own physical properties, mercury species and concentration. The separation process requires several processing and separation facilities as discussed in Sec 2.3. Separation of these light and heavy hydrocarbons in the oil and gas processing facilities yield gas and condensate streams. If mercury is present in these streams, mercury removal units (MRU) are required. The MRU is usually a fixed−bed unit filled with different adsorbents depending on the selected technology. There are several technologies that can be used to capture mercury from process streams. However, selecting the proper location and technology requires knowledge of the type of mercury species, their concentration and distribution [75]. For instance, industrial experts prefer to install mercury removal units downstream the primary separation units prior to any process treatment(as shown in Figure 2.9), but others prefer to install them after the CO_2 removal unit. Both options have drawbacks unless the distribution of mercury were properly identified. In the second option, mercury might leave with the sweetening process solvent and accumulate in the downstream facilities, while the first option might increase the size of the MRU. Computational modeling can be used to predict the concentration of mercury and its pathway through the liquid and gas streams associated with processes and help the decision makers.

The removal technologies that have been used to remove mercury from oil and gas process streams will be discussed in this section according to the stream type.

2.4.1 Mercury removal from the condensate

The condensate stream is one of the outlet streams that contains liquid light and heavy hydrocarbons. There are three types of mercury removal technologies that are widely used for the condensate streams: (i) sulphide-containing ion exchange resin material, (ii) sulphide supported by alumina, and (iii) sulphur-containing molecular sieves or sulphur-containing activated carbon. The first one is considered the most efficient process as it

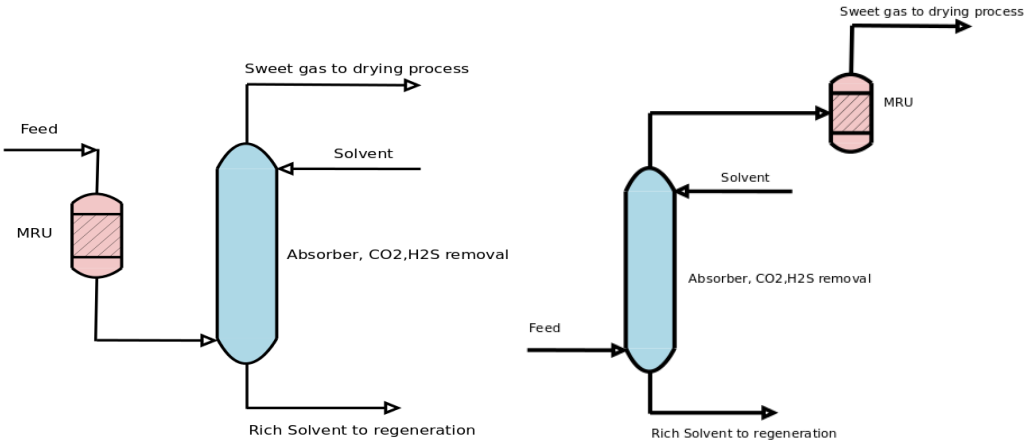

Figure 2.9: Mercury removal unit (MRU) installed upstream and downstream of CO_2 removal unit

has the ability to remove both elemental and organic mercury species, but the second one for the removal of elemental mercury only [75]. The only way to capture other mercury species using the second method is to covert mercury species to elemental mercury. This method requires more catalyst which means larger size as two catalyst types are need. The first catalyst to covert mercury species to elemental form while the second to capture the elemental form. The third technology is still under technological advancements for mercury removal from the condensate. The reaction mechanism of mercury removal using the ion exchange was reported by Monteagudo and Ortiz [76] as follows:

$$2\mathrm{R}{-}\mathrm{SO_3H} + \mathrm{Hg^{2+}} {->} \mathrm{R}{-}\mathrm{SO_3}{-}\mathrm{Hg}{-}\mathrm{O_3S}{-}\mathrm{R} + 2\mathrm{H^+} \tag{2.6}$$

$$2\mathrm{R}{-}\mathrm{SO_3H} + \mathrm{Hg_2^{2+}} {->} \mathrm{R}{-}\mathrm{SO_3}{-}\mathrm{Hg}{-}\mathrm{Hg}{-}\mathrm{O_3S}{-}\mathrm{R} + 2\mathrm{H^+} \tag{2.7}$$

where R group is the cation resin which represents polystyrene divinylbenzene, and the SO_3H group represent the functional group.

2.4.2 Mercury removal from natural gas

Fixed-bed scrubbers with a solid absorbent supported by solid material are the common capture technology for mercury vapor from the natural gas. The supported material is required in order to increase the mechanical strength of the adsorbent. There are several types of absorbents and support materials used in the industry as shown in in Table 2.5.

Table 2.5: Mercury removal scrubbers. Taken from Ref. [77].

Active Compound	Support medium	Fate of mercury
Sulfur	Carbon/ Alumina	HgS
Metal Sulfide	Carbon/ Alumina	HgS
Silver	Zeolite	Ag-Hg amalgam
Thiol/Oxidising agent/chelating	Scavenger solution	Soluble Hg compound
Metal oxide/sulfide	Metal Oxide	HgO/HgS

Sulfur with activated carbons fixed bed scrubbers are the most widely used for natural gas industry, because both the active compound (sulfur) and the support medium (activated carbon) have the ability to capture mercury. Despite of their mechanical weakness compared to oxide supports, such as alumina [77]. It requires a dry gas where in the case of condensate carry over, it creates high pressure drop. The structure of the activated carbon and the sulfur concentration in the bed as well as operating conditions play an important rule in removal efficiency [78].

2.5 Remediation cost of mercury pollution

Mercury species in the ecosystem have the ability to move from one contaminated area to another, making mercury pollution a global issue not specific to certain countries. The remediation cost of mercury polluted areas is highly dependent on the concentration of mercury and its species in the polluted location. It has been estimated that the cost of remediation of Hg polluted marine products in Greenland is around US$ 31 million [24]. Besides that it is estimated that every IQ point lost, costs Greenland US$ 59.1 million annually [24, 79]. For Minamata, compensation of US$ 1500 million was paid

by the Chisso Corporation and the Kumamoto prefectural governments from the 1950s until 2004 to the poisoned families [24]. It has been estimated that remediation cost of mercury pollution ranges from 2500 US $/kg to 1.1 million US $/kg of Hg [24].

In general, there are three ways to avoid mercury emissions from industrial sources to the environment: preventive measures, primary control measures and secondary control measures. Preventive measures can be achieved only if the source of emissions is stopped; this means fuel substitution, such as use of renewable energy or biofuels instead of mercury containing energy sources. However, this option is not popular, as oil and gas are still the main sources of energy. In primary control measures, Hg emissions are still generated but reduced to a certain value. In secondary control measures, Hg emissions exist but are removed later from exhaust gases [24]. Avoiding mercury pollution is far more cost effective than remediation of polluted areas. The selection of the best measures requires a good understanding of the behavior of mercury and its pathways through the process and the environment. Consequently, mercury exposure risks can be mitigated by determining the concentration and understanding the exposure pathways in work locations and adopting effective health and safety policies and procedures accordingly. This requires knowledge of the thermophysical properties of mercury species in pure, binary and multi-component systems. In the next section, an overview of some thermophysical properties of elemental mercury that have been measured and estimated in the open literature is discussed in detail with an emphasis on their importance to measure and mitigate mercury risks.

2.6 Thermophysical properties of mercury

Classifying mercury as a pollutant and a toxic element led to research in the measurement and estimation its thermophysical properties. Developing methods for predicting the thermophysical properties of mercury can help to understand the behavior of mercury and its distribution. This can lead to reduce its pollution rate in the environment and its exposure risks [80]. Several experimental and computational studies have been carried to measure and predict several thermophysical properties of elemental mercury as a function of temperature as it is the most dominate mercury specie in the ecosystem and in the oil and gas streams, as discussed previously in Sec 2.2 and Sec 2.3. In this section, the importance of some of the thermophysical properties of elemental mercury,

such as vapor pressure, density and solubility in measuring mercury risks are presented. In addition, the advantages and drawbacks of the previous developed methods for predicting the thermophysical properties of elemental mercury are considered.

2.6.1 Elemental mercury vapor pressure

In a risk assessment procedure, it is important to know the vapor pressure of the substance, because it is a measure of the likelihood of the substance to escape or evaporate from liquid state to the vapor state. A high vapor pressure corresponds to a fast evaporation rate. The vapor pressure is the pressure at which the liquid and its vapor are in equilibrium at a specified temperature. It also provides an indication for the state of component, and its concentration in vapor, liquid and solid phases.

Several experimental measurements and correlations have been published for pure elemental mercury vapor pressure over a wide range of temperatures [81, 82]. Huber et al. collected most of the experimental data and developed a correlation that allows the calculation of elemental mercury vapor pressure from the triple point of mercury to its critical point in the form of the Wagner equation [81]. They compared the available experimental data and the results of the previous models with the their new model and concluded that there are a limited experimental data, which have an estimated uncertainty of less than 1%. The uncertainty of their correlation was measured at three different points, near the triple point, the intermediate range and from 900 K to the critical point. The accuracy was 3%, 1% and 5%, respectively. The main drawback of the previous vapor pressure correlations is that it can only be used for a limited temperature range. These models can not be used to predict the other thermodynamic properties and phase change. Predicting the vapor pressure of mercury using a thermodynamic model that has the ability to predict the vapor pressure over a wide range of temperatures is required. It should help to predict the solubility of mercury in gas and liquid solvents at different operating conditions.

Density of a substance is one of the important properties to consider as it provides information about the mass amount that can be fit in unit volume. The next section inquires into the importance of mercury density measurements in some applications. In addition to that an overview of the previous studies that measured or predicted elemental

mercury density is discussed.

2.6.2 Density of mercury

The use of elemental mercury in several applications, such as a manometric fluid, dental amalgams and other applications, requires measurement and prediction of its density as a function of temperature. Several experimental studies have been carried out to measure liquid mercury density over a range of temperature from $-20°C$ to $300°C$. The experimental data were fitted to a temperature dependent formula by Ambrose [83]. It is useful to create a model that predicts the density as function of temperature, but it can not be used over a wide range of temperature and in the industrial applications more than one phase might be present. Another study carried out by Kitamura [84] proposed a new equation of state using a variational associating fluid theory to predict several thermodynamic quantities of mercury, including its density over a wide range of temperatures [84]. The model showed good agreement compared to the experimental values. However, the model was only tested for pure mercury, which makes it difficult to compare its accuracy with other models in predicting the thermophysical properties of other pure components or mixture.

Molecular dynamics (MD) simulation can also be used to predict the density and other properties of mercury. A recent study conducted by Belashchenko [85] to predict the density of mercury using MD over a wide range of temperatures and pressures. The study concluded that MD is capable of predicting the density of mercury if it is above $8\ g/cm^3$, but there were discrepancies at lower values.

Another property that should be measured or predicted and taken into consideration, is the solubility of mercury in liquid and gas substances. It might represent the concentration of mercury in air, water and other solvents. The pollution level of mercury in water can be identified by knowing the solubility of mercury in water. The next section, provides an overview of the importance of measuring and predicting elemental mercury solubility in binary and multi-component systems.

2.6.3 Solubility of mercury

Solubility is one of the most important physical properties of a component, as it describes the ability of a solute to dissolve in a solvent. Therefore, measuring or predicting the solubility of mercury in gas and liquid solvents is crucial. It also helps to evaluate and understand the distribution of mercury in the environment and in the solvents.

In the open literature, several experimental studies have been performed to measure the solubility of elemental mercury in binary systems, such as mercury in water, mercury in alcohols, and mercury in some hydrocarbon components, but these studies cover a limited temperature range. In addition, thermodynamic modeling of mercury solubility in gas and liquid phases at different operating conditions have not extensively studied. In the next section, an overview of the previous studies that conducted experimentally or computationally to measure or predict the solubility is discussed. The advantages and drawbacks of these studies are highlighted.

Solubility of mercury in alkanes

Normal alkanes play an important role in our daily life, where it can be found in plastic products, medicines, domestic gas, fuels and others. Therefore, predicting or measuring the solubility of mercury species in these compounds is needed to measure the risk of their use if mercury is present in them.

The main source of normal alkanes is the oil and gas where it represents more than 90% of natural gas and crude oil species. Elemental mercury is considered the dominant mercury species in the crude oil and natural gas [5, 86]. The experimental solubility data of elemental mercury in hydrocarbon systems are scarce and cover a limited temperature range. Clever et al. [87] collected and evaluated these experimental data. Most of the experimental data represent the solubility of mercury in liquid which is liquid liquid equilibrium. Some of the original authors of these experimental data fitted their results into a temperature dependent formulas. Another experimental study conducted by Miedaner et al. [88] for measuring the solubility of mercury in two normal alkanes; dodecane and octane at temperatures up to 200°C and pressures up to 6 bar. These studies cover only binary systems where multi component systems were not investigated.

For the solubility of mercury in a multi-component hydrocarbons, a recent experimental study was performed by Marsh et al.[44] to measure the solubility of elemental

mercury in light and heavy hydrocarbon mixtures. The light hydrocarbon contains 46% of methane while the heavy hydrocarbon contains around 52% of n-nonane, n-dodecane and n-hexadecane. The results of the study were fitted into a temperature dependent formula. The drawback of this formula that can not be used on a large industrial simulation scale such as refineries or outside the temperatures range of the study but it provides a framework for validating the thermodynamic modeling of mercury solubility in multi component system. All of the previous studies show that the solubility of mercury in alkanes compounds increases by increasing molecule size. In other words, solubility of mercury in octane is higher than the solubility of mercury in propane and the solubility of mercury in heavy hydrocarbon mixture is higher than in light hydrocarbon mixture.

Solubility of mercury in aromatics

Aromatic compounds, such as benzene, toluene and xylene are considered to be the main raw material for many petrochemical industries [89]. As crude oil and natural gas are the main sources of aromatics and crude oil is known to contain mercury, measuring or predicting the solubility of mercury in aromatics, is of vital importance. The experimental solubility data of mercury in benzene, toluene, and *o*-xylene were measured in a temperatures range from 273.15 K to 313.15 K at atmospheric pressure in Refs. 87 and 44. The results show that the solubility of elemental in *o*-xylene is higher than in benzene.

Solubility of mercury in alcohols

The solubility of elemental mercury in some alcohols, such as methanol and isopropanol were collected by Clever et al. [87] and evaluated. It covers a limited temperature range from 287 K to 307 K only. The solubility of mercury in alcohols that used in the industry, such as mono-ethylene glycol (MEG), triethylene glycol (TEG) and di-ethylene glycol (DEG) were not widely investigated in the literature. These alcohols are widely used in oil and gas processing as anti-freeze, water dehydration and anti-corrosion agents. Recent study conducted by Gallup et al. [90] measured the solubility of mercury in MEG and TEG at 293 K to be in range of 200 to 600 ppb and they found that the solubility of mercury decreases by increasing water concentration in these alcohols. One of the motivations of this work is to predict mercury solubility in such

alcohols.

Solubility of mercury in water

Measuring the solubility of mercury in water is of vital importance as it indicates whether water is contaminated by mercury or not. The first experiment measurement was carried out by passing water over a mercury sample and the dissolved mercury in water was reported. While most other experiments were conducted by mixing liquid mercury with water until the equilibrium reached [91]. Experimental solubility data of elemental mercury in water was collected and evaluated over a wide range of temperatures by Clever et al.[91]. Some of the obtained results were fitted with respect to temperature and a formula was generated. The disadvantage of this formula that can not be used over a wide range of operating conditions and on industrial scale where more than one component are available.

It is clear from the previous sections that fitting an experimental data into a temperature dependent formula can not be used outside the experimental operating temperature range. Thus, thermodynamic modeling is the proper approach for predicting the thermodynamic properties of pure and multi component systems. Next section provides an overview of the approaches used in the open literature to predict the thermodynamic properties of elemental mercury.

2.7 Modeling approaches

In situations where experimental data are unavailable, predictive methods are required. A competitive model should be computationally inexpensive to evaluate and require minimal parameterization [92].

One powerful method is molecular dynamics simulation, which requires force fields to be parameterized between all species in the solution. This work has been focused particularly on systems containing elemental mercury [93] and some mercury compounds in water [93, 94]. While these methods offer the possibility of predicting thermodynamic properties of system containing mercury, they are computationally intensive and not suitable for use in process scale simulations (e.g., in a refinery).

Another approach is the use of the thermodynamic models where several thermody-

namic models have been used to estimate the physical and chemical properties of a pure and multi component systems such as equations of state and activity coefficient models. The selection of a model depends on its capability of estimating the required physical and chemical properties, and predicting the phase behavior of a specific system where experimental data are unavailable. Cubic equations of state, such as Soave-Redlich-Kwong equation of state (SRK), PengRobinson (PR) or the perturbed-chain statistical associating fluid theory (PC-SAFT), are characterized by their simplicity, reliability and speed of computation and are considered the model of choice for pure and multicomponent system [95]. They are widely used for practical applications specially at high pressure. Activity coefficient models are recommended to be used at low pressure (less than 10 bar).

In terms of thermodynamic modeling, recent studies used critical-point-based modified perturbed-chain statistical association fluid theory (CP-PC-SAFT) and PR EoS's to describe the phase behavior of elemental mercury in a binary system like liquid and compressed hydrocarbon gases by Polishuk et al. [96, 97]. While the use of CP-PC-SAFT approach works well, it requires fitting binary interaction parameters k_{ij} between mercury and the specific solvents being modeled to existing experimental measurements. Moreover, the model was tested for elemental mercury hydrocarbon systems only, other solvents such as water and alcohols were not investigated even though there are an experimental data of mercury solubility in those solvents over a range of temperatures as indicated in Sec. 2.6.3. In addition to that, the k_{ij} values were assumed as a temperature independent for their studied solvents. This assumption might be applied only for some solvents over a specific range of temperatures.

Properly accounting for the interactions between molecules leads to the accurate prediction of mixture properties. Within the context of equations of state, this is typically achieved by introducing the binary interaction parameter k_{ij} between different molecular species; k_{ij} is normally used as a fitting parameter that is adjusted to minimize the differences between the calculated and experimentally measured system properties, such as VLE, LLE, density, and solubility. In a situation where experimental data are unavailable to fit the k_{ij}, predictive combining rules that account for binary interaction parameter as a function of temperature are required in order to improve model accuracy [98].

The molecules interaction can be explained by knowing the energy change in a sub-

stance. The thermodynamic concept is the only method that deals with the relationship between internal energy, pressure, density and temperature. In the next chapter, the thermodynamic concept, such as the use of potential state functions to account for the binary interaction parameter between molecules. This might improve the ability of EoS's for predicting the solubility of mercury in liquids and gases which gives an indication of mercury pathways from phase to another.

2.8 Conclusion

Mercury compounds are emitted to the biosphere from both natural and industrial sources. These compounds are classified as toxic, pollutant elements to the human and environment, and might cause corrosion and damage of industrial processing facilities. The presence of these compounds in the oil and gas can cause unplanned shutdown which is undesirable from operational and financial point of view. Therefor, predicting the physical properties of mercury compounds and modeling their distribution in oil and gas processing might eliminate their risks. This requires understanding the thermodynamic behaviour of mercury in the processing facilities and product streams. In the next chapter, the fundamentals of thermodynamic modeling for predicting mercury behavior will be discussed. The use of equations of state and phase equilibrium calculations to predict the solubility of mercury is presented in detail.

Chapter 3

Thermodynamic modelling

3.1 Introduction

Understanding the distribution of mercury in the ecosystem and oil and gas process facilities is of vital importance. Making a proper decision to mitigate or eliminate mercury pollution and its corrosion and operation problems is a challenging task as explained in Chapter 2. Refinery operators usually consider different financial scenarios in order to ensure the long-term profitability of the operations. One of these scenarios is lowering the quality of supplied crude oil to the refinery [69]. Lower quality crude oil is less expensive because it contains undesirable chemical components such as mercury and acid gases. In order to process the low quality crude oil that contains mercury, it is important to understand the fate of mercury distribution and its risk within refinery process facilities and product streams. Where, most of chemical processes require a phase contact whether vapor− liquid contact, liquid− liquid contact, liquid− solid contact or vapor−liquid−liquid contact such as separation and reaction processes. In order to design and optimize these processes, investigation of equilibrium conditions and calculation of compositions of all phases are needed. Therefore, a predictive thermodynamic approach that has the ability to predict the thermodynamic properties of the system is of essential to develop. All of the thermodynamic properties of the system, such as chemical potential, pressure, phase change, phase equilibrium and etc. can be known by knowing the thermodynamic potential state functions. In order to reduce or eliminate mercury hazards, accurate prediction of mercury distribution is of vital importance in

developing risk mitigation strategies.

In this chapter the use of fundamentals of potential state functions in combination with the EoS's for improving model ability to predict the thermophysical property of a substance are discussed. The relation between Gibbs free energy and chemical potential of an ideal gas and real solution is explained. The phase−equilibrium calculation concept for predicting the phase change properties is highlighted. Soave-Redlich-Kwong equation (SRK EoS) and perturbed-chain statistical associating fluid theory PC-SAFT are selected to carry out phase equilibrium calculations and estimate the required thermodynamic properties of mercury in several solvents. The combination of SRK EoS with a group contribution method to estimate the binary interaction parameters between elemental mercury and its solvent is introduced and discussed in this chapter.

3.2 Thermodynamic Potentials

The equilibrium behavior and the thermodynamic properties of any system can be defined by combining the thermodynamic potential state functions. There are several thermodynamic state functions such as internal energy U, free energies (Helmholtz free energy A and Gibbs free energy G) and enthalpy H . These thermodynamic state functions are very powerful and indispensable methods for the finer understanding of thermodynamics. The state function reaches their maximum or minimum values when the system approaches an equilibrium.

The internal energy can be defined after combining the first and the second laws of thermodynamic [99] as :

$$dU \leq TdS - PdV + \sum_i \mu_i dn_i \tag{3.1}$$

where U is the internal energy, V is the volume , μ_i is the chemical potential of species i in the system, n_i is the number of moles, P is the system pressure, S is the entropy of the system, and T is the absolute temperature.

The first term on the right side of Eq. (3.1) represents the amount of heat that can be absorbed by the system based on the second law of thermodynamic $dS \geq dQ/T$, while the second term represents the pressure work generated by the system at constant

pressure. All of the thermodynamic properties can be estimated using Eq. (3.1), if the internal energy of the system is known. Therfore, Eq. (3.1) is considered as the thermodynamic principal [99].

The behavior of any system and its state can be defined from the thermodynamic potential state functions by fixing the entropy, volume and number of moles. Then Eq. (3.1) becomes:

$$d(U)_{S,V,n} \leq 0 \tag{3.2}$$

Equation (3.2) is considered as one of the equilibrium criteria of the system. It indicates that neither heat nor work are given or taken from the system, if S, V, and n are kept constant.

It can be clearly seen from Eqs. (3.1) and (3.2) that the U has three natural variables; S,V and n, but S is an independent variable which can not be physically controlled. It can be replaced by another variable, such as T which can be measured and controlled. This leads to define another function called Helmholtz free energy A. The Helmholtz free energy was developed by Hermann von Helmholtz in 1882, and it measures the work that can be obtained from any given system at constant T, V, and n and is defined as:

$$A = U - TS \tag{3.3}$$

where A is the Helmholtz free energy of a system, and by substituting Eq. (3.3) into Eq. (3.1) gives:

$$dA \leq -PdV - SdT + \sum_i \mu_i dn_i \tag{3.4}$$

From Eq. (3.4), the change in the Helmholtz free energy of a system is equal to zero, if T,V and n_i are constant and Eq. (3.4) can be rewritten as:

$$d(A)_{T,V,n} \leq 0 \tag{3.5}$$

It is clearly seen from Eq. (3.5) that A can be minimized, if T,V and n_i are kept constant. This indicates that the system has reached the equilibrium state. The Helmholtz free energy depends on three natural variables; T,V,and n as can be shown in Eq. (3.4). The volume can also be replaced by P which leads to define another state function called Gibbs free energy G.

The G can also be defined from the internal energy of the system as:

$$G = U - TS + PV \tag{3.6}$$

By substituting Eq. (3.19) into Eq. (3.1) gives:

$$dG \leq VdP - SdT + \sum_i \mu_i dn_i \tag{3.7}$$

If T,P and n_i are constant, Eq. (3.7) can be rewritten as:

$$d(G)_{T,P,n} \leq 0 \tag{3.8}$$

This gives an indication that the system will reach an equilibrium state by keeping T,P and n_i constants. This indicates that the change in the G can be minimized.

These U,A, and G thermodynamic potential state functions plays an important role in predicting all of the thermophysical properties of the system as a function of their natural variables, such as $U(S, V, n_i)$, $A(T, V, n_i)$ and $G(T, P, n_i)$. Various thermodynamic properties can be derived from these functions. For instance, the pressure of a system can be obtained from the Helmholtz free energy and internal energy, if the system temperature and number of moles are kept constant as:

$$P = -\left(\frac{\partial A}{\partial V}\right)_{T,n} = -\left(\frac{\partial U}{\partial V}\right)_{S,n} \tag{3.9}$$

The temperature of the system can also be obtained, if the system volume and number

of moles are unalterable as:

$$T = -\left(\frac{\partial U}{\partial S}\right)_{V,n} \tag{3.10}$$

The entropy of the system can be obtained by fixing the volume of the system:

$$S = -\left(\frac{\partial A}{\partial T}\right)_{V,n} = -\left(\frac{\partial G}{\partial T}\right)_{P,n} \tag{3.11}$$

Taking the second derivative of Eq. (3.11) gives

$$\left(\frac{\partial S}{\partial T}\right)_{V} = -\left(\frac{\partial^2 A}{\partial^2 T}\right)_{V} = \frac{C_v}{T} \tag{3.12}$$

$$\left(\frac{\partial S}{\partial T}\right)_{P} = -\left(\frac{\partial^2 G}{\partial^2 T}\right)_{P} = \frac{C_p}{T} \tag{3.13}$$

where C_v and C_p are the heat capacity at constant volume and pressure, respectively. The chemical potential μ_i can be obtained, if the change of the thermodynamic potential state functions with respect to the number of moles is known as:

$$\mu_i = \left(\frac{\partial G}{\partial n_i}\right)_{T,P,n_j} = \left(\frac{\partial A}{\partial n_i}\right)_{T,V,n_j} = \left(\frac{\partial U}{\partial n_i}\right)_{S,V,n_j} \tag{3.14}$$

The pressure of a given system plays an important role in defining the system ideality. High pressure of a gas system indicates that the system is non ideal. In contrast, low gas pressure indicates ideal gas system. The thermodynamic potential state functions provide the benefit to model ideal and non ideal systems. This will be described in detail in the next section.

3.3 Ideal gas system

In order to describe or predict the behavior of a real gas, the concept of ideal gas is used as an approximation in the thermodynamic modelling . The molecules of an ideal gas do not attract or repel to each other. This can be approached at low system pressure. In the previous Sec. 3.2, it was demonstrated that all thermodynamic properties can be obtained from the thermodynamic potential state function. In this section, this explicitly for ideal gas models.

The ideal gas Gibbs free energy can be obtained from Eq. (3.7), if n_i and T are constant, and P at low pressure. In this case, Eq. (3.7) becomes:

$$\left(\frac{\partial G^{ig}}{\partial P}\right)_T = V^{ig} = \frac{RT}{P} \tag{3.15}$$

where the term RT/P represents the ideal gas volume based on the ideal gas law, R is the ideal gas constant. The Eq. (3.15) can also be rearranged as:

$$dG^{ig} = RTd\ln P \tag{3.16}$$

The total ideal gas Gibbs free energy G^{ig} of a system at T and P is defined as:

$$G^{ig}(T,P,y) = \sum_k n_k G_k^{o,ig}(T,P) + RT\sum_k n_k \ln y_k \tag{3.17}$$

where $G_k^{o,ig}$ is Gibbs free energy of pure ideal gas species k at given T and P, and y_k is the mole fraction of species. The reference state of an ideal gas can be defined as the state of ideal gas specie in the pure state. The ideal gas is usually selected as a reference state of non ideal fluids. Thus, Eq. (3.17) represents the Gibbs free energy of ideal gas model. It requires the pure component free energies.

The chemical potential of species i in ideal gas system can be obtained from Gibbs free energy from Eq. (3.14) as.

$$\mu_i^{ig} = \left(\frac{\partial G^{ig}}{\partial n_i}\right)_{P,T,n_j} \tag{3.18}$$

where μ_i^{ig} is the ideal gas chemical potential.

Therefore, the chemical potential of species i in ideal gas mixture:

$$\mu_i^{ig}(T, P, y_j) = \mu_i^{o,ig}(T, P_o) + RT \ln \frac{P_i}{P_o} \tag{3.19}$$

where $\mu_i^{o,ig}$ is the chemical potential of pure component i in the ideal gas state at T and P_o, P_o is the pressure of the reference state (typically taken to be 1 bar) and $P_i = y_i P$ is the partial pressure of the component i in the system.

Equation (3.19) can be rewritten at constant temperature as:

$$d\mu_i^{ig}(T, P, y_j) = RT d \ln y_i P \tag{3.20}$$

The Helmholtz free energy is widely used when its natural variables (volume, temperature and moles) are known, such as for a typical equations of state. Equations of state (EoS) provide a mathematical relationship between pressure, volume and temperature. If two variables are known, the third can be obtained. This is one of the benefits of using EoS's. The EoS's types and their selection will be discussed in detail in Sec. 3.6. The molar Helmholtz energy A^{ig} of an ideal gas can then be defined as:

$$A^{ig}(T, \rho, x_j) = \sum_{i=1} x_i \mu_i^{\circ,ig}(T, P) + RT \sum_{i=1} x_i (\ln \rho_i b_i - 1) \tag{3.21}$$

where ρ_i is the molar density of component i, and μ_i° is the standard state chemical potential at T and P.

In reality, the gas or the fluid pressure is not always low to consider it as an ideal gas. The next section covers the use of potential state functions in predicting the thermodynamic properties of non ideal system and understand its deviation from the ideal behavior.

3.4 Non ideal system

For non ideal fluids such as a gas at high system pressure where its molecules interact with each other, the reference or standard state in this case is defined as a hypothetical state. The deviations of this non ideal gas from the ideal gas behavior has to be taken into account and can not be neglected. The thermodynamic potential state functions play an important role in representing and predicting the non-ideality of the system. In order to consider real systems, defining a residual property is required. It is the difference between the property of the actual system and that of an ideal gas at the same total volume, temperature and number of moles of each species [95] and can be represented in a general formula as:

$$M^{res}(T,V,n) = M(T,V,n) - M^{ig}(T,V,n) \tag{3.22}$$

where M^{res} is any residual property.

The molar residual Helmholtz free energy A^{res} can be defined from Eq. (3.23) as:

$$A^{res}(T,V,n) = A(T,V,n) - A^{ig}(T,V,n) \tag{3.23}$$

The first term represents the Helmholtz free energy of the actual system, while the second term represents the ideal gas system Helmholtz free energy which can be obtained from Eq. (3.21). The molar residual Helmholtz free energy A^{res} can be directly determined from Eq. (3.9) by fixing system temperature and number of moles. Equation (3.9) can be written to represent residual pressure of the system as:

$$P^{res} = -\left(\frac{\partial A^{res}}{\partial V^{res}}\right)_{T,n} \tag{3.24}$$

where P^{res} is the residual pressure and can also be obtained from Eq. (3.23) as:

$$P^{res}(T,V,n) = P(T,V,n) - P^{ig}(T,V,n) \tag{3.25}$$

Substituting Eq. (3.25) into Eq. (3.24) gives:

$$A^{res} = RT \int_0^{\rho} \frac{d\rho}{\rho}(Z-1) \tag{3.26}$$

where $Z = p/(\rho RT)$ is the compressibility factor, and ρ is the molar density of the system.
It can be clearly seen from Eq. (3.26) that the residual Helmholtz free energy A^{res} can be obtained, if the system compressibility factor is known. Consequently, all of the thermopysical properties of ideal and non ideal system can be estimated. The compressibility factor can be obtained from any equation of state. This will be explored in detail in Sec 3.6.

The chemical potential of any species i in any solution at constant T can be defined from Eq. (3.19) as:

$$\mu_i(T,P,y_j) = \mu_i^o(T,P) + RT \ln \frac{f_i}{f_i^o} \tag{3.27}$$

where f_i is the fugacity of species i in the solution and f_i^o is the fugacity of species i at its reference state, μ_i^o is the chemical potential of pure component i at its reference state. The fugacity is defined as a measure of pressure of a non ideal fluid in order to satisfy the chemical potential of ideal gas. The fugacity concept is a powerful tool for phase equilibrium and reaction equilibrium modelling. It measures the likelihood of a molecule to escape from one phase to another.

The ratio f_i/f_i^o is called the activity a_i of species i in solution and Eq. (3.27) can be written as:

$$\mu_i(T,P,y_j) = \mu_i^o + RT \ln a_i \tag{3.28}$$

If the ratio of f_i/f_i^o is equal to 1, then the solution is an ideal solution.

Differentiation Eq.(3.27) gives:

$$d\mu_i(T, P, y_j) = RTd\ln f_i \tag{3.29}$$

The residual Gibbs free energy of a fluid is defined as;

$$G_i - G_i^o = RT\ln\frac{f_i}{f_i^o} \tag{3.30}$$

where G_i^o is the Gibbs free energy of pure species i at T and P,f_i is the fugacity of species i in the mixture and f_i^o is the fugacity of pure species i at the same T and P.

The chemical potential between an non ideal fluid and an ideal gas can be obtained from Eq. (3.29) and Eq. (3.20) which is the difference between system and ideal gas at the same T,P and y_j as:

$$\mu_i(T, P, y_j) - \mu_i^{ig}(T, P, y_j) = RT\ln\frac{f_i}{y_i P} \tag{3.31}$$

Eq. (3.31) can be rewritten as:

$$\mu_i(T, P, y_j) = \mu_i^{ig}(T, P, y_j) + RT\ln\frac{f_i}{y_i P} \tag{3.32}$$

The ratio $f_i/(y_i P)$ is the called the fugacity coefficient ϕ_i of species i in the solution and then Eq. (3.32) can be rearranged as:

$$\mu_i(T, P, y_j) = \mu_i^{ig}(T, P, y_j) + RT\ln\phi_i \tag{3.33}$$

The fugacity coefficient ϕ_i measures the deviation of a fluid from the idealty. If $\phi_i = 1$, this means that the system is ideal system.

The fugacity coefficient can be defined from Eq. (3.33) as:

$$\ln \phi_i = \left(\frac{\mu_i - \mu_i^{ig}}{RT} \right)_{T,P,y_j} = \left(\frac{\mu_i^{res}}{RT} \right)_{T,P,y_j} - \ln Z \tag{3.34}$$

It can be clearly seen from Eq. (3.34) that the fugacity coefficient can be estimated, if both the residual chemical potential and the compressibility factor are known. The residual chemical potential can obtained from the residual Helmholtz free energy, while the compressibility factor can be determined from any equation of state. Solving phase-equilibrium calculations requires the estimation of fugacity coefficient. Thus next section will cover the use of fugacity coefficient and the potential state functions for solving phase equilibrium problems.

3.5 Phase equilibrium

It important to perform phase equilibrium calculation prior to design chemical processing units. It provides several information, such as phase compositions, phase stability, and energy that might be absorbed or released from the system. Two techniques can be applied to perform phase-equilibrium calculations. The first technique is called $(\phi - \phi)$ approach as it requires the fugacity coefficient ϕ of all phases, while the second technique is called $\gamma - \phi$ approach which requires activity and fugacity coefficients [100]. In this study, the first techniqe is used for phase-equilibrium calculations. It is a powerful technique for solving fluid-fluid phase equilibria, such as predicting the solubility of solute into a solvent specially if the EoS is selected to carry out the thermodynamic calculations [100, 101].

From the potential state functions that were discussed in Sec. 3.2 and at constant T and P of the system, the Gibbs free energy Eq. (3.7) at equilibria can be rewritten as:

$$dG(T, P, y_j) = \sum_i \mu_i dn_i \tag{3.35}$$

As indicated in Eq. (3.8), the change in the Gibbs free energy will reach its minimum value at equilibrium state. Therefore, Eq. (3.35) can be written at equilibrium as:

$$\sum_i \mu_i dn_i = 0 \tag{3.36}$$

If two phases (I and II) are present in the system, the change in the number of moles of component i between phase I and phase II can be defined as:

$$dn_i = dn_i^I + dn_i^{II} = 0 \tag{3.37}$$

By substituting Eq. (3.37) into Eq. (3.36), given:

$$\sum_i (\mu_i^I - \mu_i^{II}) dn_i^I = 0 \tag{3.38}$$

At the equilibrium, the chemical potential between both phases I and II are equal as:

$$\mu_i^I = \mu_i^{II} \tag{3.39}$$

By combining both Eq. (3.39) and Eq. (3.27) for phase I and phase II gives:

$$f_i^I = f_i^{II} \tag{3.40}$$

The fugacity f_i^I of species i can be defined from fugacity coefficient ϕ_i as

$$f_i^I = x_i^I \phi_i^I P \tag{3.41}$$

where x_i^I is the mole fraction of component i in phase I, ϕ_i^I is the fugacity coefficient of component i in phase I and P is the system pressure.

By substituting Eq. (3.41) into Eq. (3.40) gives:

$$x_i^I \phi_i^I = x_i^{II} \phi_i^{II} \tag{3.42}$$

Equation (3.42) is the general formula of $\phi - \phi$ approach , where the composition of the components in each phase can be obtained, if the fugacity coefficient ϕ of the species is known.

It is clear that the thermophysical properties of any fluid can visibly be predicted by estimating the compressibility factor and understanding the use of potential state functions. Thus, the next section focus on the use of EoS's to estimate the compressibility factor and the fugacity coefficient of any system for the thermodynamic modeling.

3.6 Equations of State

Equations of state (EoS) play an important role in modeling of vapor-liquid, liquid-liquid and vapor-liquid-liquid equilibrium at low and high pressure [102]. As indicated in Sec 3.1 that design any processing unit requires a phase contact.

Equations of state, such as cubic equations of state or the perturbed-chain statistical associating fluid theory (PC−SAFT), are characterized by their simplicity, reliability and robustness over a wide range of conditions (e.g., high pressures), and speed of computation [95]. Therefore, they are the model of choice for many multicomponent systems and are widely used for practical applications.

Selecting the proper EoS depends on several factors, such as the nature of the components in the system, and the system applications. For instance, modeling a system that contains sour gases requires special model that takes into account the solubility of the sour gas in the used solvent. Table 3.1 shows the recommended selection of thermodynamic model based on their applications [103]. It is clear from Table 3.1 that if the system contains light and heavy hydrocarbons, both Soave-Redlich-Kwong (SRK) and Peng-Robinson (PR) EoS's are recommended. For non ideal systems, it is recommended to use activity coefficient models, such as UNIFAC, NRTL, and UNIQUAC. In the presence of water and hydrocarbon, statistical associating fluid theory (SAFT) EoS is the preferable model.

Thus, the SRK EoS and perturbed-chain statistical associating fluid theory (PC-SAFT) are selected as thermodynamic models to predict the distribution of mercury in oil and gas processing facilities. In addition that theses models are used to estimate the thermophysical properties of mercury, such as pure component vapor pressure and solubility. The Peng-Robinson (PR) EoS was not selected as it is similar to SRK EoS.

Table 3.1: Thermodynamic model selection based on system application. Taken from [103].

Application	Operating conditions	Model
General hydrocarbon	Pressure >1 bar	Soave−Redlich−Kwong
General hydrocarbon	Cryogenics and Pressure >1 bar	Peng−Robinson
Non−ideal and azeotrope	P (0−4 atm) T(275−475K)	UNIFAC
Hydrocarbon and water	—	SAFT
Non-ideal and azeotrope	—	NRTL
Non-ideal and azeotrope	—	Margules
Non-ideal and azeotrope	—	UNIQUAC
Sour Water	—	Soave−Redlich−Kwong

Moreover, the PR EoS was used by [96, 97] for predicting the solubility of elemental mercury as discussed in Sec 2.7. The SRK and PC-SAFT EoS will explored in detail in the next section. In addition to that the use of these models for modeling phase equilibrium and estimating the thermophysical properties of pure and multi components systems will be considered.

3.6.1 Soave-Redlich-Kwong equation of state

The SRK EoS is a modification of a cubic equation of state proposed by Redlich and Kwong [104] developed by Soave [105] by studying the behavior of pure compounds:

$$p = \frac{\rho RT}{1 - \rho b} - \frac{a\rho^2}{(1 + \rho b)} \tag{3.43}$$

where p is the system pressure, T is the absolute temperature, and R is the universal gas constant, ρ is the molar density of the system, and a and b are parameters of the model. The first term of Eq. (3.43) corresponds to the repulsive force and the second term corresponds to the attraction force.

The parameters a_i and b_i for a pure component i can be expressed in terms of its

critical temperature T_{ci} and critical pressure p_{ci}

$$a_i = 0.42747 \frac{R^2 T_{ci}^2}{p_{ci}} \alpha_i(T) \tag{3.44}$$

$$\alpha_i(T) = \left[1 + (0.480 + 1.57\omega_i - 0.176\omega_i^2) \left(1 - \sqrt{\frac{T}{T_{ci}}} \right) \right]^2 \tag{3.45}$$

$$b_i = 0.08664 \frac{R T_{ci}^2}{p_{ci}} \tag{3.46}$$

where ω_i is the acentric factor for component i, introduced by Pitzer [106].

To extend the SRK EOS to multi-component systems, mixing rules are required to obtain the parameters a and b for the solution from the a_i's and b_i's from the individual pure components. Many mixing rules have been proposed for cubic EoS [107, 108]. In this work, the van der Waals mixing rules are used, which are given by

$$a = \sum_{ij} x_i x_j \sqrt{a_i a_j} (1 - k_{ij}) \tag{3.47}$$

$$b = \sum_{i} x_i b_i \tag{3.48}$$

where k_{ij} in Eq. (3.47) is the binary interaction parameter, x_i is the mole fraction of component i in the mixture, and a_i and b_i are calculated from Eqs. (3.44) and (3.46). The SRK EoS Eq (3.43) can be rewritten in terms of compressibility factor Z and in the standard cubic form as:

$$Z^3 - Z^2 + (A - B - B^2)Z - AB = 0 \tag{3.49}$$

where Z is the compressibility factor.

$$A = \frac{aP}{(RT)^2} \tag{3.50}$$

$$B = \frac{bP}{RT} \tag{3.51}$$

The general form for the fugacity coefficient ϕ derived from the SRK EoS is:

$$\ln \phi_i = (BB)_i(Z-1) - \ln(Z-B) - \frac{A}{B}((AA)_i - (BB)_i)\ln\left[1+\frac{B}{Z}\right] \tag{3.52}$$

where ϕ_i is the fugacity coefficient, and Z is the compressibility factor calculated from Eq. (3.49).

$$AA_i = \frac{2}{a}\left[\sum_j \sqrt{a_i a_j}(1-k_{ij})\right] \qquad BB_i = \frac{b_i}{b} \tag{3.53}$$

The solution of Eq. (3.49) for the compressibility factor produces three roots when $T < T_c$. The largest root represents the vapor phase compressibility factor (Z_v), the smallest represents the liquid phase compressibility factor (Z_l) and the one in the middle is ignored as it has no physical meaning. When Z_v is substituted in equation (3.49), the vapor phase fugacity coefficient (ϕ_{v_i}) is obtained while the liquid phase fugacity coefficient (ϕ_{l_i}) is obtained when Z_l is used.

The compressibility factor for the SRK equation of state can be written as:

$$\begin{aligned} Z &= \frac{1}{1-\rho b} - \frac{a}{bRT}\frac{\rho b}{1+\rho b} \\ &= Z_{exc} + Z_{att} \end{aligned} \tag{3.54}$$

where Z_{exc} accounts for excluded volume interactions, and Z_{att} accounts for attractive interactions.

It is clear that by knowing the critical properties of the components, several properties can be determined, such as system pressure, fugacity coefficient, compressibility factor and others by using SRK EoS. Afterwards, phase equilibrium calculations which explored in 3.5 can be performed. The only parameter that requires binary experimental data, as VLE and LLE is the the binary interaction parameter k_{ij} in Eq. (3.47). Without

taking it into account, the accuracy of the cubic equations of state can not be assured as explored in 2 Sec 2.7. Therefore, next section investigates the possibility of estimating the k_{ij} using group contribution method by combining EoS with the potential state functions.

3.6.2 Group contribution method

In order to obtain accurate results with a cubic EoS, appropriate values for binary interaction parameters are required. Typically, the k_{ij}'s are used as fit parameters used to reproduce experimental data. However, frequently the experimental data required to develop and validate the thermodynamic models are lacking due to system toxicity as mercury species or expensive to carry out. Several empirical methods have been proposed to estimate binary interaction parameters; however, many of these correlations fail to properly predict the phase behavior at elevated pressures [109].

Alternate mixing rules to the van der Waals mixing rule (see Eqs. (3.47) and (3.48)) have been proposed as in order to improve the accuracy of EoS's. One class of these is based on combining the EoS with an activity coefficient model [110] and is typically referred to as EoS/g^E.

The use of group contribution techniques with activity coefficient models, such as UNIFAC, has been quite successful [92]. Calculating an EoS's parameters based on a group contribution method (GCM) is often more powerful than the use of activity coefficient models and can provide accurate predictions [95, 110]. The combination of an EoS with a group contribution method results in a predictive model that provides a theoretical expression for k_{ij}

Substituting Eq. (3.54) into Eq. (3.26), A^{res} can be written as:

$$A^{res} = I_{exc}(\rho b) - E(T, x)Q(\rho b) \tag{3.55}$$

where I_{exc} is the contribution from excluded volume interactions, E characterizes the dependence of the attractive interactions in the system on the composition and temperature, and Q captures the influence of density (which is related to the "frequency" of the

interactions). For the SRK EoS, these terms are explicitly given by

$$I_{exc}(\rho b) = -RT\ln(1-\rho b), \tag{3.56}$$

$$E(T,x) = \frac{a}{b^2}, \tag{3.57}$$

$$Q(\rho b) = \ln(1+\rho b). \tag{3.58}$$

In order to characterize the influence of mixing on a system, we first define an ideal solution, where the Helmholtz energy is defined as:

$$A^{id} = \sum_{i=1} x_i A_i^\circ + RT \sum_{i=1} x_i \ln x_i \tag{3.59}$$

where A_i° is the molar Helmholtz energy of pure component i, which is given by

$$A_i^\circ = \mu_i^\circ + RT(\ln \rho b_i - 1) + I_i^\circ \tag{3.60}$$

where I_i° is the molar residual Helmholtz free energy of pure i at packing fraction ρb_i and temperature T. The excess or residual property was defined in Sec 3.4 as the difference between the actual value of the property of the system and the value of an ideal mixture at the same temperature, total moles of each species and packing fraction [95]:

$$M^E(T,n,\rho b) = M(T,n,\rho b) - M^{id}(T,n,\rho b) \tag{3.61}$$

where M^E is the excess property and M^{id} is the ideal mixture property.

The excess Helmholtz free energy at constant temperature, constant volume, and constant number of moles of each species can be defined based on Eq. (3.61), Eq. (3.59) and Eq. (3.60) as:

$$A^E(T,n,\rho b) = A(T,n,\rho b) - A^{id}(T,n,\rho b) \tag{3.62}$$

$$= RT\sum_i x_i \ln\frac{b_i}{b} + I - \sum_i x_i I_i^\circ. \tag{3.63}$$

The first term represents effect of molecule size on the free energy of mixing, while the final two terms give the influence of the attractive interactions between molecules.

For an equation of state similar in form to the SRK EoS, the excess Helmholtz free

energy can be written as

$$A^E(T, n, \rho b) = RT \sum_i x_i \ln \frac{b_i}{b} + \frac{Q(\rho b)}{2b} \sum_{i,j} x_i x_j b_i b_j E_{ij} \tag{3.64}$$

where E_{ij} physically captures the free energy of interaction between a molecule of type i and a molecule of type j, and the Q term describes the frequency of the interactions. The parameter E_{ij} can be directly related to the original parameters of the SRK equation of state as

$$E_{ij} = -2\frac{a_{ij}}{b_i b_j} + \frac{a_i}{b_i^2} + \frac{a_j}{b_j^2}. \tag{3.65}$$

Using the van der Waals mixing rules (see Eqs. (3.47) and (3.48)) leads to:

$$E_{ij} = (\delta_i - \delta_j)^2 + 2\delta_i \delta_j k_{ij} \tag{3.66}$$

where $\delta_i = a_i^{1/2}/b_i$ is the Scatchard-Hildebrand solubility parameter [106, 111, 112]. It can be clearly seen that the binary interaction parameter k_{ij} describes the deviation of the interaction free energy between two molecules from that given by the regular solution model:

$$k_{ij} = \frac{E_{ij} - (\delta_i - \delta_j)^2}{2\delta_i \delta_j}. \tag{3.67}$$

The regular solution model applies to mixtures where molecules are of similar size and interact only through dispersion forces [106]. For mixtures of molecules of different size or where other forces are present (e.g., hydrogen bonding, dipole-dipole interactions, etc.), deviations from this model are to be expected. In this work, this is captured by the mixing parameter k_{ij}.

The interaction free energy E_{ij} between a molecule of type i and a molecule of type j, which appears in Eq. (3.66), can be expressed in terms of a sum of the interactions between pairs of groups within the molecules [113]

$$E_{ij} = -\frac{1}{2} \sum_{k,l} (\alpha_{ik} - \alpha_{jk})(\alpha_{il} - \alpha_{jl}) A_{kl}(T) \tag{3.68}$$

where the indices k and l run over all types of groups in the system, and α_{ik} is the fraction of molecule i occupied by group k. For example, propane has a molecular structure of CH_3-CH_2-CH_3; It contains two CH_3 groups and one CH_2 group. Therefore the total number of groups present in this molecule is three. In this case, the fraction of molecule propane occupied by group CH_2 is $\alpha_{\text{propane}-\text{CH2}} = 1/3$, and the fraction of molecule propane occupied by group CH_3 is$\alpha_{\text{propane}-\text{CH3}} = 2/3$.

The temperature dependence of the interaction parameter $A_{kl}(T)$ is given by:

$$A_{kl}(T) = A^0_{kl} \left(\frac{T_0}{T} \right)^{B^0_{kl}/A^0_{kl}-1} \tag{3.69}$$

where T is the absolute temperature, $T_0 = 298.15$ K is a reference temperature, and A^0_{kl} and B^0_{kl} are the interaction parameters between groups k and l.

The quantity $A_{kl}(T)$ represents the negative free energy of interaction between a group of type k and a group of type l. From the Gibbs-Helmholtz equation [106], we can then identify the quantity

$$B^0_{kl} \left(\frac{T_0}{T} \right)^{B^0_{kl}/A^0_{kl}-1} \tag{3.70}$$

with the attractive energy of interaction between groups, and, consequently, the quantity

$$A^0_{kl}(B^0_{kl}/A^0_{kl} - 1) \left(\frac{T_0}{T} \right)^{B^0_{kl}/A^0_{kl}-1} \tag{3.71}$$

is related with the entropy of the interaction.

This group contribution method (GCM) was used by Jaubert and Noël [110] to predict the VLE of several binary mixture of hydrocarbon components using the Peng-Robinson EoS (PR), calling this the predictive Peng-Robinson 1978 (PPR78). Noël showed that the obtained results from GCM are often more precise than EoS/g^E models. Another study used the GCM to predict k_{ij} of a system containing hydrocarbon components and carbon dioxide CO_2 using SRK EoS [114]. The study indicated its feasibility to estimate the k_{ij} of any mixture containing carbon dioxide and hydrocarbons at any temperature. A relation between the k_{ij} parameters for PPR78 and the SRK EoS has been developed [111]. This helps to predict GCM parameters of SRK EoS based on PR

EoS GCM parameters. Consequently, the values for the group interaction parameters A^0_{kl} and B^0_{kl} between a large number of different types of groups is already available. This combination between SRK EoS and GCM will be used in Chapter 4 to predict the solubility of elemental mercury in several solvents and also in Chapter 5 to predict the distribution of mercury in oil and gas processing.

3.7 Perturbed-chain statistical associating fluid theory

Due to the incompetence of cubic equations of state for predicting the vapor liquid equilibria of mixtures, predictive models that have the ability to model complex systems are demanded. This can only be achieved by implementing the statistical mechanics principles. This concept takes into account the effect of the molecule size and shape [115]. A recent thermodynamic model that obtained by applying statistical associating fluid theory (SAFT) observed by Chapman et al. [116] was successfully applied for chain mixtures. Several improvements were done to the SAFT model over the period of time, such as taking the dispersion contribution into account [117]. The SAFT model was further developed quite recently by Gross and Sadowski by applying perturbation theory [115] to became perturbed-chain statistical association fluid theory model (PC-SAFT). It was developed based upon the thermodynamic perturbation theory for chain molecules which includes a new dispersion and association interactions. The PC-SAFT is known as a new-generation equation of state as it represents the simple and complex mixture more precisely [118].

The general form of PC-SAFT EoS can be expressed in terms of Helmholtz free energy as:

$$A^{res} = A^{hc} + A^{disp} + A^{assoc} + A^{polar} + A^{elec} \tag{3.72}$$

where A^{res} is the residual Helmholtz free energy, A^{hc} is the hard chain contribution to Helmholtz free energy, A^{disp} is the dispersion contribution to Helmholtz free energy, A^{assoc} is the association contribution to Helmholtz free energy due to hydrogen bonding, A^{apolar} is the polar contribution to Helmholtz free energy, and A^{elec} is the electrolyte contribution to Helmholtz free energy accounting for the electrostatic interactions due to the charge of molecules. In this work, the polar contribution to the Helmholtz free

energy A^{polar} is not taken into account.

Figure 3.1 shows the principle of PC-SAFT for interaction accounting between molecules. The m_i in Figure 3.1 represents the number of segments per chain and σ represents the segment diameter while ϵ accounts for the depth of pair potential. For instance, if the molecule is not a long chain molecule (m_i =1), non electrolyte, non$-polar$ and non$-$associating as methane. In this case, the A^{disp} dispersion contribution to Helmholtz free energy is the only term in Eq. (3.72) that need to be taken into account. Thus in order to represent methane, σ and ϵ in Figure 3.1 are the PC-SAFT required parameters. These parameters represent the dispersion interactions between the molecules.

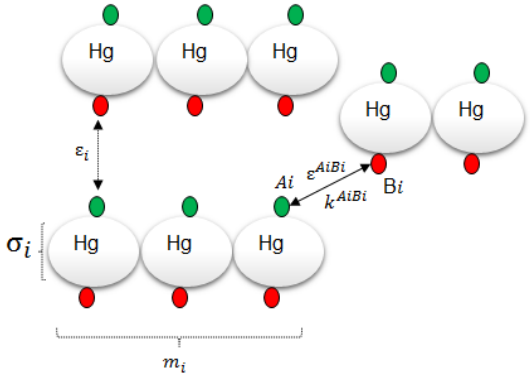

Figure 3.1: The green symbols represent the accepter sites of a molecule and the red symbols represent the donor sites of a molecule

The hard-chain contribution is defined as:

$$A^{hc} = mA^{hs} - \sum_i x_i(m_i - 1)\ln g_{ii}^{hs}(\sigma_{ii}) \tag{3.73}$$

where σ is segment diameter, g^{hs} is the radial distribution function of hard-sphere, m is the mean segment number in the mixture and is defined as

$$m = \sum_i x_i m_i \tag{3.74}$$

where:m_i is the number of segments per chain and x_i is the mole fraction of component

i.

The hard-sphere contribution to Helmholtz free energy is:

$$A^{hs} = \frac{1}{\zeta_0}\left[\frac{3\zeta_1\zeta_2}{(1-\zeta_3)} + \frac{\zeta_2^3}{\zeta_3(1-\zeta_3)^2} + \left(\frac{\zeta_2^3}{\zeta_3^2} - \zeta_0\right)\ln(1-\zeta_3)\right] \tag{3.75}$$

With the radial distribution function given as:

$$\begin{aligned} g_{ij}^{hs} = \frac{1}{(1-\zeta_3)} + \left(\frac{d_i d_j}{d_i + d_j}\right)\frac{3\zeta_2}{(1-\zeta_3)^2} + \\ \left(\frac{d_i d_j}{d_i + d_j}\right)^2 \frac{2\zeta_2^2}{(1-\zeta_3)^3} \end{aligned} \tag{3.76}$$

where ζ_n given as:

$$\zeta_n = \frac{\pi}{6}\rho\sum_i x_i m_i d_i^n \tag{3.77}$$

where d_i is the temperature-dependent segment diameter of component i defined as:

$$d_i = \sigma_i\left[1 - 0.12\exp\left(-3\frac{\epsilon_i}{kT}\right)\right] \tag{3.78}$$

where ϵ is the depth of pair potential.
The dispersion contribution to the Helmholtz free energy is given by:

$$A^{disp} = -2\pi\rho I_1(\eta, m)\overline{m^2\epsilon\sigma^3} - \pi\rho m C_1 I_2(\eta, m)\overline{m^2\epsilon^2\sigma^3} \tag{3.79}$$

$$\begin{aligned} C_1 &= \left(1 + Z^{hc} + \rho\frac{\partial Z^{hc}}{\partial\rho}\right)^{-1} \\ &= \left(1 + m\frac{8\eta - 2\eta^2}{(1-\eta)^4} + (1-m)\frac{20\eta - 27\eta^2 + 12\eta^3 - 2\eta^4}{[(1-\eta)(2-\eta)]^2}\right) \end{aligned} \tag{3.80}$$

$$\overline{m^2\epsilon\sigma^3} = \sum_i \sum_j x_i x_j m_i m_j \left(\frac{\epsilon_{ij}}{kT}\right) \sigma_{ij}^3 \tag{3.81}$$

$$\overline{m^2\epsilon^2\sigma^3} = \sum_i \sum_j x_i x_j m_i m_j \left(\frac{\epsilon_{ij}}{kT}\right)^2 \sigma_{ij}^3 \tag{3.82}$$

$$I_1(\eta, m) = \sum_{i=0}^{6} a_i(m)\eta^i \tag{3.83}$$

$$I_2(\eta, m) = \sum_{i=0}^{6} b_i(m)\eta^i \tag{3.84}$$

$$a_i(m) = a_{0i} + \frac{m-1}{m}a_{1i} + \frac{m-1}{m}\frac{m-2}{m}a_{2i} \tag{3.85}$$

$$b_i(m) = b_{0i} + \frac{m-1}{m}b_{1i} + \frac{m-1}{m}\frac{m-2}{m}b_{2i} \tag{3.86}$$

where a_{0i}, a_{1i}, a_{2i}, b_{0i}, b_{1i} and b_{2i} are the universal PC-SAFT constants given in Appendix Table B-1 [115]. The commonly combining rules were employed for the calculation of average segment diameter σ_{ij} and average dispersion energy ϵ_{ij} of unlike segments as

$$\sigma_{ij} = \frac{1}{2}(\sigma_i + \sigma_j) \tag{3.87}$$

$$\epsilon_{ij} = \sqrt{\epsilon_i \epsilon_j}(1 - k_{ij}) \tag{3.88}$$

If the molecule is an associating molecule which contains hydrogen bonding, such as water, alcohols and others, in this case accounting for the association interaction is of vital importance. The association contribution to Helmholtz free energy A^{assoc} is developed by Chapman et al. [116] as:

$$\frac{A^{assoc}}{RT} = \sum_{i}^{c} x_i \left[\sum_{A_i} \left(lnX^{A_i} - \frac{X^{A_i}}{2} \right) + \frac{1}{2} M_i \right] \tag{3.89}$$

where X^{A_i} is the mole fraction of molecule i not bonded at site A and M_i is the number of sites on molecule i. X^{A_i} is defined by.

$$X^{A_i} = \left[1 + N_{Av} \sum_{j} \sum_{B_j} \rho_j X^{B_j} \Delta^{A_i B_J} \right]^{-1} \tag{3.90}$$

where $\sum_{B_j}$ runs over all sites on molecule j. ρ_j is the molar density of component j:

$$\rho_j = x_j \rho \tag{3.91}$$

where ρ is the molar density of the solution. $\Delta^{A_i B_J}$ is the association strength and is defined as

$$\Delta^{A_i B_J} = g_{ij}^{hs} [exp(\epsilon^{A_i B_j}/kT) - 1](\sigma_{ij}^3 \kappa^{A_i B_j}) \tag{3.92}$$

The radial distribution function g_{ij}^{hs} is given by Eq. 3.76 above. The combining rules for the association energy $\epsilon^{A_i B_j}$ and the effective association volume $\kappa^{A_i B_j}$ between molecule i and j are taken from Ref. [119]:

$$\epsilon^{A_i B_j} = \frac{1}{2} (\epsilon^{A_i B_i} + \epsilon^{A_j B_j}) \tag{3.93}$$

$$\kappa^{A_i B_j} = \sqrt{\kappa^{A_i B_i} \kappa^{A_j B_j}} \left(\frac{\sqrt{\sigma_{ii} \sigma_{jj}}}{0.5(\sigma_{ii} + \sigma_{jj})} \right)^3 \tag{3.94}$$

In the presence of electrolyte molecule in the system, the electrolyte interaction between the forces should be taken into account. The Debye Huckel theory for electrolyte systems was used by Cameretti et al. [120] to account for the long range Coulomb

forces among ions in the systems is adopted. The electrolyte term is added to the original PC-SAFT [115] and the residual Helmholtz free energy of an electrolyte system is then calculated as:

$$\frac{A^{elec}}{kT} = -\frac{1}{4\pi\epsilon kT}\sum_i \frac{x_i q_i^2}{3}\kappa\chi_i \tag{3.95}$$

where

$$\chi_i = \frac{3}{(\kappa a_i)^3}\left[\frac{3}{2} + \ln(1+\kappa a_i) - 2(1+\kappa a_i) + \frac{1}{2}(1+\kappa a_i)^2\right] \tag{3.96}$$

ϵ is the dielectric constant of the medium ($\epsilon = \epsilon_0\epsilon_r$), where ϵ_0 is the vacuum permittivity and ϵ_r is the relative permittivity of the medium. x_i is the mole fraction of ion i, κ is the inverse Debye screening length and has units of inverse length and a_i is the ion diameter.

The relation between the fugacity coefficient ϕ_k and the residual chemical potential $\mu_k^{res}(T,\nu)$ can be expressed by:

$$\ln\phi_k = \frac{\mu_k^{res}(T,\nu)}{kT} - \ln Z \tag{3.97}$$

$$\begin{aligned}\frac{\mu_k^{res}(T,\nu)}{kT} = A^{res} + (Z-1) + \\ \left(\frac{\partial A^{res}}{\partial x_k}\right)_{T,\nu,x_{i\neq k}} - \sum_{j=1}^{N}\left[x_j\left(\frac{\partial A^{res}}{\partial x_j}\right)_{T,\nu,x_{i\neq j}}\right]\end{aligned} \tag{3.98}$$

It is clear from Eq. 3.97 that fugacity coefficient can be determined, if the residual Helmholtz free energy is known. Afterwards, several properties and phase equilibrium calculations can be carried out for ideal and non−ideal multi component systems. Moreover, the PC-SAFT EoS takes into account several interaction which might vanish the binary interaction parameters presented in Eq. 3.87 and makes PC-SAFT more predictive than cubic equations of state.

3.8 Conclusion

All of the thermophysical properties of a given system can be determined from the thermodynamic potential state functions. Therefore understanding the use of these potential functions helps to improve the ability of thermodynamic models for predicting pure and mixture properties. The phase equilibrium calculations, such as vapor liquid equilibrium (VLE) and liquid liquid equilibrium (LLE) are of vital importance prior to design chemical processing facilities. The use of group contribution (GCM) techniques in combination with EoS helps to understand the physical meaning of binary interaction parameters between the molecules rather than using them as a fitting parameters. The GCM in combination with SRK EoS will be used to predict the solubility of mercury in several solvents in the next Chapter 4. This combination will be validated for multi component system. Afterward its ability for predicting the distribution of elemental mercury in oil and gas processing facilities will explored in Chapter 5. The use of PC-SAFT model for predicting the distribution of elemental mercury could eliminate the binary interaction parameters as it accounts for several contribution terms, such as hard chain, dispersion, polar and association contributions. This will be investigated in Chapter 4 for solubility prediction and in Chapter 5 for predicting the distribution of elemental mercury in oil and gas processing facilities.

Chapter 4

Prediction of the thermophysical properties

4.1 Introduction

Because of mercury's toxicity and corrosive nature, it is preferable to predict its thermophysical properties rather than experimentally measured. Mercury species have lethal dose LD_{50} values ranges from $21\,mg\,kg^{-1}$ to $57.6\,mg\,kg^{-1}$ [121]. Some of the thermophysical properties of mercury, such as its vapor pressure and solubility, provide knowledge of the nature of the substance and its tendency to evaporate and diffuse in the ecosystem or in solvents. Risk mitigation strategies can not be implemented unless these properties were measured or estimated. Therefore, developing a predictive model that has the ability to predict the thermophysical properties of mercury is of vital importance. Mercury has very low solubility in some of the solvents, such as water. Due to the complex nature of water and its interaction with mercury, it restricts the ability of some the thermodynamic models to accurately predict the solubility. In Chapter 3, it was highlighted that equations of state EoS are known by their simplicity, reliability and speed of computation are considered the model of choice for multicomponent system. In addition, they are widely used for practical applications, such as oil and gas processing and refineries specially at high pressure. Thus, the widely used SRK EoS in combination with a group contribution method (GCM), and PC-SAFT EoSs described in Chapter 3 are used to predict the vapor pressure of pure components and the solubility

of elemental mercury in several solvents, such as water, hydrocarbons, aromatics and alcohols.

In this chapter, the ability of both models is tested for predicating the pure component vapor pressure of elemental mercury, water and other solvents. Then, GCM which presented in Chapter 3 was parameterized and used to estimate the SRK EoS binary interaction parameters between elemental mercury and compounds composed of CH, CH_2, CH_3,OH, H_2O, ACH and $ACCH_3$ groups which can represent water, hydrocarbons, aromatics and alcohols. This will improve the SRK ability for solubility prediction and extend its capability beyond the experimental operating range. Afterwords, the solubility of elemental mercury in several solvents, such as water, hydrocarbons, alcohols and aromatic compounds is predicted using SRK in combination with GCM. The combination of SRK with GCM is then validated for multi component systems contain light and heavy hydrocarbons.

For PC-SAFT EoS model, elemental mercury atoms is modeled as a non−bonded and bonded atoms by taking the association interaction term into account. Then, the solubility of elemental mercury in the same solvents was predicted. The PC-SAFT EoS was validated for multi component system to examine its ability for solubility prediction. Finally, the results of both models were compared for ability prediction.

4.2 Thermophysical properties prediction using SRK EoS

In this section, the vapor pressure of elemental mercury and other pure components will be estimated using the SRK EoS described in Chapter 3 in Sec. 3.6.1. The deviation in the vapor pressure between experimental values is reported for each studied component. The solubility of elemental mercury in several solvents such as water, alcohols, normal alkanes and aromatic compounds will then be predicted using SRK EoS with GCM. The ϕ-ϕ approach described in Sec. 3.5 was used for phase equilibrium calculations; vapor liquid equilibrium (VLE) and vapor liquid equilibrium (LLE). The binary interaction parameter will be estimated using Eq. (3.67) which is the combination of SRK with the group contribution. The group interaction parameters between mercury and the com-

posed groups will be obtained. The model will be validated for predicting the solubility of mercury in multi component mixtures.

As an initial step in this process, we need to ensure that the properties of the pure components such as vapor pressure are properly described using SRK EoS.

Once the pure component parameters of the SRK EoS are chosen, the values of the group interaction parameters A^0_{kl} and B^0_{kl} appearing in Eq. (3.69) between elemental mercury and various molecular groups were determined by fitting to experimental solubility data for mercury in a variety of solvents. This is done by minimizing the objective function F_{obj}

$$F_{\text{obj}} = \sum_i \left(\frac{S_i^{\text{calc}} - S_i^{\text{exp}}}{S_i^{\text{exp}}} \right)^2 \tag{4.1}$$

where S_i^{exp} is the experimental solubility of mercury in the selected solvent, and S_i^{calc} is the calculated solubility of mercury in the selected solvent.

Table 4.1: Group interaction parameters A^0 and B^0 for mercury with other groups.

group	$10^{-4}A^0$ bar^{-1}	$10^{-4}B^0$ bar^{-1}	B^0/A^0 —
CH	10.9143 ± 0.0023	7.00 ± 0.0945	0.66
CH_2	7.8864 ± 0.0057	7.0562 ± 0.065	0.89
CH_3	8.5137 ± 0.0207	7.1461 ± 0.27	0.84
OH	6.5524 ± 0.00204	5.29903 ± 0.837	0.80
ACH	7.7506 ± 0.0036	8.1350 ± 0.01	1.049
$ACCH_3$	7.5699 ± 0.028	7.9629 ± 1.1	1.052
H_2O	9.9037 ± 0.0063	3.7305 ± 0.0289	0.38

Vapor-liquid equilibrium (VLE) and liquid-liquid equilibrium (LLE) calculations were performed for the SRK equation of state using standard flash algorithms implemented in Python to obtain the solubility of mercury S_i^{calc} using ϕ-ϕ approach. The LmFit package [122] in Python was used to determine the values of the group interaction parameters A^0_{kl} and B^0_{kl} in Eq. (3.69) that minimize the objective function Eq. (4.1). LimFit depends on Levenberg-Marquardt optimization method to solve non$-$ linear optimization and curve fitting problems. The optimized values and their uncertainties are

summarized in Table 4.1. These are discussed in more detail later in this section.

4.2.1 Modelling vapor pressure of pure components using SRK EoS

In order to predict the pure component properties of a species, the SRK equation of state requires its critical pressure, critical temperature and acentric factor. In the literature, these pure fluid parameters vary slightly from reference to reference. In this work, only the acentric factor was tuned in order to achieve the minimum absolute average relative deviation error (AARD) in vapor pressure. The critical pressure, critical temperature and the adjusted acentric factor are summarized in Table 4.2. Note that these values are in good agreement with the accepted experimental critical properties for these compounds in the literature.

Table 4.2: Pure component critical properties and acentric factor.

Component	p_c bar	T_c K	ω —	Ref.
mercury	1670.0	1764	−0.2102	[123]
propane	42.55	369.92	0.152	[124]
n-butane	37.966	425.16	0.205	[124]
n-pentane	33.691	469.7	0.250	[124]
n-hexane	30.124	507.31	0.305	[124]
n-heptane	27.358	540.1	0.3525	[124]
n-octane	24.865	568.76	0.3978	[124]
n-nonane	22.879	594.56	0.4419	[124]
n-decane	21.035	617.5	0.492	[124]
benzene	48.98	562.79	0.2130	[124]
toluene	43.2	591.8	0.268	[124]
o-xylene	39.8	633.3	0.304	[124]
methanol	80.959	512.5	0.556	[124]
isopropanol	47.63	508.37	0.657	[124]
water	220.64	647.14	0.324	[125]

Figure 4.1 represents the relative deviation in the vapor pressure with respect to temperature for pure mercury, methanol, isopropanol and water. It indicates that the SRK EOS is capable of accurately predicting the vapor pressure of elemental mercury, water, and alcohols. The AARD for 99 experimental data points of elemental mercury

over a temperature range of 253.15 K to 773.15 K was 3.7%, the experimental data used in this work were taken from Refs. 126, 127, 128, and 129. These data were classified by Huber et al. as primary experimental data, because of their low experimental uncertainty of around 1% [130].

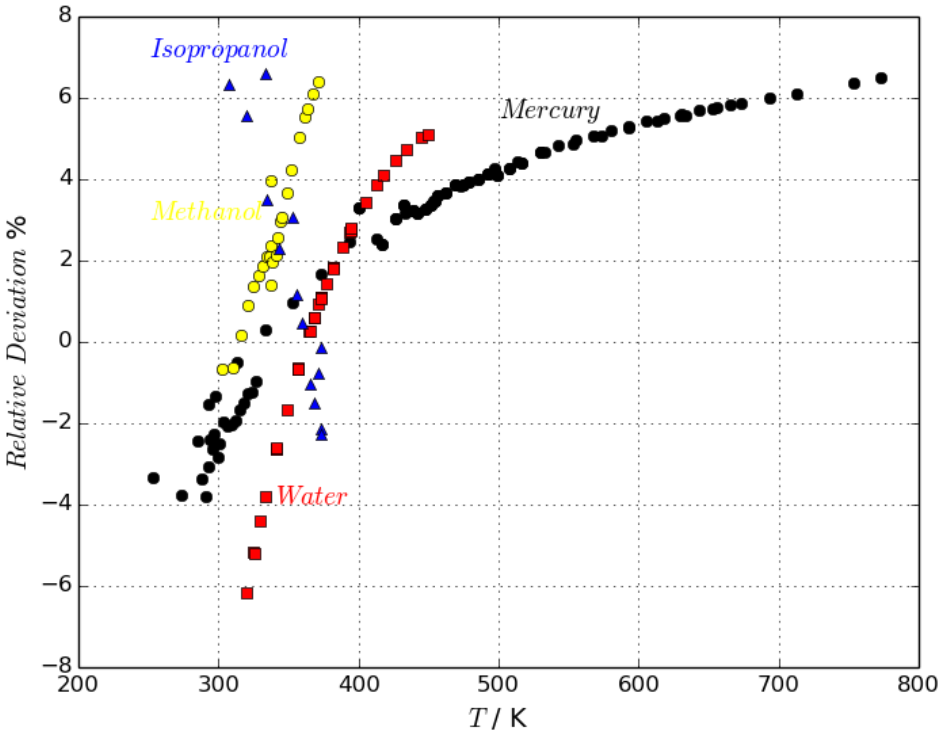

Figure 4.1: Relative deviation error between experimental and calculated values using SRK EoS in the vapor pressure of elemental mercury (black), water (red), methanol, (yellow), and isopropanol (blue) .

The AARD for the vapor pressure of water was 2.5% for 38 experimental data points over a temperature range of 319.6 K to 449.7 K; the experimental data used in this work were taken from Ref. 83. For methanol and isopropanol, the AARD was 2.8% for 24 data points and 2.6% for 14 experimental data points, respectively; the experimental data were taken from Ref. 131, 132, and 133.

Figure 4.2 shows the relative deviation of the correlations of the SRK equation of state for the vapor pressure of some n-alkanes and aromatic compounds. The AARD for propane, n-pentane, and n-decane was 0.4% for 31 experimental data points, 0.2% for 50 experimental data points, and 2.5% for 32 experimental data points respectively. the

experimental vapor pressure data were taken from Refs. 134, 135, and 136. In addition, the AARD for the vapor pressure of benzene, toluene, and o-xylene was 0.9% for 13 experimental data points, 0.3% for 17 data points, and 0.78% for 12 data points, respectively; the experimental vapor pressure data for aromatics were taken from Refs. 137, 138, and 139.

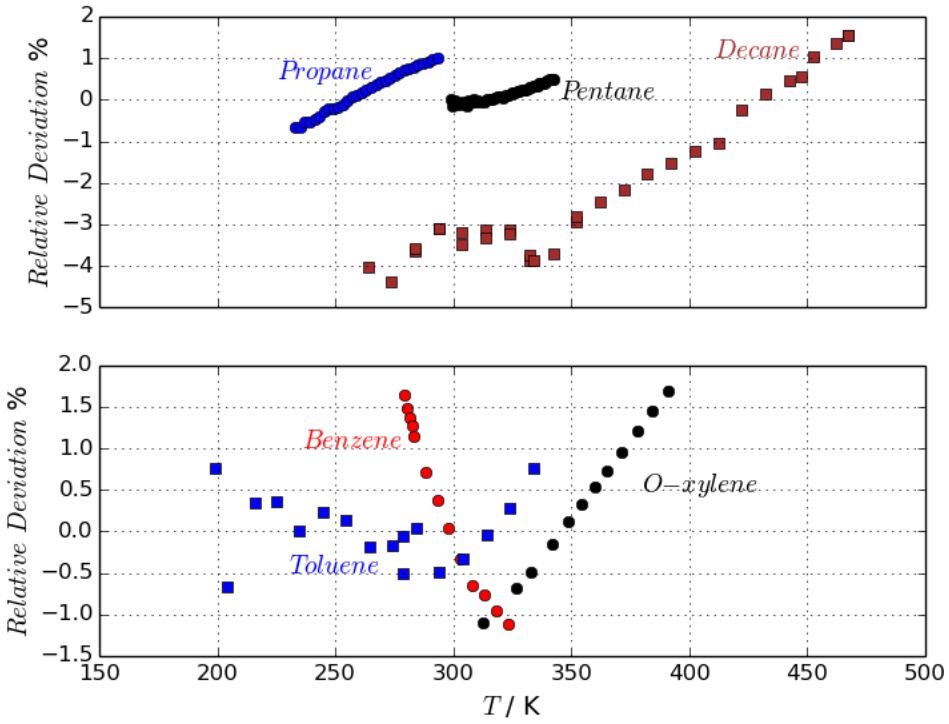

Figure 4.2: Relative deviation error between experimental and calculated values using SRK EoS in the vapor pressure of (a) n-alkanes and (b) aromatic compounds.

4.2.2 Modelling the solubility of elemental mercury in water using SRK EoS

The solubility of elemental mercury in water is available over a wide range of temperatures. The experimental data used in this work were taken from Ref. 91, which are shown as the symbols in Figure 4.3(a) over a temperature range of 273.15 K to 393.15 K. The dashed line in Figure 4.3(a) is the solubility of mercury predicted by the SRK EoS,

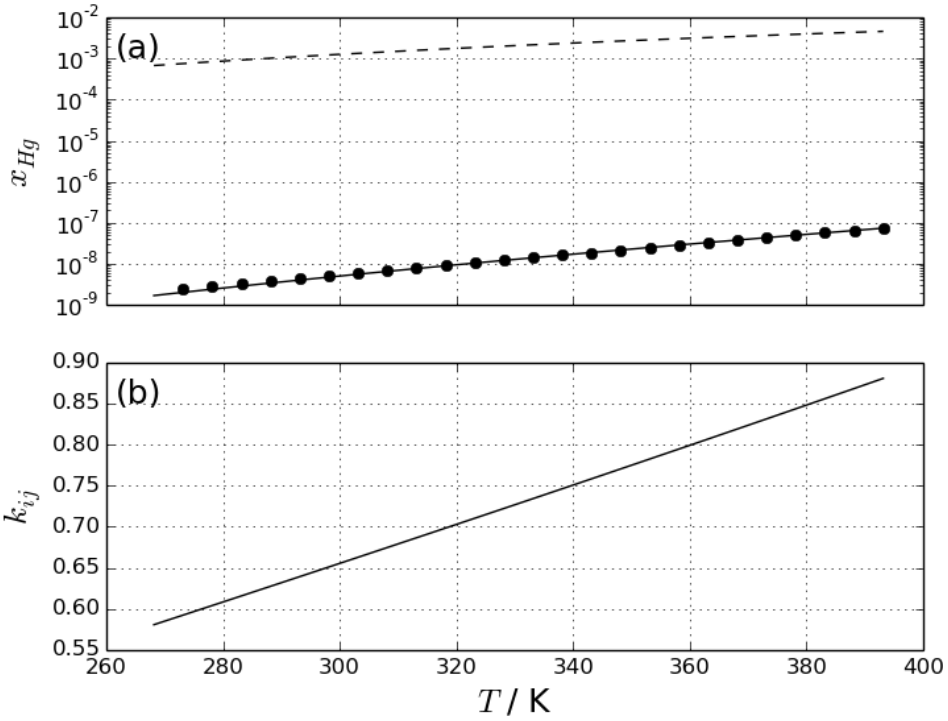

Figure 4.3: (a) Solubility of mercury in water. The symbols represent the experimental data, taken from Ref. 91. The dashed line is the correlation of the SRK EoS with $k_{ij} = 0$, and the solid line is the correlation with k_{ij} estimated using the group contribution method. (b) The variation with temperature of the binary interaction parameter between mercury and water for SRK EoS.

neglecting the binary interaction parameter (i.e. $k_{ij} = 0$); without introducing proper binary interaction parameters, the mercury solubility in water is severely overestimated.

The solid line in Figure 4.3(a) gives the correlation of the SRK EoS with the k_{ij} shown in Figure 4.3(b). The k_{ij} was estimated by using the group interaction parameters A^0_{kl} and B^0_{kl} between mercury and water which summarized in Table 4.1. For this

system, an AARD of 4.2% was obtained for 25 experimental data points. The binary interaction parameter between mercury and water is temperature dependent; it increases by 0.05 with each 20 K increase in temperature.

Thermodynamically, the ratio B^0/A^0 reflects the influence of entropy on the mixing of groups. If the ratio is less than one, the mixing process tends to increase entropy; the molecules become more disordered than in ideal mixing. If the ratio is greater than one, then entropy is lost in mixing; the molecules are more ordered than in ideal mixing. For a ratio of one, there is no excess entropy of mixing and, and enthalpy drives the process. In this case, the binary interaction parameter temperature independent.

4.2.3 Modelling the solubility of elemental mercury in normal alkanes using SRK EoS

Normal alkanes represent more than 90% of natural gas and crude oil species. Predicting mercury solubility in these species is crucial. Elemental mercury is considered the dominant mercury species in the crude oil and natural gas [5, 86]. The solubility data of elemental mercury in hydrocarbon systems are sparse and covers a limited temperature range. The experimental data used in this work are shown as the symbols in Figure 4.4(a) and Figure 4.4(b) for alkanes from C_5 to C_{10}, and Figure 4.5 (a) and Figure 4.5 (b) for C_3 and C_4. These data were taken from Ref. 87 and Ref. 88. Around 65 experimental data points for C_5 to C_{10} over a temperature range of 273.15 K to 336.15 K and atmospheric pressure, and 3 experimental data points for C_8 over a temperature range from 338.15 K to 473.15 K and 6 bar, in addition to 17 data points for C_3 and C_4 at different temperatures and pressures.

Figure 4.4(a) and Figure 4.4(b) show the predicted solubility of elemental mercury in normal alkanes from C_5 to C_{10}. The dashed lines in Figure 4.4 are the solubilities predicted by the SRK EOS, neglecting the binary interaction parameter (i.e. $k_{ij} = 0$); without introducing the proper binary interaction parameters, the mercury solubility in alkanes is nearly independent of the molecular weight of the alkanes. By introducing the binary interaction parameter which estimated using group interaction parameters A^0_{kl} and B^0_{kl} in Table 4.1 of normal alkanes , the results indicated by the solid lines in Figure 4.4 are obtained. The AARD for the solubility in normal alkanes from C_3 to C_{10} was 5.47% for 74 experimental data points.

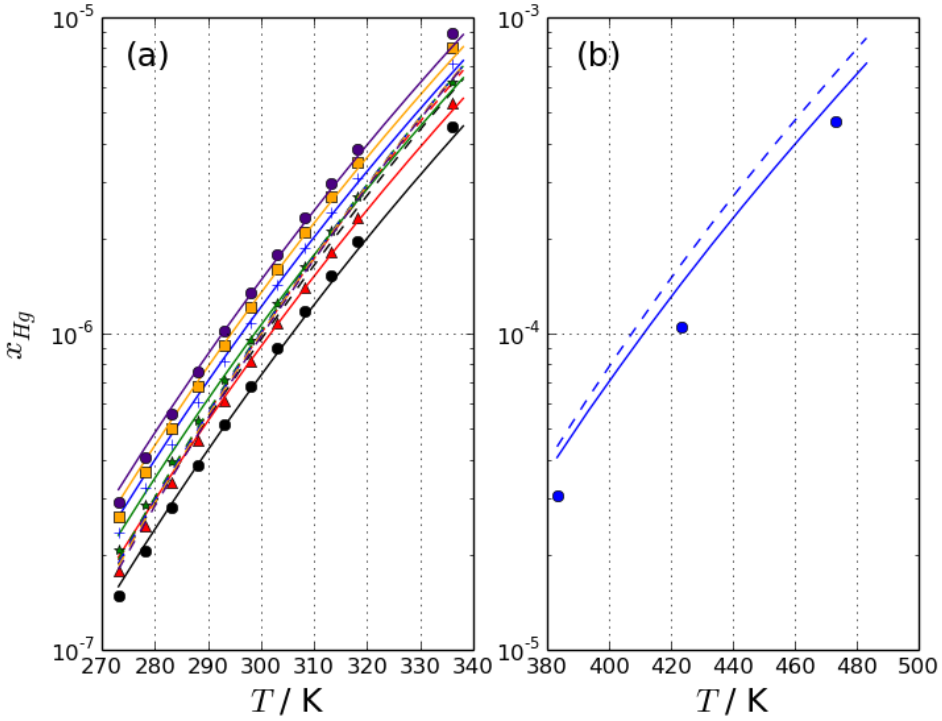

Figure 4.4: Solubility of mercury in normal alkanes: C_5 (black), C_6 (red), C_7 (green), C_8 (blue), C_9 (orange), and C_{10} (indigo). The symbols represent experimental data, taken from Ref. 87 and Ref. 88, the solid lines represent predicted solubility using SRK EoS with the binary interaction parameters estimated using the GCM, and the dashed lines represent the solubility without introducing the binary interaction parameter.

In the recent studies of Polishuk et al. [96, 97], the Peng-Robinson (PR) and CP-PC-SAFT equations of state were used to predict the properties of mercury-hydrocarbon mixtures. In their work, a single, constant value of k_{ij}, which was fixed by fitting to experimental solubility data of mercury in n-pentane, was used. The results of the study showed that within this approach, the Peng-Robinson EOS was incapable of estimating the solubility of mercury in the studied hydrocarbon systems, apart from mercury-pentane. The results obtained by CP-PC-SAFT EoS were more accurate than PR EoS. Fixing the k_{ij} is the main reason of the inadequacy of the PR EoS. The results presented in Fig. 3 of Polishuk et al. show that the predicted solubility of mercury in C_8 using PC-SAFT and the PR EoS at 298.15°C was 0.91 ppm and 3.5 ppm, respectively, while the experimental solubility was 1.08 ppm. The value obtained in this study using the

GCM was 1.10 ppm which is much closer to the experimental value.

In our study, different k_{ij} values were calculated using GCM for each mercury-hydrocarbon binary system at the system temperature and pressure. This approach improves the correlation of mercury solubility in normal alkanes more accurately than fixing k_{ij} to a single value. The solubility of elemental mercury increases with the carbon numbers, which is in consistent with the observations of Refs. 87 and 88.

Several process facilities, such as stripping columns, heat exchangers, reactors, and distillation units might operate at high temperatures in order to purify, or reach reaction desirable operating temperature; therefore, predicting mercury solubility in alkanes at high temperature is crucial. The solubility of elemental mercury in some organic solvents, including octane, dodecane, and toluene, has been experimentally and theoretically estimated over a temperature range from 100°C to 200°C and up to 6 bar [88]. Figure 4.4(b) represents the predicted solubility of elemental mercury in normal octane at 6 bar and high temperatures.

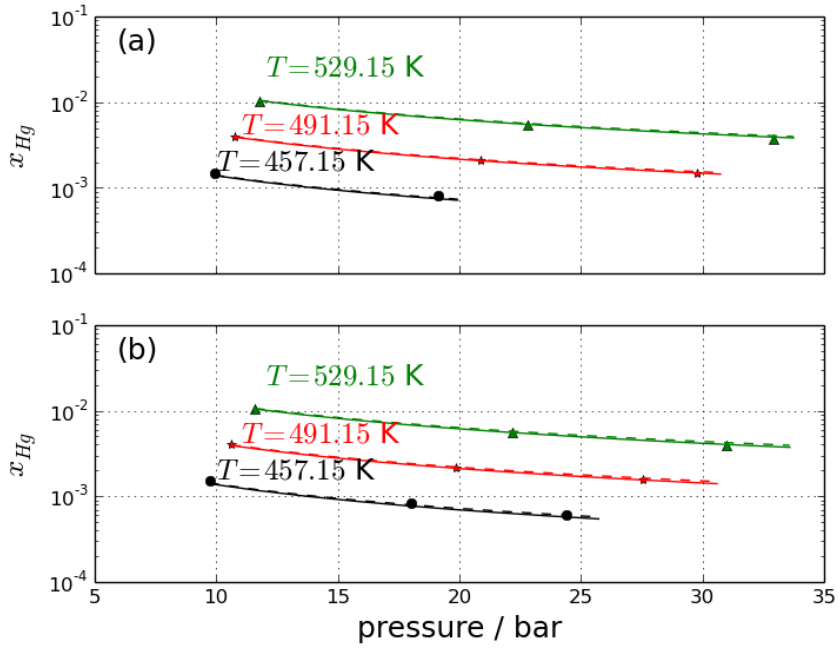

Figure 4.5: Solubility of mercury in (a) propane and (b) butane. The symbols represent experimental data, taken from Ref. 87 and Ref. 88, the solid lines represent SRK EoS predicted solubility by introducing k_{ij} estimated using the GCM, and the dashed lines represent the solubility with $k_{ij} = 0$.

Figure 4.5(a) and (b) show the solubility of mercury in propane and butane, respectively, at a range of pressures and temperatures.

It is clear that the SRK EOS predicts the solubility of elemental mercury in light hydrocarbons well. This is due to fact that cubic EOS's are capable of predicting vapor phase properties more accurately than liquid phase properties. It can be noticed that the solubility of elemental mercury in propane is almost equal to that in butane. This implies that the solubility of mercury in light hydrocarbons in the gas phase is independent of carbon number. This suggests that the interaction of elemental mercury with methane or ethane is similar to that with propane and butane. This enables the estimation of mercury solubility in methane, as the experimental data are unavailable.

The binary interaction parameters of mercury in normal alkanes from C_5 to C_{10} are shown in Figure 4.6.

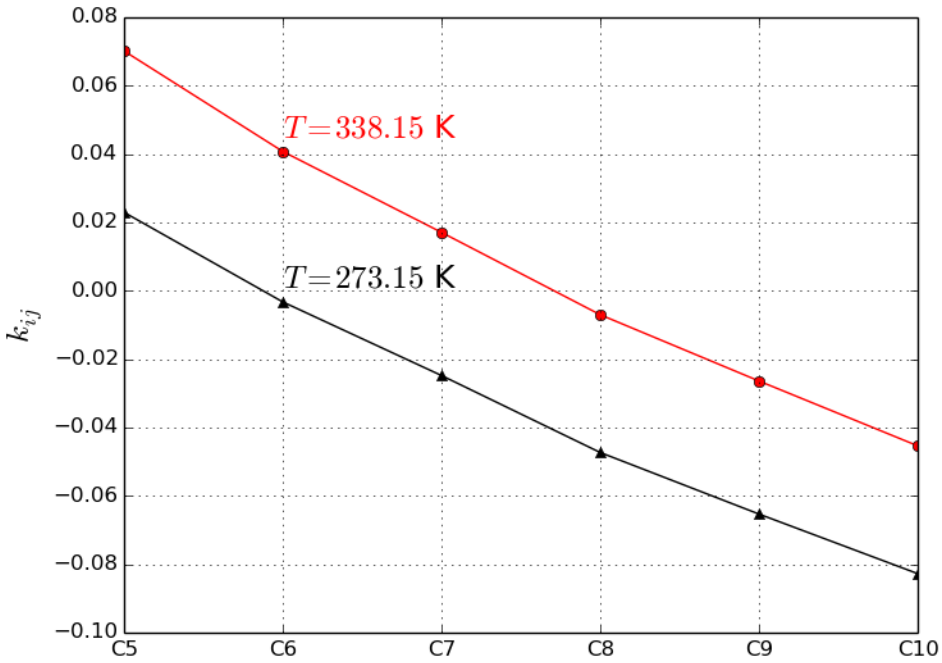

Figure 4.6: SRK EoS binary interaction parameter for mercury-alkane mixtures.

The interaction of mercury with these higher molecular weight alkanes depends on both the carbon number and temperature. Figure 4.6 clarifies that fixing the k_{ij} between mercury and normal alkanes, as assumed by Polishuk et al. [96, 97], leads to inaccurate solubility correlation.

4.2.4 Modelling the solubility of elemental mercury in aromatics using SRK EoS

Aromatics are considered to be the main raw material for many petrochemical industries [89]. The naphtha reforming process is one of main sources of aromatics. As crude oil and natural gas are the main sources of aromatics and crude oil is known to contain mercury, predicting the solubility of mercury in aromatics is vital of importance.

Figure 4.7(a) shows the solubility of elemental mercury in benzene, toluene, and *o*-xylene over a range of temperatures. The experimental data are taken from Ref. 87, which are shown as the symbols. The dashed lines are the correlations of the SRK EOS with $k_{ij} = 0$. It is clear that by neglecting the binary interaction parameters, the predicted solubility of elemental mercury in aromatics is relatively insensitive to the presence of methyl groups.

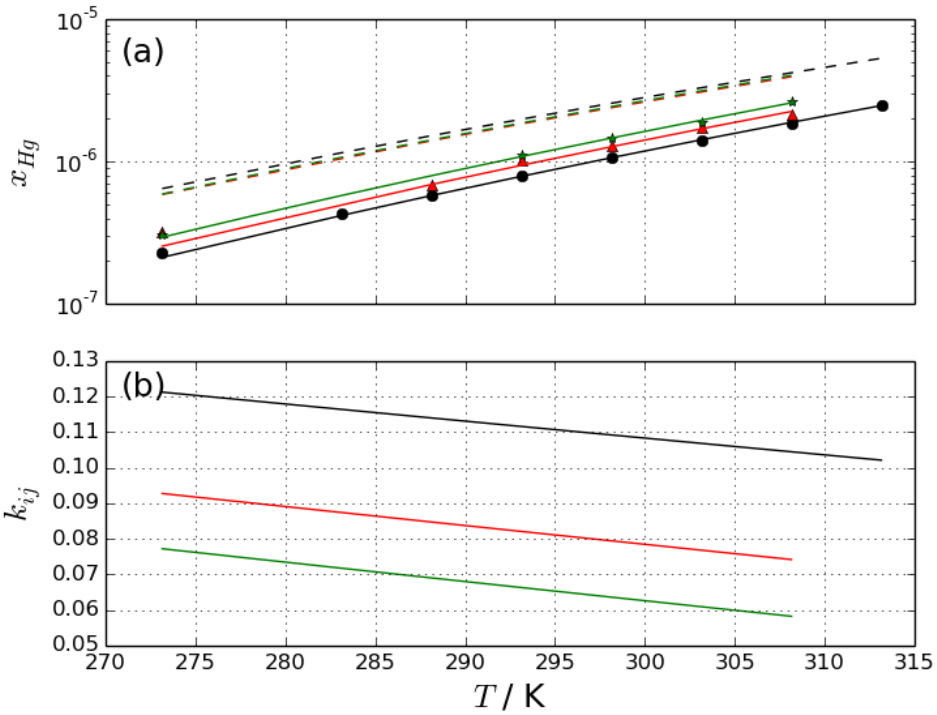

Figure 4.7: (a) Solubility and (b) binary interaction parameter of mercury with in benzene (black), toluene (red), and *o*-xylene (green)for SRK EoS. The symbols represent experimental data, taken from Ref. 87

Two types of interaction groups for benzene, toluene, and o-xylene were defined by dividing the carbons in the aromatic ring. One group ACH is an aromatic carbon that is attached to a hydrogen atom; benzene has six of these groups, while toluene has only five and o-xylene has four. The other group ACCH3 is an aromatic carbon attached to a methyl group; benzene has none of these groups, toluene has one, and o-xylene has two. The values of the interaction parameters of these groups with elemental mercury were fit to the solubility data for mercury in benzene and in o-xylene. These are summarized in Table 4.1.

The solid lines in Figure 4.7(a) show the solubilities calculated by the SRK EOS with the binary interaction parameters estimated by the group contribution method. As a test of the group contribution model, the binary interaction parameter between mercury and toluene was predicted based on the group interaction parameters obtained from mercury-benzene and mercury-o-xylene mixtures. The AARD for mercury in benzene, toluene, and o-xylene was 1.87% for 8 data points over a temperature range of 273.15 K to 313.15 K, 6.1% for 6 data points over a temperature range of 273.15 K to 308.15 K, and 2.7% for 5 data points over a temperature range of 273.15 K to 308.15 K and atmospheric pressure, respectively.

The results presented by Polishuk et al. [96] study in Fig. 4 show that the predicted solubility of mercury in toluene using PC-SAFT and PR EoS at 293.15°C was 0.91 ppm and 1.05 ppm, respectively, while the experimental solubility was 0.98 ppm. The value obtained in this work using the GCM and based on the group interaction parameters obtained from mercury-benzene and mercury-o-xylene mixtures was 0.94 ppm, which better reflects the experimental value. The GCM is capable of predicting binary interaction parameters of compounds where experimental data are unavailable.

By introducing binary interaction parameters, the solubility of elemental mercury in aromatics is found to increase with the number of methyl groups, which is consistent with what is experimentally observed. Figure 4.7(b) indicates that the interaction between mercury and aromatics is slightly independent of temperature.

4.2.5 Modelling the solubility of elemental mercury in alcohols using SRK EoS

Alcohols such as mono-ethylene glycol (MEG) and diethylene glycol (DEG) are widely used in oil and gas processing as anti-freeze and anti-corrosion agents; however, experimental data for the solubility of mercury in these alcohols are not available in the literature. One of the motivations of this work is to predict mercury solubility in such alcohols.

Experimental data are available for the solubility of mercury in methanol and isopropanol [91]. Figure 4.8(a) shows a comparison of the SRK EOS, with and without the binary interaction parameter, and experimental measurements for the solubility of mercury in methanol and isopropanol. Significant deviation can be observed between the experimental data and correlated results when $k_{ij} = 0$.

The group interaction parameters between elemental mercury and the OH group were determined by fitting experimental solubility data for alcohols (see Table 4.1). Figure 4.8(b) shows that the k_{ij} between mercury and isopropanol is more temperature dependent than methanol.

Using the group contribution method, the interaction between mercury and MEG or DEG can be easily predicted. As a test of the group contribution model, we predict the solubility of mercury in MEG. Large quantities of MEG are injected at the wellhead in order to avoid hydrate formation during transportation process. The partitioning of elemental mercury from a gas phase into MEG solutions was investigated under standard laboratory conditions [140]. It was observed that the solubility of elemental mercury in MEG ranged from 0 to 60 ppb. Using the SRK combined with GCM developed in this work to estimate k_{ij}, we predict that the solubility of mercury in MEG is 57.7 ppb. Using $k_{ij} = 0$, the solubility of mercury in MEG is 1.78 ppm. It is clear that the SRK combined with the GCM is able to predict mercury solubility in alcohol systems.

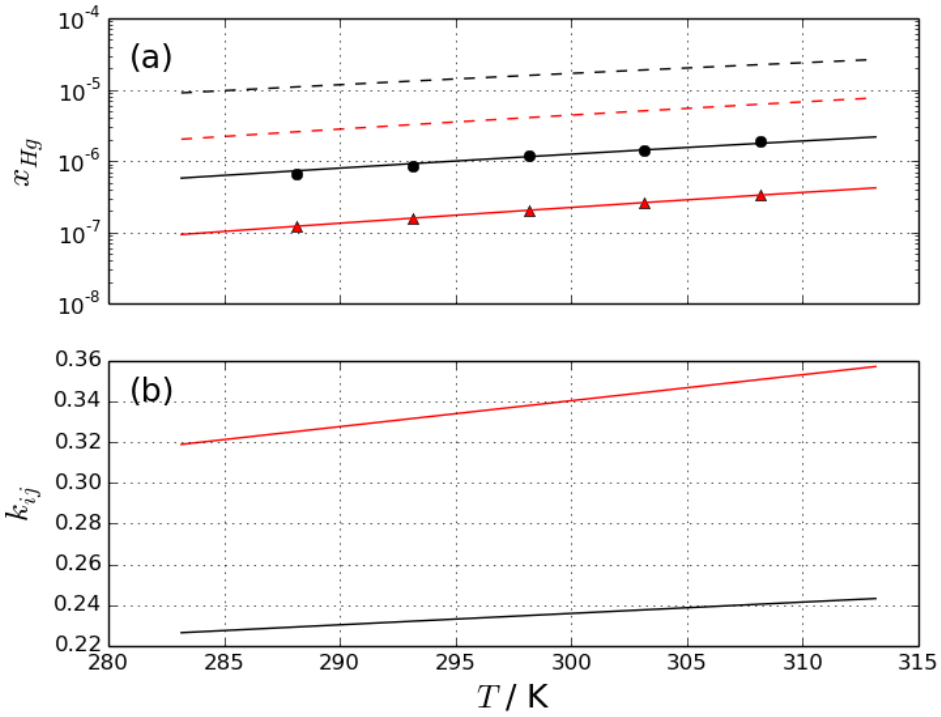

Figure 4.8: Solubility of mercury in methanol (black) and isopropanol (red). The symbols represent experimental data, taken from [91], the solid lines are predicted solubilities using SRK EoS with the binary interaction parameter estimated using the GCM, and the dashed lines are correlations with the binary interaction parameter set to zero.

4.2.6 SRK EoS model validation for predicting the soubility of elemental mercury in multi component systems

The SRK EoS in combination with GCM was validated for predicting the solubility of mercury in several pure solvents in the previous section but not for multicomponent mixtures. In order to validate the thermodynamic model for a multicomponent, Marsh et al. [44] data is used. Their study measured the solubility of elemental mercury in light hydrocarbon (LHC) and heavy hydrocarbon mixtures (HHC). Their measurements were used as a framework to validate SRK EOS for the solubility of mercury in LHC and HHC mixtures. In this work the process simulator Aspen Plus version 9.0 was used with the SRK EoS property package to validate this process.

Table 4.3 shows the composition of light and heavy hydrocarbon mixtures used

in the experiments of Marsh et al.[44]. Solubility measurements were made over the temperature range of $290.5\,\mathrm{K}$ to $359.5\,\mathrm{K}$ and pressure range of 50 bar to 95.8 bar for light hydrocarbon mixture and the temperature range of $308.9\,\mathrm{K} - 424.4\ \mathrm{K}$ and pressure range of $17.7 - 62.5$ bar for heavy hydrocarbon mixture.

Two scenarios were investigated; the first scenario was to predict the solubility of mercury in hydrocarbon mixtures using the SRK EoS without introducing binary interaction parameters k_{ij} between elemental mercury and other molecules. This scenario is the base case scenario. The second scenario was to introduce k_{ij} to the base case scenario. The k_{ij} values between elemental mercury and studied hydrocarbons were estimated at different temperatures based on GCM method discussed in Sec. 4.2. A linear temperature dependence relationship Eq. (4.2) for the k_{ij} was fit over awide range of temperatures ($273.15\,\mathrm{K} - 433.15\ \mathrm{K}$).

$$k_{ij} = k_{ij}^{(0)} + k_{ij}^{(1)} T \tag{4.2}$$

where k_{ij} is the binary interaction parameter, $k_{ij}^{(0)}$ and $k_{ij}^{(1)}$ are the equation coefficients, T is the absolute temperature in K, The linear relationship was chosen so that the model could be used in any process simulators.

Table 4.4 shows coefficients for the temperature dependence of Eq. (4.2) for each studied component. Methane was treated as CH_3 group instead of CH_4 when estimating the k_{ij} between elemental mercury and methane because there were no binary solubility data between mercury and methane in the open literature. The k_{ij} between elemental mercury and carbon dioxide, and elemental mercury and methylcyclohexane were set to zero for both scenarios because there was no binary solubility data for these molecules.

Once the composition of the hydrocarbon mixture and the k_{ij} coefficients between each component and elemental mercury are identified, they are then introduced in Aspen. Two streams were created and gathered then flashed in a three phase flash unit. The first stream contains hydrocarbon mixture, the second stream contains pure elemental mercury. Three outlet streams were connected to the flash unit; the gas stream represents light gases, the condensate stream represents heavy hydrocarbons and mercury

Table 4.3: Mole fraction of Hydrocarbon Mixtures. Taken from [44].

Component	LHC mole fraction	HHC mole fraction
carbon dioxide	0.1270	0.0
methane	0.465	0.259
ethane	0.0394	0.024
propane	0.0324	0.019
n-butane	0.0106	0.007
2-methylpropane	0.0219	0.015
n-pentane	0.0149	0.0187
2-methylbutane	0.0219	0.018
n-hexane	0.0178	0.0270
n-heptane	0.0168	0.0313
n-nonane	0.0776	0.1652
n-dodecane	0.0955	0.2653
n-hexadecane	0.0323	0.1011
methylcyclohexane	0.0255	0.0504

stream represents almost pure mercury. Both gas and condensate streams were gathered in one stream and then the solubility of elemental mercury in this stream was compared to the experimental data. The operating temperature and pressure conditions of each experimental data point were taken from Ref. 44. The feed flow rate for the hydrocarbon stream was set to $1\,\mathrm{g\,h^{-1}}$ and the first guess of pure elemental mercury flow rate was obtained by multiplying the experimental mercury concentration by $1\,\mathrm{g\,h^{-1}}$. Then pure mercury flow rate is increased until pure heavy phase of mercury is flashed out of the flash unit. This indicates that an equilibrium between mercury and hydrocarbon mixture is reached.

Figure 4.9 shows the predicted solubility of mercury in the LHC and HHC mixtures for both of the studied scenarios compared to experimental data. The predicted results demonstrates similar trend as that from experimental data where elemental mercury is more soluble in the HHC mixture than in the LHC for both investigated scenarios. The second scenario provides better results compared with the first one as it can be seen in Figure 4.9.

Table 4.4: Coefficients for the temperature dependence for Eq. (4.2)

Component	$k_{ij}^{(0)}$	$k_{ij}^{(1)}$ K^{-1}
carbon dioxide	0.0	0.0
methane	−0.2889	0.00112
ethane	−0.14413	0.00106
propane	−0.14458	0.00085
n-butane	−0.14782	0.00075
2-methylpropane	−0.17212	0.00111
n-pentane	−0.16555	0.0007
2-methylbutane	−0.1983	0.00101
n-hexane	−0.17833	0.00065
n-heptane	−0.19079	0.00061
n-nonane	−0.21873	0.00057
n-dodecane	−0.25231	0.00051
n-hexadecane	−0.3109	0.00049
methylcyclohexane	0.0	0.0
toluene	0.22193	−0.00053
water	−0.07311	0.00243

The use of SRK EoS in combination with GCM improves the solubility correlation of mercury in both light and heavy hydrocarbon mixtures. Without the use of GCM, the interaction between mercury and light, branched and long chain hydrocarbons such as methane, ethane, iso-butane, iso-pentane, and n-dodecane was impossible to estimate, as there is no experimental solubility data.

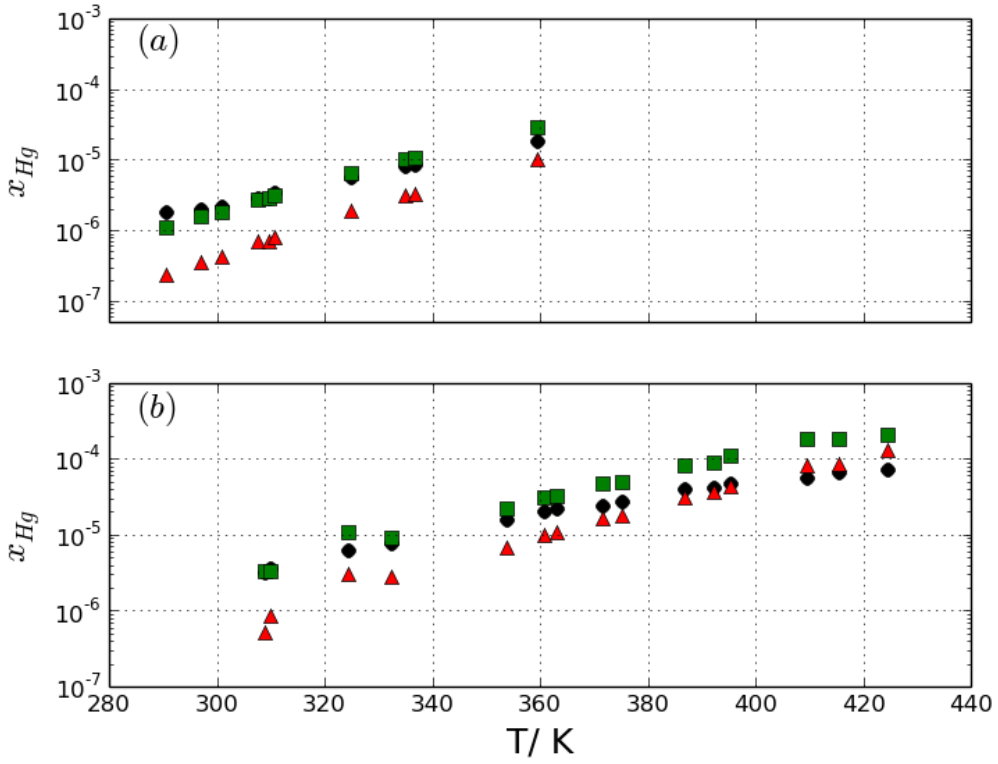

Figure 4.9: (a) Solubility of mercury in LHC mixture. The black symbols represent experimental data, taken from [44] at different pressures, and the red is the SRK correlation without k_{ij}, and the green symbols represent SRK correlation with k_{ij} estimated using the group contribution method. (b) Solubility of mercury in HHC mixture.

4.3 Thermophysical properties prediction using PC-SAFT EoS

The PC-SAFT EoS described in Chapter 3 in Sec. 3.7 was used to predict elemental mercury, water, some hydrocarbons, aromatics and alcohols vapor pressure and solubility. This equation takes into account the hard chain contribution, the dispersion, the association and the electrolyte interactions. Therefore, we will evaluate and compare its performance in predicting the thermophysical properties of elemental mercury against SRK EoS with GCM.

Two scenarios were investigated for the PC-SAFT EoS. In the first scenario, elemental mercury is considered as a non associating component. In other words, only the hard chain and dispersion contribution terms are considered to represent elemental mercury molecules behaviour. In the second scenario, elemental mercury is considered as a self associating molecule which means the association contribution term is taken into account with the hard chain and the dispersion contribution. In other words, elemental mercury molecules are assumed to be bonded with each other which leads to a bonding interaction. The PC-SAFT equations described in Sec. 3.7 were coded in Python for vapor-liquid equilibrium (VLE) and liquid-liquid equilibrium (LLE) using standard flash algorithms implemented to obtain the solubility of mercury S_i^{calc} using ϕ-ϕ approach. The required PC-SAFT parameters is usually obtained by fitting experimental vapor pressure data. The PC-SAFT parameters of the studied solvents were collected from the open literature a part from elemental mercury which will be obtained in the next section.

4.3.1 PC-SAFT prediction with non associating scenario

In the first scenario, elemental mercury atoms are treated as a non-associating molecule. Thus, the attraction and repulsion forces are the only forces that represent mercury molecules. This can be modeled by taking the hard chain and dispersion terms into account. Therefore, the general formula of PC-SAFT EoS, Eq. (3.72), becomes:

$$A^{res} = A^{hc} + A^{disp} \tag{4.3}$$

As an initial step in this scenario to ensure that the properties of the pure components, such as vapor pressure is properly described using the PC-SAFT EoS. In the next section, the vapor pressure of elemental mercury and the previous studied compounds will be predicted.

4.3.1.1 Modelling vapor pressure of pure components using PC-SAFT EoS

For non associating components, PC-SAFT EoS requires three pure component parameters σ, ε/k_B and m, as described in Sec 3.7. PC-SAFT parameters for elemental mercury

as a non−associating component were not available in the open literature. Therefore, the PC-SAFT parameters shown in Table 4.5 were detrimend for elemental mercury by fitting predicted vapor pressure to the experimental mercury vapor pressure data. The PC-SAFT parameters of other studied associated or non−associated components were obtained from Gross et al. [141] and [142] are reported in Table 4.5.

Table 4.5: PC-SAFT Pure component parameters

Molecule	T range K	Association Scheme	σ_i Å	ε_i/k_B K	m_i	$\varepsilon^{A_iB_i}/k$ K	$K^{A_iB_i}$	$Ref.$ Ref.
Mercury	293.49 – 414.92	None	3.9507	1004.21	1.0			this work
Mercury	293.49 – 414.92	2(1:1)	2.5193	610.0	1.0	2890.041	1.18619	this work
Mercury	293.49 – 414.92	4(2:2)	2.359	337.24	1.0	2447.5	0.31635	this work
propane	85– 523	None	3.6184	208.11	2.0020			[141]
n-butane	135– 573	None	3.7086	222.88	2.3316			[141]
n-pentane	143 – 469	None	3.7729	231.20	2.6896			[141]
n-hexane	177 – 503	None	3.7983	236.77	3.0576			[141]
n-heptane	182 – 623	None	3.8049	238.4	3.4831			[141]
n-octane	216 – 569	None	3.8373	242.78	3.8176			[141]
n-nonane	219– 595	None	3.8448	244.51	4.2079			[141]
n-decane	2243– 617	None	3.8384	243.87	4.6627			[141]
benzene	278– 562	None	3.6478	287.35	2.4653			[141]
toluene	178– 594	None	3.7169	285.69	2.8149			[141]
o-xylene	248– 630	None	3.7600	291.05	3.1362			[141]
methanol	178– 594	2(1:1)	3.23	188.9	1.5255	2899.5	0.035176	[142]
water	178– 594	2(1:1)	3.0007	366.51	1.0656	2500.7	0.034868	[142]
Isopropanol	185– 508	2(1:1)	3.2085	208.42	3.0929	2253.9	0.024675	[142]

Figure 4.10 represents the relative deviation in the vapor pressure with respect to temperature for pure mercury, methanol, isopropanol and water. It indicates that the PC-SAFT EoS with the dispersion term is capable of accurately predicting the vapor pressure of elemental mercury as a non associating molecule. Water and alcohols were also modeled using PC-SAFT and considered as self associating molecules with two associating sites $2(1:1)$ (one acceptor and one donor). The two associating site structure is widely used and recommended in describing water and alcohols properties using PC-SAFT EoS.

The AARD for 99 experimental data points of elemental mercury over a temperature range of 253.15 K to 773.15 K was 2.26%; the experimental data used in this work were taken from Refs. 126, 127, 128 and 129 which are the same experimental data used

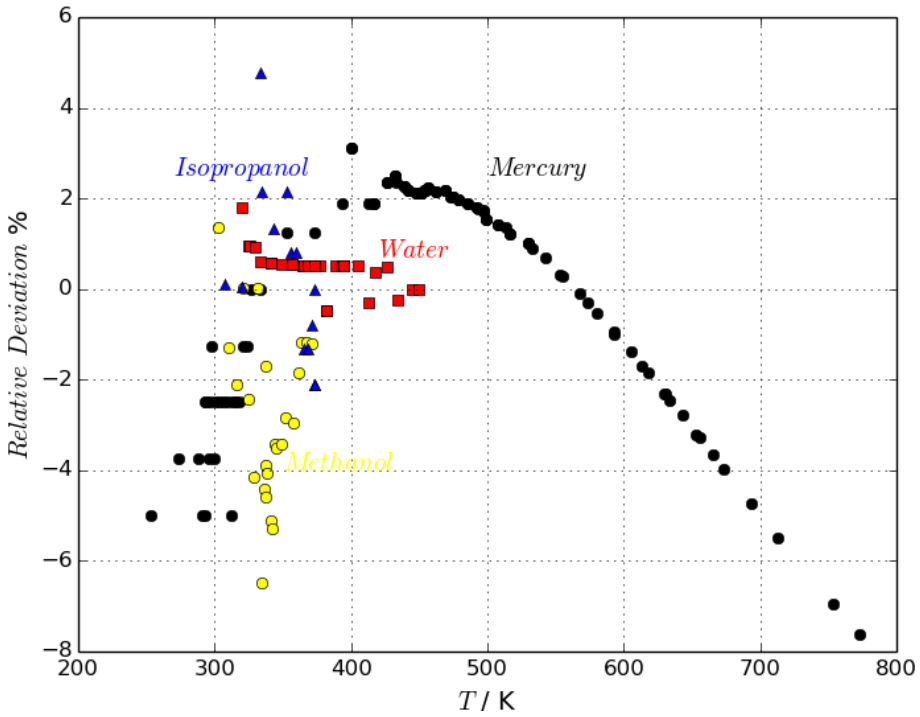

Figure 4.10: Relative deviation error between experimental and calculated values in vapor pressure using PC-SAFT for elemental mercury (black), water (red), methanol, (yellow), and isopropanol (blue).

for predicting the vapor pressure of elemental mercury using SRK EoS in the previous Sec. 4.2.1. The predictive capability of PC-SAFT EoS is better than of SRK EoS where the AARD was 3.7%

The AARD for the vapor pressure of water was 0.548% for 38 experimental data points over a temperature range of 319.6 K to 449.7 K; the experimental data were taken from Ref. 83 which is the same data used in Sec. 4.2.1. Modeling water as a self associating molecule with PC-SAFT reduces the AARD error to 1.95% compared to SRK EoS. This is due to the fact that, water hydrogen bonding plays an important role in modeling water molecules.

For methanol and isopropanol, the AARD was 2.84% for 24 data points and 1.42% for 14 experimental data points, respectively; the experimental data were taken from Refs. 131, 132 and 133 which are the same data used in Sec. 4.2.1. Almost the same

AARD obtained for methanol vapor pressure using PC-SAFT EoS and SRK EoS. For isopropanol, PC-SAFT EoS was more predictive than SRK EoS where the AARD was reduced by around 1.2%.

Figure 4.11 shows the relative deviation of the correlations of the PC-SAFT equation of state for the vapor pressure of some n-alkanes and aromatic compounds. The AARD for propane, n-pentane, and n-decane was 0.039% for 31 experimental data points, 0.36% for 50 experimental data points, and 2.65% for 32 experimental data points respectively. The experimental vapor pressure data were taken from Refs. 134, 135, and 136 which are the same experimental data used for SRK EoS correlation.

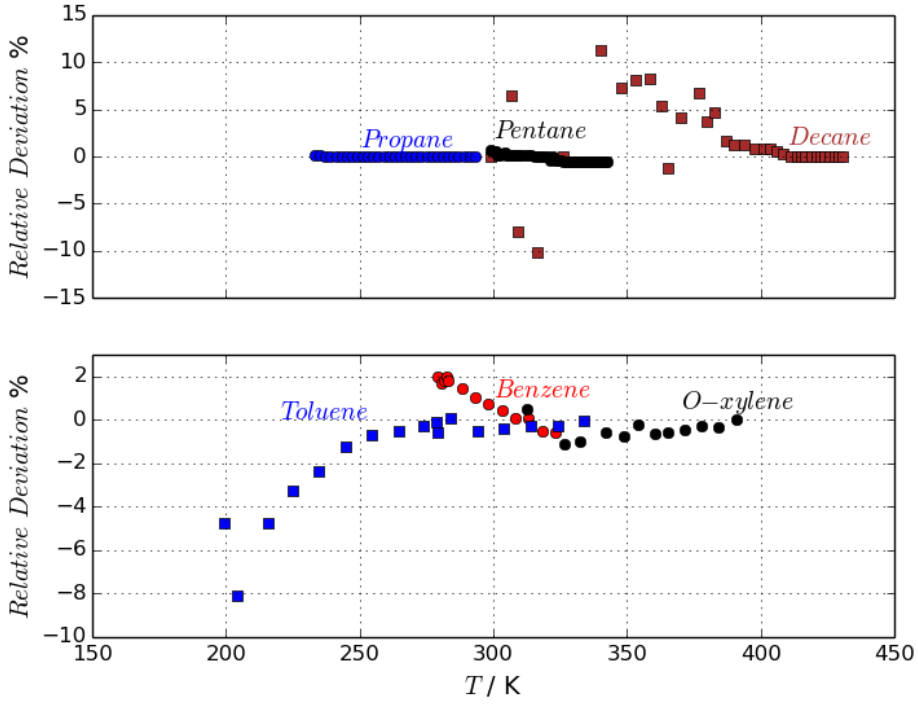

Figure 4.11: Relative deviation error between experimental and calculated values using PC-SAFT in the vapor pressure of (a) n-alkanes and (b) aromatic compounds.

In addition, the AARD for the vapor pressure of benzene, toluene, and o-xylene was 1.08% for 13 experimental data points, 1.6% for 17 data points, and 0.54% for 12 data points, respectively; the experimental vapor pressure data for aromatics were taken from Refs. 137,138, and 139. In terms of vapor pressure correlation, it is clear that

the PC-SAFT EoS is more effective than SRK EoS in predicting the vapor pressure of elemental mercury, alkanes, alcohols and water.

4.3.1.2 Modelling the solubility of elemental mercury in water using PC-SAFT EoS

Taking into account the hydrogen bonding of water molecules using PC-SAFT EoS has reduced its vapor pressure error compared to SRK EoS as shown in the previous section. This might reduce or eliminate the required binary interaction between elemental mercury and water for predicting mercury solubility in water. Figure 4.12(a) shows the solubility of elemental mercury in water using PC-SAFT EoS. The symbols

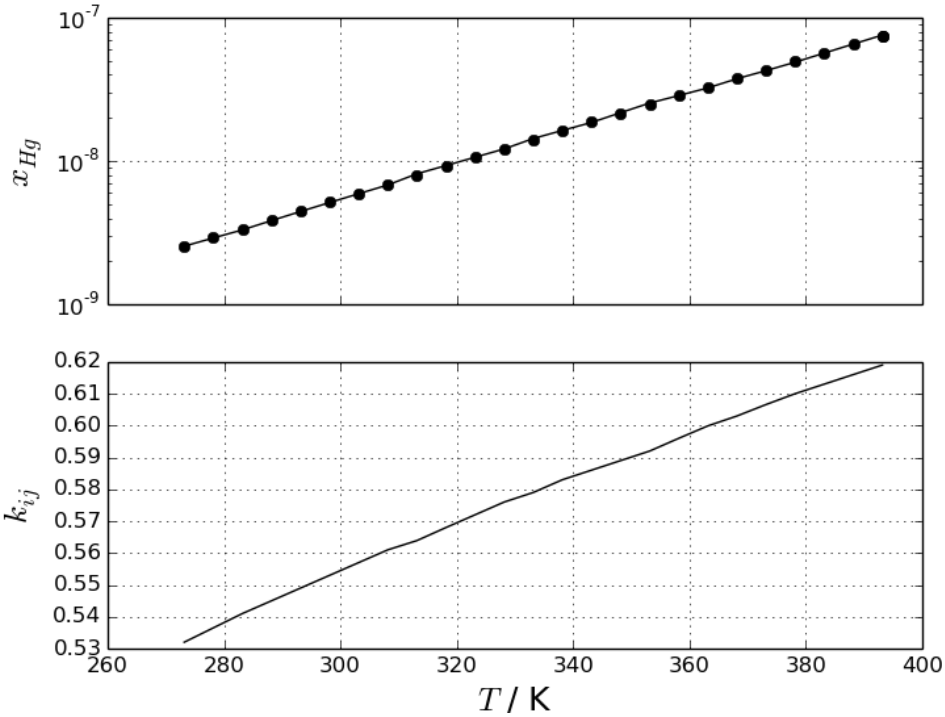

Figure 4.12: (a) Solubility of mercury in water. The symbols represent experimental data, taken from Ref. 91, The solid line is the correlation of the PC-SAFT EOS with k_{ij}. (b) The variation with temperature of the binary interaction parameter between mercury and water.

in Figure 4.12(a) represent the experimental data taken from Ref. 91, which are the same data used previously in predicting the solubility of mercury in water using SRK

EoS with GCM. The solid line in Figure 4.12(a) is the solubility of mercury predicted by the PC-SAFT EoS with binary interaction parameter. Binary interaction k_{ij} shown in Figure 4.12(b) was introduced into Eq 3.87 in order to represent the experimental solubility.

The AARD of 0.77% was obtained using PC-SAFT for 25 experimental data points compared to 4.7% using SRK EoS with GCM. A reduction of 4% in the AARD was obtained by modeling water as an associating molecule with PC-SAFT EoS. Modeling water as an associating molecule reduces the temperature dependence of the binary interaction parameter as shown in Figure 4.12(b) between mercury and water compared to its temperature dependence when SRK EoS was used.

4.3.1.3 Modelling the solubility of elemental mercury in normal alkanes using PC-SAFT EoS

Normal alkanes were modeled as a non associating molecules. The experimental data used in this work are shown as the symbols in Figure 4.13(a) and Figure 4.13(b) for alkanes from C_5 to C_{10}, and Figure 4.14(a) and (b) for C_3 and C_4. These data were taken from Ref. 87 and Refs. 88 which are the same references used for SRK GCM correlation.

Figure 4.13(a) and Figure 4.13(b) shows the predicted solubility of elemental mercury in normal alkanes from C_5 to C_{10}. The lines in Figure 4.13 are the solubilities represented by the PC-SAFT EoS, with introducing the binary interaction parameter k_{ij}. In order to accurately represent the solubility of elemental mercury in normal alkanes, temperature independent binary interaction parameters k_{ij} are required. The k_{ij} values in Table 4.6 were used for predicting the solubility of elemental mercury in the studied solvents.

Table 4.6: PC-SAFT elemental mercury$-$alkanes k_{ij}

Component	propane	n-butane	n-pentane	n-hexane	n-heptane	n-octane	n-nonane	n-dodecane
k_{ij}	0.45	0.45	0.375	0.37	0.365	0.361	0.357	0.355

Figure 4.14(a) and Figure 4.14(b) shows the predicted solubility of elemental mercury in propane C_3 and butane C_4.

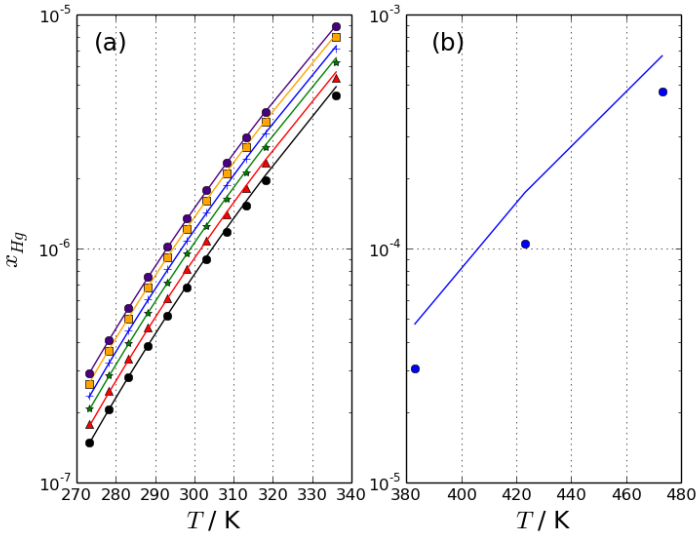

Figure 4.13: Solubility of mercury in normal alkanes: C_5 (black), C_6 (red), C_7 (green), C_8 (blue), C_9 (orange), and C_{10} (indigo). The symbols represent experimental data, taken from Ref. 87 and Refs. 88, the solid lines represent predicted solubility using PC-SAFT EoS without the association term.

By comparing the PC-SAFT results in Figure 4.14 with the SRK GCM results in Figure 4.5, it is clear that without introducing the k_{ij}, the SRK EoS is more effective than PC-SAFT as shown in the dashed lines. The AARD for the solubility in normal alkanes from C_3 to C_{10} was 4.28% for 74 experimental data points. The AARD for the solubility in normal alkanes from C_3 to C_{10} obtained by using PC-SAFT EoS is less than the AARD obtained by using SRK with GCM by 1.2%.

4.3.1.4 Modelling the solubility of elemetnal mercury in aromatics using PC-SAFT EoS

Figure 4.15 represents the solubility of elemental mercury in aromatic solvents over a range of temperatures. The experimental data are taken from Ref. 87, which are represented by the symbols.

The dashed lines are the correlations of the PC-SAFT EoS with $k_{ij} = 0$. The solid lines are the correlations of PC-SAFT EoS with an introduced k_{ij} in Table 4.7. The k_{ij} values in Table 4.7 were obtained by fitting the experimental solubilities.

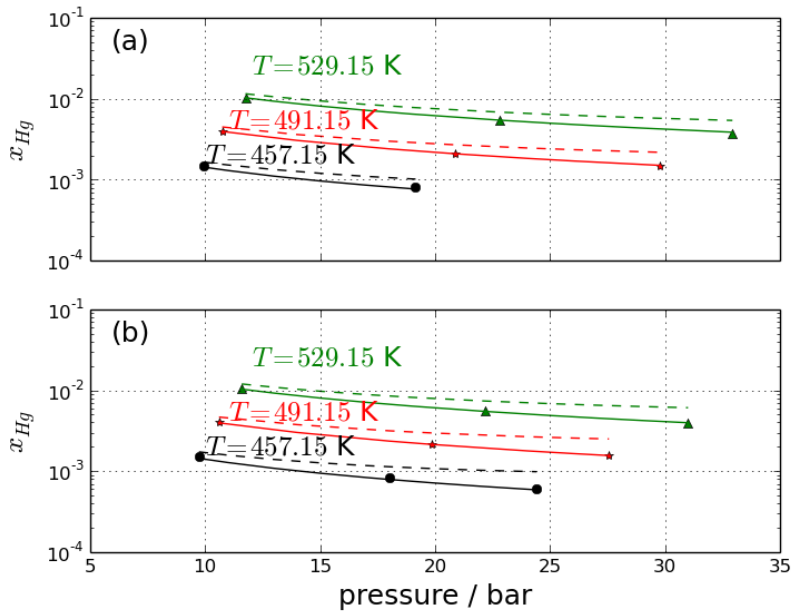

Figure 4.14: Solubility of mercury in (a) propane and (b) butane using PC-SAFT EoS. The symbols represent experimental data, taken from Ref. 87 and Refs. 88, the solid lines represent predicted solubility with the binary interaction parameters, and the dashed lines represent the solubility without introducing the binary interaction parameter.

Table 4.7: PC-SAFT elemental mercury and other solvents k_{ij}

Component	benzene	toluene	*o*-xylene	methanol	*iso*-propanol
k_{ij}	0.365	0.355	0.35	0.64	0.627

It is clear that by neglecting the binary interaction parameters, the predicted solubility of elemental mercury in aromatics are overestimated. The AARD for mercury in benzene, toluene, and *o*-xylene was 2.76% for 8 data points over a temperature range of 273.15 K to 313.15 K, 4.01% for 6 data points over a temperature range of 273.15 K to 308.15 K, and 3.42% for 5 data points over a temperature range of 273.15 K to 308.15 K and atmospheric pressure, respectively. The AARD for toluene using PC-SAFT EoS was reduced by around 1.5% but the AARD of benzene and *o*-xylene increased by 0.7% compared to SRK EoS.

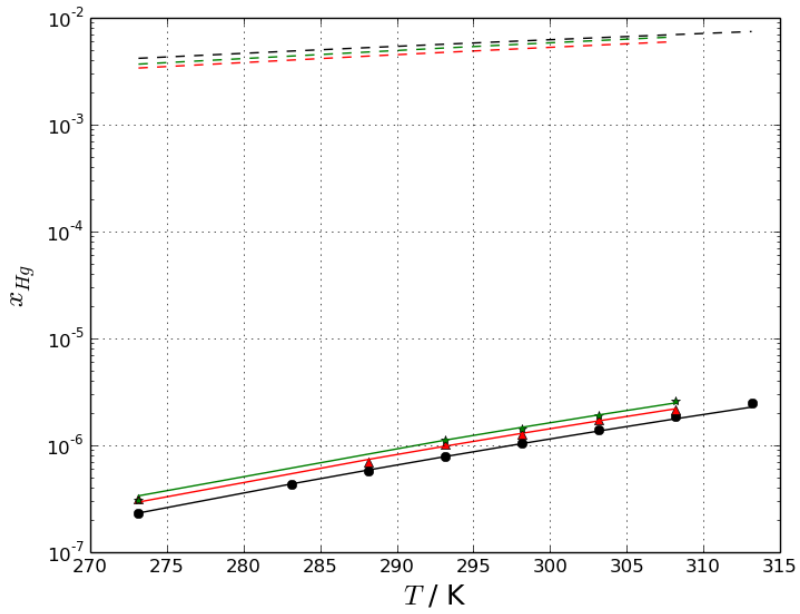

Figure 4.15: Solubility of mercury in benzene (black), toluene (red), and *o*-xylene (green), The symbols represent experimental data, taken from Ref. 87, the solid lines represent predicted solubility with the binary interaction parameters, and the dashed lines represent the solubility without introducing the binary interaction .

4.3.1.5 Modelling the solubility of elemental mercury in alcohols using PC-SAFT EoS

The solubility of elemental mercury in methanol and isopropanol was also predicted. Both alcohols were modeled as associating molecules with two sites 2(1:1). Figure 4.16 shows a comparison of the PC-SAFT EoS, with the binary interaction parameter, and experimental measurements for the solubility of mercury in methanol and isopropanol.

The experimental data taken from Ref. 91, which are the same data used previously in predicting the solubility of mercury in water using SRK EoS with GCM. The AARD for methanol was 4.85%; and for isopropanol was 2.77%.

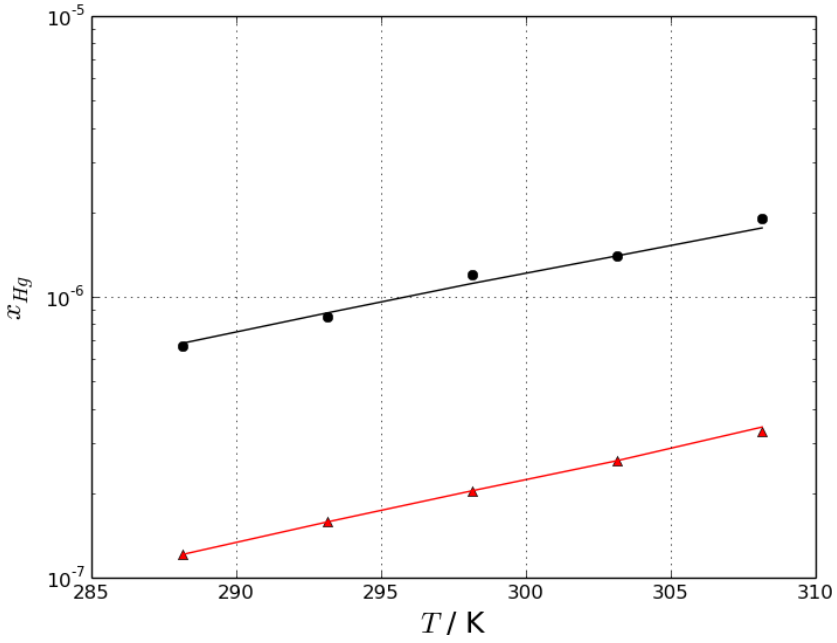

Figure 4.16: Solubility of mercury in methanol (black) and isopropanol (red). The symbols represent experimental data, taken from Ref. 91, the solid lines are predicted solubilities with the binary interaction parameter estimated using PC-SAFT

4.3.2 PC-SAFT EoS prediction with the associating scenario

In this scenario, elemental mercury is modeled as a monomeric molecule where elemental mercury atoms are bonded to each other with bonds like hydrogen bonds. This assumption might improve the PC-SAFT EoS correlation or eliminate the required binary interaction parameters. Two 2(1:1) and four 4(2:2) associating schemes for elemental mercury molecules were investigated in this section. Two more parameters $\varepsilon^{A_iB_i}/k_B$, and $K^{A_iB_i}$ were required in order to take the association term into account. The PC-SAFT parameters were obtained by fitting the experimental vapor pressure.

4.3.2.1 Modelling vapor pressure of pure components

The PC-SAFT parameters for pure elemental mercury as an associating component were not available in the open literature. Therefore, we determined the PC-SAFT pure component parameters, σ,ε/k, m, $\varepsilon^{A_iB_i}/k_B$, and $K^{A_iB_i}$ shown in Table 4.5 for elemental mercury for two and four associating sites by fitting to experimental data of mercury

vapor pressure.

Figure 4.10 indicates that significant improvement can be achieved by using PC-SAFT

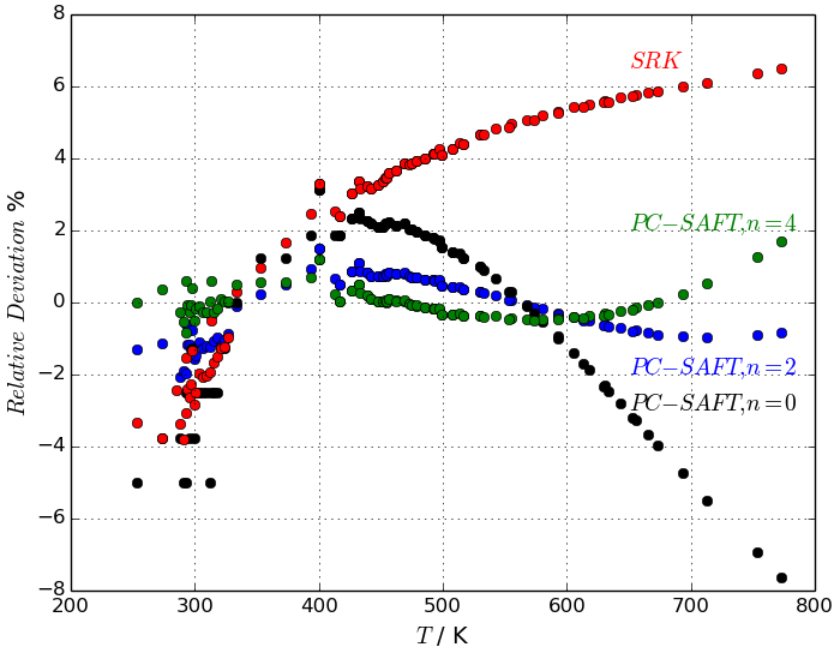

Figure 4.17: Relative deviation error between experimental and calculated vapor pressure using PC-SAFT and SRK for elemental mercury: SRK EoS (red), PC-SAFT without association (black), PC-SAFT with 2 associating site (blue), PC-SAFT with 4 associating site (green).

EoS by taking association contribution term into account. The AARD for 99 experimental data points of elemental mercury over a temperature range of 253.15 K to 773.15 K was 0.76% for two associating sites and 0.29% for four associating sites using PC-SAFT EoS . Modeling elemental mercury using PC-SAFT EoS is more predictive than SRK EoS. The AARD was reduced from 3.7% using SRK EoS to less than 1% using PC-SAFT with association contribution term.

4.3.2.2 Modelling the Solubility of elemental mercury in water using PC-SAFT EoS

Elemental mercury and water were modeled as a self associating molecules with 2(1:1) and 4(2:2) for elemental mercury and 2(1:1) associating site for water molecules. Fig-

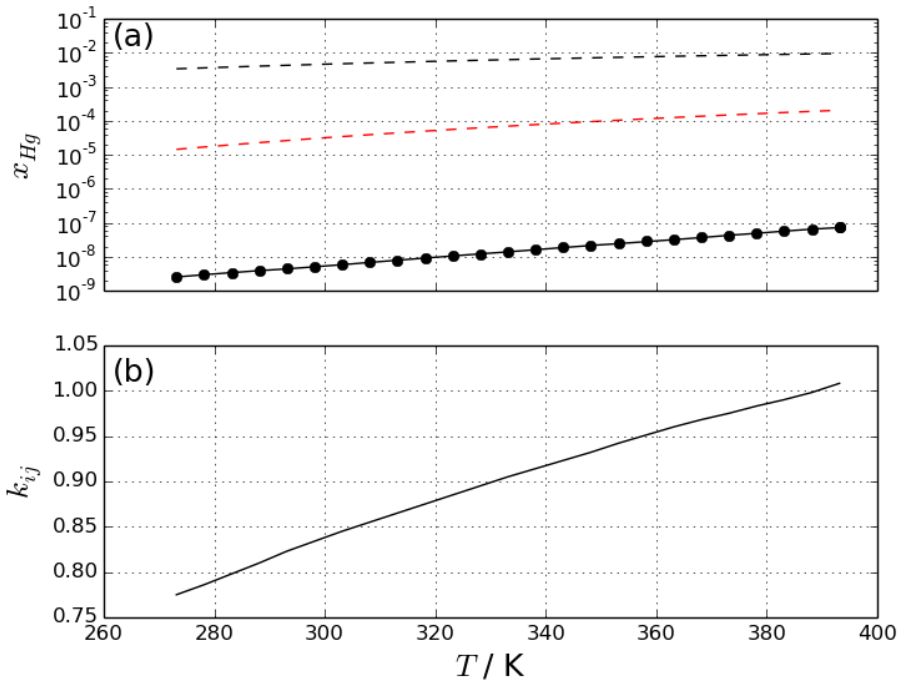

Figure 4.18: (a) Solubility of mercury in water using PC-SAFT EoS. The symbols represent the experimental data, the black dashed line is the correlation with 2(1:1) without k_{ij}, the red dashed line is the correlation with 4(2:2) without k_{ij}, and the solid line is the correlation with 2(1:1) with k_{ij}. (b) The variation with temperature of the binary interaction parameter between mercury and water.

ure 4.18 represents the solubility of elemental mercury in water. It indicates that binary interaction parameters k_{ij} are still needed between elemental mercury and water molecules for both two and four associating schemes. Without introducing k_{ij}, the solubility of mercury in water is poorly predicted. The dashed lines in Figure 4.18 (a) represent the predicted solubility when mercury has two associating sites, while the dotted dashed lines are the predicted solubilities using four associating sites. The symbols represent the experimental data which is the same experimental data used in previously. The solid line in Figure 4.18 (a) are the solubilities of elemental mercury with two associating sites after introducing k_{ij}. Figure 4.18(b) shows k_{ij} between elemental mercury and water. The k_{ij} between elemental mercury and water using PC-SAFT EoS is less temperature dependent than the k_{ij} required by SRK EoS.

The AARD was around 0.85% for 25 experimental data points by introducing k_{ij}

for two associating sites. By using PC-SAFT EoS and introducing binary interaction parameters, the AARD of mercury water system was reduced by around 4% compared to the SRK EoS.

4.3.2.3 Modelling the solubility of elemental mercury in normal alkanes using PC-SAFT EoS

Modeling elemental mercury as a self associating component with normal alkanes, improves PC-SAFT EoS correlation. Figure 4.19 and Figure 4.20 indicate that the solubility of elemental mercury in normal alkanes can be predicted without introducing k_{ij}, if mercury molecules were bonded by 2(1:1) sites. Around 65 experimental data points for C_5 to C_{10} over a temperature range of 273.15 K to 336.15 K and atmospheric pressure, and 3 experimental data points for C_8 over a temperature range from 338.15 K to 473.15 K and 6 bar. In addition to 17 data points for C_3 and C_4 at different temperatures and pressures.

Figure 4.19(a) and (b) show the predicted solubility of elemental mercury without association, 2(1:1) and 4(2:2) self associating sites in normal alkanes from C_5 to C_{10}. The dashed lines in Figure 4.19 are the solubilities predicted by PC-SAFT EoS without taking into account the association between mercury molecules. The solid lines in Figure 4.19 are the solubilities predicted with 2(1:1) self associating sites without binary interaction parameters. The dotted-dashed lines are the solubilities of elemental mercury with 4(2:2) self associating sites without introducing binary interaction parameters.

Figure 4.20 shows the predicted solubility of elemental mercury without association, 2(1:1) and 4(2:2) self associating sites in C_3 to C_4 at different pressures and temperatures. The dashed lines in Figure 4.20 are the solubilities predicted by PC-SAFT EoS without taking into account the association between mercury molecules. The solid lines are the solubilities predicted with 2(1:1) self associating sites without binary interaction parameters. The dotted dashed lines are the solubilities of elemental mercury with 4(2:2) self associating sites without introducing binary interaction parameters.

The AARD for the solubility of elemental mercury with 2(1:1) self associating sites in normal alkanes from C_3 to C_{10} was 6.95% for 74 experimental data points.

By comparing the PC-SAFT EoS results in Figure 4.19 with the SRK EoS with GCM results in Figure 4.4 for solubility of elemental mercury correlation, it is clear

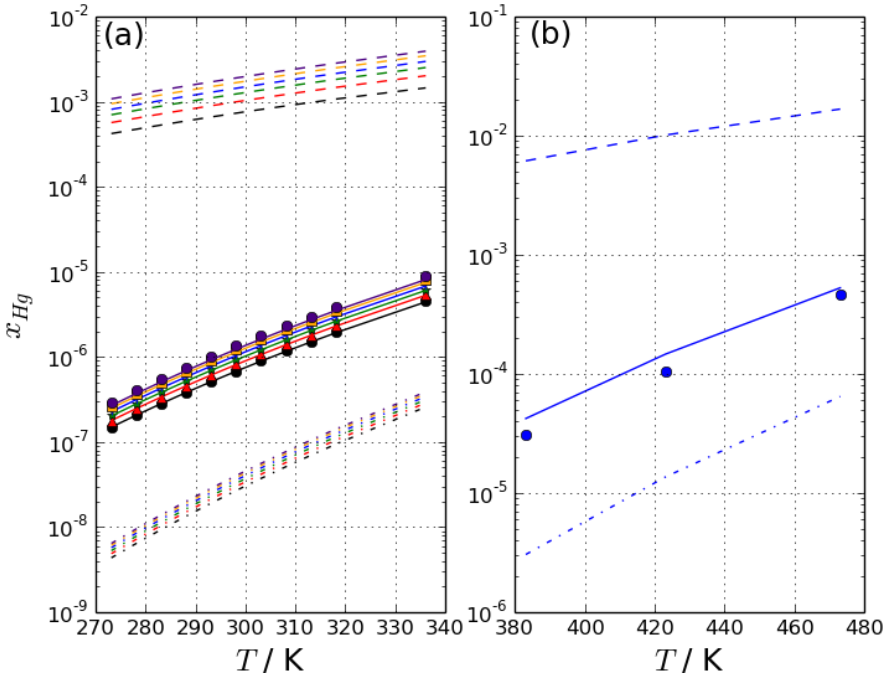

Figure 4.19: Solubility of mercury in normal alkanes: C_5 (black), C_6 (red), C_7 (green), C_8 (blue), C_9 (orange), and C_{10} (indigo). The symbols are experimental data, the dashed lines are predicted without association and k_{ij}, the solid lines are predicted using 2(1:1), and the used dotted-dashed lines are predicted using 4(2:2).

that the SRK EoS with GCM has less AARD than the PC-SAFT EoS with 2(1:1) by around 1.48% for 74 experimental data points. However, PC-SAFT EoS has the ability to predict the solubility of mercury in any alkanes unlike SRK EoS where methane is approximated by CH_3 group instead of CH_4 for its k_{ij} estimation.

4.3.2.4 Modelling the Solubility of elemental mercury in aromatics using PC-SAFT EoS

The aromatic compounds benzene, toluene and *o*-xylene were modeled as non−associating molecules like normal alkanes. Figure 4.21 shows the solubility of mercury in aromatics. It indicates that the solubility of elemental mercury in aromatics can also be predicted without introducing k_{ij}, when mercury atoms were bonded by 2(1:1) associating site.

The dashed lines in Figure 4.21 are the solubilities predicted by PC-SAFT EoS

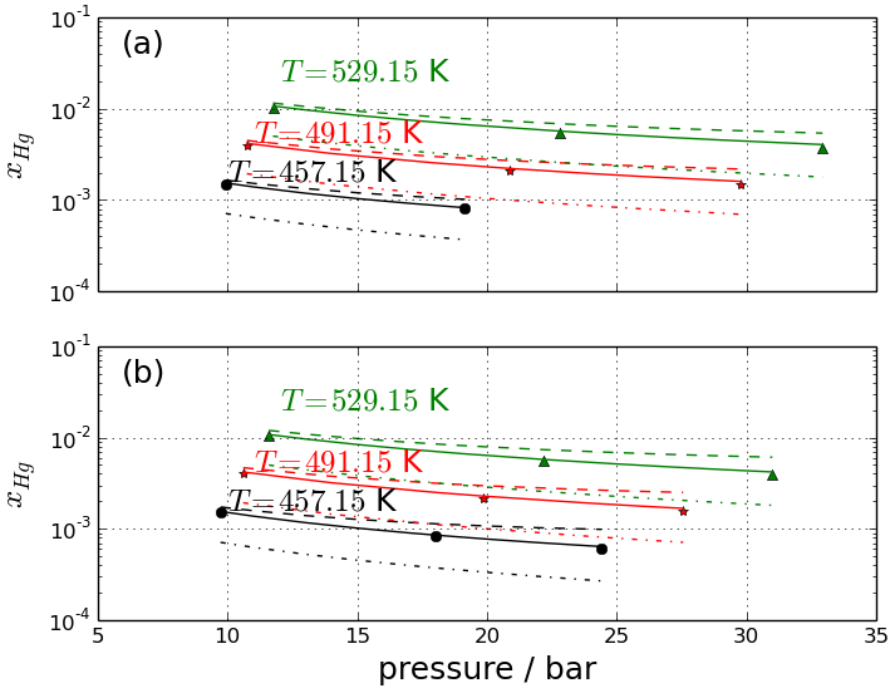

Figure 4.20: Solubility of mercury in (a) propane and (b) butane. The symbols are experimental data, the dashed lines are predicted without association and k_{ij}, the solid lines are predicted using 2(1:1), and the dotted-dashed lines are predicted using 4(2:2).

without taking the association into account between mercury atoms . The solid lines are the solubilities predicted with 2(1:1) self associating sites without binary interaction parameters. The dotted dashed lines are the solubilities of elemental mercury with 4(2:2) self associating sites without introducing binary interaction parameters. It is clear that in order to fit experimental data without taking into account the association contribution, a positive k_{ij} value has to be introduced in order to decrease the estimated solubility down as in the previous Sec 4.3.1.4. In the case of 4(2:2) sites, negative values for k_{ij} have to be introduced in order to increase the estimated solubilities.

4.3.2.5 Modelling the Solubility of elemental mercury in alcohols using PC-SAFT EoS

The solubility of elemental mercury in alcohols, methanol and isopropanol was also predicted. Alcohols are considered as a self associating molecules due to the hydrogen

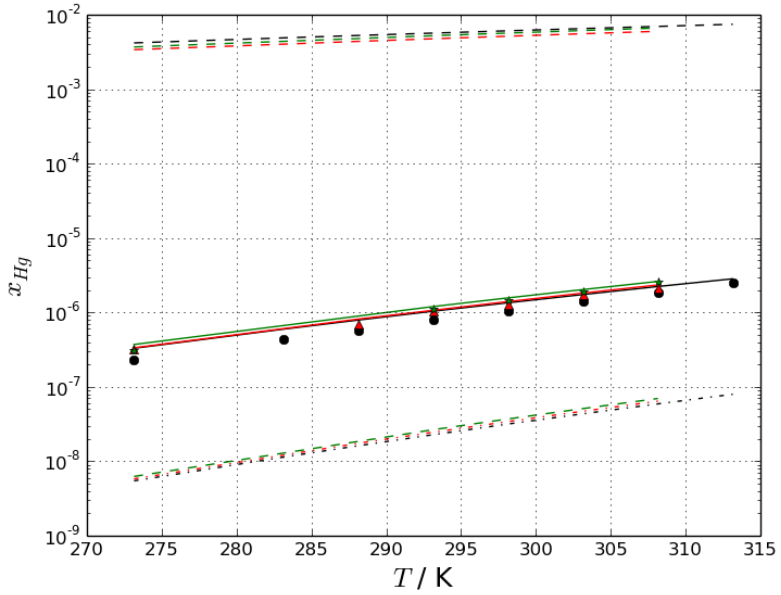

Figure 4.21: Solubility of mercury in benzene (black), toluene (red), and o-xylene (green). The symbols represent experimental data [87], the dashed lines are predicted solubilities using PC-SAFT EoS without association and introducing k_{ij}, the solid lines are predicted solubilities using PC-SAFT EoS with 2(1:1) association site, the dotted−dashed lines are predicted with 4(2:2) mercury association site

bonding in their structure. Gross and Sadowski [142] modeled those components as a self associating with 2(1:1) associating sites using PC-SAFT. Therefore both methanol and isopropanol were modeled in this section as a self associating molecules with 2(1:1) associating sites. The PC-SAFT pure component parameters for these components were taken from Gross and Sadowski [142] and are reported in Table 4.5 above.

Figure 4.22 shows that binary interaction parameters is required between elemental mercury and alcohols even if both elemental mercury and alcohol are considered as a self associating molecules.

The dashed lines in Figure 4.22 are the solubilities predicted by PC-SAFT EoS with 2(1:1) associating sites. The solid lines are the solubilities prediction with 2(1:1) associating sites with binary interaction parameters. The dotted-dashed lines are the solubilities of elemental mercury with 4(2:2) self associating sites without introducing binary interaction parameters. The AARD in the case of 2(1:1) with binary interaction parameters for methanol was 4.4%, and for isopropanol was around 2.23%.

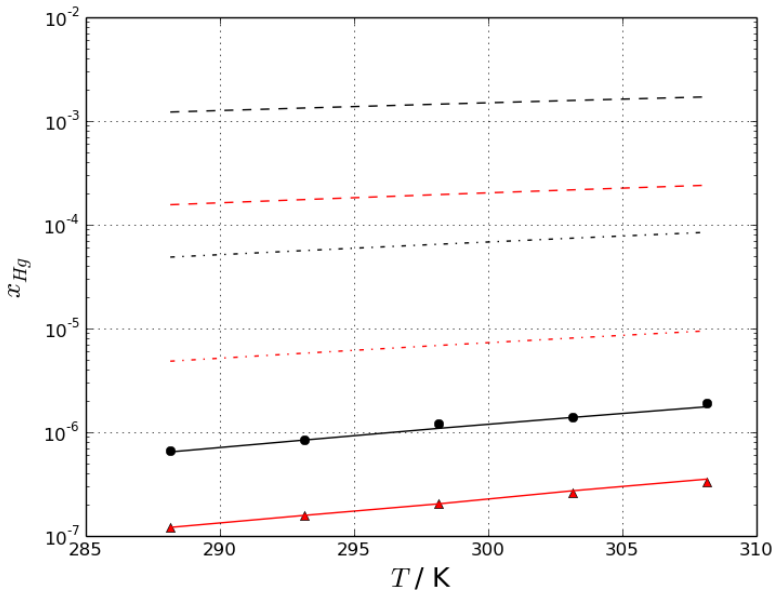

Figure 4.22: Solubility of mercury in methanol (black) and isopropanol (red). The symbols represent experimental data [91], the solid lines are predicted solubility with k_{ij} presented in Table 4.7 and the dashed lines are correlations with $k_{ij} = 0$ for 2(1:1) associating sites, and the dotted dashed lines are predicted solubilities with k_{ij} for 4(2:2) associating sites.

4.3.3 PC-SAFT model validation for predicting the solubility of elemntal mercury in multicomponent system

The PC-SAFT EoS was validated for predicting the solubility of mercury in light and heavy multicomponent hydrocarbon systems using the data of Marsh et al. [44], summarized in Table 4.3 which are the same data used for validating SRK with GCM.

In this work, Aspen Plus version 9.0 with the PC-SAFT EoS property package was used to validate this process. Two scenarios were investigated for validating PC-SAFT EoS. The first scenario was to model mercury as a non associating molecule and predict the solubility of mercury in hydrocarbon mixtures without introducing k_{ij} between elemental mercury and other molecules. The second scenario was to model elemental mercury as a self bonded molecules with 2(1:1) and 4(2:2) associating sites without introducing k_{ij} between elemental mercury and other molecules.

Figure 4.23 shows the predicted solubility of mercury in the LHC and HHC mix-

tures using PC-SAFT EoS for both of the studied scenarios and SRK with GCM compared to experimental data.

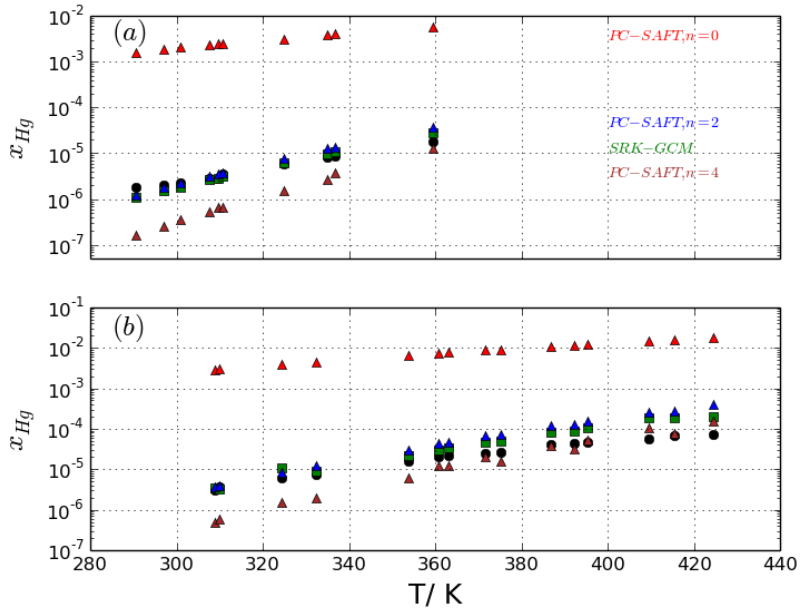

Figure 4.23: (a) Solubility of mercury in LHC mixture. The (black) symbols represent experimental data, (red) symbols are the PC-SAFT correlation without association, the (blue) symbols are PC-SAFT correlation with 2(1:1), the (brown) symbols are PC-SAFT correlation with 4(2:2), and the (green) symbols are the SRK with GCM. (b) Solubility of mercury in HHC mixture.

The results indicate that modeling elemental mercury as a non associating component using PC-SAFT without taking the k_{ij} into account leads to poor correlation. Elemental mercury with 2(1:1) self associating sites is the proper modeling scenario where there is no need to introduce k_{ij} between elemental mercury and alkanes and mercury and aromatic compounds. The results of SRK EoS with GCM are almost identical to PC-SAFT EoS with 2(1:1) associating sites. Modeling mercury molecules with 4(2:2) underestimates the solubility of mercury in hydrocarbons. Elemental mercury is more soluble in the HHC mixture than in the LHC for both investigated scenarios.

Modeling elemental mercury self associating with 2(1:1) associating sites improves

the ability of the PC-SAFT EoS to predict the solubility of elemental mercury in light and heavy hydrocarbons. This allows us to predict the behavior and the distribution of mercury when experimental data are unavailable. In the next chapter, the PC-SAFT EoS and SRK with GCM will be used for predicting the distribution of mercury in oil and gas processing facilities.

4.4 Conclusion

Predicting the solubility of mercury requires a predictive thermodynamic model that has the ability to predict the behaviour of mercury at different operating conditions. The use of SRK EoS in combination with GCM improves, the capability of SRK EoS to predict the solubility of mercury in several solvents. In this chapter, the group contribution method was parameterized to estimate the temperature dependent binary interaction parameters between elemental mercury and compounds composed of CH, CH_2, CH_3, OH, H_2O, ACH and $ACCH_3$ groups. By using these binary interaction parameters, the SRK EOS provides a good description of mercury solubility in water, alkanes, alcohols, and aromatic solvents, as compared to available experimental data. The group contribution method allows the estimation of k_{ij} of elemental mercury with a wide variety of solvents and solvent mixtures, even when experimental data are not available. It can also be used to estimate the binary interaction parameters of long chain hydrocarbon molecules as examined in Sec. 4.2.6. The group interaction parameters are already available for a wide range of systems [110, 114] and [111], making this approach immediately usable in practical applications.

The drawback of the SRK EoS with GCM that need experimental data for light hydrocarbons such as methane in order to accurately estimate its group interactions with mercury.

For the PC-SAFT EoS capability, its solubility correlation was improved by taking the association term into account. Modeling mercury atoms as a self bonded molecules with 2(1:1) associating sites discards the binary interaction parameters between elemental mercury and hydrocarbon compounds. Not only that but it also improves elemental mercury vapor pressure estimation compared to SRK EoS results. It also reduces the temperature depends of water mercury binary interaction parameters where less change in the binary interaction parameters is required. On the other hand, PC-SAFT EoS still

requires binary interaction parameters between mercury and some solvents, as water and alcohols. This drawback reduces the capability of the PC-SAFT EoS for solubility correlation outside experimental measured range. Therefore, it is recommended to take the PC-SAFT EoS electrolyte term into account while modeling electrolyte solvents, such as water and alcohols which might eliminate the binary interaction parameters.

In general, improper modeling or estimates for k_{ij} can yield extremely poor results; for instance, setting $k_{ij} = 0$, the SRK predicts that the solubility of mercury in water at 298 K is 3,374 ppm, compared to the experimental value of less than 1 ppm.

Both SRK in combination with GCM and PC-SAFT EoS's are used to predict the distribution of mercury in oil and gas processing facilities in the next chapter.

Chapter 5

Mercury distribution in an oil and gas processing plant

5.1 Introduction

Crude oil and natural gas are mixture of light and heavy hydrocarbons. This mixture of hydrocarbons can be associated with undesirable components, such as water, carbon dioxide, hydrogen sulfide and mercury. The light, heavy hydrocarbons and water mixtures are separated in a gas oil separation process into a light gas hydrocarbons, light liquid hydrocarbons which are called condensate, heavy liquid hydrocarbons which are called crude oil and water which is called produced water or oily water. The gas oil separation process consists of several processing units, such as separation, heating and cooling units, compression and pumping. The type and the number of these facilities depend on the nature of the hydrocarbon mixture, pressure and temperature of the fluid mixture, and also the presence of the undesirable components. The undesirable components have to be removed and captured prior to export because of their toxicity and corrosivity. The distribution of acid gases, carbon dioxide and hydrogen sulfide is clearly known where the sweetening process is allows located on the gas streams but the distribution of mercury in oil and gas is scattered between the phases which leads to improper location of mercury removal units. A proper mitigation strategy of mercury risks requires knowledge of the solubility of mercury in solvents, multi component systems and process streams. In order to protect the oil and gas processing facilities from

mercury risks and damage, understanding the distribution of mercury in the processing streams is of central importance. Therefore a thermodynamic prediction of mercury distribution in an ideal hydrocarbons mixture under real operating conditions is required. The thermodynamic models SRK EoS and PC-SAFT EoS described in Chapter 3 and used in Chapter 4 for predicting the solubility of mercury in binary and multi components system, need to be validated for real plant data. A gas oil separation plant called Obaiyed gas plant has been selected for validating both models in this chapter.
Therefore, this chapter is structured to provide an overview of Obaiyed gas plant and its processing facilities with an emphasis on its operating conditions and capacity. Then the distribution of elemental mercury through its processing facilities were predicted using both the widely used SRK EoS in combination with GCM, and PC-SAFT EoS. Afterward, the predictive ability of SRK and PC-SAFT models for mercury distribution was validated against the experimental data. The proper optimal location of mercury removal unit and its removal technique were identified. Finally, the benefits and the drawbacks for the use of both models will be highlighted.

5.2 Obaiyed gas processing plant

The Obaiyed gas processing plant is located in the western desert of Egypt and is the largest gas plant in that area, where it processes around 30% of the total western desert production [61]. It was designed to handle a daily contract quantity of 360 to 420 MMSCFD (million standard cubic feet per day) of a sales gas at 100 bar export pressure [61, 143, 144]. The production from different wells is gathered in one trunk line and then routed to the feed inlet of the Obaiyed processing facilities. Afterwards, the inlet stream is split into two streams and fed to two trains in order to handle a design capacity of 210 MMSCFD per train [144]. The current operating capacity of the plant is around 183 MMSCFD of gas and 15 m^3/h of condensate production per train [143].

Figure 5.1 shows the process flow diagram of the main facilities of one train, taken from Ref. 143. The distribution of elemental mercury and other mercury species was experimentally measured throughout this gas processing plant by Ezzeldin et al. [143]. Therefore, Obaiyed gas processing plant was selected as our case study for modeling the distribution of elemental mercury in oil and gas processing facilities. The blue values

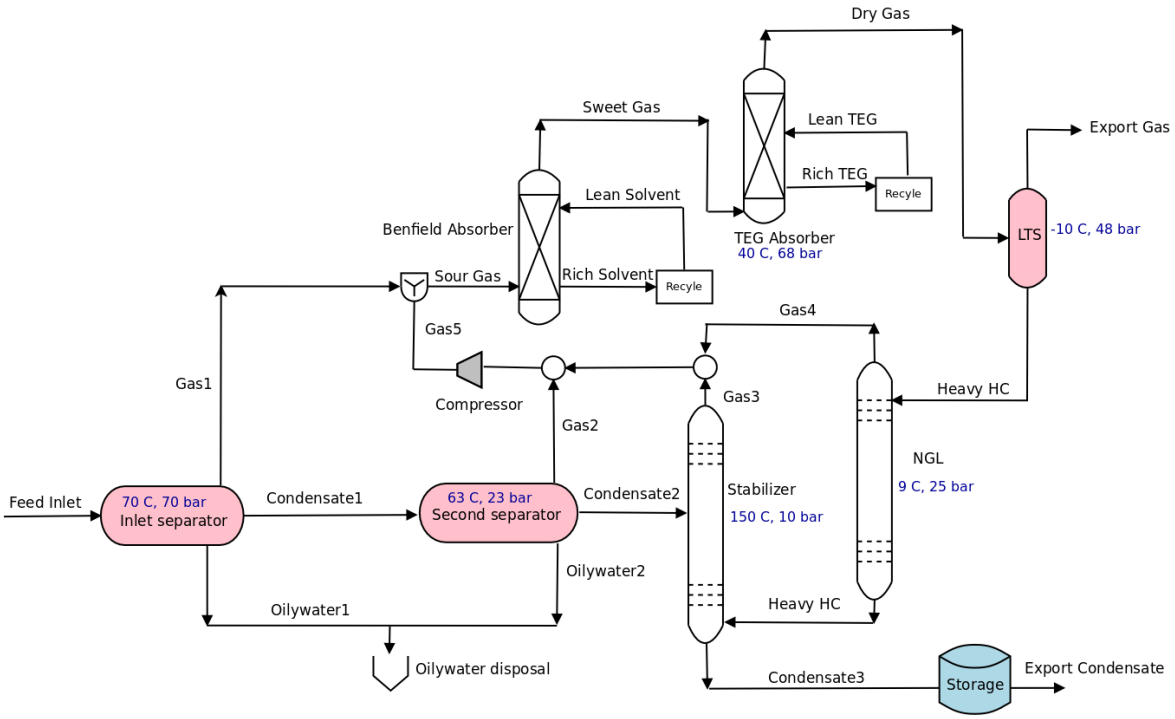

Figure 5.1: Obaiyed natural gas process flow diagram

in Figure 5.1 represent the operating conditions given in Ref. 143.

As shown in Figure 5.1, the processing facilities consist of two three-phase separators, a stripping column, acid gas removal unit, dehydration unit, low temperature separator (LTS) and storage facilities. The feed which contains light, heavy hydrocarbons and water is initially flashed in an inlet separator. The feed composition of Obaiyed gas plant was not provided in the studies that carried out by Ezzeldin [61, 143]. However, around 50 samples at different stages of Obaiyed gas plant were analysed to determine the chloride ion and hydrocarbon compositions by El Naggar et al. [144]. The hydrocarbon compositions of Obaiyed feed were characterized into six general groups by Ref. 144 as shown in Table 5.1 into; C_1 which represents methane, C_{2-5} represents light hydrocarbons from ethane to n pentane, C_{6+} represents $n-$ hexane and other hydrocarbon components heavier than $n-$ pentane, CO_2 represent carbon dioxide, N_2 represents nitrogen, and BTX represents aromatic compounds (benzene, toluene and xylene). The experimental analyses of these components in the gas and condensate were reported by El Naggar et al. [144] as shown in Figure 5.2. This characterization is difficult

to be used in any process simulators unless critical properties, density and molecular weight of the six groups were defined. Therefore, it was assumed that Obaiyed feed composition contains methane, ethane, propane, $n-$ butane, iso-butane, $n-$pentane, $iso-$pentane, carbon dioxide, nitrogen, $n-$hexane which represents C_{6+} and toluene which represents BTX as there was no information related to C_{6+} and BTX physical properties in Ref. 144 .

Table 5.1: Obaiyed plant feed characterized groups. Taken from Ref. [144].

group	Gas(Exp) mass%	Condensate (Exp) mass%
N_2	2.0	0.0
C_1	58.0	5.0
CO_2	13.0	2.0
C_{5+}	25.0	65.0
C_{6+}	2.0	14.0
BTX	0.0	14.0

The produced gas stream (Gas1) in Figure 5.1 is sent for further gas treatment, the condensate stream (Condensate1) is routed to a second three phase separator for further separation and stabilization, and the oily water stream (Oilywater1) is sent to water disposal. The flashed gas stream from the second separator (Gas2) is compressed and gathered with produced gas from the first separator. The condensate stream (Condensate2) from the second separator is further stabilized in a stripping column prior to export and storage (Condensate3). The flashed gas from the stripping column stream (Gas3) is gathered with the produced gas from the second separator and compressed via a compression unit (Compressor). The flashed gases (Gas1,Gas2,Gas3,Gas4) were gathered in one stream (Sour Gas) and sent to the acid gas removal unit (Benfield absorber) in order to capture carbon dioxide, the sweet gas is flashed out from the top of the unit while the rich solvent from the bottom of the unit (Rich solvent stream). The gas is routed to the dehydration unit shown as (TEG Absorber) in Figure 5.1 where the remaining water is removed. The dry gas from the dehydration unit was sent to low temperature separator (LTS) for hydrocarbon dew point control prior to export. The heavy hydrocarbons from the LTS unit is sent to NGL column in order to separate light

gases from condensate.

Table 5.2 shows the experimental measurements of total mercury (HgT) and some of mercury species, elemental mercury (Hg^o), inorganic mercury species (i-Hg) and Methymercury (MeHg) conducted by Ezzeldin et al. [143].

Table 5.2: Concentration of mercury species in the process streams. Taken from Ref. [143].

Stream	HgT	Hg^o	i-Hg	MeHg	sum of Hg species
Condensate1 (ng g^{-1})	1117 ± 42.9	554 ± 25.8	84 ± 6.65	11.4 ± 0.66	650 ± 50.5
Condensate2 (ng g^{-1})	154 ± 1.56	24.5 ± 1.75	66.3 ± 5.34	9.23 ± 0.46	100 ± 5.85
Condensate3 (ng g^{-1})	31.2 ± 1.28	9.75 ± 0.88	19.4 ± 1.19	4.29 ± 0.33	33.4 ± 1.98
Export Condensate (ng g^{-1})	26.7 ± 1.22	7.91 ± 0.66	12.4 ± 0.73	4.33 ± 0.47	24.6 ± 1.64
Oilywater1 (ng g^{-1})	31.2 ± 2.33	– – –	– – –	– – –	– – –
Oilywater2 (ng g^{-1})	37.7 ± 2.46	– – –	– – –	– – –	– – –
Gas1 (µg/Sm^3)	1.25 ± 0.39	– – –	– – –	– – –	– – –
Gas2 (µg/Sm^3)	37.2 ± 9.65	– – –	– – –	– – –	– – –
Gas3 (µg/Sm^3)	31.2 ± 1.28	– – –	– – –	– – –	– – –
Gas5 (µg/Sm^3)	41.6 ± 7.66	– – –	– – –	– – –	– – –
Sweet Gas(µg/Sm^3)	11.6 ± 3.04	– – –	– – –	– – –	– – –
Dry Gas(µg/Sm^3)	9.61 ± 1.88	– – –	– – –	– – –	– – –
Export Gas(µg/Sm^3)	4.11 ± 0.29	– – –	– – –	– – –	– – –

The elemental mercury was measured using WA-4 mercury analyzer (Nippon instruments Co., Japan) as reported by Ezzeldin et al. [143]. While the total mercury measurements were carried out using cold vapour atomic fluorescence spectroscopy (CV-AFS) technique. Mercury species were determined using Gas Chromatograph.
The types of inorganic mercury species (i-Hg) were not identified in Ezzeldin et al. measurements. However, they concluded due to the non volatile nature of (i-Hg) in the condensate streams, that mercury is associated with sulfides such as HgS instead of $HgCl_2$. Table 5.2 shows that the concentration of the measured total mercury (HgT) in the condensate streams are more than the sum of mercury species concentrations. This was attributed to the sampling preparation steps (derivatization reagent), solvent degradation and the use of CV-AFS technique [143, 145]. Mercury species in the oily water and gas streams were not measured by Ezzeldin et al. as indicated in Table 5.2. To identify elemental concentration in the gas and water streams, the following assumptions were taken into account: The concentration of elemental mercury in the condensate

stream was around 85% of the total sum of mercury species. As the elemental mercury is volatile specie, its concentration in the gas streams should be equal or more than 85% , therefore it was assumed in this study that 85% of the total mercury in the gas streams was elemental mercury. Because of the fact that, there are another mercury species in the feed such as organic and inorganic species and theses species have the ability to be in the gas phase even with small amount assuming 100% elemental mercury is not correct. The concentration of elemental mercury to the total mercury species in sea water and rivers were measured and it accounts for 30% to 90% as reported by Boszke et al. [146]. Therefore, it is assumed that 60% of the total mercury (HgT) in the oily water streams is elemental mercury.

5.3 Process simulation model and validation

In order to simulate any process, the feed composition, flow rate, pressure, and temperature are required. The feed composition of Obaiyed gas plant was not provided in the studies that carried out by Ezzeldin [61, 143]. Therefore the challenging step now is to obtain the mole or the weight percentage of each proposed component in the feed. This can be obtained by knowing the percentage of each group in the feed which was measured by Ref. 144 in Table 5.1, the components in the group which is already identified in the previous section, the current gas 183 MMSCFD and the condensate production 15 m^3/h of the plant per train reported by Ezzeldin et al. Ref. 143. Identifying the current production capacity of the plant is of vital importance as it impacts the calculated mercury pathways in various phases. The water production rate was not reported in Ref. 143, but it was reported in Ref. 147 that Obaiyed produces 900 bwpd (barrels of water per day).

Six groups were created, gathered and then flashed in a unit. The first group contains methane only, the second group contains hydrocarbons from ethane to $n-$pentane, the third group contains $n-$ hexane only, the fourth group contains carbon dioxide, the fifth group contains nitrogen, and the sixth group contains toluene. As a first step in this process, the flow rate of each group was set to 1 kg h^{-1}. An equimolar mixture in the second group was initially assumed as its a multicomponent group. Afterward, the flow rate of each group and its component composition were adjusted until the percent-

age of each six groups in the gas phase and liquid phase matches its reported values. The heavy components, such as n-pentane and iso-pentane in the second group were adjusted first as they represent most of condensate stream composition. In the gas phase methane is the most dominant component, if its concentration was indeterminate, the current gas production will not be meet. The percentage of propane, n-butane and iso-butane have less impact than pentane on meeting the production capacity. The obtained composition was then feed to the Obaiyed gas plant case where the current production of the plant was investigated. These steps were repeated until the current production and the percentage of each group are met. The results of this analyses were compared with the measured values provided by Ref. 144 as shown in Figure 5.2 and summarized in Table 5.3.

Table 5.3: Estimated hydrocarbon feed composition to Obaiyed plant.

group	Component	feed mole (%)	Gas(Exp) weight%	Condensate (Exp) weight %
N_2	nitrogen	1.06	2.0	0.0
C_1	methane	80.2	58.0	5.0
CO_2	carbon dioxide	5.4	13.0	2.0
C_{5+}	ethane	1.14	25.0	65.0
	propane	0.57		
	n-butane	0.57		
	iso-butane	0.57		
	n-pentane	4.00		
	iso-pentane	4.59		
C_{6+}	n-hexane	0.97	2.0	14.0
BTX	toluene	0.72	0.0	14.0

The process flow diagram of Obaiyed gas processing plant in Figure 5.1 was built in Aspen Plus version 9.0 as the hydrocarbons feed compositions; operating conditions were defined. The Benfield sweetening process was used to capture carbon dioxide from the produced gas. There was not enough information about this unit in the open literature, such as solvent flowrate, concentration, and its reaction mechanism. Therefore this gas sweetening unit was excluded from the simulation.

Three feeds, hydrocarbon, water, and mercury, were created and mixed. The hy-

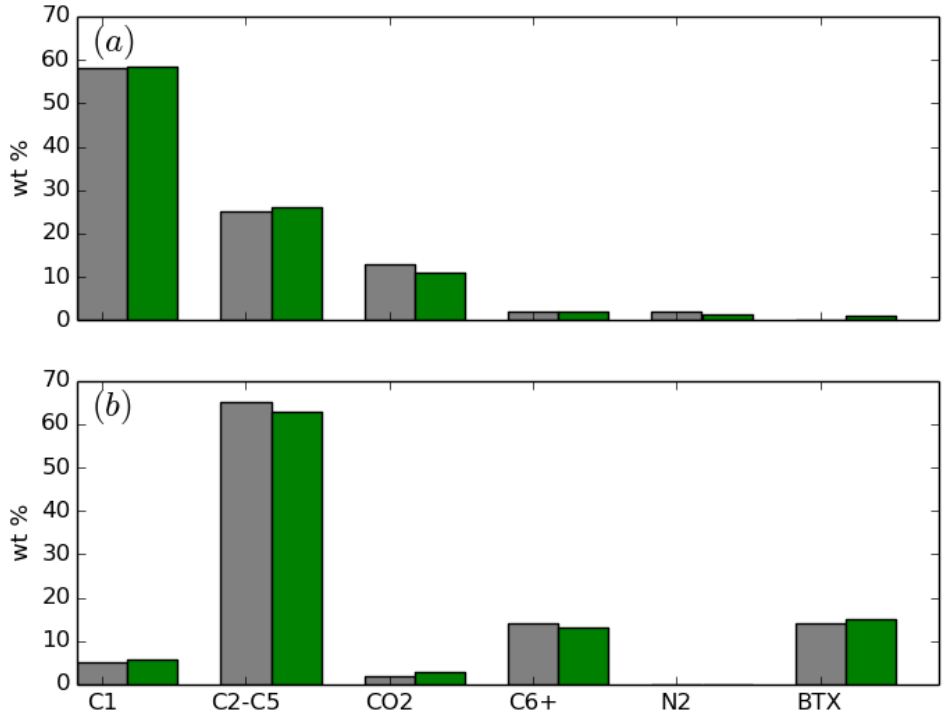

(a) Gas composition from the gas outlet stream. The (gray) bars represent experimental measurement Ref. 144, and the (green) is the estimated values (b) condensate composition from the condensate outlet stream. The (gray) bars represent experimental measurement Ref. 144, and the (green) is the estimated compositions.

Figure 5.2:

drocarbon feed contains the hydrocarbon mixture shown in Table 5.3, the water feed contains pure water, and the mercury feed contains pure mercury. As an initial step in this process, the hydrocarbon feed mass flowrate and water feed flowrate were adjusted until the current Obaiyed gas plant production capacity from gas, condensate and water achieved. Afterwards, we assumed a certain amount of mercury per day fed into the process inlet. Then based on experimental figures provided by Ezzeldin et al. [143], a mercury mass balance across the first three phase separator was carried out in order to get the second guess for mercury flow rate. Those steps were reiterated by a trial and error until converged. The final feed compostion of Obaiyed plant is obtained

in Table 5.4. This feed compostion is not a model dependent. In other words, the feed compostion in Table 5.4 was obtained using SRK EoS and the same compostion were used for PC-SAFT EoS model and it still predicts the current production capacity.

Table 5.4: Estimated feed composition to Obaiyed plant.

group	Component	mole fraction
N_2	nitrogen	0.0102
C_1	methane	0.769
CO_2	carbon dioxide	0.0522
C_{5+}	ethane	0.0110
	propane	0.0055
	n-butane	0.0055
	iso-butane	0.055
	n-pentane	0.039
	iso-pentane	0.044
C_{6+}	n-hexane	0.0093
BTX	toluene	0.0068
Hg	mercury	1.026×10^{-8}
H_2O	water	0.0424

Four scenarios were investigated for predicting the distribution of elemental mercury in Obaiyed processing facilities. The first scenario was to simulate Obaiyed gas process facilities using the SRK EOS without introducing binary interaction parameters k_{ij} between elemental mercury and other molecules. This scenario is referenced as a SRK base case scenario in the study. The second scenario was to simulate Obaiyed processing facilities using the SRK EOS in combination with GCM to estimate the k_{ij} between mercury and other species; this scenario is referred to as the SRK$-$GCM case. For the SRK$-$GCM case, the SRK EOS parameters, (i.e. pure component critical properties and acentric factor) were taken from Table 4.2, and the binary interaction parameters k_{ij} were taken from Table 4.4 in Chapter 4. The third scenario used the PC-SAFT EOS where elemental mercury is modeled as a non associating molecule without introducing binary interaction parameters k_{ij} between elemental mercury and other molecules. This scenario is referenced as a PC-SAFT base case scenario. The fourth scenario used the PC-SAFT EOS where elemental mercury is modeled as an associating molecule with 2(1:1) sites. In this scenario, only the binary interaction parameters between elemental

mercury and water was introduced.

5.4 Results and discussion

In this section, the results of both selected thermodynamic models SRK EOS and PC-SAFT EoS for predicting the distribution of elemental mercury will be compared to the experimental data. The accumulation of mercury in the processing facilities and its pathways in the gas, condensate and water streams will be investigated. The proper location of mercury removal unit will be indicated accordingly.

The three phase separator will be analysed first for mercury accumulation and distribution as it is the first unit of Obaiyed gas processing facilities as indicated in the process flow diagram given in Figure 5.1. This first separation unit was operated at high pressure $70\,\text{bar}$ and temperature $70\,^{\circ}\text{C}$. These operating conditions prevent elemental mercury from accumulating in the unit by flashing it out via the gas, condensate and water streams. The four studied scenarios indicated in Table 5.5 and Table 5.6, show that elemental mercury will not accumulate in this unit at these operating conditions. The elemental mercury mass balance across this unit indicates that the amount of elemental mercury fed into this plant was around $19\,\text{g}\,\text{h}^{-1}$ to $20.8\,\text{g}\,\text{h}^{-1}$ based on the four studied scenarios.

The PC−SAFT model provides better prediction of mercury distribution with respect to SRK with GCM compared to the experimental data. Most of the elemental mercury prefers to remain with the condensate and flows to the second separation unit via the condensate stream. Without introducing binary interaction parameters between mercury and other compounds, as in the SRK EOS and PC-SAFT EOS base case scenarios, inaccurate prediction of mercury distribution is obtained, where the mercury is predicted to leave the separator via produced water. For the SRK−GCM and PC−SAFT scenarios, the results in Table 5.5 and Table 5.6 show less elemental mercury in the water stream compared to the experimental figure obtained by Ref. 143. This could be explained by the presence of dispersed heavy hydrocarbons in the real sample. This heavy hydrocarbons in water will increase the concentration of mercury in water. This confirms that mercury is more soluble in heavy hydrocarbons as we concluded in the previous Chapter 4. For the condensate and gas streams, the SRK−GCM model pre-

dicted lower mercury levels in the condensate and more in the gas stream compared to the PC−SAFT EOS and measured quantities [143]. This might be due to the fact that in this scenario, the interaction between mercury and CH_4 was underestimated by assuming CH_4 interaction is the same as CH_3 group interaction and the C_{+6} represents n-hexane. In reality C_{6+} contains heavy hydrocarbon fractions and might have n-hexadecane or more. The prediction of the PC−SAFT EOS in the condensate, water and gas streams, is more accurate than the other studied scenarios as shown in Table 5.6. It also confirms that most of the elemental mercury tends to remain in the condensate stream and flows to the second separation unit via the condensate stream, where around $343\,\mathrm{ng\,g^{-1}}$ of elemental mercury flows to the second separator compared to $554\,\mathrm{ng\,g^{-1}}$ as an experimental figure.

Table 5.5: Elemental mercury distribution through the plant using SRK EoS

Unit	Stream name	Exp. [143]	SRK base case	SRK−GCM
inlet separator	gas1 (µg/Sm^3)	1.0625	0.108	11.19
	condensate1(ng g^{-1})	554	1.65	94.6
	oilywater1(ng g^{-1})	18.72	3286	1.43
second separator	gas2 (µg/Sm^3)	31.62	0.04	20.0
	condensate2 (ng g^{-1})	24.50	0.38	89.29
	oilywater2 (ng g^{-1})	22.62	853.8	1.45
stripping column	gas3 (µg/Sm^3)	6.001	0.0794	19.20
	condensate3 (ng g^{-1})	9.75	0.0526	0.731
compressor	gas5 (µg/Sm^3)	35.36	0.07	19.40
storage	export condensate (ng g^{-1})	7.91	0.05	0.73

The second stage separator is designed as a three phase separator and operated at 23 bar and 63 °C. Due to the high pressure and temperature drop cross this unit compared to the first stage, around $9\,\mathrm{g\,h^{-1}}$ of elemental mercury was expected to accumulate in the unit rather than flashing out based on PC−SAFT EOS scenario. Both models SRK and PC−SAFT base case scenarios show very low concentration of mercury in this unit compared to the other scenario and experimental data. This is due to the fact that in these two scenarios mercury leaves the first stage separator via the water stream. The other scenarios in Table 5.5 and Table 5.6 show that mercury in the condensate stream

Table 5.6: Elemental mercury distribution through the plant using PC−SAFT EoS

Unit	Stream name	Exp. [143]	PC−SAFT base case	PC−SAFT
inlet separator	gas1 (µg/Sm^3)	1.0625	0.0032	5.5
	condensate1(ng g^{-1})	554	2.508	343
	oilywater1 (ng g^{-1})	18.72	2944	10.39
second separator	gas2 (µg/Sm^3)	31.62	0.0018	8.78
	condensate2 (ng g^{-1})	24.50	2.066	376.65
	oilywater2 (ng g^{-1})	22..63	2059	8.8
stripping column	gas3 (µg/Sm^3)	6.001	0.00834	81.7
	condensate3 (ng g^{-1})	9.75	5.09	55.2
compressor	gas5 (µg/Sm^3)	35.36	0.07	69.7
storage	export condensate (ng g^{-1})	5.09	0.00723	55.2

is more than the experimental value which means either elemental mercury is accumulating in this unit or is speciating into other mercury species. Both mercury speciation and accumulation phenomenon are responsible for the reduction of elemental mercury concentration in the condensate stream in the experimental analysis. The oily water stream from the second separator experimentally contains more mercury than the oily water stream from the first stage and from obtained model results, this confirms that this stream contains heavy and dispersed hydrocarbons in water or another mercury species were generated in the unit.

The stripping column was operated at 150 °C in order to achieve the exported crude specifications, such as vapor pressure. This high operating temperature forces elemental mercury to leave the column from its top via the gas stream. The results of both models SRK and PC-SAFT EoS shows high concentration of mercury in the gas outlet stream (Gas3) compared to the experimental value. This indicates that the elemental mercury is converted into another mercury species and these species have not taken into account by Ezzeldin et al. [143]. For the PC-SAFT EoS scenario mercury in the condensate stream (condensate3) is also high than the experimental value and can be explained due to the accumulation of mercury.

The crude oil storage and export facilities were also affected by elemental mercury as indicated in Table 5.5 and Table 5.6. The PC−SAFT scenario shows that around

$0.61\,\mathrm{g\,h^{-1}}$ of elemental mercury will accumulate or speciate into other mercury species in the storage tank. The experimental results conducted by Ezzeldin et al. in Table 5.2 shows that the concentration of $(i-\mathrm{Hg})$ is more than the concentration of Hg in the exported condensate which means elemental mercury is converted to $(i-\mathrm{Hg})$ species.

The flashed gas from the second stage separator and stripping column were gathered and compressed to the gas processing facilities. The results in Table 5.5 and Table 5.6 indicated that this compressed gas contains a high concentration of elemental mercury where in the PC−SAFT scenario shows that this stream has around $69\,\mu\mathrm{g/Sm^3}$

5.5 Location of mercury removal unit

Selecting the proper location of mercury removal units is still a challenging task as explored in Sec 2.4 in Chapter 2. The risk of producing, transporting or processing crude oil and natural gas containing mercury is classified into various levels based on total mercury concentration. They are classified into three risk levels; low risk, medium risk and high risk which identified and reported by Wilhelm et al. [148]. These levels are summarized in Table 5.7.

Table 5.7: Mercury risk levels in crude oil and natural gas Ref. [148].

Risk levels	Hg conc.	
	Gas µg/m^3	Liquid (ppb)
Low risk	5	<5
Medium risk	5-50	5-100
High risk	>50	>100

At the high risk level, protecting the human and environment becomes more difficult in case of an oil and gas leak or spillage. This requires detailed mercury species analysis, critical observation and monitoring. Improper location and section of mercury removal units in this level is undesirable from both safety and finance point of view.

In the medium risk level, analysis of mercury species is still required, and if the concentration of elemental mercury is more than 75% of the total mercury then safety rules

must be issued to prevent workers from mercury inhalation. In this risk level, hazard areas must be monitored and restricted. Improper location and section of mercury removal units in this level is still unacceptable from both safety and finance point of view. In the low risk level, measurement of mercury species is also needed but does not require analytical uncertainties. Monitoring of mercury concentration is essential from time to time to ensure that mercury concentration did not exceed its limit at this level. Improper location and section of mercury removal units in this level is unacceptable from finance point of view.

For Obaiyd gas plant, in order to protect all of the processing facilities of this plant from mercury accumulation, it is recommended to install a mercury removal unit (MRU) upstream the second stage separator. This is the proper location of MRU. Installing the MRU in the gas stream downstream of the second stage separator as recommended by Ref. 143 will protect the processing facilities downstream of its location only, such as acid gas removal unit, dehydration unit, low temperature separator (LTS) and sales gas exporting facilities. Moreover, It will not reduce the mercury risk level of the plant specially the condensate treatment units and storage facilities. While installing it upstream second stage separator reduces the mercury risk level from high risk to low risk. Installing MRU in the condensate stream was also recommended by PETRONAS (Petroliam Nasional Berhad) in managing and executing mercury removal project to reduce project cost and complexity [149]. Figure 5.3 shows the process flow diagram of the plant with MRU located upstream of the second stage separator.

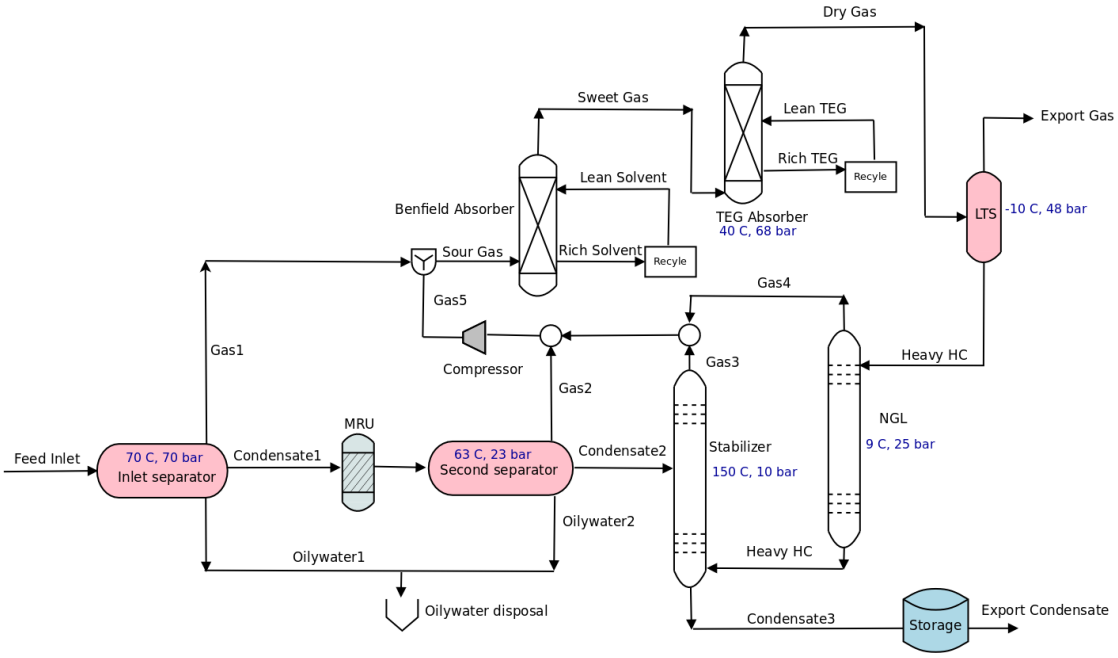

Figure 5.3: Obaiyed natural gas process flow diagram with MRU

5.6 Conclusion

Understanding mercury pathways in an ecosystem or its distribution in oil and gas process facilities requires a model that is able to predict its thermodynamic behavior in a wide variety of operating conditions. In this chapter, both the SRK EoS in combination with GCM and PC−SAFT EoS were validated for predicting the distribution of elemental mercury in oil and gas processing facilities.

Without taking into account and introducing the proper k_{ij} can yield extremely poor results. This leads to wrong decision making; for instance, setting $k_{ij} = 0$, as in the SRK EoS and PC−SAFT EoS base case scenarios, both models show that elemental mercury will be flashed out form the first stage separator via water stream instead of condensate stream. For SRK with GCM, the discrepancy in the model results compared to PC-SAFT and experimental data, is due to the fact that the interaction between elemental mercury and methane was not properly attributed due to lack of experimental data.

Reducing the operating pressure and increasing operating temperature allows more heavy hydrocarbons to flash out carrying over more mercury to the gas stream. By

comparing models results to the experimental data, it is clear that mercury species are speciating in the second separator and stripping column. It is recommended to install a mercury removal unit (MRU) upstream of second stage separator in order to protect all processing facilities and reduces its risk level from high level to low level. Increasing condensate production of the plant for example by a discovery of new well, leads to an increase in mercury feed inlet concentration, consequently, its accumulation in the process facilities. In both models, only the distribution of elemental mercury was investigated. Therefore, it is recommended to model the distribution of other mercury species, such as $i-$Hg and MeHg using PC-SAFT EoS and also take the transformation process of mercury species in oil and processing facilities into account. In the next chapter, the presence of other mercury species and their stability in oil and gas processing facilities are identified.

Chapter 6

Speciation of mercury

6.1 Introduction

Mercury species act differently where each specie has its own properties and behavior, such as solubility, toxicity, partitioning, vapor pressure, density and others. These species have the ability to transform to a more toxic or corrosive specie, such as methylmercury, and AlHg. Their presence in oil and gas processing facilities can cause several operational problems, such as corrosion and catalyst poisoning, as explained in Chapter 2. These operational problems might lead to unplanned shutdown of oil and gas, and refineries processing facilities which is operationally and financially undesirable. Thus, understanding the behavior of these species and their transformation process is of vital importance where without taking into account the speciation mechanisms of mercury species, mercury risks can not be eliminated. In addition to that, selecting the proper removal technology of mercury compounds can not be done unless mercury species and their speciation process are understood. This requires a model that has the ability to predict the transformation process of these species in oil and gas or in the ecosystem.

The transformation process depends on several parameters, such as the nature of the system in which mercury species are present, type of mercury species, its concentration, operating temperature and pressure, and other factors. For instance, oil and gas processing facilities are operated at a wide range of conditions (temperature and pressure) in order to separate and purify their feed prior to export. For instance, the Obyied gas plant

presented in Chapter 5 operated at temperatures ranging from 70°C to 150°C and pressures from 5 bar to 70 bar. This variation of operating condition might lead mercury species to transform and precipitate in the process facilities, as is the case in the second stage separator of the Obyied plant. In the second stage sperator, the significant difference between the experimentally measured values and the thermodynamically predicted values using PC-SAFT EoS can be attributed to mercury speciation or precipitation. The speciation of mercury occurs in the gas and liquid phases.

Modeling the transformation of mercury species in the ecosystem has been investigated where several models used to represent this process. These models are based on Eulerian and Lagrangian approaches [150]. Both approaches are widely used to describe fluid motion specially that associated with environmental and oceanic [151, 152]. Each one of these models has advantages and drawbacks where one of most awkward drawbacks that are modeling two and three dimensional fluid motion problems [151]. Even though the accuracy and uncertainty of these models are still a challenging task [153], they still provide an indication of mercury pathways.

Due to a lack of sufficient data and a shortage of information in the transformation process of mercury species in oil and gas, there is insufficiency modeling studies that investigated the speciation process in oil and gas processing facilities in the open literature. Therefore, this chapter provides an overview of the most dominant mercury compounds in oil and gas. In addition to that the stability of these species in the hydrocarbon mixture are explored in detail. The use the thermodynamic state functions described in Chapter 3 for predicting the thermophysical properties of mercury species and their transformation process from the thermodynamics and kinetics point of view are described in detail. The required data that needed to investigate the transformation process of these species are highlighted.

6.2 Mercury species in the oil and gas process streams

The three mercury forms, elemental Hg, organic (e.g., MeHg) and inorganic $i-$Hg (e.g., HgS, $HgCl_2$, etc.) have been reported to be present in oil and gas process streams. Separation of oil and gas mixtures in gas oil plant generates three streams; gas, condensate and produced water streams, as explained in Chapter 5. These mercury compounds

might leave the processing unit via one of these three streams or might transform and precipitate in the unit. This depends on the type of mercury compounds, its concentration and the operating conditions of the unit. For instance, elemental mercury did not precipitate or transform in the first stage separator of the Obyied gas plant presented in Chapter 5 compared to its precipitation or transformation in the second stage separator. Thus in this section, the mercury species in each processing stream will be explored in detail.

For the natural gas streams, elemental form of mercury is considered to be the dominant specie [145]. In condensate streams, the three mercury forms, elemental, organic and inorganic have been reported to be present, but the Hg and $i-$Hg species are the two main contributors [143, 145]. It has been highlighted that Hg and $i-$Hg account for more than 90% of the total mercury concentration in condensate [59, 154]. The organic mercury compounds are present in the form of monoalkyl and dialkyl mercury in condensates. The concentration of the three mercury forms were experimentally measured in the condensate streams by several authors. For instance, a study conducted by Ezzeldin et al. [143] for measuring mercury species in Obyied gas plant shows that the three forms of mercury are present in the condensate streams (see Table 5.2 in Chapter 5). It is clear that the concentrations of Hg and $i-$Hg in the condensate streams were more than the organic mercury MeHg and account for 85%, 13% and 2% respectively. The type of $i-$Hg compounds were not exactly identified in the study conducted by Ezzeldin et al., but they suggested that the $i-$Hg form is expected to be in the form of HgS. In contrast, a study conducted recently by Gajdosechova et al. [155] for measuring mercury species in petroleum hydrocarbons concluded that HgS is not the dominant $i-$Hg mercury compound in condensate and it has high stability constant and low reactivity in the presence of ligands. For produced water streams, the total mercury concentration was measured by by Ezzeldin et al., but its species were not analysed. The presence of the three mercury forms were identified in the natural water in several locations in the world where mercury chloride $HgCl_2$ and methylmercury are classified as the predominate mercury species of $i-$Hg and MeHg forms [146].

It is clear that the three mercury forms are present in the processing streams but whether they remains stability in their streams or transform to another mercury form. This will be explored in detail in the next section.

6.3 Stability of mercury species in hydrocarbons

Due to the presence of the three forms of mercury in the oil and gas streams as explored in Sec 6.2, understanding the stability of these species is of vital importance as it provides an indication of their transformation process. A study conducted by bloom [59] to analyze the stability of several pure mercury species (elemental Hg, $HgCl_2$, CH_3HgCl, $(CH_3)_2Hg$) in liquid hydrocarbon. Even thought the composition of this liquid hydrocarbon was not reported by Bloom, this study provides useful information about the stability of these species in five different materials. Bloom prepared a solution of liquid hydrocarbon with each of the previous mercury species and stored in five containers for a few days. Each container was designed from one of the following materials; glass, stainless steel 316, aluminium, Teflon FEP and polyethylene. The stability of these mercury species in the sampling containers according to Bloom study are shown in Figure 6.1.

Figure 6.1 (a) represents the stability of elemental mercury in the five materials. The solid square symbols connected by solid line represents the stability of elemental mercury in a glass container, while the diamond symbols connected by dashed line corresponds to its stability in aluminium container. The white circle and black circle symbols with dotted and dashed lines denote the stability of the elemental form in stainless steel and polyethylene materials respectively. The white triangle symbols connected by dashed line represents the stability of elemental form in Teflon FEP container. For the inorganic mercury, Figure 6.1 (b) represents the stability of $HgCl_2$ in five sampling materials. The solid square symbols connected by solid line represents the stability in a glass container, while the white diamond symbols connected by dashed line corresponds to the stability in the aluminium container. The white circle and black circle symbols with dotted and dashed lines denote the stability in stainless steel and polyethylene materials respectively. The white triangle symbols connected by dashed line represents the stability in Teflon FEP container. For the stability of organic mercury compounds, Figure 6.1 (c) and Figure 6.1 (d) represent the stability of CH_3HgCl, $(CH_3)_2Hg$ in five sampling containers. The solid square symbols connected by solid line represents the stability in a glass container, while the white diamond symbols connected by dashed line corresponds to the stability in the aluminium container. The white circle and black circle symbols with dotted and dashed lines denote the stability in stainless steel and

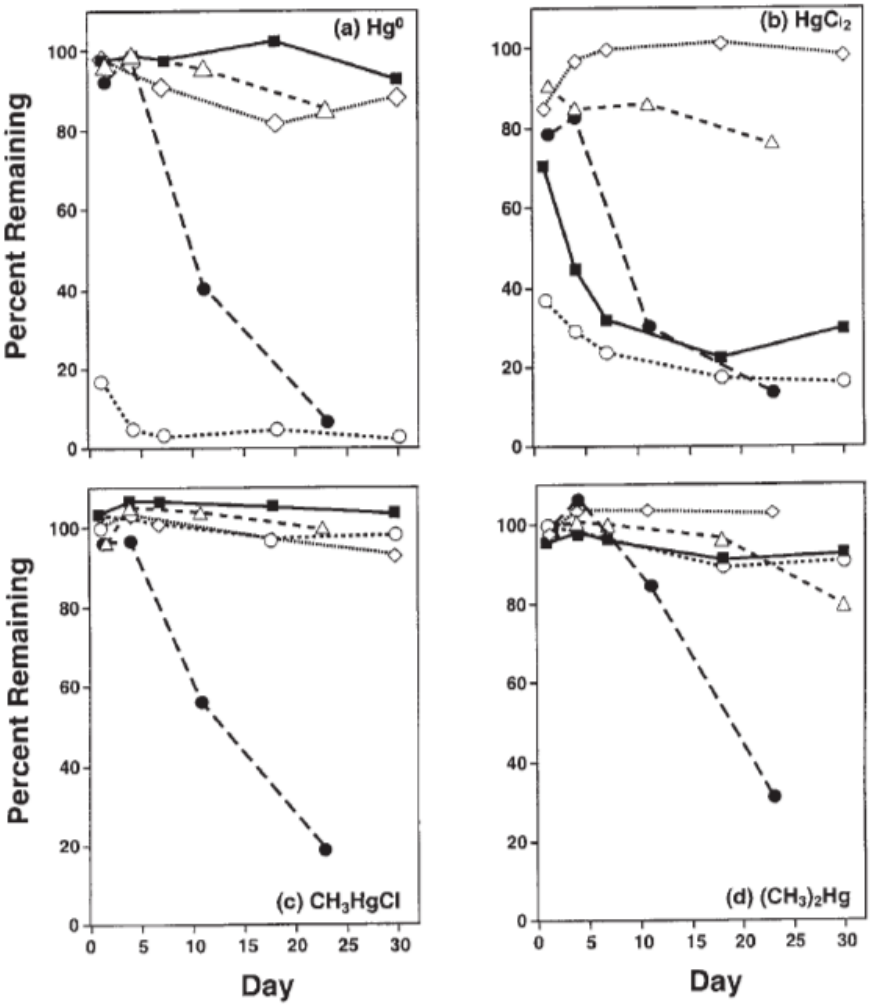

Figure 6.1: Stability of mercury species (a) elemental mercury, (b) $HgCl_2$, (c) CH_3HgCl, and (d) $(CH_3)_2Hg$) in glass (■), aluminium (◇), stainless steel (○), polyethylene (●), and Teflon (△). Taken from Ref.[59].

polyethylene materials respectively. The white triangle symbols connected by dashed line represents the stability in Teflon FEP container.

It is clear from Figure 6.1 (a) and Figure 6.1 (b) that the loss of both elemental mercury and $HgCl_2$ forms which adsorbed into the stainless steel materials as reported by Bloom, is more than 80% and 60% respectively after 3 days, while the loss of the organic mercury is less than 10%. This means that both elemental and $HgCl_2$ forms are unstable in the stainless steal SS316L material and pitting corrosion might occur after a period

of time as concluded by AL-Hinai and Nengkoda [70] for the ability of elemental mercury to corrode SS316L which explored in detail in Sec 2.3.5 in Chapter 2. The use of SS316L as a material of construction for several oil and gas processing units in the presence of elemental and $HgCl_2$ should be further investigated. Aluminium has the ability to absorb elemental mercury and $HgCl_2$ as indicated Figure 6.1 (a) and Figure 6.1 (b), where $HgCl_2$ has higher rate of absorption than elemental. Figure 6.1 (c) and Figure 6.1 (d), show that organic mercury compounds are stable in the studied materials except the polyethylene.

Another study conducted by Snell et al. [156] for investigating the stability of pure Hg, pure $HgCl_2$ and a mixture of (Hg and $HgCl_2$) in an organic solution (heptane). Where two different sampling container materials, glass and high density polyethene, were used. The results show the concentration of both Hg and $HgCl_2$ in pure heptane decreased with time and could reduced to half of their original concentration within 10 days time. The loss of Hg was faster than that of $HgCl_2$ after 4 days and 13 days from the collection time. In addition , experiments were performed when both species Hg and $HgCl_2$ were mixed tougher in heptane and found that the loss of $HgCl_2$ concentration was faster than Hg due to the formation of Hg_2Cl_2 which is hydrocarbons insoluble and precipitates according to the following reaction.

$$\mathrm{Hg} + \mathrm{HgCl_2} \longrightarrow \mathrm{Hg_2Cl_2} \tag{6.1}$$

The loss of both mercury compounds in organic solvent was attributed to the absorption of these species to the container material, and the reaction of both species together to form Hg_2Cl_2 as indicated in Eq. (6.1). Thus, it recommended to eliminate the reactions that generate Hg_2^{2+} prior to any further measurements and analysis.

It is clear that the presence of elemental mercury and $HgCl_2$ compounds in the hydrocarbon system, leads to either transformation of both species to Hg_2Cl_2 or absorption both species in the materials. In order to model the rate of transformation of these species, several parameters are required, such as reaction and equilibrium constants, reaction rate, model type and its input parameters, reaction temperature, reactants initial concentration, and reaction phases. These data are not available in the open literature. For instance, the reaction rate and reaction constant of Eq. (6.1) were not measured in the

hydrocarbon phase, but it was concluded that the reaction has a half-life time within 10 days at ambient conditions [5]. Due to the lack of data and information that required in order to model this transformation process in the hydrocarbon phase. Therefore, it is of vital importance to investigate the reaction kinetic and the thermodynamic transformation of mercury species in other phases that not far from liquid hydrocarbons, such as the transformation of mercury species with flue gases. Various studies were due to the flue gases environmental concern. This work can be considered as a framework for modeling the transformation of mercury species in the liquid hydrocarbons. Next section, provides an overview of mercury species reactions in the gas phase. In addition to that the possible reaction mechanism of these species that occurs in the flue gases according to the thermodynamic and kinetic concepts were identified.

6.4 Mercury species transformation in the flue gases

Due to the release of elemental mercury with the flue gases during fossil fuels burning, the Environmental Protection Agency (EPA) has been required to monitor the potential risks of mercury emissions from boilers [157]. The elemental mercury in the flue gases can be converted to Hg^{+2} when the temperature of the flue gas drops below 300 ^{o}C [158]. Halogenes specially chloride and hydrochloric acid HCl are considered as the main oxident of elemental mercury in the flue gases. The flue gases were reported to contain high amount of Cl_2 and HCl. A study conducted by Hall et al. [159] was the first that investigated the impact of the HCl, Cl_2, O_2 and NO_x oxidants on mercury in the flue gases. The study showed that the HCl concentration in the gas mixture plays an important role in the conversion of elemental mercury to Hg^{2+}.

Several studies were carried out to investigate the parameters that affect or speed up the speciation of mercury species in the flue gas out of the boilers. The flue gases from coal fire plants in Mongolia and Northern China contain around 85% of Hg, 15% of Hg^{2+} [160]. This investigation was in agreement with the study conducted by Widmer et al. [161]. In both studies, a one step reaction mechanism was assumed to convert Hg in the presence of HCl or Cl_2. The drawback of this mechanism is that it does not take into account the impact of other flue gases, such as O_2 and NO_x, SO_x and H_2O. Several attempts were made to understand the reaction mechanisms of Hg with chlorides and hydrochloric acid via sequences of reactions. A report issued by EPA for

the possible reaction mechanism of mercury in the presence of both HCl and Cl_2 by comparing several reactions from the thermodynamic equilibrium and reaction kinetics point of view. These reaction mechanisms and reaction constants are summarized in Table 6.1. The study concluded that the conversion of elemental mercury to $HgCl_2$ in the presence of chloride (Cl) is the possible pathway form both the thermodynamic and kinetic point of view where Hg is first converted to HgCl and then to $HgCl_2$ in the presence of Cl_2. The chloride was generated by the reaction of HCl with OH to generate Cl as indicated in Table 6.1. The results in Table 6.1 show that the reaction of elemental mercury in the presence HCl is kinetically and thermodynamically impossible to occur as it has very low rate of reaction and thermodynamic equilibrium constant. Table 6.1 also shows that elemental mercury has the ability to react with chlorine at high and low temperatures and requires less activation energy to take place. The reaction of elemental mercury with Cl_2 has less possibility to occur at high and low temperatures and requires more activation energy than the reaction of mercury with Cl. Both Cl and Cl_2 react with HgCl to form $HgCl_2$ at low and high temperatures. The specie M in some reactions in Table 6.1 represents the bath gas concentration [162]. The negative activation energy value means that the rate of reaction decreases by increasing temperature.

In conclusion, the presence of both mercury chloride $HgCl_2$ and elemental mercury in the oil and gas has a negative impact on the processing facilities and the ecosystem. These species have the ability to be absorbed in several materials as explored in Sec 6.2. In addition to that the oxidation of elemental mercury to $HgCl_2$ in the flue gases is possible. Therefore, predicting or estimating the thermophysical properties of both species is of vital importance. It leads to understand the vaporization and diffusion rates which indicates their pathways in the environment and the processing streams. The thermophysical properties and the distribution of Hg in oil and gas were predicted in Chapter 4 and Chapter 5 using both selected thermodynamic models SRK and PC-SAFT EoS. In the next section, the thermophysical properties of $HgCl_2$ such as vapor pressure, solubility and heat of vaporization were predicted using PC-SAFT EoS based on the available experimental data in the open literature.

Table 6.1: Speciation processes of mercury specie in the flue gas. Taken from [163]

Reaction Type	Temperature range	rate constant	Equilibrium constant	Activation Energy
	K	$M^{-1}\ s^{-1}$		kcal mol^{-1}
$Hg + Cl + M \rightleftharpoons HgCl + M$	298	1.57×10^{12}	1.2×10^{14}	-9.138
	600	1.74×10^{9}	6.7×10^{4}	
	1000	9.53×10^{7}	1.2×10^{1}	
	1200	2.76×10^{6}	8.3×10^{-2}	
$Hg + Cl_2 \rightleftharpoons HgCl + Cl$	298	3.68×10^{-7}	1.21×10^{-1}	88.95
	600	4.11×10^{1}	7.38×10^{2}	
	1000	6.17×10^{4}	5.0×10^{-4}	
	1200	3.84×10^{5}	1.43×10^{-5}	
$Hg + HCl \rightleftharpoons HgCl + H$	298	6.22×10^{-65}	1.9×10^{-57}	98.29
	600	1.2×10^{-28}	1.10×10^{-28}	
	1000	2.52×10^{-14}	2.7×10^{-17}	
	1200	9.59×10^{-11}	2.0×10^{-14}	
$Hg + Cl_2 + M \rightleftharpoons HgCl_2 + M$	298	2.26×10^{-16}	9.7×10^{30}	34.46
	600	8.32×10^{-2}	5.2×10^{12}	
	1000	5.11×10^{4}	3.5×10^{5}	
	1200	1.5×10^{6}	5.9×10^{3}	
$HgCl + HCl \rightleftharpoons HgCl_2$	298	3.93×10^{-15}	1.1×10^{-17}	31.22
	600	1.32×10^{-3}	3.3×10^{-10}	
	1000	4.67×10^{1}	4.2×10^{-7}	
	1200	6.4×10^{2}	2.6×10^{-6}	
$HgCl + Cl_2 \rightleftharpoons HgCl_2 + Cl$	298	1.48×10^{6}	1.21×10^{14}	4.01
	600	4.47×10^{7}	7.47×10^{1}	
	1000	1.71×10^{8}	4.04×10^{-6}	
	1200	2.40×10^{8}	4.16×10^{-8}	
$HgCl + Cl + M \rightleftharpoons HgCl_2 + M$	298	2.02×10^{14}	7.04×10^{53}	-1.28
	600	8.04×10^{9}	2.19×10^{22}	
	1000	3.17×10^{4}	1.73×10^{6}	
	1200	1.11×10^{3}	1.29×10^{2}	
$HCl + OH \rightleftharpoons Cl + H_2O$	298	4.35×10^{11}	$cm^3 mol^{-1}\ s^{-1}$	
	1200	1.89×10^{12}	$cm^3 mol^{-1}\ s^{-1}$	

6.5 Mercury chloride property prediction

Mercury chloride $HgCl_2$ is considered as one of the unstable mercury species present in the oil and gas as explored in Sec 6.3. Predicting its thermophysical properties, such as vapor pressure and solubility, leads to reduce its risks and understand its generation and transformation process. Thus this section explores the use of PC-SAFT EoS described in Chapter 3 for predicting the vapor pressure and the solubility of $HgCl_2$. Moreover, the PC-SAFT model required parameters for $HgCl_2$ will be obtained. $HgCl_2$ is one of mercury salts that has high water solubility at low temperatures [164, 165] and can be vaporized from the solid phase to the gas phase even at low temperatures. It can also be generated from the speciation of elemental mercury in the flue gases in the air and water phases.

6.5.1 Mercury chloride vapor pressure prediction

The vapor pressure of $HgCl_2$ has been experimentally measured over a range of temperatures above and below its melting temperature 277°C [164, 165]. The vapor pressure data points above the melting temperature allows us to estimate the three pure component parameters σ, ε/k_B and m of PC-SAFT model, as described in Sec 3.7. Figure 6.2 shows the predicted vapor pressure of $HgCl_2$ using PC-SAFT EoS where its the PC-SAFT parameters are obtained by fitting the vapor pressure data and are reported in the Table 6.2.

The average relative deviation error was 1.21% compared to the experimental data. The heat of vaporization and heat of sublimation of $HgCl_2$ can also be obtained from the vapor pressure data by applying the the Clausius− Clapeyron equation 6.2 below.

$$lnP = \frac{-\Delta H}{R}\frac{1}{T} + C \tag{6.2}$$

where P is the vapor pressure, ΔH is the heat of vaporization or sublimation, and C is the intercept. The slope of the red sold line in Figure 6.2 represents the $HgCl_2$ heat of vaporzation divided by ideal gas constant and the slope of the black solid line represents the heat of sublimation divided by ideal gas constant. The slopes of the red and black lines in Figure 6.2 are -7662.40 and -9577.71 , respectively. This means that the heat of vaporzation is around $63.70\,\mathrm{kJmol^{-1}}$ and the heat of sublimation is around

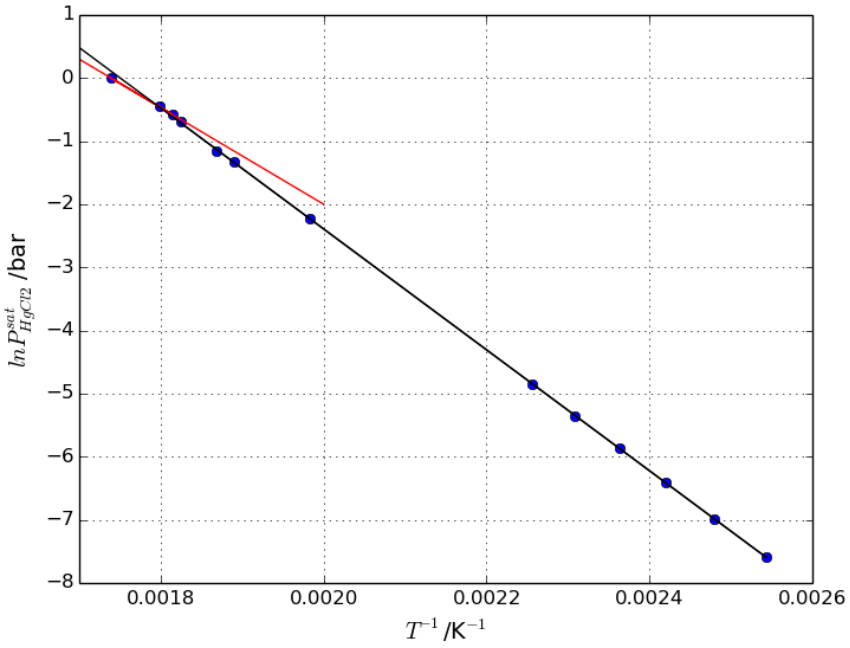

Figure 6.2: Vapor pressure of $HgCl_2$, the (blue) symbols represent experimental data, the red solid line represents the vaporization from liquid state to vapor, the black solid line represents the sublimation from solid to vapor.

$79.63\,\mathrm{kJmol^{-1}}$. Therefore the heat of fusion or melting of $HgCl_2$ can be estimated as the difference between heat of vaporization and heat of sublimation as $15.92\,\mathrm{kJmol^{-1}}$. The heat of fusion of $HgCl_2$ was reported in DETHERM according to Dortmund Data Bank as $19.4\,\mathrm{kJmol^{-1}}$ which is consistent with PC-SAFT prediction.

Table 6.2: PC-SAFT parameters for mercury species

Molecule	T range K	Association Scheme	σ_i Å	ε_i/k K	m_i	$\varepsilon^{A_iB_i}/k$ K	$K^{A_iB_i}$	$Ref.$ Ref.
Mercury chloride $HgCl_2$	2978– 302	None	2.618	1020.5	1.0			In this work
Mercuric ion Hg^{2+}	2978– 302	None	2.61812	1198.5	1.0			In this work
chloride Cl^-	2978– 302	None	3.0575	170	1.0			[166]

The PC-SAFT parameters for mercuric cation Hg^{2+} can also be obtained based on the $HgCl_2$ vapor pressure data, by modeling $HgCl_2$ as Hg^{2+} cation and Cl^- anion by

taking into account the electrolyte term that described in Sec 3.7. The Hg^{2+} PCSAFT required parameters are summarized in Table 6.2.

By knowing the PC-SAFT pure component parameters, several pure and mixture properties, such as solubility can be predicted. Not only that but also the transformation process of Hg^{2+} and other mercury species can also be predicted. Next section provides the solubility prediction of $HgCl_2$ in water using PC-SAFT model.

6.5.2 Mercury chloride solubility prediction

The solubility of mercury chloride in water has been measured at high and low temperatures [167]. This allows to predict its solubility using PC-SAFT EoS if the solid phase equilibrium is taken into account. The potential state functions and phase equilibrium calculation that explored in Sec 3.2 and Sec 3.5 in Chapter 3 can be used to represent solid liquid phase equilibrium (SLE). Eq. (3.40) can be written for solid phase as:

$$f_i^s = f_i^l \tag{6.3}$$

where f_i^s is the fugacity of pure species i and f_i^l is the fugacity of the solute in the solvent.
The fugacity of the solute in the solvent f_i^l was defined based on the fugacity at its reference state f_i^o and activity a_i in Eq. (3.28) as:

$$f_i^l = f_i^o a_i \tag{6.4}$$

where f_i^o is the fugacity of pure species i at the same T as the solution temperature.
The reference state fugacity f_i^o is defined as the fugacity of pure subcooled liquid at the solution temperature. The excess Gibbs free energy for a component from solid state to the liquid state can be defined from Eq. (3.30) as;

$$G_i^l - G_i^s = RT \ln \frac{f_i^l}{f_i^s} \tag{6.5}$$

where G_i^o is the Gibbs free energy of pure species i at T and P,f_i is the fugacity of species i in the mixture and f_i^s is the fugacity of pure species i at the same T and P.

The Gibbs free energy can also be represented, if the enthalpy and entropy of the system are changed. Thus, Eq. (3.19) can be written as:

$$\Delta G = \Delta H - T\Delta S \tag{6.6}$$

where in this case, ΔH is the enthalpy and ΔS is the entropy change from solid state to liquid state.

The enthalpy change can be defined as:

$$\Delta H = \Delta H^f + \int_{T_t}^{T} \Delta C_p dT \tag{6.7}$$

where ΔH^f is the enthalpy of fusion and T_t is the triple- point temperature.

Similarly, the entropy can be defined as:

$$\Delta S = \Delta S^f + \int_{T_t}^{T} \frac{\Delta C_p}{T} dT \tag{6.8}$$

where ΔS^f is the entropy of fusion and can be represented as $\Delta S^f = \Delta H^f / T_t$ at the triple- point temperature.

Substituting Eqs. (6.6), (6.7), (6.4) and (6.8) into (6.5), gives:

$$\ln \frac{f_i^o a_i}{f_i^s} = \frac{\Delta H^f}{RT_t}\left(\frac{T_t - T}{T}\right) - \frac{\Delta C_p}{R}\left(\frac{T_t - T}{T}\right) + \frac{\Delta C_p}{R} \ln \frac{T_t}{T} \tag{6.9}$$

The the activity a_i can also be expressed replaced by $a_i = x_i^l \gamma_i^l$, where γ_i^l is the activity coefficient of species i in solution and x_i^l is the solubility of the solute in the solution. Eq. (6.9) becomes:

$$\ln \frac{x_i^l \gamma_i^l f_i^o}{f_i^s} = \frac{\Delta H^f}{RT_t}\left(\frac{T_t - T}{T}\right) - \frac{\Delta C_p}{R}\left(\frac{T_t - T}{T}\right) + \frac{\Delta C_p}{R} \ln \frac{T_t}{T} \tag{6.10}$$

where f_i^o / f_i^s term is equal to 1 at melting temperature.

The solubility of a salt in a solvent using PC-SAFT was expressed by Pontes et al. [168] based on Eq. (6.10) as:

$$x_i^l \gamma_i^l = exp\left[(\frac{\Delta H_i^{sl}}{RT_{mi}})(\frac{T - T_{mi}}{T})\right] \tag{6.11}$$

where x_i^l is the mole fraction of component i in the liquid phase l,γ_i^l is the activity of component i in the liquid phase l, ΔH_i^{sl} is the heat of melting of component i, T_{mi} is the melting temperature of component i. The last two terms in Eq. (6.10) were neglected.

The Eq. (6.11) was used in PC-SAFT model predict the solubility of $HgCl_2$ in water. The $\phi - \phi$ approach explored in Sec 3.5 in Chapter 3 was applied for SLE phase equilibrium calculation. The binary interaction parameters was introduced using the formula in Eq. (6.12). Figure 6.3 shows the experimental and predicted solubility of $HgCl_2$ in water.

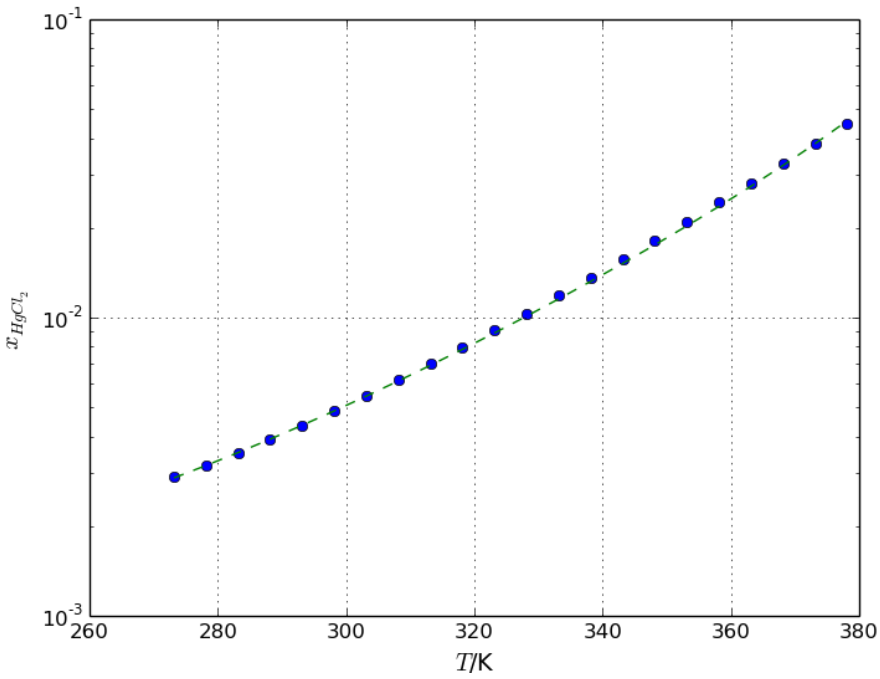

Figure 6.3: Solubility of $HgCl_2$, the symbols represent experimental data. The green dashed line represents the predicted solubility using PC-SAFT EoS.

$$k_{ij} = k_{ij}^{(0)} + k_{ij}^{(1)}T + k_{ij}^{(2)}T^2 \tag{6.12}$$

where $k_{ij}^{(0)} = -0.19393$,$k_{ij}^{(1)} = 0.002946$, $k_{ij}^{(2)} = -6.40x10^{-6}$, and T is in K.

The symbols represent the experimental data taken from [167], while the dashed line represents the predicted solubility. The AARD for 22 experimental data points was 1.36%.

It is clear that PC-SAFT EoS has the ability to predict the solubility of solid mercury species. This helps to predict mercury species precipitation quantity in oil and gas processing facilities. Moreover, It can also identify mercury species drop out temperature and pressure.

6.6 Species transformation

Understanding the transformation of any chemical specie requires both the thermodynamic and kinetic knowledge as chemical reactions might occur in different phases, gas, liquid and solid. The thermodynamics can provide several information, such as equilibrium conversion, feasibility of occurrence spontaneously, and reaction direction (forward or backward). This can be defined by knowing the potential state functions which explained in Chapter 3. The kinetic concept can provide, the rate of reaction, conversion, and the reaction controlling step. This section highlights the thermodynamic concept of species transformation according to the potential state functions. In addition to that explores the required parameters from thermodynamic and kinetic modeling point of view.

By considering mercury speciation reaction provided in Eq. (6.1) as a transformation example in this section :

$$\nu_{\mathrm{Hg}}\mathrm{Hg} + \nu_{\mathrm{HgCl_2}}\mathrm{HgCl_2} \longrightarrow \nu_{\mathrm{Hg_2Cl_2}}\mathrm{Hg_2Cl_2} \tag{6.13}$$

where ν_i is the stoichiometry of species i. The number of moles of the reactants and products can be defined as:

$$n_i = n_i^0 - \nu_i \varepsilon \tag{6.14}$$

where n_i^0 is the initial number of moles of species i, and ε is the the extent of the reaction. Due to the changes of moles between reactants and products as in Eq. (6.1), the general form of Gibbs free energy change in a system described in Eq. (3.7) can be expressed as:

$$d(nG) = (nV)dP - (nS)dT + \sum_i \nu_i \mu_i d\varepsilon \tag{6.15}$$

Therefore, at constant T, P Eq. (6.15) becomes:

$$\sum_i \nu_i \mu_i = \left[\frac{d(nG)}{d\varepsilon}\right]_{P,T} \tag{6.16}$$

The rate of change in the total Gibbs free energy with respect to the reaction coordinate at constant T and P is equal to zero, Eq. (6.16) becomes:

$$\sum_i \nu_i \mu_i = 0 \tag{6.17}$$

By combining Eq (3.28) with Eq (6.17), gives an equilibrium state of a chemical reaction:

$$\sum_i \nu_i \mu_i^o(T,P) + RT \sum_i \ln(a_i)^{\nu_i} = 0 \tag{6.18}$$

where μ_i^o is the chemical potential of pure component i at its reference state.
The reference state is a hypothetical state used as a reference point where its temperature and pressure should be defined. The Eq (6.18) can be re-arranged as :

$$\prod_i (a_i)^{\nu_i} = \exp\left(-\frac{\sum_i \nu_i \mu_i^o(T,P)}{RT}\right) \tag{6.19}$$

The change in the Gibbs free energy of any reaction at its reference state can be defined as:

$$\Delta G^o_{rxn} = \sum_i \nu_i \mu^o_i \tag{6.20}$$

Therefore, the equilibrium constant for any reaction is defined as:

$$K \equiv \exp\left(-\frac{\Delta G^o_{rxn}}{RT}\right) \tag{6.21}$$

$$K = \prod_i (a_i)^{\nu_i} \tag{6.22}$$

where K is the reaction equilibrium constant.

It is clear from Eq (6.18) that by specifying the reference state of the system, knowing the reaction mechanism, and estimating the activity a_i of species, the reaction conversion and its directions can be identified. Next section highlights the relation of reaction equilibrium constant in case of ideal gas, and dilute reference state functions are specified.

6.6.1 Ideal gas equilibrium reaction

The chemical potential of an ideal gas system as a reference state was expressed in Chapter 3 in Eq (3.33) as:

$$\mu_i = \mu_i^{o,ig} + RT \ln y_i \phi_i \tag{6.23}$$

Therefore, for mixture with an ideal gas reference state of pure i at T and P, the reaction constant becomes:

$$K^{o,ig} = \prod_i (\phi_i y_i)^{\nu_i} \equiv \exp\left(-\frac{\Delta G^{o,ig}_{rxn}}{RT}\right) \tag{6.24}$$

The Eq (6.24) can be used for ideal and non ideal gas reactions which allows to predict the reaction conversion, the direction of the reaction, and the composition of the reactants and products after reaction completion. This requires several parameters that some of each need to be experimentally measured, such as initial concentration of the reactants and products and reference state Gibbs free energy of the species, and a thermodynamic model that the ability to predict fugacity coefficient of reaction species. In addition to that, model input parameters need to be obtained, for instance PC-SAFT EoS as described in Chapter 3 and applied in Chapter 4 requires pure component parameters ($\sigma_i, \varepsilon_i/k, m_i$). This requires fitting some of thermophysical properties as vapor pressure. Next section provides the thermodynamic relation between non ideal gas equilibrium reaction constant and ideal gas equilibrium constant.

6.6.2 Non ideal system equilibrium reaction

The chemical reactions might occur in an ideal and non ideal solutions as in ideal and non ideal gases. The solution may be concentrated or dilute. For a reaction in a dilute system, the solvent has the ability to impact the thermodynamic and kinetic equilibrium. As a result, understanding its effect is of vital importance. Therefore this section provides the relation between the ideal gas equilibrium reaction constant and non ideal system equilibrium constant. Moreover, the impact of a solvent to a solute to transform is investigated.

The activity coefficient γ_i of a liquid species in the mixture can be defined as:

$$\gamma_i = \frac{a_i}{x_i} \tag{6.25}$$

where γ_i is the activity coefficient of species i in the mixture.
The chemical potential of a dilute species i in concentrated liquid solvent can be defined from The Eq (3.28) as:

$$\mu_i = \mu_i^{\infty} + RT \ln x_i \gamma_i^{\infty} \tag{6.26}$$

where μ_i^{∞} is the chemical potential of pure species i at dilute state where T,P, and concentration must be identified. when $\gamma_i^{\infty} \to 1$, concentration of $C_i \to 0$ and $x_i \to 0$, the chemical potential can be expressed in terms of mol fraction and concentration as:

$$\mu_i = \mu_i^{\infty} + RT \ln x_i \tag{6.27}$$

This can be written as:

$$\mu_i = \mu_i^{\theta} + RT \ln \frac{C_i}{C^{\theta}} \tag{6.28}$$

where C^{θ} is the standard concentration arbitrarily defined as 1M.
By combining Eq (6.23) with Eq (6.27) and Eq (6.28) , the chemical potential of a dilute solute in concentrated solvent becomes:

$$\sum_i \nu_i \mu_i^{\theta} = \sum_i \nu_i \mu_i^{o,ig} + RT \sum_i \nu_i \ln C^{\theta} V_W^o \phi_i^{\infty} \tag{6.29}$$

Therefore, the reaction equilibrium constant can be defined based on the ideal gas state reaction constant as:

$$K^{\theta} = K^{o,ig} \exp\left(- \frac{\sum_i \nu_i \ln C^{\theta} V_W^o \phi_i^{\infty}}{RT} \right) \tag{6.30}$$

where K^{θ} is the reaction equilibrium constant in a dilute system, V_W^o is the molar volume of the pure solvent at the same T and P.

It is clear form Eq (6.30) that the solvent type, concentration, and fugacity coefficient ϕ_i of species have an impact on the reaction and transformation of any specie.

Both Eq (6.24) and Eq (6.30) represent the relation between thermodynamic and kinetic of a species i in a system. In order to understand the transformation of mercury species in oil and gas processing or in the environment, the thermophysical properties of the species, such as fugacity coefficient ϕ_i, reaction rate constant $K^{o,ig}$, K^{θ}, reaction

Gibbs free energy G_{rxn}, and reaction kinetics are required. The fugacity coefficient ϕ_i can be estimated from the EoS's such as SRK or PC-SAFT, if model required input parameters are known as explained in Chapter 3 and used in Chapter 4. The reaction equilibrium constant should be measured experimentally by measuring the concentration of the reactants and products or predicted by knowing the Gibbs free energy of the reaction. For instance, in order to model the transformation of Hg to $HgCl_2$ in the presence of Cl in the flue gas, the properties of HgCl such as solubility or vapor pressure are required for model parameters estimation but these properties are unavailable in the open literature. The influence of kinetic resistances (diffusional, convective, thermal) and other resistances in the plant should be taken into account.

6.7 Conclusion

The presence of both elemental mercury and $HgCl_2$ in oil and gas processing facilities and streams have been reported. Theses compounds have been classified as an unstable species in the hydrocarbon system and have the ability to react with several materials and also with each other to generate another mercury species, such as mercury chloride. Their reaction mechanism in the hydrocarbons was not intensively investigated in the open literature where neither reaction rates nor equilibrium constants were reported. Therefor, it is recommended to investigate its reaction mechanism and measure the rate of reaction and constants. It is clear that elemental mercury in the flue gases has the ability to converted to HgCl and then to $HgCl_2$ in the presence of Cl at high and low temperatures. In order to model this transformation mechanism, it is recommended to measure the obtain some experimental data for HgCl in some liquids such as water and hydrocarbon. The reaction of mercury species with sampling material should be taken into account which might impact the the measurements.

Chapter 7

Conclusions and recommendations

7.1 Conclusions

Mercury is not only a toxic pollutant in the environment, but it is also a corrosive element to the processing facilities as explained in detail in Chapter 1 and Chapter 2. The presence of mercury in the most consumable nonrenewable energy sources (oil and gas) impacts negatively its processing facilities, and its price in the market. Different mercury species behave differently and each specie has its distinct thermophysical properties. These species may precipitate or transform to a more toxic specie as explored in Chapter 5 and Chapter 6. Therefore, it is of vital importance to protect the processing facilities to avoid unit failure which might lead to unplanned shutdown. This can only be achieved by understanding the distribution of mercury species and their transformation process in the processing facilities.

This work is aimed at the thermodynamic modeling of mercury distribution in oil and gas processing facilities. This approach has the ability to predict mercury behavior over a wide variety of operating conditions and solvents. Two thermodynamic models were used; SRK EoS in combination with group contribution was the first model, while the second model was the PC-SAFT EoS.

For the SRK EoS, a group contribution method was parameterized to estimate the temperature dependent binary interaction parameters between elemental mercury and compounds composed of CH, CH_2, CH_3, OH, H_2O, ACH and $ACCH_3$ groups. By using these binary interaction parameters, it has been found that the SRK EoS provides

a good description of mercury solubility in water, alkanes, alcohols, and aromatic solvents, as compared to available experimental data. Improper estimates for k_{ij} can yield extremely poor results; for instance, setting k_{ij} = 0, the SRK predicts that the solubility of mercury in water at 298K is 3,374 ppm, compared to the experimental value of less than 1ppm. The GCM allows the estimation of kij of elemental mercury with a wide variety of solvents and solvent mixtures, even when experimental data are not available. The group interaction parameters are already available for a wide range of systems [110, 111, 114], making this approach immediately usable in practical applications. Therefore, the SRK in combination with group contribution method was used to predict the partitioning of elemental mercury through a gas processing facility. The results of this model has been validated against field data.

For the PC-SAFT EoS two scenarios were investigated to improve the PC-SAFT EoS ability for predicting the thermophysical properties of elemental mercury, such as vapor pressure, and solubility in a wide variety of solvents and conditions. In the first scenario, elemental mercury atoms were modeled as an non− bonded atoms, while in the second scenario, the atoms were modeled as bonded atoms with 2(1:1) and 4(2:2) associating schemes by taking the association term into account. The second scenario with 2(1:1) associating scheme has significantly improved the PC-SAFT EoS ability for predicting the vapor pressure of elemental mercury and also its solubility in light and heavy hydrocarbon mixtures. The results indicated that there is no need to introduce the binary interaction between elemental mercury and normal alkanes, if elemental mercury atoms are considered as a bonded atoms with 2(1:1) associating scheme. This achievement is of a great interest, where it helps to predict the solubility of mercury in light hydrocarbons, such as methane and ethane where there is a lack of experimental data in the open literature.

The PC-SAFT EoS was then used to model the distribution of elemental mercury through a gas processing facility as explained in Chapter 5. The results were compared against field data. It is clearly seen that, the PC-SAFT EoS is more predictive than SRK EoS in combination with GCM for predicting the distribution of elemental mercury in oil and gas processing facilities. This is due to the fact that PC-SAFT takes into account several terms, such as hard chain, association, and dispersion. These terms eliminate the need for introducing the binary interaction parameters between mercury and alkanes.

Moreover, in the SRK EoS the interaction between mercury and methane was assumed to be the same as that between mercury and CH_3 group due to the lack of experimental data between mercury and methane in the open literature.

Water molecule was modeled as an associating molecule with 2(1:1) scheme. This assumption improved the ability of the PC-SAFT model to predict the solubility of mercury in water. For the stability of mercury species in the hydrocarbon system, both elemental mercury and inorganic mercury have been reported to be unstable compounds. They have the ability to react with each other, with stainless steel, and other materials.

7.2 Recommendations and future work

While this work has shown the importance of using the thermodynamic modeling for predicting the distribution of elemental mercury in oil and gas process facilities, and estimating the thermophysical properties of elemental mercury and other organic and inorganic pure components, it is recommended to experimentally measure the distribution of organic and inorganic mercury species in oil and gas processing facilities. This would progress the work to take into account the distribution of other mercury species. This also requires the experimental measurements of the thermopysical properties of the present species in order to estimate the input parameters of the models.

It has been shown that, there is an accumulation or transformation of mercury species in the second stage separator of Obaiyed gas processing plant for both models, SRK and PC-SAFT EoS. Thus, it is recommended to install mercury removal unit upstream of second stage separator in order to protect the whole processing facilities from mercury accumulation, which in turn reduces mercury risk level in the plant. Moreover, elemental mercury is more soluble in the condensate phase than gas and water phases. A discovery of new condensate well that contains mercury and connecting it into the Obaiyed processing facilities will increase the accumulation and concentration of mercury in the second stage separator.

As the PC-SAFT EoS is found to be more promising model than SRK EoS for predicting the distribution of mercury and thrmophysical properties of elemental mercury and mercury chloride as explored in Chapter 4, Chapter 5, and Chapter 6. Consequently, it is recommended to use this model for modeling the transformation of mercury species in oil and gas processing facilities as it is of vital importance to consider. This requires

the estimation of PC-SAFT input parameters, such as σ_i,ε_i/k, m_i, $\varepsilon^{A_iB_i}/k$ and $K^{A_iB_i}$. In order to estimate these, a pure component property, such as vapor pressure or density as function of temperature are needed. Thus, it is recommended to measure these properties for organic and inorganic mercury species as there is a lack of experimental data. For modelling the transformation of any mercury species in oil and gas or in the environment such as transformation of Hg to $HgCl_2$ in the presence of Cl in the flue gas, the properties of HgCl and reaction equilibrium constant should be measured experimentally.

In order to improve the ability of the PC-SAFT model, it is recommended to consider both the polar and the electrolyte terms for modeling polar and electrolyte molecules such as water. This might eliminate the requirement of interaction parameters between mercury and water which makes the PC-SAFT more predictive.

For the SRK with GCM model, it is recommended to measure the solubility of elemental mercury in methane experimentally and obtain the group interaction parameters A^0 and B^0 between elemental mercury and methane rather than modeling methane as CH_3 group. This will improve the ability of the model for predicting the distribution of mercury in natural gas.

.1 Appendix A

For the flash calculations the following equations were used;

$$K_i = \frac{\phi_{l_i}}{\phi_{v_i}} \tag{A-1}$$

where K_i is equilibrium constant.
Rachford-Rice objective function was used (equation A-2);

$$\sum_{i=1}^{c} \frac{z_i(K_i - 1)}{1 + \alpha_v(K_i - 1)} = 0 \tag{A-2}$$

where z_i is the mole fraction of component i in the feed stream and α_v is the vapor fraction of the feed. By assuming a value for z_i, the value of α_v that minimises the above objective function can be obtained and used to find the vapor and liquid phase compositions as follows

$$x_i = \frac{z_i}{1 + \alpha_v(K_i - 1)} \tag{A-3}$$

$$y_i = K_i x_i \tag{A-4}$$

where y_i and x_i are the component vapor and liquid phase compositions respectively.

.2 Appendix B

Perturbed-Chain Statistical Associating Fluid Theory Equation of State (PCS-AFT EOS)

The general form of PCSAFT EOS can be expressed in terms of Helmholtz free energy as:

$$a^{res} = a^{hc} + a^{disp} + a^{assoc} + a^{polar} + a^{elec} \tag{B-1}$$

Table B-1: Universal PC-SAFT model constants

i	a_{0i}	a_{1i}	a_{2i}	b_{0i}	b_{1i}	b_{2i}
0	0.9105631445	-0.3084016918	-0.0906148351	0.7240946941	-0.5755498075	0.0976883116
1	0.6361281449	0.1860531159	0.4527842806	2.2382791861	0.6995095521	-0.2557574982
2	2.6861347891	-2.5030047259	0.5962700728	-4.0025849485	3.8925673390	-9.155856153
3	-26.547362491	21.419793629	-1.7241829131	-21.00357681	-17.215471648	20.642075974
4	97.759208784	-65.25588533	-4.1302112531	26.855641363	192.67226447	-38.804430052
5	-159.59154087	83.31868048	13.776631870	206.55133841	-161.82646165	93.626774077
6	91.297774084	-33.746922930	-8.6728470368	-355.60235612	-165.20769346	-29.666905585

The density in PCSAFT EOS is determined through iterative procedures. First, the reduced density η is set to 0.5 for the vapor phase and 10^{-10} for the liquid phase as starting values suggested by [115]. Then the reduced density is adjusted until the calculated pressure is equal to the system pressure.

$$\rho = \frac{6}{\pi}\eta\left(\sum_i x_i m_i d_i^3\right)^{-1} \tag{B-2}$$

$$\hat{\rho} = \frac{\rho}{N_{AV}}\left(10^{10}\frac{\mathring{A}}{m}\right)^3\left(10^{-3}\frac{kmol}{mol}\right) \tag{B-3}$$

$$\zeta_{n,xk} = \left(\frac{\partial \zeta_n}{\partial x_k}\right)_{T,\rho,x_{j\neq k}} = \frac{\pi}{6}\rho m_k (d_k)^n \qquad n \in \{0,1,2,3\} \tag{B-4}$$

The partial derivative of the Hard-Chain reference contribution to Helmholtz free energy

is:

$$\left(\frac{\partial a^{hc}}{\partial x_k}\right)_{T,\rho,x_{j\neq k}} = m_k a^{hs} + \bar{m}\left(\frac{\partial a^{hs}}{\partial x_k}\right)_{T,\rho,x_{j\neq k}} - \sum_i x_i(m_i-1)(g_{ii}^{hs})^{-1}\left(\frac{\partial g_{ii}^{hs}}{\partial x_k}\right)_{T,\rho,x_{j\neq k}} \tag{B-5}$$

The partial derivative of the Hard-Sphere contribution is:

$$\begin{aligned}\left(\frac{\partial a^{hs}}{\partial x_k}\right)_{T,\rho,x_{j\neq k}} = &-\frac{\zeta_{0,xk}}{\zeta_0}a^{hs}+ \\ &\frac{1}{\zeta_0}[\frac{3(\zeta_{1,xk}\zeta_2+\zeta_1\zeta_{2,xk})}{(1-\zeta_3)}+ \\ &\frac{3\zeta_1\zeta_2\zeta_{3,xk}}{(1-\zeta_3)^2}+\frac{3\zeta_2^2\zeta_{2,xk}}{\zeta_3(1-\zeta_3)^2}+\frac{\zeta_2^3\zeta_{3,xk}(3\zeta_3-1)}{\zeta_3^2(1-\zeta_3)^3}+ \\ &\left(\frac{3\zeta_2^2\zeta_{2,xk}\zeta_3-2\zeta_2^3\zeta_{3,xk}}{\zeta_3^3}-\zeta_{0,xk}\right)\ln(1-\zeta_3)+ \\ &\left(\zeta_0-\frac{\zeta_2^3}{\zeta_3^2}\right)\frac{\zeta_{3,xk}}{(1-\zeta_3)}]\end{aligned} \tag{B-6}$$

$$\begin{aligned}\left(\frac{\partial g_{ij}^{hs}}{\partial x_k}\right)_{T,\rho,x_{j\neq k}} = &\frac{\zeta_{3,xk}}{(1-\zeta_3)^2}+ \\ &\left(\frac{d_i d_j}{d_i+d_j}\right)\left(\frac{3\zeta_{2,xk}}{(1-\zeta_3)^2}+\frac{6\zeta_2\zeta_{3,xk}}{(1-\zeta_3)^3}\right)+ \\ &\left(\frac{d_i d_j}{d_i+d_j}\right)^2\left(\frac{4\zeta_2\zeta_{2,xk}}{(1-\zeta_3)^3}+\frac{6\zeta_2^2\zeta_{3,xk}}{(1-\zeta_3)^4}\right)\end{aligned} \tag{B-7}$$

The partial derivative of the dispersion contribution to Helmholtz free energy is:

$$\begin{aligned}\left(\frac{\partial a^{disp}}{\partial x_k}\right)_{T,\rho,x_{j\neq k}} = &-2\pi\rho[I_{1,xk}\overline{m^2\epsilon\sigma^3}+I_1(\overline{m^2\epsilon\sigma^3})_{xk}]- \\ &\pi\rho([m_k C_1 I_2+mC_{1,xk}I_2+ \\ &mC_1 I_{2,xk}]\overline{m^2\epsilon^2\sigma^3}+mC_1 I_2(\overline{m^2\epsilon^2\sigma^3})_{xk})\end{aligned} \tag{B-8}$$

$$(\overline{m^2\epsilon\sigma^3})_{xk} = 2m_k \sum_j x_j m_j \left(\frac{\epsilon_{kj}}{kT}\right) \sigma_{kj}^3 \tag{B-9}$$

$$(\overline{m^2\epsilon^2\sigma^3})_{xk} = 2m_k \sum_j x_j m_j \left(\frac{\epsilon_{kj}}{kT}\right)^2 \sigma_{kj}^3 \tag{B-10}$$

$$\begin{aligned} C_{1,xk} = C_2\zeta_{3,xk} - \\ C_1^2 \left[m_k \frac{8\eta - 2\eta^2}{(1-\eta)^4} - m_k \frac{20\eta - 27\eta^2 + 12\eta^3 - 2\eta^4}{[(1-\eta)(2-\eta)]^2} \right] \end{aligned} \tag{B-11}$$

$$I_{1,xk} = \sum_{i=0}^{6} [a_i(m) i \zeta_{3,xk} \eta^{i-1} + a_{i,xk}\eta^i] \tag{B-12}$$

$$I_{2,xk} = \sum_{i=0}^{6} [b_i(m) i \zeta_{3,xk} \eta^{i-1} + b_{i,xk}\eta^i] \tag{B-13}$$

$$a_{i,xk} = \frac{m_k}{m^2} a_{1i} + \frac{m_k}{m^2}\left(3 - \frac{4}{m}\right) a_{2i} \tag{B-14}$$

$$b_{i,xk} = \frac{m_k}{m^2} b_{1i} + \frac{m_k}{m^2}\left(3 - \frac{4}{m}\right) b_{2i} \tag{B-15}$$

Compressibility factor using PC-SAFT

The compressibility factor Z can be derived from the Helmholtz free energy A using the following relation

$$Z = \rho \left(\frac{\partial(A/RT)}{\partial\rho}\right)_{N_\alpha, T} \tag{B-16}$$

As PC-SAFT accounts for hard chain, dispersion, association and electrolyte Helmholtz free energy, the total Z is the sum of these free energy as:

$$Z = 1 + Z^{hc} + Z^{disp} + Z^{assoc} + Z^{elec} \tag{B-17}$$

The residual hard-chain contribution to the compressibility factor is:

$$Z^{hc} = mZ^{hs} - \sum_i x_i(m_i - 1)(g_{ii}^{hs})^{-1}\rho\frac{\partial g_{ii}^{hs}}{\partial\rho} \tag{B-18}$$

The residual contribution of the hard-sphere fluid is:

$$Z^{hs} = \frac{\zeta_3}{(1-\zeta_3)} + \frac{3\zeta_1\zeta_2}{\zeta_0(1-\zeta_3)^2} + \frac{3\zeta_2^3 - \zeta_3\zeta_2^3}{\zeta_0(1-\zeta_3)^3} \tag{B-19}$$

where

$$\begin{aligned}\rho\frac{\partial g_{ii}^{hs}}{\partial\rho} = &\frac{\zeta_3}{(1-\zeta_3)^2} + \\ &\left(\frac{d_i d_j}{d_i + d_j}\right)\left(\frac{3\zeta_2}{(1-\zeta_3)^2} + \frac{6\zeta_2\zeta_3}{(1-\zeta_3)^3}\right) + \\ &\left(\frac{d_i d_j}{d_i + d_j}\right)^2\left(\frac{4\zeta_2^2}{(1-\zeta_3)^3} + \frac{6\zeta_2^2\zeta_3}{(1-\zeta_3)^4}\right)\end{aligned} \tag{B-20}$$

The dispersion contribution to the compressibility factor is:

$$Z^{disp} = -2\pi\rho\frac{\partial(\eta I_1)}{\partial\eta}\overline{m^2\epsilon\sigma^3} - \pi\rho m\left[C_1\frac{\partial(\eta I_2)}{\partial\eta} + C_2\eta I_2\right]\overline{m^2\epsilon^2\sigma^3} \tag{B-21}$$

$$\frac{\partial(\eta I_1)}{\partial\eta} = \sum_{i=0}^{6} a_j(m)(j+1)\eta^j \tag{B-22}$$

$$\frac{\partial(\eta I_2)}{\partial\eta} = \sum_{i=0}^{6} b_j(m)(j+1)\eta^j \tag{B-23}$$

$$\begin{aligned}C_2 &= \frac{\partial C_1}{\partial\eta} \\ &= -C_1^2\left(\bar{m}\frac{-4\eta^2 + 20\eta + 8}{(1-\eta)^5} + (1-\bar{m})\frac{2\eta^3 + 12\eta^2 - 48\eta + 40}{[(1-\eta)(2-\eta)]^3}\right)\end{aligned} \tag{B-24}$$

The association contribution to the compressibility factor is defined as:

$$Z^{assoc} = \rho\left(\frac{\partial(A^{assoc}/RT)}{\partial\rho}\right) \tag{B-25}$$

where $\frac{\partial(A^{assoc}/RT)}{\partial\rho}$ is the derivative of eq 3.89 above and is given as:

$$\frac{\partial(A^{assoc}/RT)}{\partial\rho} = \sum_i x_i\left[\sum_{A_i}\left[\frac{1}{X^{A_j}} - \frac{1}{2}\right](\frac{\partial X^{A_i}}{\partial\rho})\right] \tag{B-26}$$

and

$$\begin{aligned}\frac{\partial X^{A_i}}{\partial\rho} = -(X^{A_i})^2[\sum_j\sum_{B_j} x_j X^{B_j}\Delta^{A_iB_j} + \rho\sum_j\sum_{B_j} x_j\frac{\partial X^{B_j}}{\partial\rho}\Delta^{A_iB_j} + \\ \rho\sum_j\sum_{B_j} x_j X^{B_j}\frac{\partial\Delta^{A_iB_j}}{\partial\rho}]\end{aligned} \tag{B-27}$$

where

$$\frac{\partial\Delta^{A_iB_j}}{\partial\rho} = (\sigma_{ij})^3\kappa^{A_iB_j}\left(\frac{\partial g_{ij}^{hs}}{\partial\rho}\right)\left[\exp(\epsilon^{A_iB_j}/kT) - 1\right] \tag{B-28}$$

where

$$\begin{aligned}\frac{\partial g_{ij}^{hs}}{\partial\rho} = \left(\frac{1}{\rho}\right)[\frac{\zeta_3}{(1-\zeta_3)^2} + \frac{3d_id_j}{d_i+d_j}[\frac{\zeta_2}{(1-\zeta_3)^2} + \\ \frac{2\zeta_3\zeta_2}{(1-\zeta_3)^3}] + 2[\frac{d_id_j}{d_i+d_j}]^2[\frac{2\zeta_2^2}{(1-\zeta_3)^3} + \frac{3\zeta_3\zeta_2^2}{(1-\zeta_3)^4}]]\end{aligned} \tag{B-29}$$

The electrostatic contribution to the compressibility factor Z^{elec} is given by equation B-30 below

$$Z^{elec} = \frac{P^{elec}}{\rho_N kT} = -\left(\frac{\partial A^{elec}/kT}{\rho_N \partial \upsilon}\right)_{T,N} = \frac{\kappa}{24\pi kT\epsilon}\sum_k x_k q_k^2 \sigma_k \tag{B-30}$$

where σ_k is given by equation B-31

$$\sigma_k = \left(\frac{\partial(\kappa\chi_k)}{\partial\kappa}\right)_{T,N} = -2\chi_k + \frac{3}{1+\kappa a_k} \tag{B-31}$$

ρ_N is the number density of the system and q_k is the ion charge. The electrostatic contribution to the chemical potential μ_j^{elec} is given by equation B-32 below

$$\frac{\mu_j^{elec}}{kT} = \left(\frac{\partial A^{elec}/kT}{\partial N_j}\right)_{T,V,N_i \neq N_j} = -\frac{q_j^2\kappa}{24\pi kT\epsilon}\left[2\chi_j + \frac{\sum_k x_k q_k^2 \sigma_k}{\sum_k x_k q_k^2}\right] \tag{B-32}$$

.3 Appendix C

Fluid Phase Equilibria 432 (2017) 76–84

Contents lists available at ScienceDirect

Fluid Phase Equilibria

journal homepage: www.elsevier.com/locate/fluid

A group contribution method for predicting the solubility of mercury

Mansour Khalifa*, Leo Lue

Department of Chemical and Process Engineering, University of Strathclyde, James Weir Building, 75 Montrose Street, Glasgow G1 1XJ, United Kingdom

ARTICLE INFO

Article history:
Received 20 May 2016
Received in revised form
13 October 2016
Accepted 21 October 2016
Available online 24 October 2016

Keywords:
Mercury
Solubility
Equation of state
Group contribution method

ABSTRACT

Mercury is a toxic and corrosive element, and understanding its partitioning within ecosystems and industrial processes is of vital importance. The solubility of mercury in normal alkanes, aromatics, water and alcohols is predicted using widely used Soave-Redlich-Kwong equation of state in combination with a group contribution method to estimate binary interaction parameters. The interaction parameters between elemental mercury and seven other molecular groups were determined in this work by fitting available solubility data for mercury. The solubility in the studied solvents was accurately described. This work allows the prediction of the thermodynamic behavior of elemental mercury in a wide variety of solvents, solvent mixtures, and operating conditions where experimental data are unavailable.

1. Introduction

Mercury occurs naturally in the environment and can be found in soil, air, and water. Due to its toxicity and accumulative nature, it is considered a highly dangerous element [1–3]. The sources of mercury in the biosphere can be divided into natural and anthropogenic sources. Both are considered to be equally important causes of mercury accumulation in the environment. Natural sources include volcanic activity, erosion of terrain, and dissolution of mercury minerals in the oceans, lakes and rivers [4]. Anthropogenic sources include cement manufacturing, paper milling, the combustion of coal, oil, and gas as fuel to generate power, flared gas from onshore and offshore oil and gas platforms, and produced water discharged from oil and gas processing facilities, refineries and chemical plants [5–7].

In addition to its contribution to environmental pollution, mercury has a negative impact on the production and processing of oil and gas. As mercury is present in many major oil fields, maintenance and operation teams can be exposed to this highly dangerous element on a daily basis. Activities that expose workers to mercury include equipment cleaning, oil sampling, vessel and tank inspections and hot work activities on restricted areas. The risks are proportional to the concentration of mercury in the process facilities [8]. Mercury not only poses health risks, it is also corrosive and can cause equipment degradation and damage, catalyst poisoning, etc. [9]. It has an ability to accumulate on primary and secondary process treatment units (e.g., amine units, glycol units, cryogenic units and heat exchangers), eventually causing process failure [8].

In general, there are three ways to avoid mercury emissions from industrial sources to the environment: preventive measures, primary control measures and secondary control measures. Preventive measures can be achieved only if the source of emissions is prevented; this means fuel substitution, such as use of renewable energy or biofuels instead of mercury containing energy sources. However, this option is not popular as oil and gas are still the main source of energy. In primary control measures, Hg emissions are still generated but reduced to a certain value. In secondary control measures, Hg emissions exist but are removed later from exhaust gases [10]. The selection of the best measures requires a good understanding of the behavior of mercury and its pathways through the process and the environment. Consequently, mercury exposure risks can be mitigated by determining the concentration and understanding the exposure pathways in work locations and adopting effective health and safety policies and procedures accordingly. Understanding mercury pathways in industrial processes and the ecosystem requires knowledge of the thermodynamic behavior of mercury and its interactions with other compounds, such as process fluids (e.g., water, hydrocarbon mixtures, etc.).

Many physical properties of mercury, such as density, thermal expansion and compressibility as a function of temperature and pressure have been measured [11]. Vapor pressure is one of the

* Corresponding author.
E-mail addresses: khalifa.manssor@strath.ac.uk (M. Khalifa), leo.lue@strath.ac.uk (L. Lue).

http://dx.doi.org/10.1016/j.fluid.2016.10.025
0378-3812/

most important properties, as it indicates the state of mercury and its concentration in vapor, liquid, and solid phases. Several experimental measurements and correlations have been published for the calculation of mercury vapor pressure over wide range of temperatures [12,13].

Predicting the solubility of mercury in liquids and gases gives an indication of mercury pathways from one phase to another. Accurate prediction of mercury solubility plays an important role in developing a risk mitigation strategy. In general, however, the available experimental data are limited, in part, due to the difficulty in working with mercury. Experiments involving mercury can be time consuming and costly, and it is difficult to anticipate the wide range of process conditions and fluids that may be encountered.

In situations where experimental data are unavailable, predictive methods are required. A competitive model should be computationally inexpensive to evaluate and require minimal parameterization [14]. One powerful method is molecular simulation, which requires force fields to be parameterized between all species in the solution. This work has been focused particularly on systems containing elemental mercury [15] and some mercury compounds [15,16] in water. While these methods offer the possibility of predicting thermodynamic properties of system containing mercury, they are computationally intensive and not suitable for use in process scale simulations (e.g., in a refinery).

Another approach is to use thermodynamic models, such as an equations of state (EOS) or an activity coefficient model [17]. These models have been successfully used for the estimation of physical and chemical properties of pure and multicomponent systems. The selection of a model depends on its capability of estimating the required physical and chemical properties, and predicting the phase behavior of a specific system where experimental data are unavailable. Equations of state, such as cubic equations of state or the perturbed-chain statistical associating fluid theory (PCSAFT), are characterized by their simplicity, reliability and robustness over a wide range of conditions (e.g., high pressures), and speed of computation [18]. Therefore, they are the model of choice for many multicomponent systems and are widely used for practical applications.

A recent study used PCSAFT to describe the phase behavior of elemental mercury in liquid and compressed hydrocarbon gases [19]. While this approach works well, it requires fitting binary interaction parameters k_{ij} between mercury and the specific solvents being modeled to existing experimental measurements. Properly accounting for the interactions between molecules is vital to the accurate prediction of mixture properties. Within the context of equations of state, this is typically achieved by introducing the binary interaction parameter k_{ij} between different molecular species; k_{ij} is normally used as a fitting parameter that is adjusted to minimize the differences between the calculated and experimentally measured system properties, such as VLE, LLE, density, and solubility. This limits its usage to solvents where measurements with mercury exist.

One approach developed in order to overcome this issue is the group contribution method (GCM). In the GCM, molecules are subdivided into a series of groups which consist of individual atoms or collections of atoms [20]. The binary interaction parameters between two molecules is then given as the sum of the interaction parameters between the various pairs of groups on each of the molecules. This allows the prediction of k_{ij} for a large number of compounds where experimental data are unavailable and at operating conditions outside the range of measurements.

In this work, we parameterize a group contribution method to estimate the binary mixing parameters for the Soave-Redlich-Kwong (SRK) equation of state to the estimation of the thermodynamic properties of elemental mercury in mixtures of water, alkanes, aromatics, and alcohols. The SRK EOS is used in this work because of its simplicity, computational efficiency, and ability to predict vapor-liquid equilibria (VLE) and liquid-liquid equilibria (LLE) at high and low pressures. The k_{ij} of elemental mercury was predicted using the GCM developed by Peneloux and co-workers [20]. This has the advantage that the group interaction parameters already exist [21–23] for the SRK EOS for a wide range of molecular groups, and so the method can be immediately used in practical calculations. Combined with a group contribution method, the SRK EOS allows the prediction of mercury solubility and partitioning between phases.

In the next section, we briefly review the SRK EOS and its application to mixtures. We then present the group contribution method that is used to predict the binary interaction parameters required by the equation of state. In Section 3, this theory is compared against experimental measurements for the solubility of mercury in water, *n*-alkanes, aromatic solvents, and alcohols. Finally, the main points of this paper are summarized in Section 4, and directions for future work are discussed.

2. Methodology

The SRK EOS is a modification of a cubic equation of state proposed by Redlich and Kwong [24] developed by Soave [25] by studying the behavior of pure compounds:

$$p = \frac{\rho RT}{1-\rho b} - \frac{a\rho^2}{(1+\rho b)} \tag{1}$$

where p is the system pressure, T is the absolute temperature, and R is the universal gas constant, ρ is the molar density of the system, and a and b are parameters of the model. The first term of Eq. (1) corresponds to the repulsive force and the second term corresponds to the attraction force. The parameters a_i and b_i for a pure component i can be expressed in terms of its critical temperature T_{ci} and critical pressure p_{ci}

$$a_i = 0.42747\frac{R^2T_{ci}^2}{p_{ci}}\alpha_i(T) \tag{2}$$

$$\alpha_i(T) = \left[1 + \left(0.480 + 1.57\omega_i - 0.176\omega_i^2\right)\left(1 - \sqrt{\frac{T}{T_{ci}}}\right)\right]^2 \tag{3}$$

$$b_i = 0.08664\frac{RT_{ci}^2}{p_{ci}} \tag{4}$$

where ω_i is the acentric factor for component i, introduced by Pitzer [17].

To extend the SRK EOS to multi-component systems, mixing rules are required to obtain the parameters a and b for the solution from the a_i's and b_i's from the individual pure components. Many mixing rules have been proposed for cubic EOS [26,27]. In this work, we use the van der Waals mixing rules, which are given by

$$a = \sum_{ij} x_i x_j \sqrt{a_i a_j}(1 - k_{ij}) \tag{5}$$

$$b = \sum_i x_i b_i \tag{6}$$

where k_{ij} in Eq. (5) is the binary interaction parameter, x_i is the mole fraction of component i in the mixture, and a_i and b_i are calculated from Eqs. (2) and (4).

2.1. The Helmholtz energy

From knowledge of the Helmholtz energy as a function of the temperature, volume, and component densities, all thermodynamic properties of a system can be determined. For an ideal gas, the molar Helmholtz energy A^{ig} is given by

$$A^{ig}(T,\rho) = \sum_{i=1} x_i \mu_i^\circ + RT \sum_{i=1} x_i (\ln \rho_i b_i - 1) \tag{7}$$

where ρ_i is the molar density of component i, and μ_i° is the standard state chemical potential.

In order to consider real systems, we define a residual property as the difference between the property of the actual system and that of an ideal gas at the same total volume, temperature and number of moles of each species [18]

$$M^{res}(T,V,n) = M(T,V,n) - M^{ig}(T,V,n) \tag{8}$$

where M^{res} is any residual property.

The molar residual Helmholtz energy A^{res} can be directly determined from the equation of state by

$$A^{res} = RT \int_0^\rho \frac{d\rho}{\rho}(Z-1) = I \tag{9}$$

where $Z = p/(\rho RT)$ is the compressibility factor, and ρ is the molar density of the system.

The compressibility factor for the SRK equation of state can be written as:

$$\begin{aligned} Z &= \frac{1}{1-\rho b} - \frac{a}{b^2 RT}\frac{\rho b}{1+\rho b} \\ &= Z_{exc} + Z_{att} \end{aligned} \tag{10}$$

where Z_{exc} accounts for excluded volume interactions, and Z_{att} accounts for attractive interactions. Substituting Eq. (10) into Eq. (9), A^{res} can be written as:

$$A^{res} = I_{exc}(\rho b) - E(T,x)Q(\rho b) \tag{11}$$

where I_{exc} is the contribution from excluded volume interactions, E characterizes the dependence of the attractive interactions in the system on the composition and temperature, and Q captures the influence of density (which is related to the "frequency" of the interactions). For the SRK EOS, these terms are explicitly given by

$$I_{exc}(\rho b) = -RT\ln(1-\rho b), \tag{12}$$

$$E(T,x) = \frac{a}{b^2}, \tag{13}$$

$$Q(\rho b) = \ln(1+\rho b). \tag{14}$$

In order to characterize the influence of mixing on a system, we first define an ideal solution, where the Helmholtz energy is defined as:

$$A^{id} = \sum_{i=1} x_i A_i^\circ + RT \sum_{i=1} x_i \ln x_i \tag{15}$$

where A_i° is the molar Helmholtz energy of pure component i, which is given by

$$A_i^\circ = \mu_i^\circ + RT(\ln \rho b_i - 1) + I_i^\circ \tag{16}$$

where I_i° is the molar residual Helmholtz free energy of pure i at packing fraction ρb_i and temperature T. We also define an excess property as the difference between the actual value of the property of the system and the value of an ideal mixture at the same temperature, total moles of each species and packing fraction [18]:

$$M^E(T,n,\rho b) = M(T,n,\rho b) - M^{id}(T,n,\rho b) \tag{17}$$

where M^E is the excess property and M^{id} is the ideal mixture property.

The excess Helmholtz free energy at constant temperature, constant volume, and constant number of moles of each species can be defined based on Eq. (17) as:

$$\begin{aligned} A^E(T,n,\rho b) &= A(T,n,\rho b) - A^{id}(T,n,\rho b) \\ &= RT\sum_i x_i \ln\frac{b_i}{b} + I - \sum_i x_i I_i^\circ . \end{aligned}$$

The first term represents effect of molecule size on the free energy of mixing, while the final two terms give the influence of the attractive interactions between molecules.

For an equation of state similar in form to the SRK EOS, the excess Helmholtz free energy can be written as

$$A^E(T,n,\rho b) = RT\sum_i x_i \ln\frac{b_i}{b} + \frac{Q(\rho b)}{2b}\sum_{i,j} x_i x_j b_i b_j E_{ij} \tag{18}$$

where E_{ij} physically captures the free energy of interaction between a molecule of type i and a molecule of type j, and the Q term describes the frequency of the interactions. The parameter E_{ij} can be directly related to the original parameters of the SRK equation of state as

$$E_{ij} = -2\frac{a_{ij}}{b_i b_j} + \frac{a_i}{b_i^2} + \frac{a_j}{b_j^2}. \tag{19}$$

Using the van der Waals mixing rules (see Eqs. (5) and (6)) leads to:

$$E_{ij} = (\delta_i - \delta_j)^2 + 2\delta_i\delta_j k_{ij} \tag{20}$$

where $\delta_i = a_i^{1/2}/b_i$ is the Scatchard-Hildebrand solubility parameter [17,22,28]. So we see that the binary interaction parameter k_{ij} describes the deviation of the interaction free energy between two molecules from that given by the regular solution model:

$$k_{ij} = \frac{E_{ij} - (\delta_i - \delta_j)^2}{2\delta_i\delta_j}. \tag{21}$$

The regular solution model applies to mixtures where molecules are of similar size and interact only through dispersion forces [17]. For mixtures of molecules of different size or where other forces are present (e.g., hydrogen bonding, dipole-dipole interactions, etc.), deviations from this model are to be expected. In this work, this is captured by the mixing parameter k_{ij}.

2.2. Group contribution method

In order to obtain accurate results with a cubic EOS, appropriate values for binary interaction parameters are required. Typically, the k_{ij}'s are used as fit parameters used to reproduce experimental data.

However, frequently the experimental data required to develop and validate the thermodynamic models are lacking. Several empirical methods have been proposed to estimate binary interaction parameters; however, many of these correlations fail to properly predict the phase behavior at elevated pressures [29].

Alternate mixing rules to the van der Waals mixing rule (see Eqs. (5) and (6)) have been proposed as in order to improve the accuracy of EOS's. One class of these is based on combining the EOS with an activity coefficient model [21] and is typically referred to as EOS/g^E.

The use of group contribution techniques with activity coefficient models, such as UNIFAC, has been quite successful [14]. Calculating an EOS's parameters based on a group contribution method (GCM) is often more powerful than the use of activity coefficient models and can provide accurate predictions [18,21]. The combination of an EOS with a group contribution method results in a predictive model that provides a theoretical expression for k_{ij}

The interaction free energy E_{ij} between a molecule of type i and a molecule of type j, which appears in Eq. (20), can be expressed in terms of a sum of the interactions between pairs of groups within the molecules [20]

$$E_{ij} = -\frac{1}{2}\sum_{k,l}\left(\alpha_{ik} - \alpha_{jk}\right)\left(\alpha_{il} - \alpha_{jl}\right)A_{kl}(T) \tag{22}$$

where the indices k and l run over all types of groups in the system, and α_{ik} is the fraction of molecule i occupied by group k. For example, propane has a molecular structure of CH_3–CH_2–CH_3; It contains two CH_3 groups and one CH_2 group. Therefore the total number of groups present in this molecule is three. In this case, the fraction of molecule *propane* occupied by group CH_2 is $\alpha_{\text{propane}-\text{CH2}} = 1/3$, and the fraction of molecule *propane* occupied by group CH_3 is$\alpha_{\text{propane}-\text{CH3}} = 2/3$.

The temperature dependence of the interaction parameter $A_{kl}(T)$ is given by:

$$A_{kl}(T) = A^0_{kl}\left(\frac{T_0}{T}\right)^{B^0_{kl}/A^0_{kl}-1} \tag{23}$$

where T is the absolute temperature, $T_0 = 298.15$ K is a reference temperature, and A^0_{kl} and B^0_{kl} are the interaction parameters between groups k and l.

The quantity $A_{kl}(T)$ represents the negative free energy of interaction between a group of type k and a group of type l. From the Gibbs-Helmholtz equation [17], we can then identify the quantity

$$B^0_{kl}\left(\frac{T_0}{T}\right)^{B^0_{kl}/A^0_{kl}-1}$$

with the attractive energy of interaction between groups, and, consequently, the quantity

$$A^0_{kl}\left(B^0_{kl}/A^0_{kl} - 1\right)\left(\frac{T_0}{T}\right)^{B^0_{kl}/A^0_{kl}-1}$$

is related with the entropy of the interaction.

This group contribution method (GCM) was used by Jaubert and Noël [21] to predict the VLE of several binary mixture of hydrocarbon components using the Peng-Robinson EOS (PR), calling this the predictive Peng-Robinson 1978 (PPR78). Noël showed that the obtained results from GCM are often more precise than EOS/g^E models. Another study used the GCM to predict k_{ij} of a system containing hydrocarbon components and carbon dioxide CO_2 using SRK EOS [23]. The study indicated its feasibility to estimate the k_{ij} of any mixture containing carbon dioxide and hydrocarbons at any temperature. A relation between the k_{ij} parameters for PPR78 and the SRK EOS has been developed [22]. This helps to predict GCM parameters of SRK EOS based on PR EOS GCM parameters. Consequently, the values for the group interaction parameters A^0_{kl} and B^0_{kl} between a large number of different types of groups is already available.

3. Results and discussion

In this section, we determine the values of the group interaction parameters A^0_{kl} and B^0_{kl} appearing in Eq. (23) between elemental mercury and various molecular groups. As an initial step in this process, we need to ensure that the properties of the pure components are properly described by the SRK equation of state. This is done by ensuring the vapor pressure curves are accurately reproduced, which is described in the next section.

Once the pure component parameters of the SRK EOS are chosen, the values of the group interaction parameters are determined by fitting experimental solubility data for mercury in a variety of solvents. This is done by minimizing the objective function F_{obj}

$$F_{\text{obj}} = \sum_i \left(\frac{S_i^{\text{calc}} - S_i^{\text{exp}}}{S_i^{\text{exp}}}\right)^2 \tag{24}$$

where S_i^{exp} is the experimental solubility of mercury in the selected solvent, and S_i^{calc} is the calculated solubility of mercury in the selected solvent.

Vapor-liquid equilibrium (VLE) and liquid-liquid equilibrium (LLE) calculations were performed for the SRK equation of state using standard flash algorithms implemented in Python to obtain the solubility of mercury S_i^{calc}. The LmFit package in Python was used to determine the values of the group interaction parameters A^0_{kl} and B^0_{kl} in Eq. (23) that minimize the objective function. The optimized values and their uncertainties are summarized in Table 1. These are discussed in more detail in the following parts of this section.

3.1. Vapor pressure

In order to predict the pure component properties of a species, the SRK equation of state requires its critical pressure, critical temperature and acentric factor. In principle, these can be obtained.

In the literature, pure fluid parameters vary slightly from reference to reference. In this work, the acentric factor was only tuned in order to achieve the minimum absolute average relative deviation error (AARD) in vapor pressure. The adjusted acentric factor and critical pressure, critical temperature are summarized in Table 2. Note that these values are in good agreement with the accepted experimental critical properties for these compounds in the literature.

Fig. 1 indicates that the SRK EOS is capable of accurately

Table 1
Group interaction parameters A^0 and B^0 for mercury with other groups.

Group	$10^{-4}A^0$ bar^{-1}	$10^{-4}B^0$ bar^{-1}	B^0/A^0 –
CH	10.9143 ± 0.0023	7.00 ± 0.0945	0.66
CH_2	7.8864 ± 0.0057	7.0562 ± 0.065	0.89
CH_3	8.5137 ± 0.0207	7.1461 ± 0.27	0.84
OH	6.5524 ± 0.00204	5.29903 ± 0.837	0.80
ACH	7.7506 ± 0.0036	8.1350 ± 0.01	1.049
$ACCH_3$	7.5699 ± 0.028	7.9629 ± 1.1	1.052
H_2O	9.9037 ± 0.0063	3.7305 ± 0.0289	0.38

Table 2
Pure component critical properties and acentric factor.

Component	p_c bar	T_c K	ω –	Ref.
mercury	1670.0	1764	−0.2102	[44]
propane	42.55	369.92	0.152	[45]
n-butane	37.966	425.16	0.205	[45]
n-pentane	33.691	469.7	0.250	[45]
n-hexane	30.124	507.31	0.305	[45]
n-heptane	27.358	540.1	0.3525	[45]
n-octane	24.865	568.76	0.3978	[45]
n-nonane	22.879	594.56	0.4419	[45]
n-decane	21.035	617.5	0.492	[45]
benzene	48.98	562.79	0.2130	[45]
toluene	43.2	591.8	0.268	[45]
o-xylene	39.8	633.3	0.304	[45]
methanol	80.959	512.5	0.556	[45]
isopropanol	47.63	508.37	0.657	[45]
water	220.64	647.14	0.324	[46]

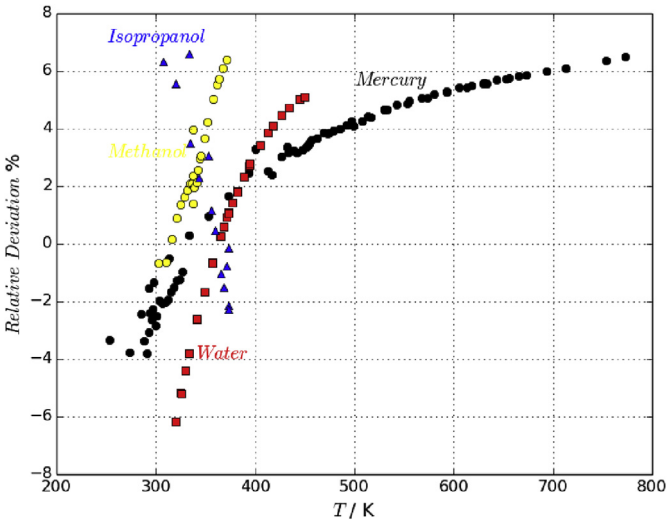

Fig. 1. Relative deviation in vapor pressure for elemental mercury (black), water (red), methanol, (yellow), and isopropanol (blue). (For interpretation of the references to colour in this figure legend, the reader is referred to the web version of this article.)

predicting the vapor pressure of elemental mercury, water, and alcohols. The AARD for 99 experimental data points of elemental mercury over a temperature range of 253.15 K–773.15 K was 3.7%, the experimental data used in this work were taken from Refs. [30–33]. These data were classified by Huber et al. as primary experimental data, because of their low experimental uncertainty of around 1% [12].

The AARD for the vapor pressure of water was 2.5% for 38 experimental data points over a temperature range of 319.6 K–449.7 K; the experimental data used in this work were taken from Ref. [34]. For methanol and isopropanol, the AARD was 2.8% for 24 data points and 2.6% for 14 experimental data points, respectively; the experimental data were taken from Refs. [35–37].

Fig. 2 shows the relative deviation of the predictions of the SRK equation of state for the vapor pressure of some *n*-alkanes and aromatic compounds. The AARD for propane, *n*-pentane, and *n*-decane was 0.4% for 31 experimental data points, 0.2% for 50 experimental data points, and 2.5% for 32 experimental data points respectively. the experimental vapor pressure data were taken from Refs. [38–40]. In addition, the AARD for the vapor pressure of benzene, toluene, and *o*-xylene was 0.9% for 13 experimental data points, 0.3% for 17 data points, and 0.78% for 12 data points,

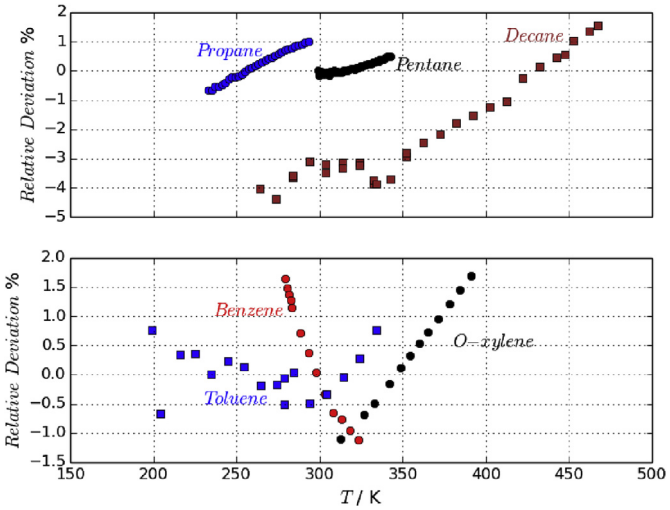

Fig. 2. Relative deviation in vapor pressure of (a) *n*-alkanes and (b) aromatic compounds.

respectively; the experimental vapor pressure data for aromatics were taken from Refs. [41–43].

3.2. Solubility of mercury in water

The solubility of elemental mercury in water is available over a wide range of temperatures. The experimental data used in this work were taken from Ref. [47], which are shown as the symbols in Fig. 3(a) over a temperature range of 273.15 K–393.15 K. The dashed line in Fig. 3(a) is the solubility of mercury predicted by the SRK EOS, neglecting the binary interaction parameter (i.e. $k_{ij} = 0$); without introducing proper binary interaction parameters, the mercury solubility in water is severely overestimated. The solid line in Fig. 3(a) gives the prediction of the SRK EOS with the k_{ij} shown in Fig. 3(b). For this system, an AARD of 4.2% was obtained for 25 experimental data points. The binary interaction parameter between mercury and water is temperature dependent; it increases by 0.05 with each 20 K increase in temperature.

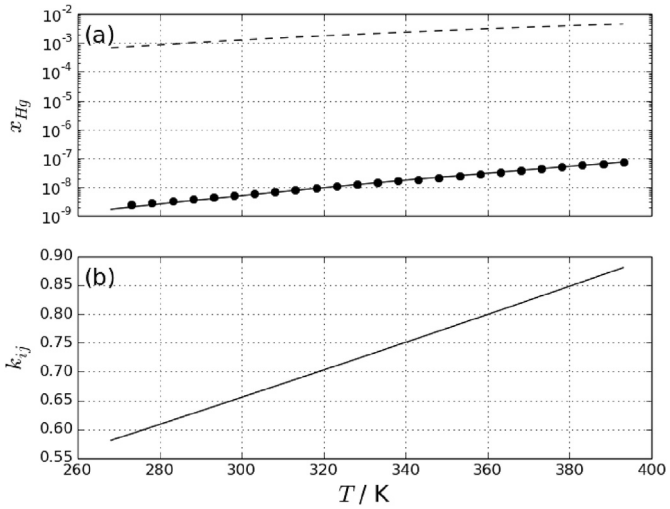

Fig. 3. (a) Solubility of mercury in water. The dashed line is the prediction of the SRK EOS with $k_{ij} = 0$, and the solid line is the prediction with k_{ij} estimated using the group contribution method. (b) The variation with temperature of the binary interaction parameter between mercury and water.

Thermodynamically, the ratio B^0/A^0 reflects the influence of entropy on the mixing of groups. If the ratio is less than one, the mixing process tends to increase entropy; the molecules become more disordered than in ideal mixing. If the ratio is greater than one, then entropy is lost in mixing; the molecules are more ordered than in ideal mixing. For a ratio of one, there is no excess entropy of mixing and, and enthalpy drives the process. In this case, the binary interaction parameter temperature independent.

3.3. Solubility of mercury in normal alkanes

Normal alkanes represent more than 90% of natural gas and crude oil species. Predicting mercury solubility in these species is crucial. Elemental mercury is considered the dominant mercury species in the crude oil and natural gas [9,48]. The solubility data of elemental mercury in hydrocarbon systems are sparse and covers a limited temperature range, The experimental data used in this work are shown as the symbols in Fig. 4(*a*) and (*b*) for alkanes from C_5 to C_{10}, and Fig. 5(*a*)and (*b*) for C_3 and C_4. These data were taken from Refs. [49,50]. Around 65 experimental data points for C_5 to C_{10} over a temperature range of 273.15 K–336.15 K and atmospheric pressure, and 3 experimental data points for C_8 over a temperature range from 338.15 K to 473.15 K and 6 bar. In addition to 17 data points for C_3 and C_4 at different temperatures and pressures.

Fig. 4(a) and (b) show the predicted solubility of elemental mercury in normal alkanes from C_5 to C_{10}. The dashed lines in Fig. 4 are the solubilities predicted by the SRK EOS, neglecting the binary interaction parameter (i.e. $k_{ij} = 0$); without introducing the proper binary interaction parameters, the mercury solubility in alkanes is nearly independent of the molecular weight of the alkanes. By introducing the binary interaction parameter, the results indicated by the solid lines in Fig. 4 are obtained. The AARD for the solubility in normal alkanes from C_3 to C_{10} was 5.47% for 74 experimental data points.

In the recent study of Polishuk et al. [19], the Peng-Robinson (PR) and PC-SAFT equations of state were used to predict the properties of mercury-hydrocarbon mixtures. In their work, a single, constant value of k_{ij}, which was fixed by fitting to experimental solubility data of mercury in *n*-pentane, was used. The results of the study showed that within this approach, the Peng-Robinson EOS was incapable of estimating the solubility of mercury in the studied hydrocarbon systems, apart from mercury-pentane. The results presented in Fig. 3 of Polishuk et al. show that the predicted solubility of mercury in C_8 using PC-SAFT and the PR EoS at 298.15 °C was 0.91 ppm and 3.5 ppm, respectively, while the experimental solubility was 1.08 ppm. The value obtained in this study using the GCM was 1.10 ppm which is much closer to the experimental value.

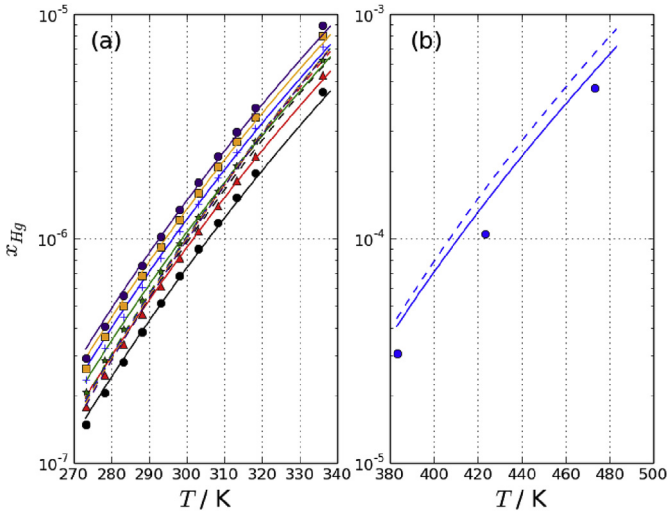

Fig. 4. Solubility of mercury in normal alkanes: C_5 (black), C_6 (red), C_7 (green), C_8 (blue), C_9 (orange), and C_{10} (indigo). The symbols represent experimental data, the solid lines represent predicted solubility with the binary interaction parameters estimated using the GCM, and the dashed lines represent the solubility without introducing the binary interaction parameter. (For interpretation of the references to colour in this figure legend, the reader is referred to the web version of this article.)

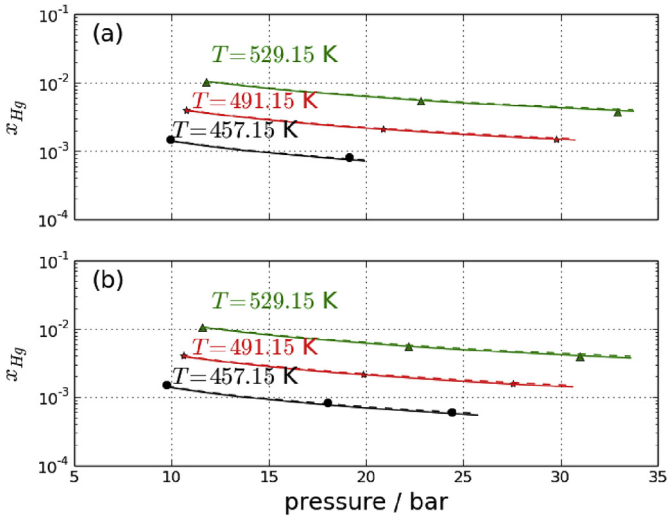

Fig. 5. Solubility of mercury in (a) propane and (b) butane.

In our study, different k_{ij} values were calculated using GCM for each mercury-hydrocarbon binary system at the system temperature and pressure. This approach improves the prediction of mercury solubility in normal alkanes more accurately than fixing k_{ij} to a single value. The solubility of elemental mercury increases with the carbon numbers, which is in consistent with the observations of Refs. [49,50].

Several process facilities, such as stripping columns, heat exchangers, reactors, and distillation units operate at high temperatures; therefore, predicting mercury solubility in alkanes at high temperature is crucial. The solubility of elemental mercury in some organic solvents, including octane, dodecane, and toluene, has been experimentally and theoretically estimated over a temperature range from 100 °C to 200 °C and up to 6 bar [50]. Fig. 4(b) represents the predicted solubility of elemental mercury in normal octane at 6 bar and high temperatures.

Fig. 5(*a*) and (*b*) show the solubility of mercury in propane and butane, respectively, at a range of pressures and temperatures. It is clear that the SRK EOS predicts the solubility of elemental mercury in light hydrocarbons well. This is due to fact that cubic EOS's are capable of predicting vapor phase properties more accurately than liquid phase properties. It can be noticed that the solubility of elemental mercury in propane is almost equal to that in butane. This implies that the solubility of mercury in light hydrocarbons in the gas phase is independent of carbon number. This suggests that the interaction of elemental mercury with methane or ethane is similar to that with propane and butane. This enables the estimation of mercury solubility in methane, as the experimental data are unavailable.

The binary interaction parameters of mercury in normal alkanes from C_5 to C_{10} are shown in Fig. 6. The interaction of mercury with these higher molecular weight alkanes depends on both the carbon number and temperature.

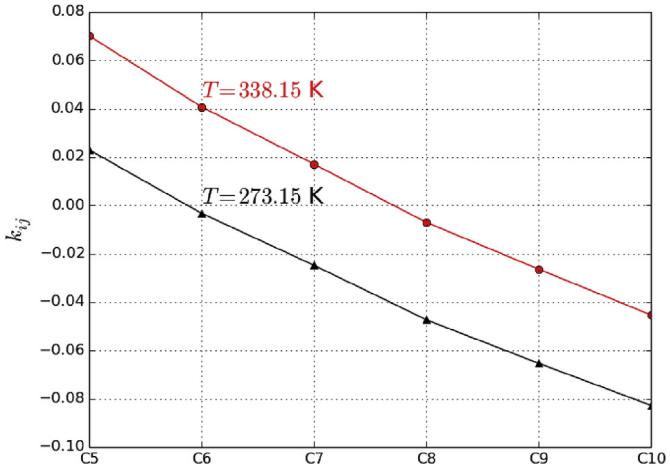

Fig. 6. Binary interaction parameter for mercury-alkane mixtures.

3.4. Solubility of mercury in aromatics

Aromatics are considered to be the main raw material for many petrochemical industries [51]. The naphtha reforming process is one of main sources of aromatics. As crude oil and natural gas are the main sources of aromatics and crude oil is known to contain mercury, predicting the solubility of mercury in aromatics is vital of importance.

Fig. 7(a) shows the solubility of elemental mercury in benzene, toluene, and *o*-xylene over a range of temperatures. The experimental data are taken from Ref. [49], which are shown as the symbols. The dashed lines are the predictions of the SRK EOS with $k_{ij} = 0$. It is clear that by neglecting the binary interaction parameters, the predicted solubility of elemental mercury in aromatics is relatively insensitive to the presence of methyl groups.

Two types of interaction groups for benzene, toluene, and *o*-xylene were defined by dividing the carbons in the aromatic ring. One group ACH is an aromatic carbon that is attached to a hydrogen atom; benzene has six of these groups, while toluene has only five and *o*-xylene has four. The other group ACCH3 is an aromatic carbon attached to a methyl group; benzene has none of these groups, toluene has one, and *o*-xylene has two. The values of the interaction parameters of these groups with elemental mercury were fit to the solubility data for mercury in benzene and in *o*-xylene. These are summarized in Table 1.

The solid lines in Fig. 7(a) show the solubilities calculated by the SRK EOS with the binary interaction parameters estimated by the group contribution method. As a test of the group contribution model, the binary interaction parameter between mercury and toluene was predicted based on the group interaction parameters obtained from mercury-benzene and mercury-*o*-xylene mixtures. The AARD for mercury in benzene, toluene, and *o*-xylene was 1.87% for 8 data points over a temperature range of 273.15 K–313.15 K, 6.1% for 6 data points over a temperature range of 273.15 K–308.15 K, and 2.7% for 5 data points over a temperature range of 273.15 K–308.15 K and atmospheric pressure, respectively.

The results presented in Fig. 4 of the Polishuk et al. [19] study show that the predicted solubility of mercury in toluene using PC-SAFT and PR EoS at 293.15 °C was 0.91 ppm and 1.05 ppm, respectively, while the experimental solubility was 0.98 ppm. The value obtained in this work using the GCM and based on the group interaction parameters obtained from mercury-benzene and mercury-*o*-xylene mixtures was 0.94 ppm, which better reflects the experimental value. The GCM is capable of predicting binary interaction parameters of compounds where experimental data are unavailable.

By introducing binary interaction parameters, the solubility of elemental mercury in aromatics is found to increase with the number of methyl groups, which is consistent with what is experimentally observed. Fig. 7(b) indicates that the interaction between mercury and aromatics is fairly independent of temperature.

3.5. Solubility of mercury in alcohols

Alcohols such as mono-ethylene glycol (MEG) and diethylene glycol (DEG) are widely used in oil and gas processing as anti-freeze and anti-corrosion agents; however, experimental data for the solubility of mercury in these alcohols are not available in the literature. One of the motivations of this work is to predict mercury solubility in such alcohols.

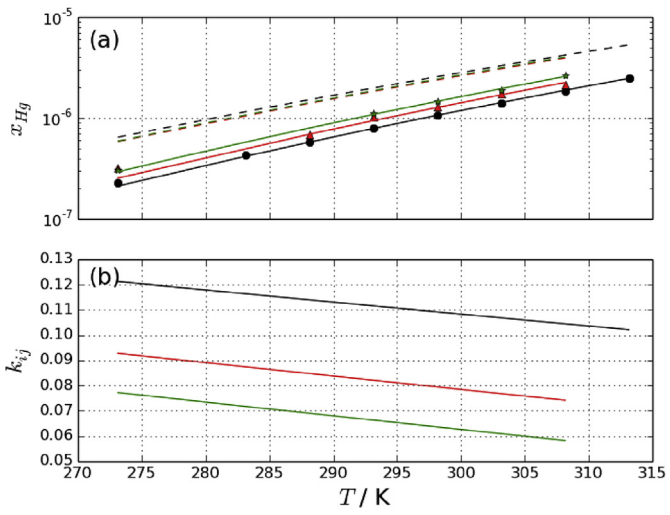

Fig. 7. (a) Solubility and (b) binary interaction parameter of mercury with in benzene (black), toluene (red), and *o*-xylene (green). (For interpretation of the references to colour in this figure legend, the reader is referred to the web version of this article.)

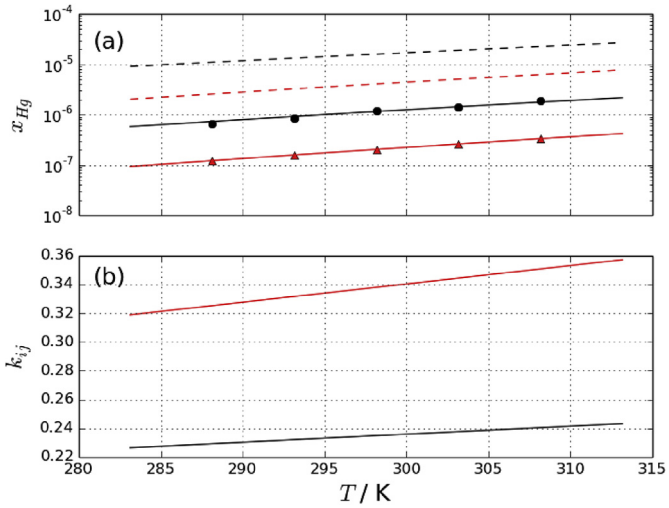

Fig. 8. Solubility of mercury in methanol (black) and isopropanol (red). The symbols represent experimental data, the solid lines are predicted solubilities with the binary interaction parameter estimated using the GCM, and the dashed lines are predictions with the binary interaction parameter set to zero. (For interpretation of the references to colour in this figure legend, the reader is referred to the web version of this article.)

Experimental data are available for the solubility of mercury in methanol and isopropanol [47]. Fig. 8(*a*) shows a comparison of the SRK EOS, with and without the binary interaction parameter, and experimental measurements for the solubility of mercury in methanol and isopropanol. Significant deviation can be observed between the experimental data and correlated results when $k_{ij} = 0$.

The group interaction parameters between elemental mercury and the OH group were determined by fitting experimental solubility data for alcohols (see Table 1). Fig. 8(b) shows that the k_{ij} between mercury and isopropanol is more temperature dependent than methanol.

Using the group contribution method, the interaction between mercury and MEG or DEG can be easily predicted. As a test of the group contribution model, we predict the solubility of mercury in MEG. Large quantities of MEG are injected at the wellhead in order to avoid hydrate formation during transportation process. The partitioning of elemental mercury from a gas phase into MEG solutions was investigated under standard laboratory conditions [52]. It was observed that the solubility of elemental mercury in MEG ranged from 0 to 60 ppb. Using the SRK combined with GCM developed in this work to estimate k_{ij}, we predict that the solubility of mercury in MEG is 57.7 ppb. Using $k_{ij} = 0$, the solubility of mercury in MEG is 1.78 ppm. It is clear that the SRK combined with the GCM is able to predict mercury solubility in alcohol systems.

4. Conclusions

Mercury is not only a toxic pollutant in the environment, but it is also a corrosive element to processing equipment. Understanding mercury pathways in an ecosystem or its distribution in process facilities requires a model that is able to predict its thermodynamic behavior in a wide variety of conditions and solvents. In this work, we parameterize a group contribution method to estimate the temperature dependent binary interaction parameters between elemental mercury and compounds composed of CH, CH_2, CH_3, OH, H_2 O, ACH and $ACCH_3$ groups. By using these binary interaction parameters, we find that the SRK EOS provides a good description of mercury solubility in water, alkanes, alcohols, and aromatic solvents, as compared to available experimental data. Improper estimates for k_{ij} can yield extremely poor results; for instance, setting $k_{ij} = 0$, the SRK predicts that the solubility of mercury in water at 298 K is 3374 ppm, compared to the experimental value of less than 1 ppm. The group contribution method allows the estimation of k_{ij} of elemental mercury with a wide variety of solvents and solvent mixtures, even when experimental data are not available. The group interaction parameters are already available for a wide range of systems [21–23], making this approach immediately usable in practical applications.

Currently, we are using this group contribution model to estimate the partitioning of elemental mercury through a gas processing facility and validating the calculations against field data. In future, we intend to extend this approach to organic mercury compounds to examine the speciation and distribution of mercury.

Acknowledgments

MK is grateful to the Department of Chemical and Process Engineering Department at the University of Strathclyde and to the Libyan Ministry of Higher Education and Scientific Research for financial support. The authors are thankful to Dr. Karen Johnston for useful discussions.

References

[1] A. Maulvault, P. Anacleto, V. Barbosa, J.J. Sloth, R. Rasmussen, A. Tediosi, M. Fernandez-Tejedor, F.H. van den Heuvel, M. Kotterman, A. Marques, Toxic elements and speciation in seafood samples from different contaminated sites in Europe, Part B, Environ. Res. 143 (2015) 72–81, http://dx.doi.org/10.1016/j.envres.2015.09.016.

[2] H.D. Choi, J. Huang, S. Mondal, T.M. Holsen, Variation in concentrations of three mercury (Hg) forms at a rural and a suburban site in New York State, Sci. Total Environ. 448 (2013) 96–106, http://dx.doi.org/10.1016/j.scitotenv.2012.08.052.

[3] C. Deng, D. Zhang, X. Pan, F. Chang, S. Wang, Toxic effects of mercury on {PSI} and {PSII} activities, membrane potential and transthylakoid proton gradient in microsorium pteropus, J. Photochem. Photobiol. B 127 (2013) 1–7, http://dx.doi.org/10.1016/j.jphotobiol.2013.07.012.

[4] R. Ferrara, B. Mazzolai, E. Lanzillotta, E. Nucaro, N. Pirrone, Volcanoes as emission sources of atmospheric mercury in the Mediterranean basin, Sci. Total Environ. 259 (1–3) (2000) 115–121, http://dx.doi.org/10.1016/S0048-9697(00)00558-1.

[5] Q. Liu, Mercury concentration in natural gas and its distribution in the Tarim Basin, Sci. China Earth Sci. 56 (8) (2013) 1371–1379, http://dx.doi.org/10.1007/s11430-013-4609-2.

[6] F. Wang, S. Wang, L. Zhang, H. Yang, Q. Wu, J. Hao, Mercury enrichment and its effects on atmospheric emissions in cement plants of China, Atmos. Environ. 92 (2014) 421–428, http://dx.doi.org/10.1016/j.atmosenv.2014.04.029.

[7] N. Pirrone, S. Cinnirella, X. Feng, R.B. Finkelman, H.R. Friedli, J. Leaner, R. Mason, A.B. Mukherjee, G.B. Stracher, D.G. Streets, K. Telmer, Global mercury emissions to the atmosphere from anthropogenic and natural sources, Atmos. Chem. Phys. 10 (2010) 5951–5964, http://dx.doi.org/10.5194/acp-10-5951-2010.

[8] S.M. Wilhelm, Avoiding exposure to mercury during inspection and maintenance operations in oil and gas processing, Process Saf. Prog. 18 (3) (1999) 178–188, http://dx.doi.org/10.1002/prs.680180311.

[9] S.M. Wilhelm, N. Bloom, Mercury in petroleum, Fuel Process. Technol. 63 (1) (2000) 1–27, http://dx.doi.org/10.1016/S0378-3820(99)00068-5.

[10] L.D. Hylander, M.E. Goodsite, Environmental costs of mercury pollution, Sci. Total Environ. 368 (1) (2006) 352–370, http://dx.doi.org/10.1016/j.scitotenv.2005.11.029.

[11] G.J.F. Holman, C.A. ten Seldam, A critical evaluation of the thermophysical properties of mercury, J. Phys. Chem. Ref. Data 23 (5) (1994) 807–827, http://dx.doi.org/10.1063/1.555952.

[12] M.L. Huber, A. Laesecke, D.G. Friend, Correlation for the vapor pressure of mercury, Ind. Eng. Chem. 45 (2006) 7351–7361, http://dx.doi.org/10.1021/ie060560s.

[13] A. Merlone, C. Musacchio, The mercury vapour pressure vs. temperature relation between (500 and 665)K, J. Chem. Thermodyn. 42 (1) (2010) 38–47, http://dx.doi.org/10.1016/j.jct.2009.07.012.

[14] C.-C. Chen, P.M. Mathias, Applied thermodynamics for process modeling, AIChE J. 48 (2) (2002) 194–200, http://dx.doi.org/10.1002/aic.690480202.

[15] M.H. Abraham, J. Gil-Lostes, W.E. Acree Jr., J. Enrique Cometto-Muniz, W.S. Cain, Solvation parameters for mercury and mercury(ii) compounds: calculation of properties of environmental interest, J. Environ. Monit. 10 (2008) 435–442, http://dx.doi.org/10.1039/B719685G.

[16] M.H. Lagache, J. Ridard, P. Ungerer, A. Boutin, Force field optimization for organic mercury compounds, J. Phys. Chem. B 108 (24) (2004) 8419–8426, http://dx.doi.org/10.1021/jp049676x.

[17] J.M. Prausnitz, R.N. Lichtenthaler, E.G. de Azevedo, Molecular Thermodynamics of Fluid-phase Equilibria, second ed., Prentice-Hall, Englewood Cliffs, NJ, 1986.

[18] M.B. Ewing, C.J. Peters, Fundamental considerations, in: C.P.J.V. Sengers, R.F. Kayser, H. White (Eds.), Equations of State for Fluids and Fluid Mixtures, vol. 5, Elsevier, 2000, pp. 5–34, http://dx.doi.org/10.1016/S1874-5644(00)80013-2. Experimental Thermodynamics.

[19] I. Polishuk, F. Nakonechny, N. Brauner, Predicting phase behavior of metallic mercury in liquid and compressed gaseous hydrocarbons, Fuel 174 (2016) 197–205, http://dx.doi.org/10.1016/j.fuel.2016.02.002.

[20] A. Peneloux, W. Abdoul, E. Rauzy, Excess functions and equations of state, Fluid Phase Equilib. 47 (23) (1989) 115–132, http://dx.doi.org/10.1016/0378-3812(89)80172-4.

[21] J.-N. Jaubert, F. Mutelet, VLE predictions with the Peng-Robinson equation of state and temperature dependent k_{ij} calculated through a group contribution method, Fluid Phase Equilib. 224 (2) (2004) 285–304, http://dx.doi.org/10.1016/j.fluid.2004.06.059.

[22] J.-N. Jaubert, R. Privat, Relationship between the binary interaction parameters (k_{ij}) of the Peng-Robinson and those of the Soave-Redlich-Kwong equations of state: Application to the definition of the PR2SRK model, Fluid Phase Equilib. 295 (1) (2010) 26–37, http://dx.doi.org/10.1016/j.fluid.2010.03.037.

[23] N. Abedi, K. Nasrifar, Group contribution method for predicting the phase behavior of binary mixtures containing carbon dioxide, Iran. J. Chem. Eng. 9 (1) (2012) 12–22.

[24] O. Redlich, J.N.S. Kwong, On the thermodynamics of solutions. V. An equation of state. Fugacities of gaseous solutions, Chem. Rev. 44 (1) (1949) 233–244, http://dx.doi.org/10.1021/cr60137a013.

[25] G. Soave, Equilibrium constants from a modified Redlich-Kwong equation of state, Chem. Eng. Sci. 27 (6) (1972) 1197–1203, http://dx.doi.org/10.1016/0009-2509(72)80096-4.

[26] T. Kwak, G. Mansoori, Van der waals mixing rules for cubic equations of state, applications for supercritical fluid extraction modelling, Chem. Eng. Sci. 41 (5)

(1986) 1303–1309.
[27] D.S.H. Wong, S.I. Sandler, A theoretically correct mixing rule for cubic equations of state, AIChE J. 38 (5) (1992) 671–680, http://dx.doi.org/10.1002/aic.690380505.
[28] G.K.F. Georgios, M. Kontogeorgis, Thermodynamic Models for Industrial Applications from Classical and Advanced Mixing Rules to Association Theories, John Wiley and Sons Ltd, 2010.
[29] D. Minicucci, X.-Y. Zou, J. Shaw, The impact of liquid-liquid-vapour phase behaviour on coke formation from model coke precursors, Fluid Phase Equilib. 194–197 (2002) 353–360, http://dx.doi.org/10.1016/S0378-3812(01)00787-7.
[30] H. Ernsberger, F.M. Pitmam, New absolute manometer for vapor pressure in the micron range, Rev. Sci. Instrum. 26 (4) (1955) 584–588, http://dx.doi.org/10.1063/1.1715251.
[31] D. Ambrose, C.H.S. Sprake, The vapor pressure of mercury, J. Chem. Thermodyn. 4 (4) (1972) 603–620, http://dx.doi.org/10.1016/0021-9614(72)90082-1.
[32] C. Merlone, A. Musacchio, The mercury vapour pressure versus temperature relation between 500 and 665 k, J. Chem. Thermodyn. 42 (1) (2010) 38–47, http://dx.doi.org/10.1016/j.jct.2009.07.012.
[33] T.B. Douglas, A.F. Ball, D.C. Ginnings, Heat capacity of liquid mercury between 0° and 450 °C; Calculation of certain thermodynamic properties of the saturated liquid and vapor, J. Res. Natl. Bur. Stand 46 (4) (1951) 2204.
[34] D. Ambrose, M.B. Ewing, N.B. Ghiassee, J.C.S. Ochoa, The ebulliometric method of vapor-pressure measurement: vapor pressures of benzene, hexafluorobenzene, and naphthalene, J. Chem. Thermodyn. 22 (6) (1990) 589–605, http://dx.doi.org/10.1016/0021-9614(90)90151-F.
[35] C.S. Moreira Gomes, H.N.M. de Oliveira, O. Chiavone-Filho, E.L. Foletto, Vapor-liquid equilibria for ethyl acetate + methanol and ethyl acetate + ethanol mixtures: experimental verification and prediction, Chem. Eng. Res. Des. 92 (19) (2014) 2861–2866, http://dx.doi.org/10.1016/j.cherd.2014.07.010.
[36] D.S.M. Constantino, C.S.M. Pereira, S. a. P. Pinho, V.M.T.M. Silva, A.E. Rodrigues, Isobaric vaporliquid equilibrium data for binary system of glycerol ethyl acetal and acetonitrile at 60.0 kpa and 97.8 kpa, J. Chem. Eng. Data 58 (6) (2013) 1717–1723, http://dx.doi.org/10.1021/je400138m.
[37] S.A. Iwarere, J.D. Raal, P. Naidoo, D. Ramjugernath, Vapour-liquid equilibrium of carboxylic acid-alcohol binary systems: 2-propanol + butyric acid, 2-butanol + butyric acid and 2-methyl-1-propanol + butyric acid, Fluid Phase Equilib. (2014) 18–27, http://dx.doi.org/10.1016/j.fluid.2014.07.025.
[38] X. Dong, M. Gong, J. Liu, J. Wu, Experimental measurement of vapor pressures and (vapor + liquid) equilibrium for 1,1,1,2-tetrafluoroethane (R134a) + propane (R290) by a recirculation apparatus with view windows, J. Chem. Thermodyn. 43 (3) (2011) 505–510, http://dx.doi.org/10.1016/j.jct.2010.11.001.
[39] R. Rós, J. Ortega, L. Fernández, I. de Nuez, J. Wisniak, Improvements in the experimentation and the representation of thermodynamic properties iso-p VLE and y^E of alkyl propanoate + alkane binaries, J. Chem. Eng. Data 59 (1) (2014) 125–142, http://dx.doi.org/10.1021/je4009415.
[40] C. Viton, M. Chavret, E. Behar, J. Jose, Vapor pressure of normal alkanes from decane to eicosane at temperatures from 244 k to 469 k and pressures from 0.4 pa to 164 kp, ELDATA Int, Electron. J. Phys. Chem. Data 2 (1996) 215–224.
[41] M. Nicolae, F. Oprea, Vaporliquid equilibrium for the binary mixtures of dipropylene glycol with aromatic hydrocarbons: Experimental and regression, Fluid Phase Equilib. 370 (2014) 34–42, http://dx.doi.org/10.1016/j.fluid.2014.03.003.
[42] R. Garriga, P. Perez, M. Gracia, Total vapor pressure and excess Gibbs energy for binary mixtures of 1,1,2,2-tetrachloroethane or tetrachloroethene with benzene at nine temperatures, Fluid Phase Equilib. 227 (1) (2005) 79–86, http://dx.doi.org/10.1016/j.fluid.2004.02.021.
[43] I. Mokbel, E. Rauzy, J.P. Meille, J. Jose, Low vapor pressures of 12 aromatic hydrocarbons. experimental and calculated data using a group contribution method, Fluid Phase Equilib. 147 (1998) 271–284, http://dx.doi.org/10.1016/S0378-3812(98)00234-9.
[44] V. Kozhevnikov, D. Arnold, E. Grodzinskii, S. Naurzakov, Phase transitions and critical phenomena in mercury fluid probed by sound, Fluid Phase Equilib. 125 (1) (1996) 149–157, http://dx.doi.org/10.1016/S0378-3812(96)03099-3.
[45] G. Liessmann, W. Schmidt, S. Reiffarth, Data Compilation of the Saechsische Olefinwerke Boehlen 1.
[46] B.E. Poling, J.M. Prausnitz, J. O'Connell, The Properties of Gases and Liquids, fifth ed., McGraw-Hill, New York, 2000.
[47] H.L. Clever (Ed.), Mercury in Liquids, Compressed Gases, Molten Salts and Other Elements, IUPAC Solubility Data Series, 1987, http://dx.doi.org/10.1016/B978-0-08-035935-9.50011-X. Pergamon, Amsterdam.
[48] S.M. Wilhelm, L. Liang, D. Cussen, D.A. Kirchgessner, Mercury in crude oil processed in the United States (2004), Environ. Sci. Technol. 41 (13) (2007) 4509–4514, http://dx.doi.org/10.1021/es062742j.
[49] H.L. Clever, M. Iwamoto, Solubility of mercury in normal alkanes, Ind. Eng. Chem. Res. 26 (2) (1987) 336–337, http://dx.doi.org/10.1021/ie00062a026.
[50] M.M. Miedaner, A.A. Migdisov, A.E. Williams-Jones, Solubility of metallic mercury in octane, dodecane and toluene at temperatures between 100 °C and 200 °C, Geochim. Cosmochim. Acta 69 (23) (2005) 5511–5516, http://dx.doi.org/10.1016/j.gca.2005.06.029.
[51] T. Kimura, N. Hata, K. Sakashita, S. Asaoka, Production of aromatics from heavier n-paraffins on hybrid cracking-reforming catalyst, Catal. Today 185 (1) (2012) 119–125, http://dx.doi.org/10.1016/j.cattod.2011.09.027.
[52] Y.M. Sabri, S.J. Ippolito, J. Tardio, P. Morrison, S.K. Bhargava, Studying mercury partition in monoethylene glycol (MEG) used in gas facilities, Fuel 159 (2015) 917–924, http://dx.doi.org/10.1016/j.fuel.2015.07.047.

Bibliography

[1] R. C. Gupta, Chapter 39 - Mercury, in: R. C. Gupta (Ed.), Veterinary Toxicology (Second Edition), second edition Edition, Academic Press, Boston, 2012, pp. 537 – 543. doi:10.1016/B978-0-12-385926-6.00039-9. 19

[2] Z. F. Anual, Exposure assessment for mercury and other metals in commonly consumed fish of west peninsular malaysia, Ph.D. thesis, Faculty of Education, Science, Technology & Mathematics, University of Canberra (2014). 19

[3] S. M. Wilhelm, Mercury in petroleum and natural gas: Estimation of emissions from production, processing, and combustion, Tech. rep., US environmental Protection Agancy (2001). 19, 25, 27, 31, 37

[4] C. T. Driscoll, R. P. Mason, H. M. Chan, D. J. Jacob, N. Pirrone, Mercury as a global pollutant: Sources, pathways, and effects, Environmental Science & Technology 47 (10) (2013) 4967–4983. doi:10.1021/es305071v. 19

[5] S. M. Wilhelm, N. Bloom, Mercury in petroleum, Fuel Processing Technology 63 (1) (2000) 1 – 27. doi:10.1016/S0378-3820(99)00068-5. 19, 20, 27, 48, 86, 137

[6] S. Azimi, M. S. Moghaddam, Effect of mercury pollution on the urban environment and human health, Environment and Ecology Research 1 (2013) 12 – 20. doi:10.13189/eer.2013.010102. 19, 23, 24

[7] Q. Liu, Mercury concentration in natural gas and its distribution in the Tarim Basin, Sci. China Earth Sci. 56 (8) (2013) 1371–1379. doi:10.1007/s11430-013-4609-2. 19, 38

[8] V. V. Ryzhov, N. R. Mashyanov, N. A. Ozerova, S. E. Pogarev, Regular variations of the mercury concentration in natural gas, Science of The Total Environment 304 (13) (2003) 145 – 152. doi:10.1016/S0048-9697(02)00564-8. 19, 31

[9] M. S. Wilhelm, L. Lian, K. David, Identification and properties of mercury species in crude oil, Energy & Fuels 20 (1) (2006) 180–186. doi:10.1021/ef0501391. 19, 31

[10] J. Li, G. Chen, T. Hayat, A. Alsaedi, Mercury emissions by beijings fossil energy consumption: Based on environmentally extended inputoutput analysis, Renewable and Sustainable Energy Reviews 41 (0) (2014) 1167 – 1175. doi:10.1016/j.rser.2014.08.073. 20

[11] S. M. Wilhelm, Avoiding exposure to mercury during inspection and maintenance operations in oil and gas processing, Process Saf. Prog. 18 (3) (1999) 178–188. doi:10.1002/prs.680180311. 20

[12] E. Ha, N. Basu, S. Bose-OReilly, J. G. Drea, E. McSorley, M. Sakamoto, H. M. Chan, Current progress on understanding the impact of mercury on human health, Environmental Research 152 (2017) 419 – 433. doi:10.1016/j.envres.2016.06.042. 23

[13] K. Murata, M. Sakamoto, Minamata disease, in: Reference Module in Earth Systems and Environmental Sciences, Elsevier, 2013, pp. –. doi:10.1016/B978-0-12-409548-9.02075-3. 23

[14] S. Ekino, M. Susa, T. Ninomiya, K. Imamura, T. Kitamura, Minamata disease revisited: An update on the acute and chronic manifestations of methyl mercury poisoning, Journal of the Neurological Sciences 262 (1) (2007) 131 – 144, environmental Neurology. doi:10.1016/j.jns.2007.06.036. 23

[15] E.-G. Brunke, C. Walters, T. Mkololo, L. Martin, C. Labuschagne, B. Silwana, F. Slemr, A. Weigelt, R. Ebinghaus, V. Somerset, Mercury in the atmosphere and in rainwater at cape point, south africa, Atmospheric Environment 125 (2016) 24 – 32. doi:10.1016/j.atmosenv.2015.10.059. 23, 25

[16] Y. Huang, M. Deng, T. Li, J. Japenga, Q. Chen, X. Yang, Z. He, Anthropogenic mercury emissions from 1980 to 2012 in china, Environmental Pollution 226 (2017) 230 – 239. doi:10.1016/j.envpol.2017.03.059. 23

[17] P. Chakraborty, Mercury exposure and alzheimer's disease in india - an imminent threat?, Science of The Total Environment 589 (2017) 232 – 235. doi:org/10.1016/j.scitotenv.2017.02.168. 23

[18] P. Johansen, G. Mulvad, H. S. Pedersen, J. C. Hansen, F. Riget, Human accumulation of mercury in greenland, Science of The Total Environment 377 (2) (2007) 173 – 178. doi:10.1016/j.scitotenv.2007.02.004. 24

[19] T. Yorifuji, S. Kashima, T. Tsuda, M. Harada, What has methylmercury in umbilical cords told us? minamata disease, Science of The Total Environment 408 (2) (2009) 272 – 276. doi:10.1016/j.scitotenv.2009.10.011. 24

[20] T. McGuire. Mercury detoxification: The natural way to remove mercury from your body [online] (2014). 24

[21] P. Johansen, D. Muir, G. Asmund, F. Riget, Human exposure to contaminants in the traditional greenland diet, Science of The Total Environment 331 (1) (2004) 189 – 206, contaminants in the Greenland Environment: an update. doi:10.1016/j.scitotenv.2004.03.029. 24

[22] W. Zhang, G. Zhen, L. Chen, H. Wang, Y. Li, X. Ye, Y. Tong, Y. Zhu, X. Wang, Economic evaluation of health benefits of mercury emission controls for china and the neighboring countries in east asia, Energy Policy 106 (2017) 579 – 587. doi:10.1016/j.enpol.2017.04.010. 24

[23] N. R. Council, Toxicological effects of methylmercury, Washington, DC, USA: National Academy Press, 2000. 24

[24] L. D. Hylander, M. E. Goodsite, Environmental costs of mercury pollution, Sci. Total Environ. 368 (1) (2006) 352 – 370. doi:10.1016/j.scitotenv.2005.11.029. 24, 44, 45

[25] N. Pirrone, S. Cinnirella, X. Feng, R. B. Finkelman, H. R. Friedli, J. Leaner, R. Mason, A. B. Mukherjee, G. B. Stracher, D. G. Streets, K. Telmer, Global mercury emissions to the atmosphere from anthropogenic and natural sources, Atmospheric Chemistry and Physics 10 (13) (2010) 5951–5964. doi:10.5194/acp-10-5951-2010. 25, 26

[26] M. S. Gustin, S. E. Lindberg, K. Austin, M. Coolbaugh, A. Vette, H. Zhang, Assessing the contribution of natural sources to regional atmospheric mercury budgets, Science of The Total Environment 259 (1) (2000) 61 – 71. doi:10.1016/S0048-9697(00)00556-8. 25

[27] M. C. Hernandez-Soriano (Ed.), Environmental Risk Assessment of Soil Contamination, InTech, 2014. doi:10.5772/57086. 26, 29

[28] R. Mason, W. Fitzgerald, F. Morel, The biogeochemical cycling of elemental mercury: Anthropogenic influences, Geochimica et Cosmochimica Acta 58 (15) (1994) 3191 – 3198. doi:10.1016/0016-7037(94)90046-9. 26

[29] G. Asmund, S. P. Nielsen, Mercury in dated greenland marine sediments, Science of The Total Environment 245 (1) (2000) 61 – 72. doi:10.1016/S0048-9697(99)00433-7. 26

[30] K. M. W.-J. J. Gworek B, Bemowska-Kaabun O, Mercury in marine and oceanic watersa review, Water, Air, and Soil Pollutiondoi:10.1007/s11270-016-3060-3. 26

[31] N. O. Guangliang Liu, Yong Cai (Ed.), Environmental Chemistry and Toxicology of Mercury, of John Wiley & Sons, 2010. 26, 27, 28

[32] S. Zhao, Y. Duan, T. Yao, M. Liu, J. Lu, H. Tan, X. Wang, L. Wu, Study on the mercury emission and transformation in an ultra-low emission coal-fired power plant, Fuel 199 (2017) 653 – 661. doi:10.1016/j.fuel.2017.03.038. 26

[33] M. M. Veiga, G. Angeloci-Santos, J. A. Meech, Review of barriers to reduce mercury use in artisanal gold mining, The Extractive Industries and Society 1 (2) (2014) 351 – 361. doi:10.1016/j.exis.2014.03.004. 27

[34] M.-K. Kim, K.-D. Zoh, Fate and transport of mercury in environmental media and human exposure, Journal of Preventive Medicine and Public Health 45 (6) (2012) 335–343. doi:doi:10.3961/jpmph.2012.45.6.335. 28

[35] Z. W. Park J-D, Human exposure and health effects of inorganic and elemental mercury, Journal of Preventive Medicine and Public Health 6 (45) (2012) 344–352. doi:10.3961/jpmph.2012.45.6.344. 28

[36] R. W. Macdonald, T. Harner, J. Fyfe, Recent climate change in the Arctic and its impact on contaminant pathways and interpretation of temporal trend data, Sci. Total Environ. 342 (1-3) (2005) 5 – 86. doi:10.1016/j.scitotenv.2004.12.059. 28

[37] S. Ayrinhac, M. Gauthier, L. E. Bove, M. Morand, G. Le Marchand, F. Bergame, J. Philippe, F. Decremps, Equation of state of liquid mercury to 520 k and 7 gpa from acoustic velocity measurements, The Journal of Chemical Physics 140 (24) (2014) 244201. doi:10.1063/1.4882695. 28

[38] J. Zyk, Y. Roustan, A. Wyrwa, Modelling of the atmospheric dispersion of mercury emitted from the power sector in poland, Atmospheric Environment 112 (Supplement C) (2015) 246 – 256. doi:10.1016/j.atmosenv.2015.04.040. 28

[39] L. Zhang, S. X. Wang, L. Wang, J. M. Hao, Atmospheric mercury concentration and chemical speciation at a rural site in beijing, china: implications of mercury emission sources, Atmospheric Chemistry and Physics 13 (20) (2013) 10505–10516. doi:10.5194/acp-13-10505-2013. 28

[40] M.-K. Kim, K.-D. Zoh, Fate and transport of mercury in environmental media and human exposure, Journal of preventive medicine and public health 6 (45) (2012) 335–343. doi:10.3961/jpmph.2012.45.6.335. 28

[41] H. Hu, H. Lin, W. Zheng, S. Tomanicek, A. Johs, X. Feng, D. Elias, L. Liang, B. Gu, Oxidation and methylation of dissolved elemental mercury by anaerobic bacteria 6 (2013) 751–754. 28

[42] A. T. Reis, J. P. Coelho, I. Rucandio, C. M. Davidson, A. C. Duarte, E. Pereira, Thermo-desorption: A valid tool for mercury speciation in soils and sediments?, Geoderma 237 (2015) 98 – 104. doi:10.1016/j.geoderma.2014.08.019. 29

[43] R. T. Di Giulio, E. A. Ryan, Mercury in soils, sediments, and clams from a north carolina peatland, Water, Air, and Soil Pollution 33 (1) (1987) 205–219. doi:10.1007/BF00191389. 29

[44] K. N. Marsh, J. W. Bevan, J. C. Holste, D. L. McFarlane, M. Eliades, W. J. Rogers, Solubility of mercury in liquid hydrocarbons and hydrocarbon mixtures, Journal of Chemical & Engineering Data 61 (8) (2016) 2805–2817. doi:10.1021/acs.jced.6b00173. 29, 48, 49, 93, 94, 95, 97, 113

[45] J. Jumal, B. M. Yamin, M. Ahmad, L. Y. Heng, Mercury ion-selective electrode with self-plasticizing poly(nbuthylacrylate) membrane based on 1,2-bis-(nbenzoylthioureido)cyclohexane as ionophore, APCBEE Procedia 3 (2012) 116 – 123, 2nd International Conference on Chemistry and Chemical Process (ICCCP 2012) May 5-6, 2012. doi:10.1016/j.apcbee.2012.06.056. 29

[46] C. P. Jones, S. N. Lyman, D. A. Jaffe, T. Allen, T. L. O'Neil, Detection and quantification of gas-phase oxidized mercury compounds by gc/ms, Atmospheric Measurement Techniques 9 (5) (2016) 2195–2205. doi:10.5194/amt-9-2195-2016. 29

[47] J. Conti, International energy outlook 2016 with projections to 2040, Tech. rep., U.S. Energy Information Administration (2016). 30, 31

[48] G. Chen, X. Wu, Energy overview for globalized world economy: Source, supply chain and sink, Renewable and Sustainable Energy Reviews 69 (2017) 735 – 749. doi:10.1016/j.rser.2016.11.151. 30

[49] D. D., Production and processing of sour crude and natural gas - challenges due to increasing stringent regulations, Tech. rep., Norwegian University of Science and Technology (2013). 30

[50] M. G. David Lang, J. Holmes, Mercury arising from oil and gas production in the United Kingdom and UK continental shelf, Tech. rep., University of Oxford Department of Earth Sciences (2012). 31, 34, 37

[51] R. H. Filby, Origin and nature of trace element species in crude oils, bitumens and kerogens: implications for correlation and other geochemical studies, Geological Society, London, Special Publications 78 (1) (1994) 203–219. 31, 36, 37

[52] Global liquid fuels [online] (2017). 32, 33

[53] P. Boschee. Advancements in the removal of mercury from crude oil [online] (2013). 32

[54] S. M. Wilhelm, L. Liang, D. Cussen, D. A. Kirchgessner, Mercury in crude oil processed in the United States (2004), Environ. Sci. Technol. 41 (13) (2007) 45094514. doi:10.1021/es062742j. 33, 34

[55] J. H. Won, J. Y. Park, T. G. Lee, Mercury emissions from automobiles using gasoline, diesel, and lpg, Atmospheric Environment 41 (35) (2007) 7547 – 7552. doi:10.1016/j.atmosenv.2007.05.043. 35

[56] S. C. B. J.-K. G. Hoyer M., Baldauf1 R.V., Mercury emissions from motor vehicles, 13th International Emission Inventory Conference, 2004. 35

[57] K. C. Rice, Trace-element concentrations in streambed sediment across the conterminous united states, Environmental Science & Technology 33 (15) (1999) 2499–2504. doi:10.1021/es990052s. 35

[58] L. Liang, M. Horvat, P. Danilchik, A novel analytical method for determination of picogram levels of total mercury in gasoline and other petroleum based products, Science of The Total Environment 187 (1) (1996) 57 – 64. doi:10.1016/0048-9697(96)05129-7. 35

[59] N. S. Bloom, Analysis and stability of mercury speciation in petroleum hydrocarbons, Fresenius' Journal of Analytical Chemistry 366 (5) (2000) 438–443. doi:10.1007/s002160050089. 35, 134, 135

[60] S. Mokhatab, W. A. Poe, J. Y. Mak, Chapter 3 - Basic Concepts of Natural Gas Processing, in: S. M. A. P. Y. Mak (Ed.), Handbook of Natural Gas Transmission and Processing (Third Edition), Gulf Professional Publishing, Boston, 2015, pp. 123 – 135. doi:10.1016/B978-0-12-801499-8.00003-1. 36

[61] M. F. Ezzeldin, Mercury distribution in an egyption natural gas processing, Ph.D. thesis, University of Aberdeen (2012). 36, 38, 117, 119, 121

[62] J. S. Giacomo C., K. C., Mercury removal from natural gas and liquid streams, Tech. rep., UOP LLC. 37

[63] R. Jacobs, R. Grant, J. Kwant, J. Marquenie, E. Mentzer, The composition of produced water from Shell operated oil and gas production in the north sea, Vol. 46, 1992. 37

[64] G. Z. C. Ebenezer T. Igunnu, Produced water treatment technologies, International Journal of Low-Carbon Technologies 9 (2014) 157–177. doi:10.1093/ijlct/cts049. 37

[65] T. Bakke, J. Klungsyr, S. Sanni, Environmental impacts of produced water and drilling waste discharges from the norwegian offshore petroleum industry, Mar. Environ. Res. 92 (0) (2013) 154 – 169. doi:10.1016/j.marenvres.2013.09.012. 37

[66] M. D. Bingham, Field Detection and Implications of Mercury in Natural Gas, SPE-19357-PAdoi:10.2118/19357-PA. 38, 40, 41

[67] S. Santos, Mercury(hg) in oxy-coal fired power plant with coal fired power plant with co2 capture, Tech. rep., IEA Greenhouse Gas R&D Programme Cheltenham, UK (2004). 38

[68] S. S. T Pojtanabuntoeng, C Saiwan, D. L. Gallup, Effect of mercury on corrosion in production wells in gulf of thailand, Corrosion Engineering, Science and Technology. 39, 41

[69] R. Hadden, T. Moss, Dealing with mercury in refinery processes, Digital Refining. 39, 53

[70] . A.-H. Z. M. Nengkoda, A., Understanding of mercury corrosion attack on stainless steel material at gas wells: Case study, International Petroleum Technology Conference, 2009. doi:10.2523/IPTC-13368-MS. 39, 40, 136

[71] S. M. Wilhelm, The effect of elemental mercury on engineering materials used in ammonia plants, Plant/Operations Progress 10 (4) (1991) 189–193. doi:10.1002/prsb.720100404. 39, 41

[72] Galvanic corrosion [online] (2018). 41

[73] J. E. Leeper. Mercury lng's problem [online] (1980). 41

[74] S. Mishra, Mercury treatment options for natural gas plants, Digital Refining. 41

[75] A. Shafawi, L. Ebdon, M. Foulkes, P. Stockwell, W. Corns, Preliminary evaluation of adsorbent-based mercury removal systems for gas condensate, Analytica Chimica Acta 415 (12) (2000) 21 – 32. doi:10.1016/S0003-2670(00)00838-2. 42, 43

[76] J. M. Monteagudo, M. J. Ortiz, Removal of inorganic mercury from mine waste water by ion exchange, Journal of Chemical Technology & Biotechnologydoi:10.1002/1097-4660(200009)75:9<767::AID-JCTB281>3.0.CO;2-1. 43

[77] Abai, Mahpuzah and Atkins, Martin P. and Hassan, Amiruddin and Holbrey, John D. and Kuah, Yongcheun and Nockemann, Peter and Oliferenko, Alexander A. and Plechkova, Natalia V. and Rafeen, Syamzari and Rahman, Adam A. and Ramli, Rafin and Shariff, Shahidah M. and Seddon, Kenneth R. and Srinivasan, Geetha and Zou, Yiran, An ionic liquid process for mercury removal from natural gas, Dalton Trans. 44 (2015) 8617–8624. doi:10.1039/C4DT03273J. 44

[78] X. F. E. B. Wenguo Feng, Seokjoon Kwon, M. Radisav D. Vidic, Sulfur impregnation on activated carbon fibers through h2s oxidation for vapor phase mercury remova, Journal of Environmental Engineering. 44

[79] L. Trasande, P. J. Landrigan, C. Schechter, Public Health and Economic Consequences of Methyl Mercury Toxicity to the Developing Brain, Environmental Health Perspectives 113 (5) (2005) 590–596. doi:10.1289/ehp.7743. 44

[80] . Marcia L. Huber, A. Laesecke, , D. G. Friend, Correlation for the vapor pressure of mercury, Industrial & Engineering Chemistry Research 45 (21) (2006) 7351–7361. doi:10.1021/ie060560s. 45

[81] M. L. Huber, A. Laesecke, D. G. Friend, Correlation for the vapor pressure of mercury, Industrial & Engineering Chemistry Research 45 (21) (2006) 7351–7361. doi:10.1021/ie060560s. 46

[82] A. Merlone, C. Musacchio, The mercury vapour pressure vs. temperature relation between (500 and 665)K, J. Chem. Thermodyn. 42 (1) (2010) 38 – 47. doi:10.1016/j.jct.2009.07.012. 46

[83] D. Ambrose, M. B. Ewing, N. B. Ghiassee, J. C. S. Ochoa, The ebulliometric method of vapor-pressure measurement: Vapor pressures of benzene, hexafluorobenzene, and naphthale, J. Chem. Thermodyn. 22 (6) (1990) 589–605. doi:10.1016/0021-9614(90)90151-F. 47, 84, 100

[84] H. Kitamura, Equation of state for expanded fluid mercury: Variational theory with many-body interaction, The Journal of Chemical Physics 126 (13) (2007) 134509. doi:10.1063/1.2712443. 47

[85] D. K. Belashchenko, Molecular dynamics simulation of the thermodynamic properties of mercury at pressures below 2.5 gpa and temperatures below 10000 k, Russian Journal of Physical Chemistry A 91 (8) (2017) 1392–1400. doi:10.1134/S0036024417080052. 47

[86] S. M. Wilhelm, L. Liang, D. Cussen, D. A. Kirchgessner, Mercury in crude oil processed in the United States (2004), Environ. Sci. Technol. 41 (13) (2007) 4509–4514. doi:10.1021/es062742j. 48, 86

[87] H. L. Clever, M. Iwamoto, Solubility of mercury in normal alkanes, Ind. Eng. Chem. Res. 26 (2) (1987) 336–337. doi:10.1021/ie00062a026. 48, 49, 86, 87, 88, 90, 102, 103, 104, 110

[88] M. M. Miedaner, A. A. Migdisov, A. E. Williams-Jones, Solubility of metallic mercury in octane, dodecane and toluene at temperatures between 100°C and

200°C, Geochim. Cosmochim. Acta 69 (23) (2005) 5511 – 5516. doi:doi.org/10.1016/j.gca.2005.06.029. 48, 86, 87, 88, 102, 103

[89] T. Kimura, N. Hata, K. Sakashita, S. Asaoka, Production of aromatics from heavier n-paraffins on hybrid cracking-reforming catalyst, Catal. Today 185 (1) (2012) 119 – 125. doi:10.1016/j.cattod.2011.09.027. 49, 90

[90] D. L. Gallup, D. J. O'Rear, R. Radford, The behavior of mercury in water, alcohols, monoethylene glycol and triethylene glycol, Fuel 196 (2017) 178 – 184. doi:10.1016/j.fuel.2017.01.100. 49

[91] H. L. Clever (Ed.), Mercury in Liquids, Compressed Gases, Molten Salts and Other Elements, IUPAC Solubility Data Series, Pergamon, Amsterdam, 1987. doi:10.1016/B978-0-08-035935-9.50011-X. 50, 85, 86, 92, 93, 101, 105, 111

[92] C.-C. Chen, P. M. Mathias, Applied thermodynamics for process modeling, AIChE J. 48 (2) (2002) 194–200. doi:10.1002/aic.690480202. 50, 69

[93] M. H. Abraham, J. Gil-Lostes, W. E. Acree, Jr, J. Enrique Cometto-Muniz, W. S. Cain, Solvation parameters for mercury and mercury(ii) compounds: calculation of properties of environmental interest, J. Environ. Monit. 10 (2008) 435–442. doi:10.1039/B719685G. 50

[94] M. H. Lagache, J. Ridard, P. Ungerer, A. Boutin, Force field optimization for organic mercury compounds, J. Phys. Chem. B 108 (24) (2004) 8419–8426. doi:10.1021/jp049676x. 50

[95] M. B. Ewing, C. J. Peters, Fundamental considerations, in: C. P. J.V. Sengers, R.F. Kayser, H. White (Eds.), Equations of State for Fluids and Fluid Mixtures, Vol. 5 of Experimental Thermodynamics, Elsevier, 2000, pp. 5 – 34. doi:10.1016/S1874-5644(00)80013-2. 51, 60, 65, 69, 70

[96] I. Polishuk, F. Nakonechny, N. Brauner, Predicting phase behavior of metallic mercury in liquid and compressed gaseous hydrocarbons, Fuel 174 (2016) 197 – 205. doi:10.1016/j.fuel.2016.02.002. 51, 66, 87, 89, 91

[97] I. Polishuk, A. Vilk, M. Chorewski, Predicting phase behavior of metallic mercury in liquid and compressed gaseous hydrocarbons ii: Further examination of cp-pc-saft in the light of new data, Fuel 203 (Supplement C) (2017) 686 – 689. doi:10.1016/j.fuel.2017.05.032. 51, 66, 87, 89

[98] G. Soave, S. Gamba, L. A. Pellegrini, Srk equation of state: Predicting binary interaction parameters of hydrocarbons and related compounds, Fluid Phase Equilibria 299 (2) (2010) 285 – 293. doi:10.1016/j.fluid.2010.09.012. 51

[99] L. R. N. . A.-E. G. Prausnitz, J. M., Molecular Thermodynamics of Fluid-Phase Equilibria, Upper Saddle River, N.J: Prentice Hall PTR, 1999. 54, 55

[100] R. Privat, J.-N. Jaubert, Y. Privat, A simple and unified algorithm to solve fluid phase equilibria using either the gammaphi or the phiphi approach for binary and ternary mixtures, Computers & Chemical Engineering 50 (2013) 139 – 151. doi:doi.org/10.1016/j.compchemeng.2012.11.006. 63

[101] M.-O. Coppens, Thermodynamics. fundamentals for applications. von john p. o'connell und j. m. haile., Angewandte Chemie 118 (8) (2006) 1202–1202. doi:10.1002/ange.200585336. 63

[102] H. Orbey, S. Sandler, Modeling Vapor-liquid Equilibria: Cubic Equations of State and Their Mixing Rules, Cambridge series in chemical engineering, Cambridge University Press, 1998. 65

[103] E. E. John, Process modelling selection of thermodynamic methods, Tech. rep., P & I Design Ltd (2008). 65, 66

[104] O. Redlich, J. N. S. Kwong, On the thermodynamics of solutions. V. An equation of state. Fugacities of gaseous solutions., Chem. Rev. 44 (1) (1949) 233–244. doi:10.1021/cr60137a013. 66

[105] G. Soave, Equilibrium constants from a modified Redlich-Kwong equation of state, Chem. Eng. Sci. 27 (6) (1972) 1197 – 1203. doi:10.1016/0009-2509(72)80096-4. 66

[106] J. M. Prausnitz, R. N. Lichtenthaler, E. G. de Azevedo, Molecular Thermodynamics of Fluid-Phase Equilibria, 2nd Edition, Prentice-Hall, Englewood Cliffs, NJ, 1986. 67, 71, 72

[107] T. Kwak, G. Mansoori, Van der waals mixing rules for cubic equations of state, applications for supercritical fluid extraction modell, Chem. Eng. Sci. 41 (5) (1986) 1303–1309. 67

[108] D. S. H. Wong, S. I. Sandler, A theoretically correct mixing rule for cubic equations of state, AIChE J. 38 (5) (1992) 671–680. doi:10.1002/aic.690380505. 67

[109] D. Minicucci, X.-Y. Zou, J. Shaw, The impact of liquid-liquid-vapour phase behaviour on coke formation from model coke precursors, Fluid Phase Equilib. 194-197 (2002) 353 – 360. doi:10.1016/S0378-3812(01)00787-7. 69

[110] J.-N. Jaubert, F. Mutelet, VLE predictions with the Peng-Robinson equation of state and temperature dependent k_{ij} calculated through a group contribution method, Fluid Phase Equilib. 224 (2) (2004) 285 – 304. doi:10.1016/j.fluid.2004.06.059. 69, 72, 114, 153

[111] J.-N. Jaubert, R. Privat, Relationship between the binary interaction parameters (k_{ij}) of the Peng-Robinson and those of the Soave-Redlich-Kwong equations of state: Application to the definition of the PR2SRK model, Fluid Phase Equilib. 295 (1) (2010) 26 – 37. doi:10.1016/j.fluid.2010.03.037. 71, 72, 114, 153

[112] G. K. F. Georgios M. Kontogeorgis, Thermodynamic Models for Industrial Applications From Classical and Advanced Mixing Rules to Association Theories, John Wiley and Sons Ltd, 2010. 71

[113] A. Peneloux, W. Abdoul, E. Rauzy, Excess functions and equations of state, Fluid Phase Equilib. 47 (23) (1989) 115 – 132. doi:10.1016/0378-3812(89)80172-4. 71

[114] N. Abedi, K. Nasrifar, Group contribution method for predicting the phase behavior of binary mixtures containing carbon dioxide, Iran. J. Chem. Eng. 9 (1) (2012) 12–22. 72, 114, 153

[115] J. Gross, G. Sadowski, Perturbed-chain saft: an equation of state based on a perturbation theory for chain molecules, Industrial & Engineering Chemistry Research 40 (4) (2001) 1244–1260. doi:10.1021/ie0003887. 73, 76, 78, 159

[116] W. G. Chapman, K. E. Gubbins, G. Jackson, M. Radosz, New reference equation of state for associating liquids, Industrial & Engineering Chemistry Research 29 (8) (1990) 1709–1721. doi:10.1021/ie00104a021. 73, 76

[117] S. H. Huang, M. Radosz, Equation of state for small, large, polydisperse, and associating molecules: extension to fluid mixtures, Industrial & Engineering Chemistry Research 30 (8) (1991) 1994–2005. doi:10.1021/ie00056a050. 73

[118] P. Hosseinifar, S. Jamshidi, Determination of perturbed-chain statistical association fluid theory parameters for pure substances, single carbon number groups, and petroleum fractions using cubic equations of state parameters, Industrial & Engineering Chemistry Research 54 (45) (2015) 11448–11465. doi:10.1021/acs.iecr.5b03103. 73

[119] K. Nasrifar, A. H. Tafazzol, Vaporliquid equilibria of acid gasaqueous ethanolamine solutions using the pc-saft equation of state, Industrial & Engineering Chemistry Research 49 (16) (2010) 7620–7630. arXiv:http://dx.doi.org/10.1021/ie901181n, doi:10.1021/ie901181n. 77

[120] L. F. Cameretti, G. Sadowski, J. M. Mollerup, Modeling of aqueous electrolyte solutions with perturbed-chain statistical associated fluid theory, Industrial & Engineering Chemistry Research 44 (9) (2005) 3355–3362. doi:10.1021/ie0488142. 77

[121] R. A. Youn, Toxicity summary for methylmercury, Ph.D. thesis, Biomedical and Environmental Information Analysis Section (1992). 80

[122] M. N. Non-linear least-squares minimization and curve-fitting for python [online] (2017). 82

[123] V. Kozhevnikov, D. Arnold, E. Grodzinskii, S. Naurzakov, Phase transitions and critical phenomena in mercury fluid probed by sound, Fluid Phase Equilibria 125 (1) (1996) 149 – 157. doi:10.1016/S0378-3812(96)03099-3. 83

[124] G. Liessmann, W. Schmidt, S. Reiffarth, Data compilation of the saechsische olefinwerke boehlen 1. 83

[125] J. M. P. Bruce E. Poling, J. P., The Properties of Gases and Liquids, fifth edition Edition, McGraw-Hill,New York, 2000. 83

[126] H. Ernsberger, F.M.;Pitmam, New absolute manometer for vapor pressure in the micron range, Rev. Sci. Instrum. 26 (4) (1955) 584–588. doi:doi.org/10.1063/1.1715251. 84, 99

[127] D. Ambrose, C. H. S. Sprake, The vapor pressure of mercury, J. Chem. Thermodyn 4 (4) (1972) 603–620. doi:10.1016/0021-9614(72)90082-1. 84, 99

[128] A. Merlone, C. Musacchio, The mercury vapour pressure versus temperature relation between 500 and 665 k, J. Chem. Thermodyn. 42 (1) (2010) 38–47. doi:10.1016/j.jct.2009.07.012. 84, 99

[129] T. B. Douglas, A. F. Ball, D. C. Ginnings, Heat capacity of liquid mercury between 0° and 450°C; Calculation of certain thermodynamic properties of the saturated liquid and vapor, J. Res. Natl. Bur. Stand. 46 (4) (1951) 2204. 84, 99

[130] M. L. Huber, A. Laesecke, D. G. Friend, Correlation for the vapor pressure of mercury, Ind. Eng. Chem. 45 (2006) 7351–7361. doi:10.1021/ie060560s. 84

[131] C. S. Moreira Gomes, H. N. M. de Oliveira, O. Chiavone-Filho, E. L. Foletto, Vapor-liquid equilibria for ethyl acetate + methanol and ethyl acetate + ethanol mixtures: Experimental verification and prediction, Chem. Eng. Res. Des. 92 (19) (2014) 2861–2866. doi:10.1016/j.cherd.2014.07.010. 84, 100

[132] D. S. M. Constantino, C. S. M. Pereira, S. a. P. Pinho, V. M. T. M. Silva, A. E. Rodrigues, Isobaric vaporliquid equilibrium data for binary system of glycerol ethyl acetal and acetonitrile at 60.0 kpa and 97.8 kpa, J. Chem. Eng. Data 58 (6) (2013) 1717–1723. doi:10.1021/je400138m. 84, 100

[133] S. A. Iwarere, J. D. Raal, P. Naidoo, D. Ramjugernath, Vapour-liquid equilibrium of carboxylic acid-alcohol binary systems: 2-propanol + butyric acid, 2-butanol + butyric acid and 2-methyl-1-propanol + butyric acid, Fluid Phase Equilib. (2014) 18–27doi:10.1016/j.fluid.2014.07.025. 84, 100

[134] X. Dong, M. Gong, J. Liu, J. Wu, Experimental measurement of vapor pressures and (vapor + liquid) equilibrium for 1,1,1,2-tetrafluoroethane (R134a) + propane (R290) by a recirculation apparatus with view windows, J. Chem. Thermodyn. 43 (3) (2011) 505 – 510. doi:10.1016/j.jct.2010.11.001. 84, 100

[135] R. Rós, J. Ortega, L. Fernández, I. de Nuez, J. Wisniak, Improvements in the experimentation and the representation of thermodynamic properties iso-p VLE and y^E of alkyl propanoate + alkane binaries, J. Chem. Eng. Data 59 (1) (2014) 125–142. doi:10.1021/je4009415. 84, 100

[136] C. Viton, M. Chavret, E. Behar, J. Jose, Vapor pressure of normal alkanes from decane to eicosane at temperatures from 244 k to 469 k and pressures from 0.4 pa to 164 kp, ELDATA Int. Electron. J. Phys. Chem. Data 2 (1996) 215–224. 84, 100

[137] M. Nicolae, F. Oprea, Vaporliquid equilibrium for the binary mixtures of dipropylene glycol with aromatic hydrocarbons: Experimental and regression, Fluid Phase Equilibria 370 (2014) 34 – 42. doi:10.1016/j.fluid.2014.03.003. 84, 101

[138] R. Garriga, P. Perez, M. Gracia, Total vapor pressure and excess Gibbs energy for binary mixtures of 1,1,2,2-tetrachloroethane or tetrachloroethene with benzene at nine temperatures, Fluid Phase Equilib. 227 (1) (2005) 79–86. doi:10.1016/j.fluid.2004.02.021. 84, 101

[139] I. Mokbel, E. Rauzy, J. P. Meille, J. Jose, Low vapor pressures of 12 aromatic hydrocarbons. experimental and calculated data using a group contribution method, Fluid Phase Equilib. 147 (1998) 271–284. doi:10.1016/S0378-3812(98)00234-9. 84, 101

[140] Y. M. Sabri, S. J. Ippolito, J. Tardio, P. Morrison, S. K. Bhargava, Studying mercury partition in monoethylene glycol (MEG) used in gas facilities, Fuel 159 (2015) 917 – 924. doi:10.1016/j.fuel.2015.07.047. 92

[141] J. Gross, G. Sadowski, Perturbed-chain saft: an equation of state based on a perturbation theory for chain molecules, Industrial & Engineering Chemistry Research 40 (4) (2001) 1244–1260. doi:10.1021/ie0003887. 98, 99

[142] J. Gross, G. Sadowski, Application of the perturbed-chain saft equation of state to associating systems, Industrial & Engineering Chemistry Research 41 (22) (2002) 5510–5515. doi:10.1021/ie010954d. 98, 99, 111

[143] M. F. Ezzeldin, Z. Gajdosechova, M. B. Masod, T. Zaki, J. Feldmann, E. M. Krupp, Mercury speciation and distribution in an egyptian natural gas processing plant, Energy & Fuels 30 (12) (2016) 10236–10243. doi:10.1021/acs.energyfuels.6b02035. 117, 118, 119, 120, 121, 122, 124, 125, 126, 127, 129, 134

[144] A. Y. El Naggar, Y. M. Moustafa, S. Faramawy, A. M. Elfadly, E. S. Abdullah, M. A. Ebiad, Monitoring of trace chloride ions at different stages of the gas production process, Arabian Journal of Chemistry 8 (1) (2015) 15–24. doi:10.1016/j.arabjc.2011.03.004. 117, 119, 121, 122, 123

[145] Bouyssiere, B., Baco, F., Savary, L., Lobinski, R., Analytical methods for speciation of mercury in gas condensates: Critical assessment and recommendations, Oil & Gas Science and Technology - Rev. IFP 55 (6) (2000) 639–648. doi:10.2516/ogst:2000048. 121, 134

[146] a. S. J. Boszke L., Glosinska G., Some aspects of speciation of mercury in a water environment, Polish Journal of Environmental Studies 11 (4) (2002) 285–298. 121, 134

[147] D. N. Egypt. Bapetco achieves highest production record in 15 years [online] (2015). 122

[148] M. A. A. I. S. Mark Wilhelm, S. Safri, Mercury in se asia produced fluids holistic approach to managing offshore impacts, International Petroleum Technology Conference. 128

[149] M. R. Sainal, T. M. U. Tg Mat, A. B. Shafawi, A. J. Mohamed, Mercury Removal Project: Issues and Challenges in Managing and Executing a Technology Project, in: SPE-110118-MS, Society of Petroleum Engineers, SPE, 2007. doi:10.2118/110118-MS. 129

[150] A. Ryaboshapko, O. R. Bullock, J. Christensen, M. Cohen, A. Dastoor, I. Ilyin, G. Petersen, D. Syrakov, R. S. Artz, D. Davignon, R. R. Draxler, J. Munthe, Intercomparison study of atmospheric mercury models: 1. comparison of models with short-term measurements, Science of The Total Environment 376 (1) (2007) 228 – 240. doi:10.1016/j.scitotenv.2007.01.072. 133

[151] P. J. F., Lagrangian and eulerian representations of fluid flow: Kinematics and the equation of motion, Tech. rep., Woods Hole Oceanographic Institution (2006). 133

[152] H. Jnicke, G. Scheuermann, Measuring complexity in lagrangian and eulerian flow descriptions, Computer Graphics Forum 29 (6) (2010) 1783–1794. doi:10.1111/j.1467-8659.2010.01648.x. 133

[153] S. Y. Kwon, N. E. Selin, Uncertainties in atmospheric mercury modeling for policy evaluation, Current Pollution Reports 2 (2) (2016) 103–114. doi:10.1007/s40726-016-0030-8. 133

[154] B. Bouyssiere, F. Baco, L. Savary, R. Lobiski, Speciation analysis for mercury in gas condensates by capillary gas chromatography with inductively coupled plasma mass spectrometric detection, Journal of Chromatography A 976 (1) (2002) 431 – 439, 7th International Symposium on Hyphenated Techniques in Chromatography and Hyphenated Chromatographic Analyzers. doi:10.1016/S0021-9673(02)01151-2. 134

[155] Z. Gajdosechova, M. S. Boskamp, F. Lopez-Linares, J. Feldmann, E. M. Krupp, Hg speciation in petroleum hydrocarbons with emphasis on the reactivity of hg particles, Energy & Fuels 30 (1) (2016) 130–137. doi:10.1021/acs.energyfuels.5b02080. 134

[156] J. Snell, J. Qian, M. Johansson, K. Smit, Stability and reactions of mercury species in organic solution[dagger], Analyst 123 (1998) 905–909. doi:10.1039/A708391B. 136

[157] J. R. Edwards, R. K. Srivastava, J. D. Kilgroe, A study of gas-phase mercury speciation using detailed chemical kinetics, Journal of the Air & Waste Management Association 51 (6) (2001) 869–877. doi:10.1080/10473289.2001.10464316. 138

[158] L. Zhang, S. Wang, Q. Wu, F. Wang, C.-J. Lin, L. Zhang, M. Hui, M. Yang, H. Su, J. Hao, Mercury transformation and speciation in flue gases from anthropogenic emission sources: a critical review, Atmospheric Chemistry and Physics 16 (4) (2016) 2417–2433. doi:10.5194/acp-16-2417-2016. 138

[159] B. Hall, P. Schager, J. Weesmaa, The homogeneous gas phase reaction of mercury with oxygen, and the corresponding heterogeneous reactions in the presence of activated carbon and fly ash, Chemosphere 30 (4) (1995) 611 – 627. doi:10.1016/0045-6535(94)00428-W. 138

[160] S. Tang, L. Wang, X. Feng, Z. Feng, R. Li, H. Fan, K. Li, Actual mercury speciation and mercury discharges from coal-fired power plants in inner mongolia, northern china, Fuel 180 (Supplement C) (2016) 194 – 204. doi:10.1016/j.fuel.2016.04.037. 138

[161] N. C. Widmer, J. A. Cole, W. R. Seeker, J. A. Gaspar, Practical limitation of mercury speciation in simulated municipal waste incinerator flue gas, Combustion Science and Technology 134 (1-6) (1998) 315–326. doi:10.1080/00102209808924138. 138

[162] J. Wilcox, D. C. Marsden, P. Blowers, Evaluation of basis sets and theoretical methods for estimating rate constants of mercury oxidation reactions involving

chlorine, Fuel Processing Technology 85 (5) (2004) 391 – 400. doi:10.1016/j.fuproc.2003.09.007. 139

[163] B. P. Wendt, Jost O.L., Fundamentals of mercury speciation kinetics: A theoretical and experimental study, Tech. rep., University of Arizona (2004). 140

[164] K. O. Awitor, L. Bernard, B. Coupat, J. P. Fournier, P. Verdier, Measurement of mercurous chloride vapor pressure, New J. Chem. 24 (2000) 399–401. doi:10.1039/B000238K. 139, 141

[165] F. M. G. Johnson, The vapor pressures of mercuric chloride, bromide and iodide., Journal of the American Chemical Society 33 (6) (1911) 777–781. arXiv:http://dx.doi.org/10.1021/ja02219a001, doi:10.1021/ja02219a001. 139, 141

[166] C. Held, T. Reschke, S. Mohammad, A. Luza, G. Sadowski, epc-saft revised, Chemical Engineering Research and Design 92 (12) (2014) 2884 – 2897, advances in Thermodynamics for Chemical Process and Product Design. doi:doi.org/10.1016/j.cherd.2014.05.017. 142

[167] H. L. Clever, S. A. Johnson, M. E. Derrick, The solubility of mercury and some sparingly soluble mercury salts in water and aqueous electrolyte solutions, Journal of Physical and Chemical Reference Data 14 (3) (1985) 631–680. doi:10.1063/1.555732. 142, 145

[168] P. V. Pontes, E. A. Crespo, M. A. Martins, L. P. Silva, C. M. Neves, G. J. Maximo, M. D. Hubinger, E. A. Batista, S. P. Pinho, J. A. Coutinho, G. Sadowski, C. Held, Measurement and pc-saft modeling of solid-liquid equilibrium of deep eutectic solvents of quaternary ammonium chlorides and carboxylic acids, Fluid Phase Equilibria 448 (Supplement C) (2017) 69 – 80, deep Eutectic Solvents. doi:10.1016/j.fluid.2017.04.007. 144